LA-11906-MS

Los Alamos National Laboratory is operated by the University of California for the United States Department of Energy under contract W-7405-ENG-36

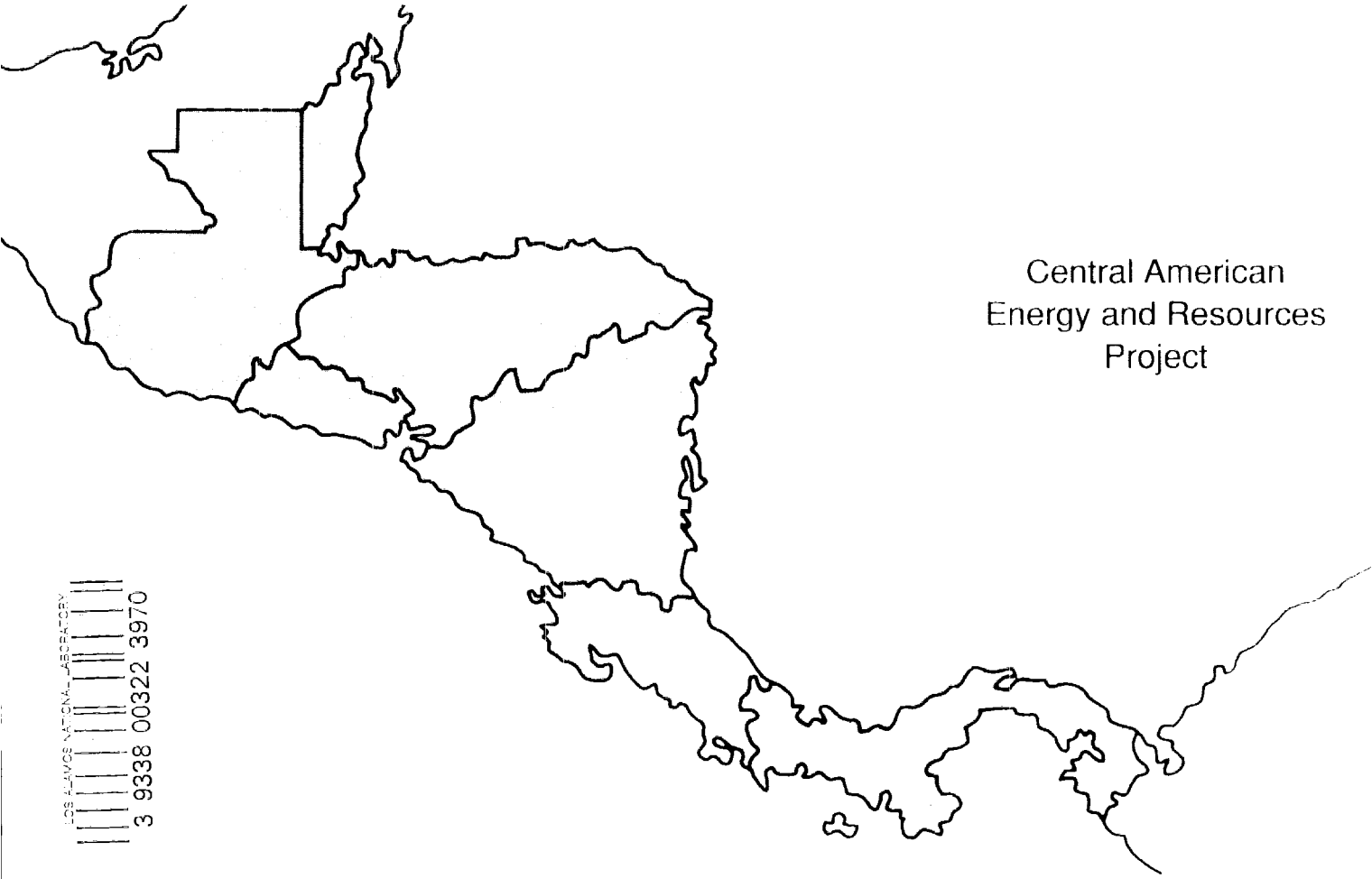

Central American
Energy and Resources
Project

An Evaluation of the Geothermal Potential of the Tecuamburro Volcano Area of Guatemala

Los Alamos National Laboratory
Los Alamos, New Mexico 87545

This work was supported by the US Agency for International Development.

An Affirmative Action/Equal Opportunity Employer

LA-11906-MS

UC-000
Issued: September 1990

An Evaluation of the Geothermal Potential of the Tecuamburro Volcano Area of Guatemala

Edited by
G. Heiken
*W. Duffield**

**US Geological Survey, 2255 N. Gemini, Flagstaff, AZ 86001.*

Los Alamos National Laboratory
Los Alamos, New Mexico 87545

CONTENTS

AN EVALUATION OF THE GEOTHERMAL POTENTIAL OF THE TECUAMBURRO VOLCANO AREA OF GUATEMALA

Edited by
G. Heiken and W. Duffield

ABSTRACT

Radiometric ages indicate that the Tecuamburro Volcano and three adjacent lava domes grew during the last 38300 years, and that a 360-m-wide phreatic crater, Laguna Ixpaco, was formed near the base of these domes about 2900 years ago. Laguna Ixpaco is located within the Chupadero crater, from which pyroxene pumice deposits were erupted 38300 years ago. Thus, the likelihood is great for a partly molten or solid-but-still-hot near-surface intrusion beneath the area. Fumaroles and hot springs issue locally from the Tecuamburro volcanic complex and near Laguna Ixpaco. Analyses of gas and fluid samples from these and other nearby thermal manifestations yield chemical-geothermometer temperatures of about 150° to 300°C, with the highest temperatures at Ixpaco. The existence of a commercial-grade geothermal reservoir beneath the Ixpaco area seems likely.

EXECUTIVE SUMMARY

Field studies of the Tecuamburro Volcano geothermal area were conducted by scientists from the Los Alamos National Laboratory (LANL), the US Geological Survey (USGS), and the Instituto Nacional de Electrificatión (INDE) in 1988 and 1989. The program included geologic studies with an emphasis on the history of volcanism, thermal sources and structural framework; a soil-radon survey aimed at identifying zones of enhanced permeability; hydrogeochemical studies that include analysis and interpretation of fumarolic gases and thermal and nonthermal waters; and geophysical surveys with emphasis on measurements of electrical resistivity; The results of the integrated surveys indicate that there is a substantial crustal heat source beneath the area of youngest volcanism, especially at the Laguna Ixpaco phreatic crater. The young volcanism (<100000 years), the high chemical geothermometer fumarolic gas temperatures at Ixpaco (~300°C), and the presence of a highly conductive, WNW-trending zone that passes through Laguna Ixpaco all indicate the intersection between a fault zone with several craters, along which there is upflow of geothermal fluids. The Laguna Ixpaco and fumarole fields all lie within the 4-km-diameter Chupadero crater that may be the source for 38000-year-old pyroxene pumice deposits.

Tecuamburro lies within the southern end of a N-S-trending, 20-km-wide graben. The Jalpatagua strike-slip fault zone terminates the northern end of the graben and the Pacific coastal plain sediments bury the southern end. Andesitic composite cone complexes flank the graben, with Pueblo Nuevo Viñas on the west and Ixhuatán on the east; these

volcanic complexes have ages of 2.6 Ma and 1.2 Ma, respectively. Ages of some of the volcanic rocks erupted within the graben may partly overlap those of the relatively older flanking volcanoes. Most of the volcanoes within the graben decrease in age from north to south; exceptions are the scoria cones near Barberena and Cuilapa. Radiometric ages range from 1.18 Ma in the north-central part of the graben to 38300 years for a pyroclastic unit farther south to somewhat younger for Tecuamburro summit eruptions that overlie this pyroclastic unit. Tecuamburro and adjacent lava domes represent the youngest magmatic eruptions in the area and consist of several km^3 of lava. We estimate that about 55 km^3 of magma was erupted from closely spaced vents in the Tecuamburro area during the last 100000 years.

North- and WNW-trending normal faults are common within the Tecuamburro graben with many thermal manifestations located along them. Vents of the Tecuamburro dome complex are aligned along the WNW trend and the electrical resistivity survey defines a WNW-trending conductive zone that passes through Laguna Ixpaco and fumaroles located west of the laguna. The WNW-trending faults are important zones of permeability for geothermal fluids.

Chemical and isotopic analyses of thermal and nonthermal waters and gases collected at springs and fumaroles of the Tecuàmburro geothermal area provide information about possible geothermal reservoir temperatures and such processes as mixing and boiling. Three types of thermal waters have been identified: (1) steam-heated, (2) acid-sulfate, and (3) neutral-chloride. These waters are restricted to the northern highlands within the graben, the Laguna Ixpaco (Chupadero crater) area, and along the course of the Río Los Esclavos.

The steam-heated waters are relatively dilute and are composed mostly of near-surface ground water heated either by condensation of steam from an underlying boiling reservoir and/or from elevated crustal heat flow. Acid-sulfate waters have pH ≤ 3, are high in sulfate, and presumably form from H_2S, which rises from a boiling, high-temperature reservoir and oxidizes in ground water to form sulfuric acid. These waters are associated with fumaroles at Laguna Ixpaco. Fumaroles of similar gas composition issue from the sulfur mine at the base of the Peña Blanca and San Francisco domes. Neutral-chloride springs typically have pH 7 and relatively high chloride content. These probably represent lateral outflow from a geothermal reservoir with or without dilution by mixing with shallow meteoric ground water.

Chemical geothermometry was applied to both water and gas samples. Gases collected at fumaroles of Laguna Ixpaco yield geothermometer temperatures as high as 300°C. These gases presumably rise more or less vertically from a geothermal reservoir located beneath the Ixpaco area, within the Chupadero crater. Temperatures calculated for thermal water range from 150° to 200°C. Thermal waters along the Río Los Esclavos show evidence of mixing with shallow meteoric ground water and are interpreted to represent lateral outflow from a hydrothermal convection system or systems located below the higher terrain to the west.

Two interpretations are possible: (1) a single geothermal system of ~300°C centered beneath the Laguna Ixpaco-Tecuamburro Volcano area feeds all hot springs along the Río Los Esclavos and a zone of steam-heated waters to the north by means of two to three lateral flow paths; and (2) two adjacent systems separated by a WNW-trending fault-zone aquitard extending from El Corozal near the Río Los Esclavos, westward to Joyas de San Nicolas. In the latter interpretation one system is centered beneath the Laguna Ixpaco-Tecuamburro area as stated in (1) and the second system of ~165°C is centered beneath the Fumarole Infiernitos-Finca Las Delicias area.

We conclude that there are active geothermal systems within this area and that geothermal gradient coreholes should be drilled to test the most promising of these systems. The first corehole should be drilled to the west of the Laguna Ixpaco phreatic crater, 700 m WNW of the center of Ixpaco, along the zone of low resistivity that was defined by the electrical and soil-radon surveys.

A second corehole should be sited several kilometers north of Ixpaco, along one of the faults that cross older andesitic volcanoes. A geothermal reservoir or reservoirs located along these faults may be the sources for neutral-chloride waters samples at Colmenares. A WNW-trending fault-zone that crosses the northern rim of Chupadero crater may be an aquitard; a second corehole, located north of this fault, is needed to determine if there is one large system or two separate systems in the Tecuamburro region.

ACKNOWLEDGEMENTS

This work was funded by the Regional Office, Central American Project (ROCAP), of the US Agency for International Development, under the auspices of the US Department of Energy. We thank Carl Duisberg (ROCAP), Andres Caicedo (INDE), and A. W. Laughlin, E. Van Eeckhout, and S. Booth (LANL) for handling the planning and paperwork required for this project. Oscar Pinzon, formerly of INDE, worked with us in the field as a colleague during the first field season. We also thank Anthony Garcia, Marcia Jones, H. Cummings, and Marge Wilson for illustrating, typing, and editing of this report.

I. GEOLOGY AND GEOTHERMAL POTENTIAL OF THE TECUAMBURRO VOLCANO AREA OF GUATEMALA

([1]W. A. Duffield*, G. H. Heiken**, K. H. Wohletz**, L. W. Maassen**, G. Dengo†, and E. H. McKee††)

A. INTRODUCTION

The Tecuamburro geothermal area is a promising commercial geothermal resource, based on recent geological and hydrogeochemical studies made by the Los Alamos National Laboratory (LANL), the U. S. Geological Survey (USGS), and Instituto Nacional de Electrificación (INDE). The area is located in southeastern Guatemala along the Central American chain of active volcanoes and is dominated by Tecuamburro Volcano, which rises ~800 m above its surroundings. Thermal manifestations, which are found over an area of nearly 400 km^2 within the Cuilapa and northern portions of the Chiquimulilla topographic sheets, appear to be linked to recent volcanic activity around Tecuamburro volcano. Major hot spring and fumarolic areas are located at Laguna Ixpaco, within a poorly-defined crater immediately north of Tecuamburro Volcano, and along the Río Los Esclavos east and northeast of the volcano; these manifestations have chemical geothermometer temperatures of 150° to 300°C.

The Tecuamburro volcanic complex has no record of historic activity, but its well-preserved edifice suggests that it is Pleistocene (e.g., Williams et al., 1964; Carr, 1984; Reynolds, 1987). Previous mapping by students from Dartmouth University (Beaty et al., 1980) identified major rock units and some of the volcanic structure of the Cuilapa Sheet. New radiometric ages obtained for this study suggest that Tecuamburro Volcano is younger than 38300 ± 1000 years and that powerful phreatic explosions about 2900 years ago formed a crater that contains Laguna Ixpaco. It thus seems likely that magma still resides within the crust beneath this area.

---

[1] * US Geological Survey, 2255 N. Gemini, Flagstaff, AZ 86001.
**Los Alamos National Laboratory, Earth and Environmental Sciences Division, Los Alamos, NM 87545.
†Centro de Estudios Geológicos de America Central, Apartado 468, Guatemala City, Guatemala.
††US Geological Survey, 345 Middlefield Road, Menlo Park, CA 94025.

The objectives of this study concern (1) the volcanic history of the Tecuamburro area, (2) the structural setting, (3) the volcanic and structural framework of the hydrothermal systems, and (4) recommendations for future exploration by completion of geothermal gradient and lithologic studies at one or more site-specific coreholes.

Field geological work was completed during July, 1988 and February-March, 1989. A 1:50,000 scale geologic map of the region has been produced (Plate 1), which defines major structural and stratigraphic elements. Over 80 rock samples collected during field mapping have been characterized by optical microscopy, scanning electron microscope (SEM), and electron probe analysis. Most of those samples were also analyzed by X-ray fluorescence. Several samples have yielded new radiometric ages by both ^{14}C and K-Ar dating methods.

B. REGIONAL GEOLOGIC SETTING

Tecuamburro Volcano is located within the west-tapering tail of the Caribbean lithospheric plate (Fig. I.1). This plate is bounded on the south by the Middle America Trench and related subduction zone, above which is a chain of active volcanoes. It is bounded on the north by the Polochic and Motagua system of left-lateral transform faults.

A system of roughly N-S-trending grabens forms a series of active tectonic structures in southern Guatemala that are readily identifiable as far east as the Honduran depression, but they appear to be buried beneath volcanic rocks in western Guatemala (Burkhart and Self, 1985).

Tecuamburro Volcano and the related Pliocene and Pleistocene volcanoes located immediately north of and adjacent to Tecuamburro are located within one of these N-S-trending grabens that we informally call the "Tecuamburro graben." The composite cone of Pueblo Nuevo Viñas, similar in size to Tecuamburro, rises to the west of this graben; the Ixhuatan volcanic shield complex is on the eastern side. The Tecuamburro graben terminates to the north against the WNW-trending Jalpatagua strike-slip fault and lies beneath Quaternary sedimentary rocks of the Pacific coastal plain in the south. Part of the graben-bounding fault system was seismically active in 1979-1980 along north-trending faults that cut across the Ixhuatan complex. First motion analysis of the earthquakes in this swarm indicates downthrow to the west along steeply west-dipping planes (White et al., 1980); the Tecuamburro graben continues to grow.

The regional setting is evident on a Space Shuttle Imaging Radar image of the region (Fig. I.2), which extends SW-NE from the Pacific shoreline to Ayarza caldera. The most apparent feature in this image is the Jalpatagua fault zone, which appears to be several kilometers wide. The Jalpatagua fault zone divides 6 km east of Cuilapa, with the main fault zone trending N70W and the subsidiary fault N55W; both continue NW until they are buried by pyroclastic deposits from the Amatitlán caldera. Apparently diverted courses of drainages suggest that the Jalpatagua fault zone is a right-lateral strike-slip fault, whereas the apparent offset of lines of cinder cones suggests left-lateral movement. The Tecuamburro

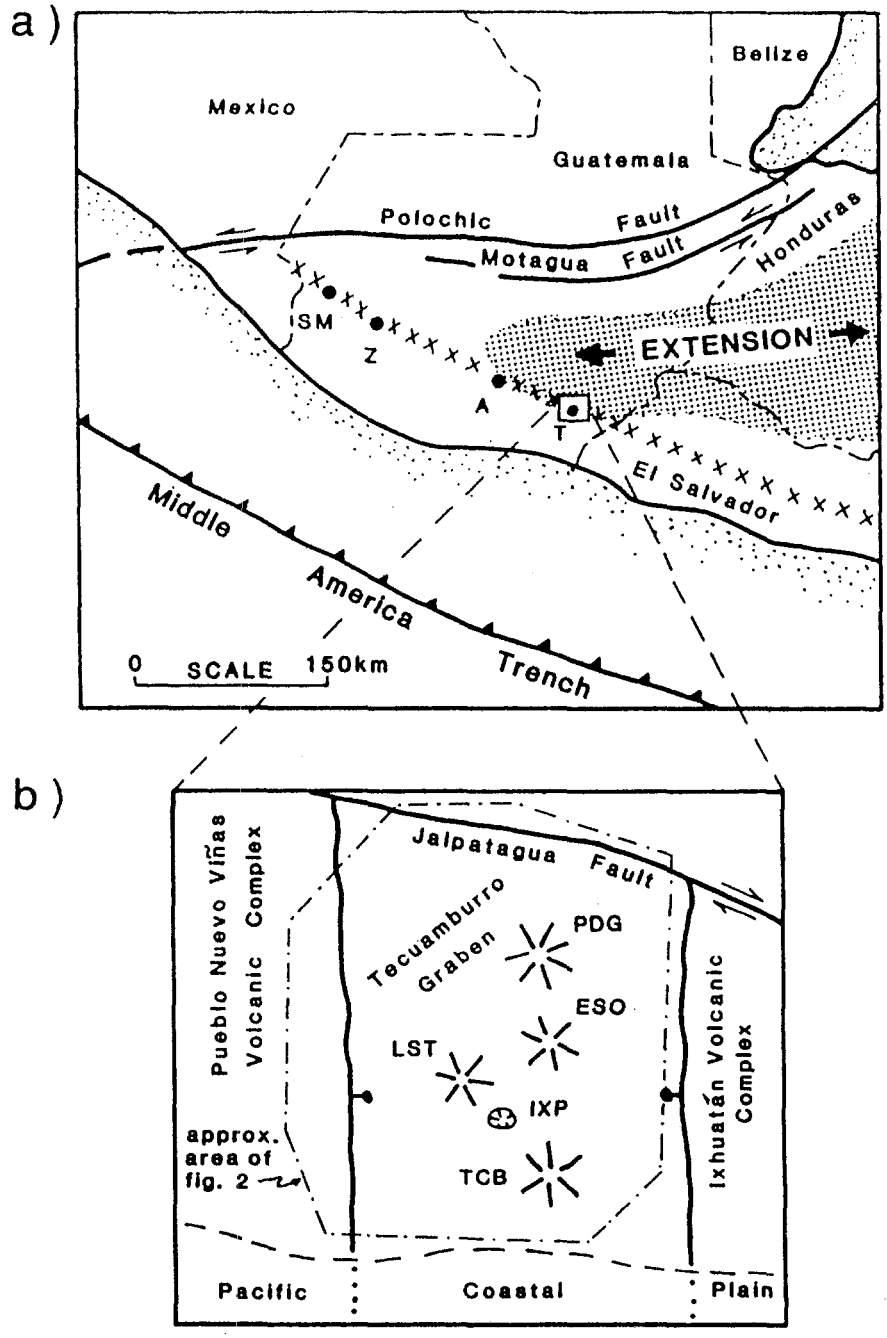

Fig. I.1. Index maps of Guatemala and the Tecuamburro Volcano area. (a) Lithospheric plate boundaries in Honduras, Guatemala, and El Salvador. The Polochic and Motagua Faults form a left-lateral transform boundary between the Caribbean and North American plates. The Middle America Trench is the surface expression of a subduction zone boundary between the Caribbean and Cocos plates. The chain of active volcanoes is generalized as xxxxxxxxx. Principal Geothermal fields of Guatemala are San Marcos (SM); Zunil (Z); Amatitlan (A); Tecuamburro (T). (b) Schematic structural map of the Tecuamburro area. The graben is about 20 km wide. Patterns of radiating lines mark principal vent areas of volcanic complexes within the graben. IXP is the Ixpaco phreatic crater and tuff ring.

Fig. I.2a. Space Shuttle Imaging Radar image of southeastern Guatamala. Most of the structural features discussed in the text are visible, including the Tecuamburro graben, the Jalpatagua fault zone, and Ixhuatan, Pueblo Nuevo Viñas, Tecuamburro, and Ayarza volcanoes. (Image was provided by Ron Blom, NASA-Jet Propulsion Laboratory, Pasadena, California)

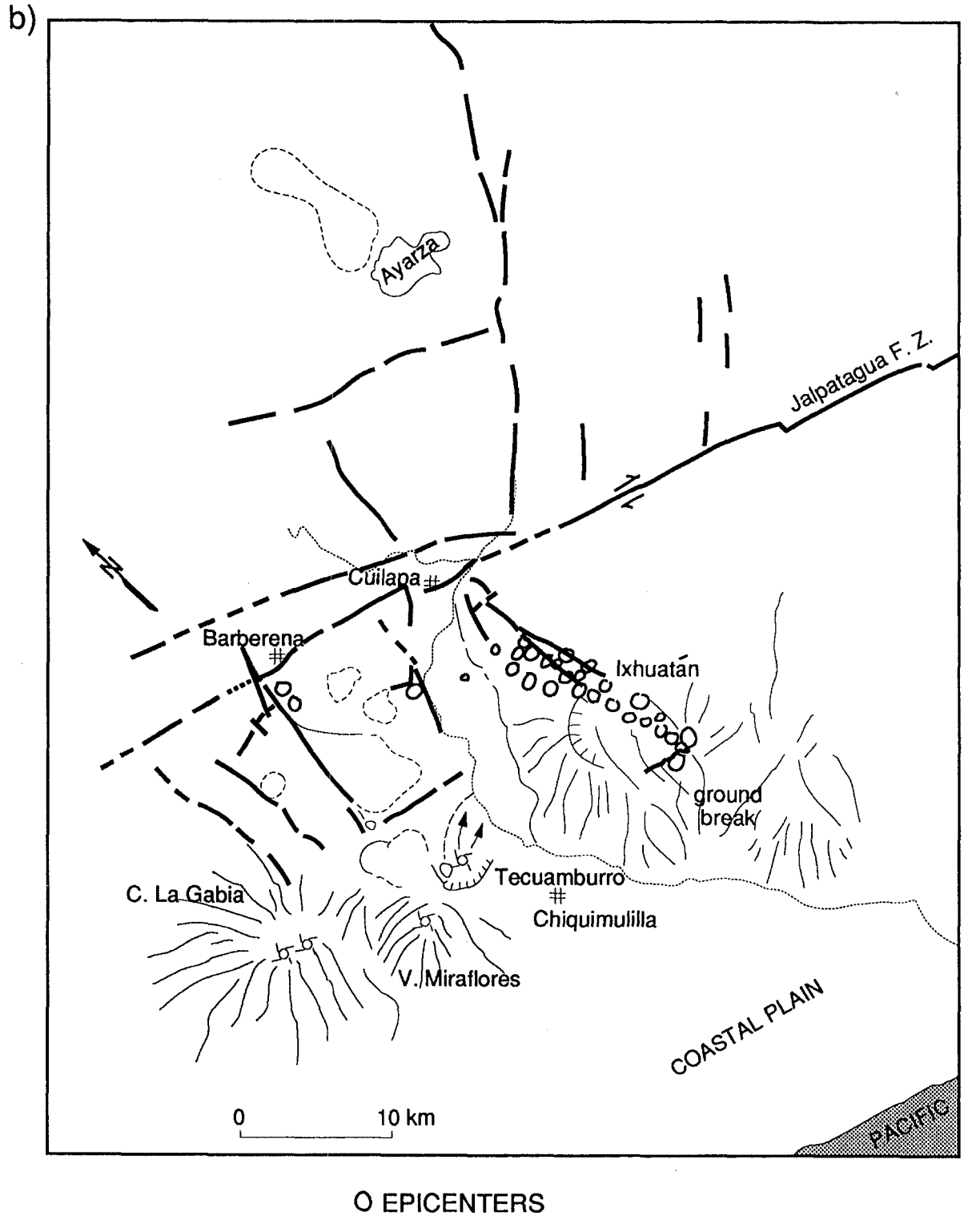

Fig. 1.2b. Sketch map of stuctural features visible on the Space Shuttle Imaging Radar image.

graben is also visible on this image (Fig. I.2a), with normal north-south faults bounding the graben and crossing the older volcanic massifs of Pueblo Nuevo Viñas (marked Cerro La Gabia on Fig. I.2b) and Ixhuatán volcanoes. Also visible on the image are the sector collapse crater of Volcán Miraflores, the Chupadero crater (containing the Laguna Ixpaco crater), and zones of hydrothermal alteration within the older composite cones north of Tecuamburro.

North of Tecuamburro Volcano, the Tecuamburro graben contains several older volcanoes that range in age from >1.8 Ma to 0.8 Ma, including Piedra Grande, El Sordo, and Los Sitios. These volcanoes contain large areas of hydrothermal alteration, arcuate crater rims and collapse features, and a large crater or caldera informally named "Chupadero" crater. These volcanoes are crossed by N- and NW-trending normal and reverse (thrust) faults. Many of these NW-trending faults, especially the reverse faults, may be second-order structures related to the strike-slip regime of the Jalpatagua fault.

C. STRATIGRAPHY AND PETROLOGY

The stratigraphic succession, as indicated by field relations, is summarized in Fig. I.3. Some age assignments are equivocal, and adjacent vent areas likely had overlapping periods of activity. Broadly speaking, however, andesitic and dacitic volcanoes are progressively younger to the south. Volcanoes flanking the Tecuamburro graben are interpreted to predate most, if not all, of the volcanic rocks erupted within the graben.

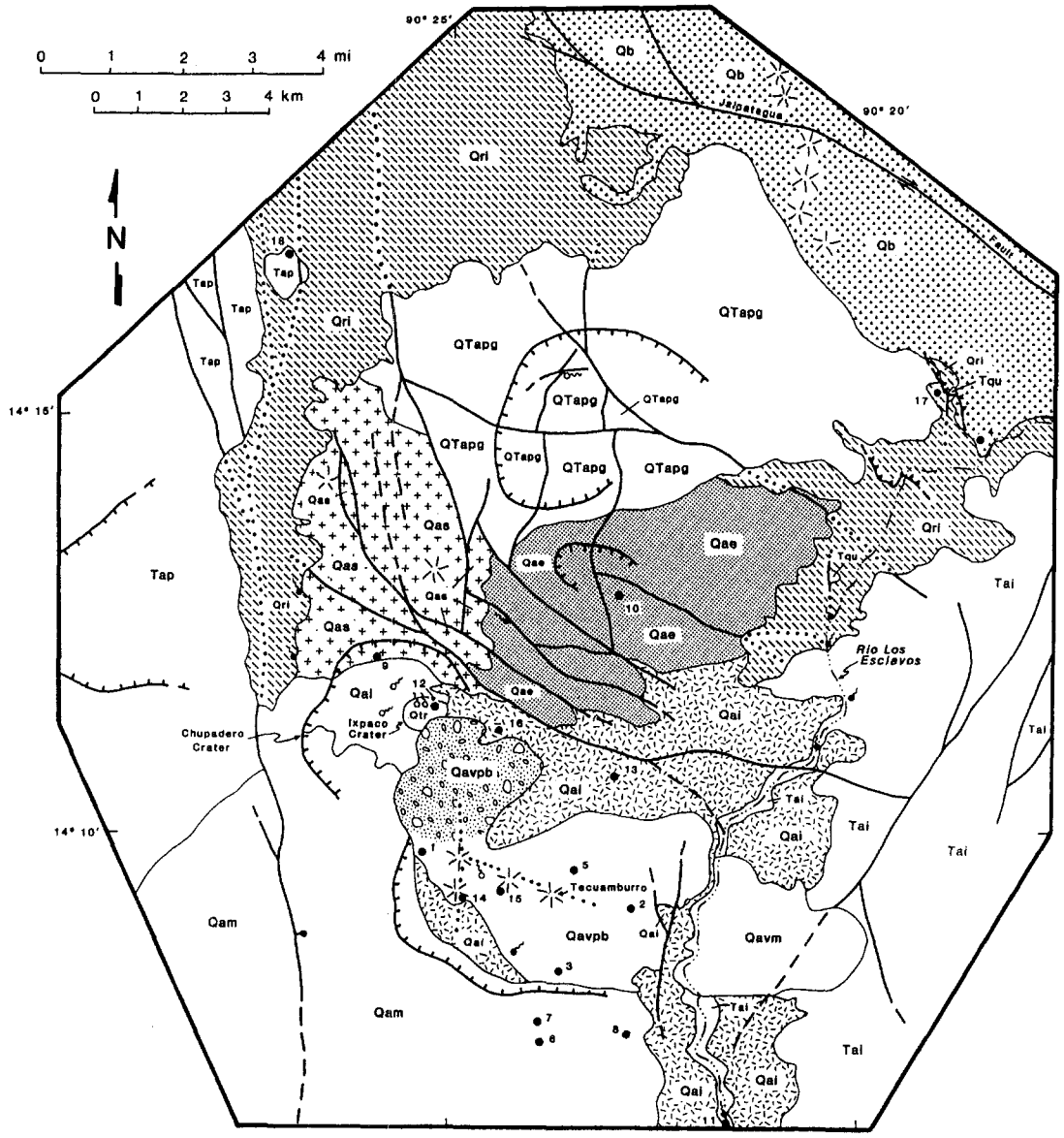

Fig. I.3a. Geologic map of Tecuamburro Volcano and adjacent areas. Compiled by Wendell A. Duffield; mapping by Duffield, G. Heiken, K. Wohletz, L. Maassen, G. Dengo, and O. Pinzon. Supplementary information came from the Geologic Map of Guatemala, Cuilapa Sheet (1980).

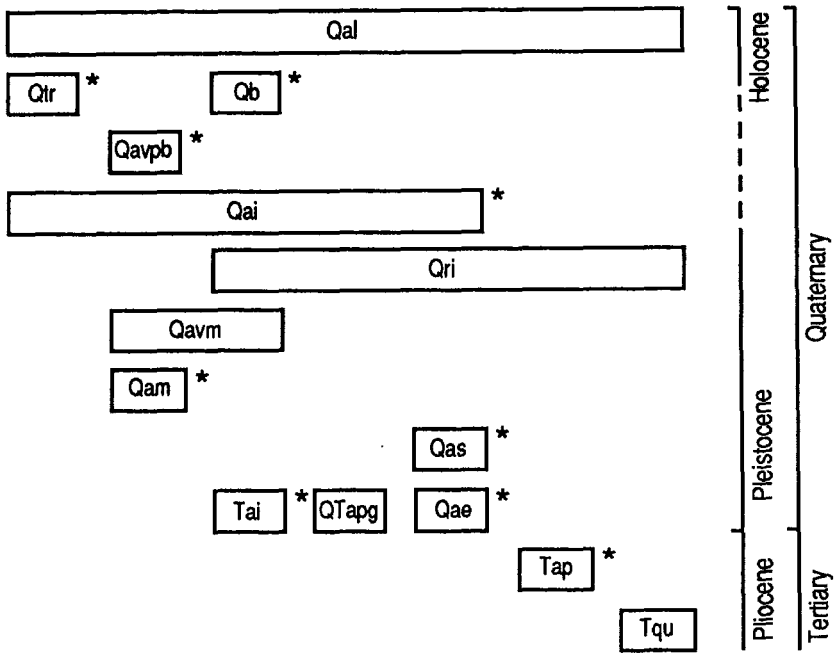

Fig. 1.3b. Legend for the geologic map presented in Fig. 1.3a.

Radiometric ages are generally consistent with field-defined stratigraphy (Table I.1 and Fig. I.4). The four oldest ages (2.6 ± 0.3 Ma, 1.16 ± 0.048 Ma, 1.18 ± 0.080 Ma, and 0.8 ± 0.080 Ma) were determined for rocks from the flanking Pueblo Nueva Viñas and Ixhuatán volcanic complexes, and the northern part of the Tecuamburro graben. In the southern part of the graben, the stratovolcano that is ancestral to Tecuamburro (Miraflores) is about 0.1 Ma. This volcano was modified by a large sector collapse that formed the hummocky terrain across the Río Los Esclavos, east of the Miraflores-Tecuamburro complex. At some time after this sector collapse, two-pyroxene andesitic pumice deposits were erupted; the location of a vent for this eruption is not known, although the distribution of the pumice fallout (stippled pattern on the geologic map) suggests a vent at Chupadero Crater or beneath Tecuamburro. The subsequently erupted Tecuamburro rocks are too young to yield accurate K-Ar ages, but their calculated ages and associated uncertainties (Table I.1) are consistent with the <38.3 ka ^{14}C age determined from a log in the pyroxene pumice deposits.

TABLE I.1. RADIOMETRIC AGES FOR SAMPLES FROM THE TECUAMBURRO VOLCANO AREA. (See Plate 1 for sample locations.)

K-Ar[a]

Sample	Map Unit	K_2O (%)	^{40}Ar (mol/gm)	^{40}Ar (% Rad.)	Age (Ma)
1	Qat	1.085	3.0663×10^{-13}	0.16	0.019 ± 0.056
2	Qat	0.528	7.5074×10^{-14}	0.50	0.096 ± 0.105
3	Qat	0.576	-4.8337×10^{-14}	-0.3[b]	-0.056 ± 0.098
4	Qb	0.765	4.0044×10^{-14}	0.29	0.036 ± 0.064
5	Qat	0.671	-1.0465×10^{-13}	-0.9[b]	-0.108 ± 0.130
6	Qam	0.769	1.1921×10^{-13}	6.85	0.108 ± 0.045
7	Qam	0.910	1.2675×10^{-13}	0.14	0.094 ± 0.263
8	Qam	0.936	1.8283×10^{-13}	5.39	0.131 ± 0.039
9	Qas	1.300	1.4977×10^{-12}	5.13	0.800 ± 0.061
10	Qal	0.748	1.2758×10^{-12}	7.32	1.180 ± 0.080
11	Tai	1.257	2.1009×10^{-12}	10.60	1.160 ± 0.050
18	Tap				2.6 ± 0.3[c]

^{14}C

Sample	Map Unit	Material Dated	Age (years)
12	Qtr	Sediment	2,910 ± 70
13	Qai	Wood	38,300 ± 1,000

[a] All K-Ar ages are on whole-rock samples of lava flows.

[b] The negative ^{40}Ar and age are artifacts of the method of calculating radiogenic ^{40}Ar. The experiment shows that the sample contains too little radiogenic ^{40}Ar to be detectable, presumably an indication of a very young age.

[c] Reported by Reynolds (1987).

Note: The K-Ar age determination of sample 5 was carried out at the laboratory of the Institute of Human Origins, Berkeley, California. All others were done at the USGS, Menlo Park, California. The ^{14}C age determinations were carried out by S. Robinson and D. Trimble in the USGS laboratories at Menlo Park. Samples were crushed, sieved to 60-100 mesh, washed in water, treated for 30 minutes in 14% HNO_3 and then for 2 minutes in 5% HF. This procedure removes extraneous argon from whole-rock samples. Samples were also boiled in water for 12 hours before loading them into an ultrahigh-vacuum fusion-extraction system for collection of argon. This procedure inhibits adsorption of atmospheric ^{40}Ar, hence it increases the proportion of radiogenic ^{40}Ar recovered from a sample. Potassium was analyzed by a lithium metaborate flux fusion-flame photometry technique, with the lithium serving as an internal standard (Ingamells, 1970). Argon was analyzed by isotope dilution, using a five-collector system for simultaneous measurement of argon ratios in a static mass spectrometer (Stacey et al., 1978) at the USGS and by a 10-cm Reynolds-type gas-source spectrometer at Berkeley. The ± values represent analytical uncertainty at one standard deviation, as determined by experience with replicate analyses. Radioactive-decay constants and abundance of ^{40}Ar are from Steiger and Jager (1977).

A conservative interpretation suggests that all of the ≤0.1 Ma rocks within the southern part of the graben were erupted from closely spaced vents, which also implies an equally long-lived residence of crustal magma bodies beneath the area.

Monogenetic basaltic vents and associated lavas along the Jalpatagua fault zone at the northern margin of the map (Fig. I.3) are inferred to represent the youngest magmatic eruptions in the study area. These olivine-phyric basalts and basaltic andesites are the most primitive rocks of those analyzed (see Table I.3).

With the exception of local, small-volume deposits of alluvium and minor lacustrine beds, most of the Tecuamburro area is underlain by two-pyroxene andesitic lavas. Complexly twinned and zoned plagioclase is a nearly ubiquitous phenocryst; hornblende and olivine are minor constituents of some of the rocks. Andesites range from sparsely to moderately porphyritic and occur as lava domes and flows, laharic breccias, and ignimbrites, fallout, and surge pyroclastic deposits. SiO_2 contents of all rocks range from 48 to 64% (Table I.2) and all analyzed rocks comprise a weakly calc-alkaline suite.

Silicic rocks are restricted to rhyodacitic ignimbrites that partly fill valleys along the east and west sides of the Tecuamburro graben (Fig. I.3, Qri) and to inliers of similarly silicic quartz-phyric rocks that are interpreted as Tertiary "basement" (Fig. I.3, Tqu). These latter rocks are exposed only in two small upfaulted blocks, and their subsurface extent is unknown. The ignimbrites contain phenocrysts of sanidine, plagioclase, biotite, and hornblende; these rocks are similar in age, petrographic characteristics, and chemical composition to part of the outflow sheets erupted from Amatitlàn caldera, which is located 50 km to the northwest (Fig. I.5). This correlation is also suggested by the fact that the ignimbrites in the northwestern part of the map area can be traced almost continuously back to Amatitlán caldera. Those Qri ignimbrites exposed along the Río Los Esclavos, in the eastern part of our map area, are interpreted to have flowed over an intervening drainage divide during emplacement, or possibly along a valley now buried by the basaltic lavas that post-date them. The only other nearby caldera young enough to be a potential source for the ignimbrites is Ayarza, located ~50 km northeast of Tecuamburro Volcano; however, the Ayarza outflow sheet is considerably more silicic than that from Amatitlán and the older ignimbrites within the map area (Fig. I.5).

TABLE 1.2. Whole-rock chemical analyses of rocks from the Tecuamburro area. Map Unit designations are referred to in the text and Plate 1.

0 Map Unit	1 sample #	2 SiO2	3 TiO2	4 Al2O3	5 Fe2O3	6 MnO	7 MgO	8 CaO	9 K2O	10 Na2O	11 P2O5	12 Total
1 Qb	LM-4	48.37	1.30	17.27	9.97	0.16	6.92	9.39	0.81	3.63	0.29	98.11
2 Qb	LM-4	49.64	1.32	18.11	10.12	0.16	7.00	9.53	0.78	3.05	0.30	100.02
3 Qat	7-9-88-6a	52.01	0.89	19.20	10.16	0.18	4.49	8.23	0.44	2.82	0.14	98.57
4 Qat	7-9-88-6A	52.16	0.90	19.02	10.10	0.17	4.38	8.29	0.45	2.94	0.14	98.55
5 Qat	7-9-88-2	52.32	0.76	18.00	8.60	0.16	5.00	8.88	0.56	3.42	0.15	97.84
6 Qat	7-9-88-6b	52.81	0.83	20.65	9.38	0.17	2.93	5.90	0.44	3.24	0.11	96.47
7 Qat	7-9-88-6b	52.82	0.84	20.60	9.46	0.17	2.88	5.89	0.44	2.95	0.11	96.16
8 Qat	7-9-88-3	52.83	0.78	18.83	8.63	0.15	4.94	8.93	0.56	3.46	0.15	99.25
9 Qat	7-9-88-2	52.97	0.79	18.23	8.79	0.16	5.09	8.86	0.55	3.18	0.16	98.78
10 Tai	GH-3-1-89-2	53.11	0.87	19.03	9.28	0.17	3.94	8.24	0.85	3.11	0.21	95.68
11 Qat	7-9-88-3	53.21	0.78	18.86	8.58	0.15	4.93	8.99	0.56	3.42	0.16	99.63
12 Tai	GH-3-1-89-2	53.41	0.86	19.17	9.23	0.16	4.11	8.13	0.87	3.22	0.21	99.41
13 Tai	GH-3-1-89-3	53.71	0.91	25.00	8.52	0.13	0.42	1.25	0.61	1.10	0.04	92.52
14 Tai	GH-3-1-89-2	53.77	0.87	18.98	9.19	0.16	3.98	8.10	0.88	3.27	0.21	99.41
15 Tai	GH-3-1-89-3	54.01	0.92	25.34	8.57	0.13	0.46	1.25	0.61	1.20	0.03	99.01
16 Qtr	GH2-25-89-3D	54.26	0.82	26.18	7.29	0.05	1.39	0.43	0.36	0.91	0.06	91.60
17 Qtr	GH2-25-89-3D	54.30	0.82	26.22	7.35	0.05	1.42	0.44	0.35	0.59	0.07	91.61
18 Qb	LM-3	55.00	1.07	16.96	8.61	0.13	3.72	8.82	0.74	2.94	0.24	98.22
19 Qb	LM-3	55.18	1.07	16.92	8.61	0.13	3.74	8.79	0.72	2.83	0.24	98.23
20 Qtr	GH2-25-89-3C	55.50	0.73	16.97	15.94	0.03	1.84	0.22	0.32	0.39	0.24	91.77
21 Qas	GH-2-24-89-5	55.56	0.77	23.55	8.71	0.16	1.00	0.43	0.40	0.68	0.06	91.58
22 Qas	GH-2-24-89-5	55.61	0.76	23.69	8.70	0.16	1.03	0.45	0.41	0.70	0.06	98.63
23 Qai	GH-2-24-89-4	55.74	0.80	18.45	8.27	0.17	3.22	7.42	0.72	3.63	0.20	99.08
24 Qtr	GH2-25-89-3C	55.92	0.75	16.91	16.05	0.03	1.81	0.23	0.32	0.46	0.25	92.19
25 Qai	GH-2-24-89-4	56.00	0.80	18.48	8.29	0.17	3.28	7.47	0.73	3.66	0.20	99.08
26 Qasf	7-8-88-3	56.06	0.74	19.59	8.25	0.16	3.29	4.83	0.67	3.12	0.09	96.81
27 Qas	GH-2-24-89-5	56.07	0.86	22.94	9.05	0.14	1.39	1.39	0.79	1.69	0.04	94.36
28 Qas	GH-2-24-89-5	56.20	0.85	22.88	8.92	0.14	1.37	1.36	0.79	1.63	0.05	94.35
29 Qasf	7-8-88-3	56.27	0.76	19.71	8.33	0.17	3.39	4.85	0.63	3.05	0.09	97.25
30 Qam	7-11-88-1	56.45	0.73	18.21	8.46	0.18	3.35	7.79	0.85	3.71	0.19	99.91
31 Qam	7-11-88-1	56.67	0.73	18.31	8.39	0.18	3.33	7.83	0.86	3.68	0.19	100.17
32 Qas	LM-7	57.07	0.71	18.07	7.94	0.14	3.17	7.58	1.26	3.23	0.12	99.29
33 Tai	LM-1	57.20	0.59	18.56	8.11	0.18	2.51	6.82	1.27	4.60	0.30	87.02
34 Tai	GH-3-1-89-1	57.46	0.72	19.67	5.90	0.13	1.58	7.03	1.87	3.48	0.27	99.39
35 Qai	GH-2-22-89-4	57.65	0.65	18.98	7.32	0.14	2.81	5.05	0.96	3.00	0.10	96.84
36 Tai	GH-3-1-89-1	57.76	0.72	19.72	5.95	0.13	1.60	6.95	1.87	3.57	0.27	98.11
37 Qai	GH-2-22-89-4	57.87	0.64	19.12	7.30	0.14	2.79	5.10	0.96	2.82	0.10	99.05
38 Qas	LM-7	58.55	0.72	18.49	8.16	0.15	3.34	7.74	1.29	3.47	0.12	102.02
39 Tai	GH-3-1-89-4	58.60	0.71	19.82	5.93	0.09	1.31	6.53	1.84	3.88	0.30	99.14
40 Tai	GH-3-1-89-4	58.66	0.71	19.81	5.88	0.09	1.29	6.58	1.84	3.97	0.30	99.13
41 Qtr	GH2-25-89-3B	58.88	0.85	17.37	12.22	0.02	1.51	0.23	0.28	0.40	0.10	92.33
42 Qtr	GH2-25-89-3B	59.17	0.84	17.53	12.27	0.02	1.50	0.24	0.28	0.39	0.10	92.34
43 Qai	GH-2-24-89-2	59.42	0.67	18.69	7.54	0.13	3.29	5.82	0.72	3.19	0.13	94.18
44 Qai	GH-2-24-89-2	59.58	0.68	18.51	7.50	0.13	3.30	5.81	0.73	2.88	0.13	99.62
45 Qap	GH-2-22-89-6	59.80	0.58	18.36	6.80	0.14	3.18	5.25	1.01	3.37	0.10	98.59
46 Qap	GH-2-22-89-6	59.95	0.59	18.49	6.85	0.14	3.24	5.27	1.03	3.40	0.10	98.59
47 Qat	7-8-88-4	60.07	0.64	17.30	6.89	0.14	2.81	6.19	1.22	3.71	0.13	99.10
48 Qai	7-9-88-12	60.26	0.58	17.11	6.40	0.14	2.46	5.50	1.23	3.06	0.06	96.80
49 Qai	GH-2-25-89-4	60.44	0.57	17.10	6.21	0.12	2.70	5.74	1.19	3.19	0.12	98.59
50 Qat	7-8-88-4	60.54	0.66	17.24	6.92	0.14	2.80	6.23	1.25	4.12	0.13	100.02
51 Qai	7-9-88-12	60.78	0.58	17.11	6.48	0.14	2.47	5.47	1.21	3.23	0.06	97.53
52 Qai	GH-2-25-89-4	60.78	0.57	16.95	6.26	0.13	2.67	5.74	1.21	3.00	0.12	97.39
53 Qap	GH-2-22-89-5	61.22	0.60	17.79	6.28	0.13	2.84	5.27	1.15	3.36	0.11	99.14
54 Qap	GH-2-22-89-5	61.51	0.63	17.64	6.42	0.13	2.85	5.30	1.15	3.41	0.10	99.14

TECUAMBURRO CHEMICAL ANALYSES

0 Map Unit	1 sample #	2 SiO2	3 TiO2	4 Al2O3	5 Fe2O3	6 MnO	7 MgO	8 CaO	9 K2O	10 Na2O	11 P2O5	12 Total
55 Qdpb	7-8-88-1	62.34	0.56	16.75	6.06	0.13	2.47	5.77	1.36	3.56	0.10	99.12
56 Qdpb	7-8-88-1	62.49	0.55	16.67	6.08	0.13	2.48	5.75	1.32	3.42	0.11	98.99
57 Qtr	GH2-25-89-3A	63.20	0.91	22.30	3.34	0.04	2.31	0.18	0.44	0.33	0.07	91.86
58 Qtr	GH2-25-89-3A	63.24	0.90	22.29	3.33	0.04	2.33	0.17	0.44	0.30	0.07	93.11
59 Qtapg	KW7-88-5	63.42	0.67	17.75	6.96	0.11	0.69	1.84	2.36	1.84	0.04	98.81
60 Qtapg	GH-2-25-89-7	63.45	0.51	16.65	5.38	0.11	1.68	4.37	2.24	3.10	0.11	98.19
61 Qtapg	GH-2-25-89-7	64.07	0.51	16.52	5.40	0.11	1.69	4.39	2.27	3.13	0.10	98.19
62 Qri	7-9-88-16	66.14	0.50	15.19	3.62	0.10	0.90	2.82	3.50	3.69	0.09	96.55
63 Qri	7-9-88-16	66.52	0.48	15.42	3.61	0.10	0.93	2.81	3.53	3.70	0.09	97.20
64 n.a.	GH-2-22-89-1	75.89	0.12	13.13	0.77	0.05	0.09	0.46	4.24	3.51	0.03	98.44
65 n.a.	GH-2-22-89-1	76.04	0.12	12.99	0.78	0.05	0.10	0.47	4.27	3.59	0.03	98.74

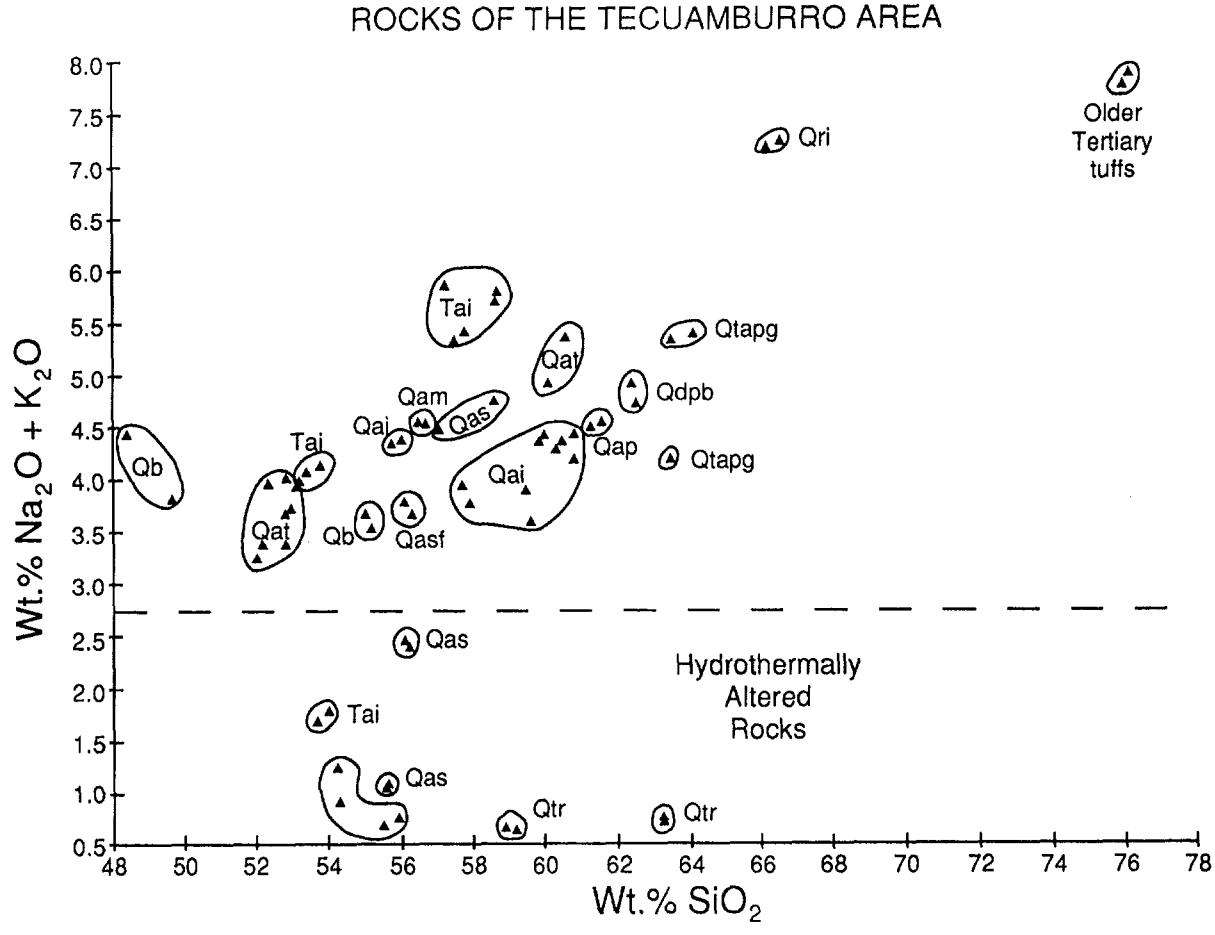

Fig. I.4. Plot of SiO_2 vs $Na_2O + K_2O$ for samples collected from the Tecuamburro Area.

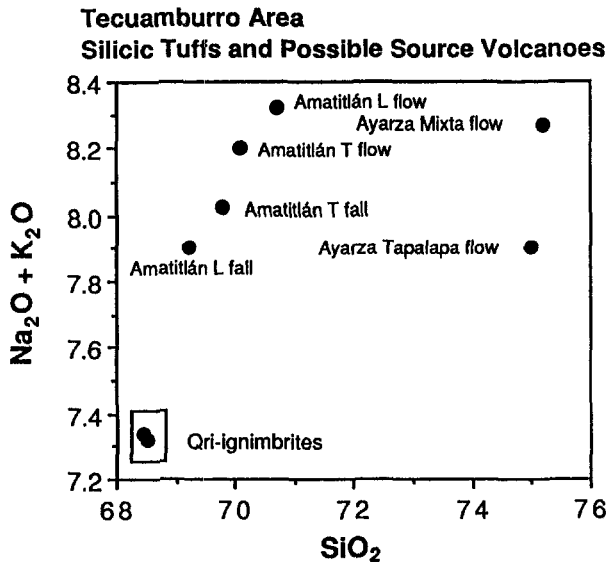

Unit	SiO_2	TiO_2	Al_2O_3	FeO	MgO	CaO	K_2O	Na_2O	P_2O_5	Total
(Qri) Valley Ignimbrite-East	68.50	0.52	15.73	3.75	0.93	2.92	3.50	3.82	0.09	100
(Qri) Valley Ignimbrite-East	68.44	0.49	15.86	3.71	0.93	2.89	3.53	3.81	0.09	100
Amatitlán T Flow	70.10	0.39	14.70	2.40	0.51	1.50	4.20	4.00	0.06	100
Amatitlán T Fall	69.80	0.38	14.70	2.35	0.51	1.50	4.00	4.02	0.06	100
Amatitlán T Flow	70.70	0.52	15.60	0.66	0.66	1.80	4.15	4.17	0.07	100
Amatitlán T Fall	69.20	0.49	15.80	3.20	0.80	2.10	3.80	4.10	0.07	100
Ayarza Mixta Flow	75.20	0.14	14.10	1.30	0.20	0.70	4.37	3.90	0.05	99.96
Ayarza Tapalapa Flow	75.00	0.13	14.70	1.32	0.10	0.82	3.70	4.20	0.03	100.00

Fig. 1.5. a. SiO_2 vs. $Na_2O + K_2O$ plot for silicic tuffs of the Tecuamburro area (Qri-valley ignimbrite) and a comparison with ignimbrites from Amatitlán caldera (Wunderman and Rose, 1984), and Ayarza calderas (Peterson and Rose, 1985). b. Tabulated XRF analyses for the tuffs shown in a.

Two nested craters are located near the northwest base of the Tecuamburro (Fig. I.3). The larger crater, informally called Chupadero, is older and more poorly defined. It is in rocks with ages of 0.8 and 0.1 Ma (Fig. I.3 Qas and Qam) and in turn contains some of the 38.3 Ka pyroclastic deposits of map unit Qai and part of the Tecuamburro dome complex. Chupadero crater may be the vent of the Qai, whose pumice falls and ignimbrites once blanketed adjacent hills and filled the lower part of the Cañon de Río Los Esclavos.

The younger crater, Laguna Ixpaco, has yielded a ^{14}C age of 2.91 ± 0.07 ka on an organic-rich zone with the tuff ring around the crater. A debris avalanche from the nearest of the closest Tecuamburro dome has buried the southeastern edge of the Ixpaco tuff ring. Thus dome growth may have been as recent as <2.91 ka, although an event unrelated to and younger than dome growth >2.91 and <38.3 Ka could have triggered the avalanche.

Rock Unit Descriptions

Pliocene

Undifferentiated Quartz-Bearing Lavas (Tqu)

Two small outcrops of quartz-bearing altered volcanic rocks occur along Highway 16 between Los Esclavos and Finca La Concepción. These outcrops are partly bounded by both normal and reverse faults and are partly overlain by basalt flows and ignimbrite (Fig. I.3, units Qri and Qb). Age relations with other rocks in the project area are unknown, but we infer that these upfaulted rocks are part of the Tertiary basement and may be correlative with the Miocene Padre Miguel Group (Williams and McBirney, 1969).

The mineralogy of these "basement" rocks and their pervasive hydrothermal alteration and silicification is distinct from younger andesitic rocks of the area. Rock types identified include felsic porphyries and an altered rhyolitic welded tuff. One of these coarse-grained porphyries crops out in a road cut (UTM 789.6, 1577.3) and superficially resembles a granite, consisting of euhedral, rounded quartz phenocrysts (~10%) up to 2 mm long in a strongly altered groundmass. Euhedral plagioclase and K-feldspar phenocrysts (~25%) are up to 2 mm long and are completely altered to clays; only a relict texture remains. Hornblende and biotite make up less than 5% of this rock.

Underlying the coarse-grained porphyry is an altered rhyolitic welded tuff, which in turn overlies another felsic porphyry. Because of the hydrothermal alteration, these rocks resemble andesitic lavas in the field. The welded tuff contains nearly 15% rounded and embayed quartz phenocrysts (up to 3 mm long), lesser amounts of broken and altered feldspar phenocrysts, and a few percent hornblende. A devitrified, fine-grained groundmass shows relict, compacted shard textures.

Mineralogy typical of silicic rocks and strong alteration suggest that these rocks may be one of the widespread Tertiary-age silicic lava and tuff sequences commonly found behind the active volcanic arc in Guatemala (Carr, 1984). These rocks may be representative of the Tertiary basement underlying the younger andesitic rocks of the stratovolcanoes north of Tecuamburro, and we infer this relationship in cross sections.

Andesitic Volcanoes of Pueblo Nuevo Viñas (Tap and Tapbr)

The village of Pueblo Nuevo Viñas is on an avalanche breccia from a composite cone similar in size to Tecuamburro, which is centered several kilometers soouthwest of the town. All of the volcanic rocks west of the Tecuamburro Graben have been grouped together as the andesites of Pueblo Nuevo Viñas composite cone. Although an age of 2.6 ± 0.3 Ma is recorded for a lava from the northern end of this complex (Reynolds, 1987), most of the lavas from this cone appear to be stratigraphically higher; they are from a cone as well-preserved as Miraflores volcano. It thus seems likely that these andesites are Plio-Pleistocene.

The Pueblo Nuevo Viñas composite cone is over 10 km wide at its base and reaches elevations of over 1800 m. The summit area has been

modified by sector collapse that left an amphitheater open to the northeast. Within the amphitheater collapse and avalanche breccias, laharic breccias, and lava boulders several meters in diameter (Tapbr) form an irregular hummocky terrain that extends to the northeast, where they are buried by the younger hornblende-biotite rhyodacite (Qri).

Lavas of the Pueblo Nuevo Viñas composite cone are of two main types: (1) older oxyhornblende-bearing andesites and dacites and younger two-pyroxene andesites. Both are porphyritic and contain over 20% plagioclase phenocrysts.

Although the age relationships are equivocal, we suggest the following stratigraphy for the Pueblo Nuevo Viñas volcano: (1) lavas make up most of the older cone, exposed at the base of the amphitheater and in basal outflow units on the western flanks; and (2) two-pyroxene lavas form the upper cone flanks, including a dike near the summit. One of the older lavas sampled at the base of the amphitheater is dacitic and contains 10% quartz, 20% oligoclase, 5% oxyhornblende, and 1% hypersthene phenocrysts. The dike rock from the summit is a dark black, fine-grained, two-pyroxene basaltic andesite. Magma compositions apparently became more mafic with time in the Pueblo Nuevo Viñas complex. The complex may consist of two overlapping eruptive centers or may have been formed by eruptions of both basaltic andesite and andesite and dacite.

Pliocene-Pleistocene

Andesitic Volcanoes of Ixhuatán (Tai)

The volcanic complex of Ixhuatán is named after the town of Santa Maria Ixhuatán, located near the summit. The Ixhuatán complex forms a shield 20 x 12.5 km with a maximum elevation of 1718 m, which is cut by faults on the eastern side of the Tecuamburro graben. The northern end of Ixhuatán is bounded by the Jalpatagua fault zone and the southern end slopes onto the coastal plain. The name "Ixhuatan" was assigned to this volcanic complex by Beaty et al. (1980). The one K-Ar date for an Ixhuatán lava is 1.16 ± 0.050 Ma. The age of this complex is reflected also in a deep (~4 m) weathering profile over much of the summit. Much of the topography appears to be controlled by faults, with very few of the original volcanic landforms still in place.

The lowest slopes of Ixhuatán, exposed along the Río Los Esclavos, below Sinacantán, consist of massive gray porphyritic andesite (Table I.2 and Appendix B). The rock contains 37% phenocrysts in a trachytic groundmass; these include zoned plagioclase, pigeonite and Fe-Ti oxides. Upstream, roughly east of Tecuamburro, laharic breccias and some silicic pyroclastic rocks are interbedded with the lavas.

Exposures along the summit regions of the Ixhuatán complex consist of mostly rubbly or platy lava flow tops, scoria cones, and vulcanian breccias. The porphyritic lavas and scoria have andesitic and basaltic andesitic compositions (Table I.2). The lavas and scoria are

petrographically unique within this region; they are characterized by abundant (35 to 50%) phenocrysts of plagioclase and minor orthopyroxene and Fe-Ti oxide. The zoned plagioclase phenocrysts have distinctive hopper shapes not seen anywhere else in the mapped area.

A weathered lithic tuff, with relict phenocrysts of plagioclase, hornblende, and biotite, is exposed intermittently across the Llano Grande, along the northern end of the Ixhuatán complex. It is petrographically similar to the hornblende-biotite ignimbrites of the valley of Río Los Esclavos, but it is much more deeply weathered than those deposits.

Pyroxene Andesite Volcanic Complex of Piedra Grande (QTapg)

The Piedra Grande volcanic complex occupies approximately the northern third of the Tecuamburro graben. Lavas, laharic breccias, and welded tuffs make up this eroded composite cone (cross section F-F') that we infer to overlie felsic lavas and tuffs of Tqu. The cone, eroded and faulted, is about 7 km wide at the base and reaches elevations of 1600 m at Cerro la Torre. The cone is flanked and overlain by younger andesites of Los Sitios (Qas) to the west, Quaternary basalts to the northeast, Quaternary hornblende-biotite ignimbrite (Qri) to the north and northwest, and basalts of El Sordo (Qae) to the south; this suggests that the volcano is older than about 1.2 Ma (K-Ar age for the stratigraphically younger El Sordo Volcano).

Lavas from Cerro la Torre and a welded tuff from Finca Los Suquinayes are dacitic (SiO_2=63-64%). The welded tuff consists of 14% plagioclase (<3 mm), 7% oxidized hornblende (<3 mm), 4% sanidine (0.4 mm), 2% Fe-Ti oxides, and a trace of orthopyroxene. The lavas are also porphyritic. Laharic breccias in outflow units to the north and east contain boulders of two-pyroxene andesite and dacite.

Much of the upper part of the cone of Piedra Grande volcano is hydrothermally altered and fresh samples could not be found. The alteration is most extensive near Finca Las Delicias and to the west and northwest of the finca. Alteration products include opal CT, tridymite, cristobalite, smectite, and pyrite. The alteration may be associated with a collapse event that produced the distinctive, semicircular volcanic landform. Activity at Fumarole Infiernitos (TM-32 in chapter III) may represent late stage vestiges of a larger, earlier hydrothermal alteration event.

Pyroxene Andesite Volcanic Complex of El Sordo (Qae)

El Sordo is an eroded and faulted composite cone located in the central part of the mapped area. The lavas of El Sordo are basaltic (50-53 Wt.% SiO_2) and overlie and interfinger with the southern flanks of the Piedra Grande volcano; they are overlain by lavas and scoria of Los Sitios (Qas) volcanoes to the west and valley-filling ignimbrites (Qri) to the east. A lava sampled about 1.5 km southeast of the El Sordo summit yielded a K-Ar date of 1.18 Ma.

The lavas are mostly two-pyroxene basalts; blocky, euhedral phenocrysts include 25-35% plagioclase (<3 mm long), 2-8%

hypersthene (<1 mm), and 1% pigeonite (<1.5 mm). The hyalopilitic groundmass shows patchy devitrification and sometimes trachytic alignment of clinopyroxene and plagioclase microlites. One sample contains up to 2.5% olivine. A sample from near the El Sordo summit contains 4% hornblende, completely replaced by Fe-Ti oxides. All of these lavas contain glomeroporphyritic clots of hypersthene and plagioclase. Laharic breccias mostly cover the outer flanks of El Sordo . Near Finca La Concepción laharic breccias partly bury a basaltic scoria cone.

Pleistocene

Pyroxene Andesite Lavas and Scoria Cones of Los Sitios (Qas)

Los Sitios andesites (57-58 Wt.% SiO_2) crop out north of Chupadero crater, along the western flanks of El Sordo and Piedra Grande volcanoes. A sample from the northern rim of Chupadero crater yielded a K-Ar date of 0.8 Ma. Two major vents are the scoria and lava cone of Cerro San Luis El Volcancito and the lava cone west of Finca Miramar. These rocks may overlie lavas and laharic breccias of Piedra Grande (QTapg) and Pueblo Nuevo Viñas (cross-section G-G') in the north-trending valley along the west side of the larger Tecuamburro graben.

The rocks are mostly two-pyroxene andesitic lavas with a pilotaxitic groundmass of plagioclase laths. Phenocrysts include 25% plagioclase (<2 mm), 1-2% clinopyroxene (<0.5 mm), 1% Fe-Ti oxides, and a trace of olivine with reaction rims. They also contain traces of pyroxene-plagioclase glomeroporphyritic clots. Where faults cut these lavas, they are silicified and altered to clays.

Pyroxene Andesite Stratovolcano Complex of Miraflores (Qam)

The base upon which the younger Tecuamburro and associated domes (Fig. I.3, map unit Qavpb) are constructed is the Miraflores stratovolcano. It has an approximately14 km diameter base. The highest elevation is 945 m; at one time it was higher but the cone was truncated by sector collapse. Exposures along the southern slopes are poor, but generally there are massive andesitic lavas above and laharic breccias below elevations of between 700 and 800 m (there is a distinct break in slope around the southern flanks of the volcano at this level). There are also intermittent exposures of lavas in the crescent-shaped, east-facing scarp that wraps around the bowl in which the Tecuamburro domes grew.

Miraflores lavas sampled are porphyritic andesites (Table I.2 and Appendix B). The rocks contain 45 to 50% phenocrysts of mostly zoned plagioclase, with lesser hypersthene and Fe-Ti oxides. Many of the phenocrysts are bound up in glomeroporphyritic clots. Three sampled Miraflores andesitic lavas have K-Ar ages of 0.108 ± .045 Ma, 0.094 ± 0.263 Ma, and 0.131 ± 0.039 Ma.

Avalanche Deposits From Partial Collapse of the Miraflores Volcano (Qavm).

The large crescent-shaped crater of Miraflores Volcano, open to the east, was the basis for a search for a deposit resulting from sector collapse. Sector collapse of stratovolcanoes (composite cones) is a common phenomenon, observed most recently at the 1980 eruption of Mount St. Helens in the United States (Voight, et al.,1981; Siebert, 1984). Sector collapse may be caused by (1) deformation and steepening of a volcano's slopes by magma intrusion, (2) weakening of the volcano core by hydrothermal alteration, or (3) an earthquake. Deposits consist of megabreccias, frequently with blocks up to hundreds of meters wide, and have a characteristic hummocky surface. Hummocky terrain that is fairly common along the coastal plain of Guatemala is mostly the result of sector collapse of stratovolcanoes that form the Guatemalan highlands (W. I. Rose, Michigan Technological University, personal communication).

The base of the Miraflores/Tecuamburro stratovolcanoes are exposed in the west wall of the canyon of the Río Los Esclavos. Ixhuatán rocks are exposed along the river. East of the Río, on the lower slopes of Ixhuatán volcano, is a lobe of hummocky terrain, 3.8 km long, 3.2 to 2 km wide, and ~100 to 300 m thick. The river cuts through this hummocky terrain, and resulting canyon walls are the sites of huge landslides with movement down toward the river. The hummocky terrain is overlain by deposits of pyroxene-phyric pumice falls and ignimbrites.

In the face of the active landslides, near the Río Los Esclavos, the hummocky terrain consists of massive tuffaceous breccia, consisting of angular clasts of gray, red, and black porphyritic andesite a few cm to 2 m in diameter. Lithic clasts make up ~60% of the deposit. The matrix consists of coarse-ash- to block-size pyroxene-bearing pumice (not the younger pyroxene pumice, which overlies these deposits). A sample from similar deposits on the top of the hummocky surface (along the Quebrada de Agua) is a hydrothermally-altered, block-bearing tuff; lithic clasts contain ~40% phenocrysts of zoned plagioclase and orthopyroxene. Also exposed in the hummocky terrain are (1) conglomerates consisting of boulders of andesite or basaltic andesite and (2) massive andesitic lavas.

Little or no evidence of a large sector collapse avalanche deposit is visible along the western canyon wall of the Río Los Esclavos. Instead, younger deposits of pyroxene pumice ignimbrite, overlain by Tecuamburro lavas, are visible down nearly to river level. In a few spots, the ignimbrite overlies orangish-tan breccias, which appear to have been hydrothermally altered and are interpreted here as avalanche deposits or laharic breccias of the Ixhuatán complex. Upstream 1.5 km from the northern boundary of the mapped avalanche deposits, large slabs (tens of m long) of bedded tuffaceous mudstone, conglomerate, and laharic breccia tilt randomly in all directions and are unconformably overlain by volcanic breccias of Tecuamburro. These may have been part of a sector collapse, but the evidence for this is weak.

Isolated outcrops in the hummocky terrain are not convincing evidence for a large avalanche deposit. However, the hummocky terrain,

best seen from a distant high point, on the map, or on aerial photographs, argues that the avalanche deposit theory reasonably explains the following observations: (1) the change in geomorphic expression of the slopes of the Ixhuatán volcanic complex; (2) the location of deposits from collapse that may have formed the large crescent-shaped crater on Miraflores volcano (no sector collapse breccias are visible on the coastal plain below Chiquimulilla); (3) andesite blocks within this hummocky terrain are not similar to the distinctive andesites of Ixhuatán volcano, with their hopper-shaped plagioclase phenocrysts, but more like those of Miraflores and Tecuamburro; and (4) the Río Los Esclavos has been dammed in the past, either by collapse avalanche deposits or lava flows, allowing the ponding and deposition of lacustrine sediments and ignimbrites upstream from the hummocky terrain.

Pyroxene Andesite Lavas of La Perla (Qap)

Within the crescent-shaped crater of Miraflores volcano, but overlain by the lava domes of Tecuamburro, are poorly exposed massive andesitic lavas (Table I.2 and Appendix B) formed during an early eruptive phase of Tecuamburro. The lavas are not distinctive, consisting of 35 to 50% phenocrysts of zoned plagioclase and lesser orthopyroxene.

Pyroxene Andesite Pumice Fallout, Ignimbrite and Surge Deposits (Qai)

Distinctive andesitic pyroxene-phyric pumice ignimbrite and surge deposits are exposed below lavas of Tecuamburro Volcano in the valley and canyon of the Río Los Esclavos, northeast, east, and southeast of Tecuamburro, and along the main stream through the Finca Vainillal. A similar pumice fall deposit drapes the terrain in the area of Tecuamburro and north for about 10 km (mappable deposit—stipple pattern, Plate 1). Carbonized wood collected from a 4-m-thick section of the pyroxene pumice northeast of Tecuamburro along Highway 16 (Table I.3; Fig. I.6) was dated, using the ^{14}C method, and has an age of 38300 ± 1000 years. Because of intermittent outcrops, it is difficult to measure a volume for this deposit; it is, however, a major pyroclastic unit in this volcanic field. There appear to be several subunits within the pyroxene pumice deposits, but it is beyond the scope of this study to subdivide them.

Table I.3. XRF analyses of pyroxene pumice deposits (Qai).

0 LOCATION	1 sample #	2 SiO2	3 TiO2	4 Al2O3	5 Fe2O3	6 MnO	7 MgO	8 CaO	9 K2O	10 Na2O	11 P2O5	12 Total
F. Piedra Parada	GH-2-24-89-4	55.74	0.80	18.45	8.27	0.17	3.22	7.42	0.72	3.63	0.20	99.08
-"-	GH-2-24-89-4	56.00	0.80	18.48	8.29	0.17	3.28	7.47	0.73	3.66	0.20	99.08
C. Pena Blanca	GH-2-22-89-4	57.65	0.65	18.98	7.32	0.14	2.81	5.05	0.96	3.00	0.10	96.84
-"-	GH-2-22-89-4	57.87	0.64	19.12	7.30	0.14	2.79	5.10	0.96	2.82	0.10	99.05
Chiquimulilla	GH-2-24-89-2	59.42	0.67	18.69	7.54	0.13	3.29	5.82	0.72	3.19	0.13	94.18
-"-	GH-2-24-89-2	59.58	0.68	18.51	7.50	0.13	3.30	5.81	0.73	2.88	0.13	99.62
Chupadero	7-9-88-12	60.26	0.58	17.11	6.40	0.14	2.46	5.50	1.23	3.06	0.06	96.80
F. S. Francisco	GH-2-25-89-4	60.44	0.57	17.10	6.21	0.12	2.70	5.74	1.19	3.19	0.12	98.59
Chupadero	7-9-88-12	60.78	0.58	17.11	6.48	0.14	2.47	5.47	1.21	3.23	0.06	97.53
F. S. Francisco	GH-2-25-89-4	60.78	0.57	16.95	6.26	0.13	2.67	5.74	1.21	3.00	0.12	97.39

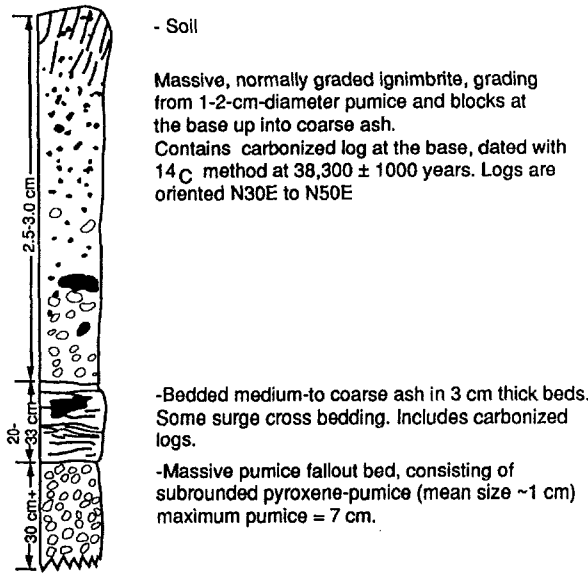

Fig. I.6. Pyroxene Pumice deposits (Qai) exposed along the lower northeastern flank of Tecuamburro Volcano.

Pyroxene Pumice Deposits Near Chupadero Crater (Qai). North and east of the Chupadero crater (Fig. I.3), the older andesitic stratovolcanoes are partly covered by pumice fallout deposits with a maximum measured thickness of >4 m (at Finca San Francisco). Thicknesses of this pumice mantle decrease toward the east and west; e.g., the mantle thins to 1 m at Finca Concepción. The pumice mantle thickens toward both the Chupadero crater and the vents for the earliest eruptions of Tecuamburro. The massive deposits consist of mostly light tan pumice lapilli in a coarse ash matrix; at this location, there are no visible lithic clasts. The pumices are porphyritic, containing about 15% phenocrysts of zoned plagioclase, orthopyroxenes, and Fe-Ti oxides. The vesicularity ranges from 62 to 69%; vesicles are ovoid, ranging in length from 10 to 200 μm and are radial to phenocryst surfaces (Fig. I.7).

Two meters of light tan massive ignimbrite are exposed intermittently along the road between Finca Vainilla and the village of Chupadero, near Laguna Ixpaco and west of Ixpaco village. This unit consists of 4 to10-cm-diameter, equant pumices in a medium ash matrix.

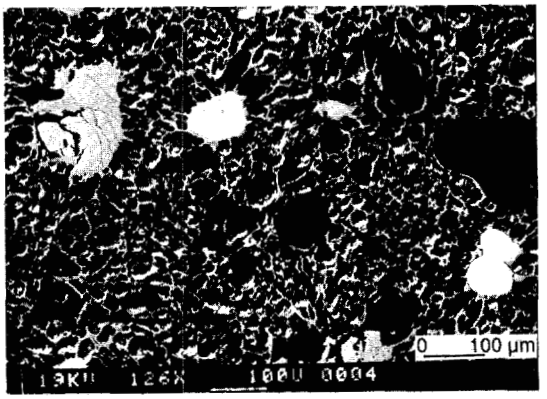

Fig. I.7. Scanning electron micrograph of a polished thin section of a pyroxene pumice clast collected from a 4-m-thick pumice fallout deposit north of Chupadero crater. Vesicles make up 65% of these pumices, which contain 15% phenocrysts of plagioclase, orthopyroxene, and Fe-Ti oxides. Note the radial vesicle orientations around phenocryst surfaces.

The pumice contains 20% phenocrysts of plagioclase and minor K-feldspar, orthopyroxene, and Fe-Ti oxides and has a vesicularity of 36%.

Pumice deposits near Chupadero crater are similar, but not identical to pyroxene pumice deposits along the eastern slopes of Tecuamburro and along the Río Los Esclavos. The pumices in the fallout deposits have vesicularities ranging from 62 to 69%, whereas the pumices from the ignimbrite have a vesicularity of around 35%. The Chupadero pumices are more silicic (60.2 to 60.8 Wt.% SiO_2) than the deposits east of the area (55.7 to 59.6 Wt.% SiO_2) (Table I.3). These may be different phases of one eruption, as they are all about the same level stratigraphically, but they could also be interpreted as being from separate eruptions.

Pyroxene Pumice Deposits Along the Río Los Esclavos (Qai). The best exposures (and most inaccessible) of the pyroxene pumice tuff deposits are along the Río Los Esclavos, where they occur as arroyo- and valley-fills. These deposits range in thickness from 5 to 6 m on the slopes of Tecuamburro and to 150 m on the slopes adjacent to the Río Los Esclavos, east of Tecuamburro.

The arroyo-filling pyroxene pumice deposits east of Tecuamburro, with maximum thicknesses ranging from 60 to 150 m consist of a basal pumice fallout (<2 m thick), overlain by massive, nonwelded pinkish-tan ignimbrite. There are stringers of lithic clasts throughout the ignimbrite (Fig. I.8). The river has cut down through these deposits to underlying river gravels that appear to identify its pre-eruption level. Along terraces above the river, between paleoarroyos, the deposits consist of a thin (<5 m) sequence of pumice fallout, overlain by wood-bearing, cross-bedded surges and thin ignimbrites (Fig. I.6). There is a thin grey pumice fallout and ignimbrite (3m thick) 3 km below the entrance to the canyon of the Río Los Esclavos that is interbedded between two thin tan ignimbrites; this gray ash was not seen anywhere else in the area.

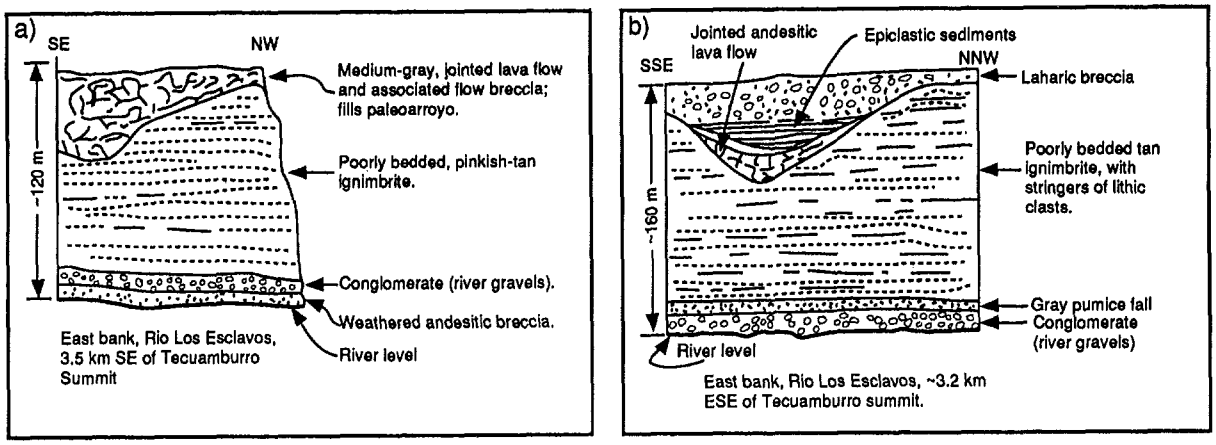

Fig. I.8. Sketches of stratigraphic sections of cliffs along the Rio Los Esclavos, east and southeast of Tecuamburro Volcano, showing thick pyroxene pumice ignimbrites, canyons cut into those ignimbrites, and valley-filling andesitic lava flows from Tecuamburro Volcano.

Upstream from the deep canyon of the Río Los Esclavos, within the broad valley below Cuilapa, some of the distal portions of the pyroxene pumice tuffs are exposed near the contact with overlying biotite-hornblende ignimbrites. An exposed section near Finca Concepción consists of 30 cm of pumice fallout, overlain by two nonwelded ignimbrites, separated by 10 cm of coarse ash fallout (Fig. I.9).

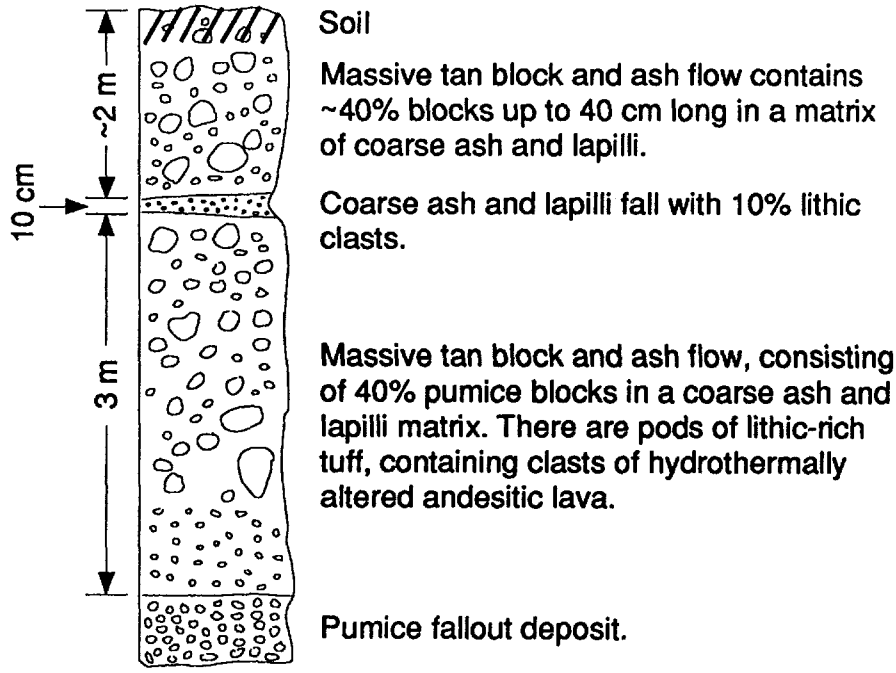

Fig. I.9. Stratigraphic section of distal pyroxene pumice deposits (Qai), near Finca la Concepción.

Downstream, near Chiquimulilla, the pyroxene pumice ignimbrites spread out onto the coastal plain. Thicknesses range from 5 to 10 m. The pinkish-tan, graded ignimbrites consist of equant, subrounded pumices (up to 12 cm in diameter) in a matrix of coarse ash. They contain <1% andesitic lava lithic clasts.

Most of the ignimbrites consist of porphyritic pumices with 18 to 21% broken(subhedral) phenocrysts (plagioclase>> orthopyroxene> clinopyroxene> Fe-Ti oxides) and vesicularities of 45% (Fig. I.10). Vesicles are spherical to ovoid and 10 to 100 μm long; there is radial vesicle growth from phenocryst surfaces. Distal deposits, exposed near Finca La Concepción, are coarse crystal tuffs, with concentrations of phenocrysts (72%) and andesitic and sandstone lithic clasts (14%). SiO_2 contents range from 55.7 to 59.6% (Table I.3); these pumices are also more calcic than those around the Chupadero crater.

A *minimum* estimate of the volume of pyroxene pumice deposits is 0.8 km^3; the dense rock equivalent (DRE) is 0.41 km^3. This is a substantial amount of pyroclastic material for a dome complex (*if* it is from Tecuamburro), where volumes are usually <0.1 km^3 (Heiken and Wohletz, 1987). It is a reasonable volume for pyroclastic material erupted from a small caldera, which may be indirect evidence for its eruption from Chupadero crater.

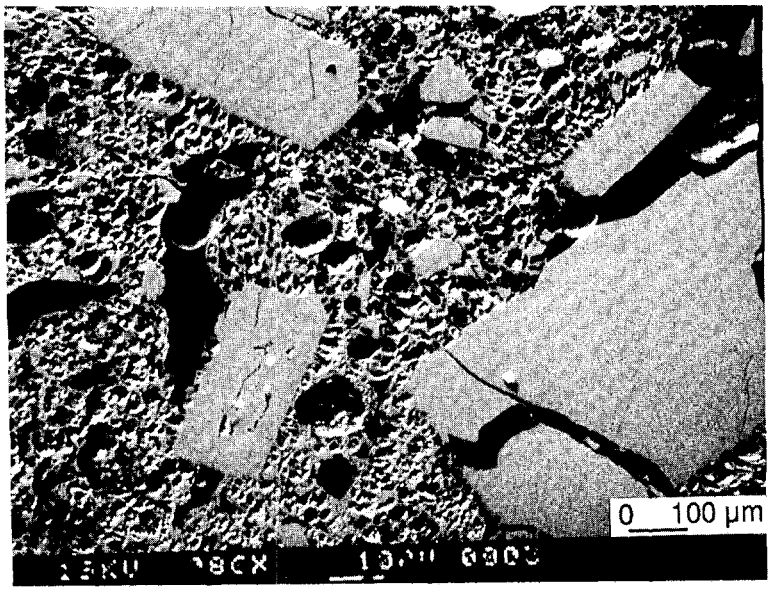

Fig. I.10. SEM of polished thin section of pumice collected from the pyroxene pumice deposits (Qai) near Chiquimulilla. Pumice vesicularity is 45%; it contains 21% phenocrysts of plagioclase, orthopyroxene, clinopyroxene, and Fe-Ti oxides.

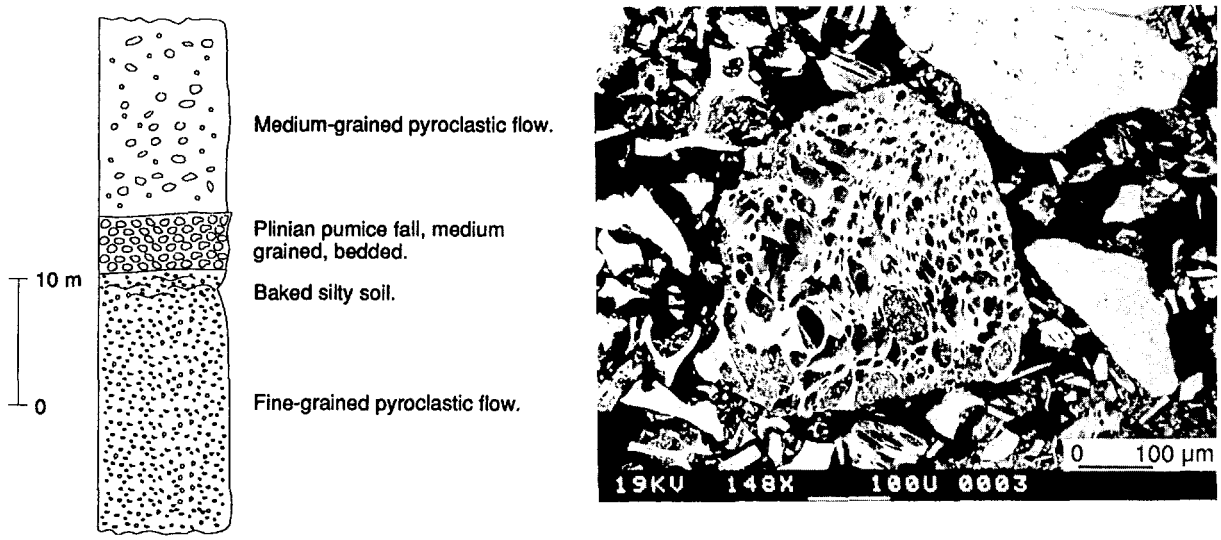

Fig. I.11. (a). Stratigraphic section of rhyolitic ignimbrite along the Río El Azufre. (b). SEM of the valley-filling hornblende-biotite rhyodacitic tuff . Rounded pumice clasts are scattered throughout a matrix of pointed and angular shards.

Hornblende-Biotite Rhyodacitic Ignimbrite (Qri)

The northern ends of north-south-trending valleys that flank the volcanoes within the Tecuamburro graben are partly filled with biotite-hornblende-bearing rhyodacitic ignimbrites (Figs. I.3, I.11a).

Ignimbrites exposed in the valley of the Río Los Esclavos are massive, nonwelded, light tan or gray, consisting of 1-4-cm pumice clasts in a matrix of medium ash. The medium- to fine-grained ash consists of mostly (63%) colorless shards derived from a pumiceous melt with narrow, elongate vesicles; disruption of this melt produced needle- and tube-shaped shards (Fig. I.11b). It also contains 10.4% phenocrysts (plagioclase>K-feldspar>biotite>Fe-Ti oxides>hornblende; see Appendix B) and rounded andesitic and siltstone lithic clasts (9.3%). These ignimbrites have not been dated, but they are probably too young for K-Ar dating techniques. They best correlate with the Amatitlán L deposits, with their petrographic characteristics and bulk chemical composition (Wunderman and Rose, 1984), and with SiO_2 contents of 68.5 to 71% (Fig. I.5; Table I.3). They are notably less silicic than tuffs of the Ayarza calderas, which are 50 km north of the area and on the same watershed (Fig. 1.5; analyses from Peterson and Rose, 1985).

Within the western mapped area, the ignimbrites are well exposed by erosion along the Ríos La Plata, Las Cadeñas, and El Azufre and in western areas along the Río Aquacapa, where it fills valleys and has thicknesses of up to 40 m; these ignimbrites contain pumices 15-20 cm long. Along the Río El Azufre two major ignimbrite flow units are separated by 4 m of Plinian pumice fallout (Fig. I.11a), which contains 4 mm-diameter pumices and abundant basaltic/andesitic lava lithic clasts. Within the northeastern part of the mapped area, Qri becomes noticeably finer grained (maximum pumices of 5 cm) and the phenocryst content decreases to <1%.

Pyroxene Andesite Lava Dome of Tecuamburro (Qat)

Volcán Tecuamburro, with elevations of 1640 m (summit crater) and 1845 m (Cerro La Soledad), consists of a WNW-trending ridge made up of mostly lava flows with interbedded laharic breccias and vulcanian tuffs. The volcano was built within the collapse crater of Miraflores volcano on a base sloping to the east at about 11°. The base of the Tecuamburro volcano is about 4 x 5 km. A closed summit crater is 250 x 150 m, 20 m deep, and is located in a flat summit area.

At the summit and along the upper slopes of Tecuamburro, there appear to be mostly massive gray to light gray basaltic andesite flows (SiO_2=52.01 to 53.21%). An exception to this is the overlapping andesitic dome of Cerro la Soledad, with a SiO_2 content of 60.2%. All lavas overlie the pyroxene pumice, dated at 38300 ± 1000 years. The lavas are too young for accurate dating with the K-Ar method (Table I.1).

Along the lower slopes there are matrix-supported laharic breccias interbedded with the lava flows (Fig. I.12). There are also interbeds of scoria, with bombs up to 10 cm long, and surge deposits consisting of lithic tuffs containing accretionary lapilli and traces to 12% pumice (Fig. I.13 and Appendix B). At the base of the volcano, lava flows and laharic breccias are restricted to paleocanyons, cut into the underlying pyroxene pumice ignimbrites.

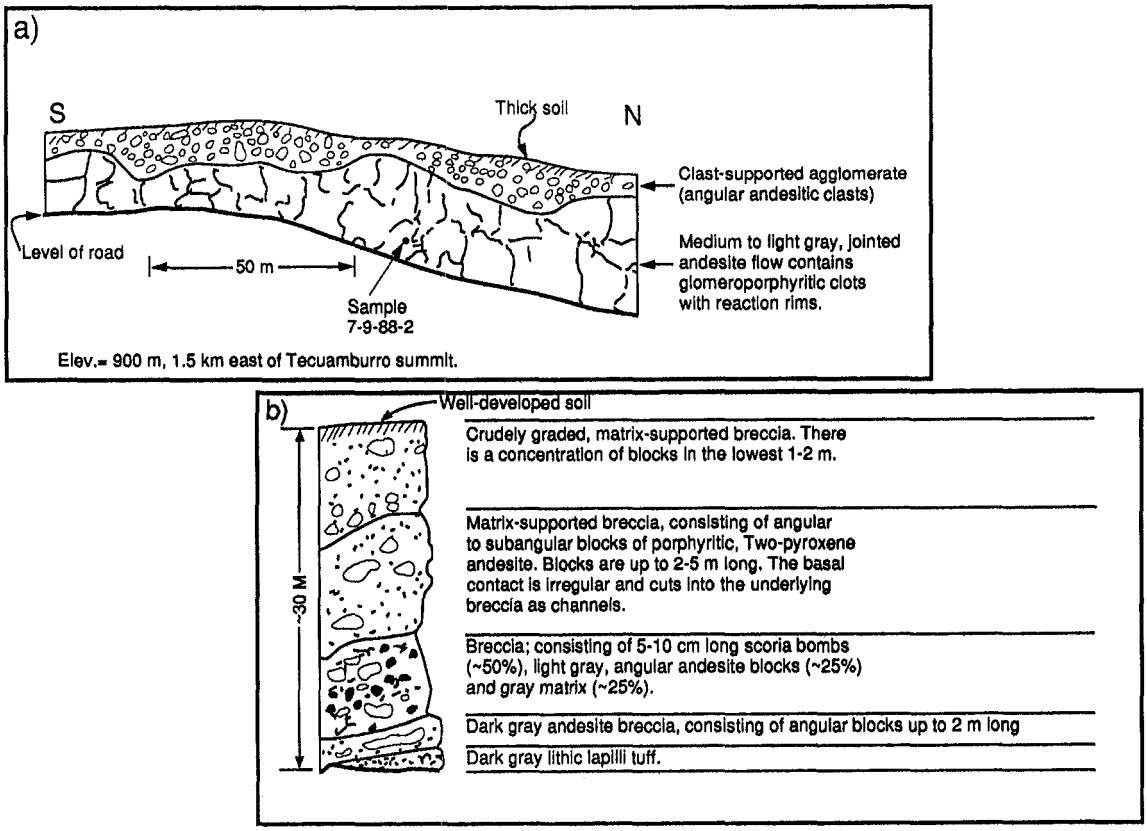

Fig. I.12. Stratigraphic sections along the eastern slopes of Tecuamburro Volcano. (a). Massive andesitic lava flows, overlain by a clast-supported agglomerate. (b). Laharic breccias and vulcanian agglomerates interbedded with andesitic lava flows.

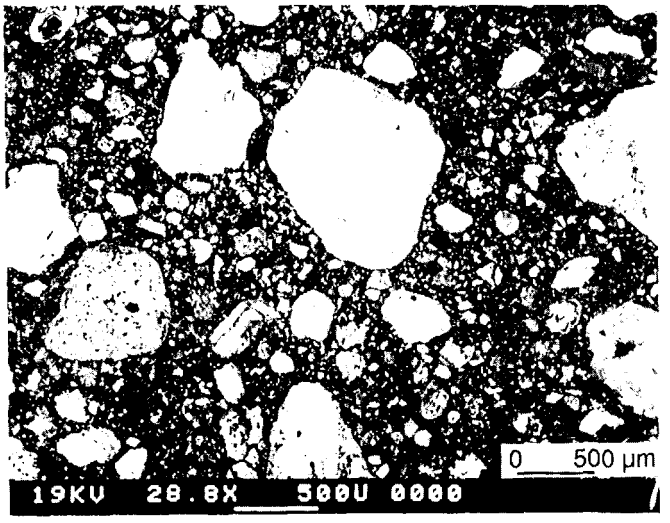

Fig. I.13. SEM of a polished thin section of lithic ash from tephras interbedded with lava flows on the eastern slopes of Tecuamburro Volcano. Most of the pyroclasts consist of largely andesitic lava clasts and mineral fragments but contain 12% andesitic pumices. Most of the clasts are rounded and show some degree of hydrothermal alteration.

The lavas are porphyritic, with 46 to 50% individual phenocrysts (100 µm to 3 mm) and glomeroporphyritic clots consisting of mostly zoned plagioclase, with lesser orthopyroxene (hypersthene) ≥ clinopyroxene (augite) > olivine > Fe-Ti oxides (see Appendix B).

Pyroxene Andesite Lava Dome of San Francisco (Qasf)

A 1.5-km-diameter crater immediately west of the Tecuamburro lava dome(s) contains the fumaroles of Mina de Azufre, the dome of San Francisco (named after Finca San Francisco Tecuamburro), and the dome of Cerro Peña Blanca. The crater cuts the pyroxene andesitic lavas of La Perla (Qap) and the lavas of Tecuamburro (Qat). Rocks along the southeastern margin of the crater are hydrothermally altered to tridymite, cristobalite, and an amorphous phase and contain active fumaroles.

The San Francisco dome is 750 m in diameter, 120 m high, and has a 120-m-diameter, shallow crater located on the western summit area. It consists of medium gray, flow-banded andesite. The lower flanks of the dome are covered with a breccia collar that could be talus from the dome or a small tuff ring; the exposures are poor.

The porphyritic andesite lava of the San Francisco dome consists of 45% phenocrysts in a glassy, diktytaxitic groundmass. It is a two-pyroxene andesite (hypersthene and augite) with Fe-Ti oxides and a trace of hornblende.

Hornblende Dacite Dome of Peña Blanca (Qdpb)

Peña Blanca Dome, with an elevation of 1840 m and a basal diameter of about 1.5 km, is one of the largest domes of the Tecuamburro complex. It is located within the crater of Mina de Azufre and rises 500 m above the crater floor. The northern part of the dome has collapsed, leaving a 1-km-wide scarp above a debris avalanche; the avalanche is described below.

Lava at the base of the dome is a massive light gray dacite (verging on the classification border with andesite, with a SiO_2 content of 62.4%). Sulfur-depositing fumaroles are located at the base of the avalanche scarp, which is nearly vertical.

The dome rock near the summit is a porphyritic andesitic dacite with 50% phenocrysts of plagioclase >> orthopyroxene (hypersthene) > hornblende in a hyalocrystalline matrix (Appendix B). The hornblende occurs as glomeroporphyritic clots with plagioclase and orthopyroxene.

Undifferentiated Olivine-Bearing Basaltic Scoria Cones and Lavas (Qb)

Within the northern part of the map area, the youngest rock units are the scoria cones and associated lava flows that lie across the Jalpatagua fault zone near the towns of Cuilapa and Barberena. These probably are Holocene, overlying the nonwelded ignimbrites of Amatitlán; the cones and flows are well preserved and often have poorly-developed soil profiles.

The lavas consist of 10 to 34% phenocrysts of plagioclase, clinopyroxene, olivine, and Fe-Ti oxides in a trachytic, diktytaxitic groundmass. The clinopyroxenes, usually pigeonite and aegerine-augite, occur in glomeroporphyritic clots. One of the lava samples contains quartzose sandstone xenoliths; the quartz has reaction rims and the clay matrix is altered to chlorite (Appendix B). These lavas are closest in chemical composition to alkali-olivine basalts (Table I.2).

Phreatic Tuff Ring and Enclosed Acid lake of Laguna Ixpaco (Qtr)

Laguna Ixpaco is an acid sulfurous lake 360 m in diameter, located within the Chupadero crater, 3 km north of Cerro Peña Blanca. The crater lake is surrounded by a tuff ring with a diameter of about 1 km and a 10 to 20-m-high crater rim. The southern part of the crater rim is partly buried by an avalanche deposit from Cerro Peña Blanca.

The tuff ring consists of poorly bedded, white to light gray breccia that consists of relict acid-altered pumice and crystal and lithic clasts. Where exposed along the eastern crater rim, there are two depositional units: (1) a lower, 6-m-thick, massive white breccia, and (2) an upper, 4-m-thick, poorly bedded unit, consisting of alternating white and pink, 4-cm- to 1-m-thick beds (Fig. I.14a).

Along the northeastern rim of the crater are two exposed units: (1) massive, acid-altered tuff, thickness unknown; and (2) a poorly-bedded, acid-altered, pumice-rich unit, with patches of orange stain. Separating these two units is a 5- to 40-cm-thick organic-rich zone that was dated using the ^{14}C method at 2910 ± 70 years (Fig. I.14b). The lower unit appears to be in place and may be the "country rock" through which the Ixpaco phreatic crater erupted, or it may be a lower phreatic ejecta deposit, for which we do not see the base. If the latter hypothesis is correct, then there have been two phreatic eruptions at Ixpaco, separated by enough time for several centimeters of organic material to accumulate.

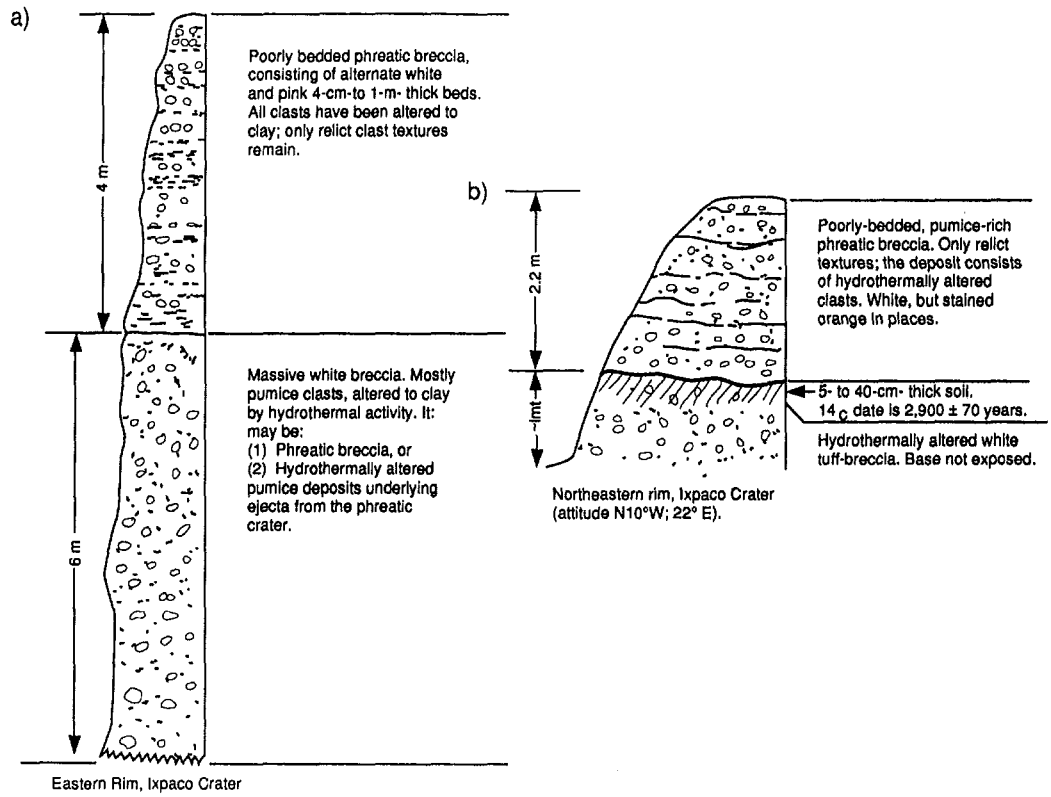

Fig. I.14. Stratigraphic sections through the phreatic tuff ring around Laguna Ixpaco: (a). Eastern rim, behind the abandoned sulfur works. (b). Northeastern rim, along the road to Ixpaco village.

The two units above the organic-rich zone have been altered to mostly smectite and kaolinite, with lesser amounts of alunite, authigenic quartz and feldspar, jarosite, and cristobalite. The breccias underlying the organic-rich zone are mostly kaolinite and halloysite (?), with lesser quartz, cristobalite, feldspar, and alunite (?).

The phreatic breccias were sampled to determine what rock types are represented to infer what underlies the phreatic crater. The rocks are completely altered by acid fluids, but relict textures remain. Enhanced SEM images allow identification of clast types (Fig. I.15), which include (1) medium-ash size to blocks of pumice, with 40 to 50% vesicles (small, ovoid shapes), (2) andesitic lithic clasts, and (3) plagioclase and pyroxene. A comparison of these samples with the clast types, shapes, and sizes was made with Tecuamburro lithic ashes and the pyroxene pumice deposits (Fig. I.16). The phreatic deposits are most similar to the pyroxene pumice deposits when numerical comparisons are made between clast size and shape; this is reasonable, for in outcrops closest to Laguna Ixpaco there are pyroxene pumice ignimbrites.

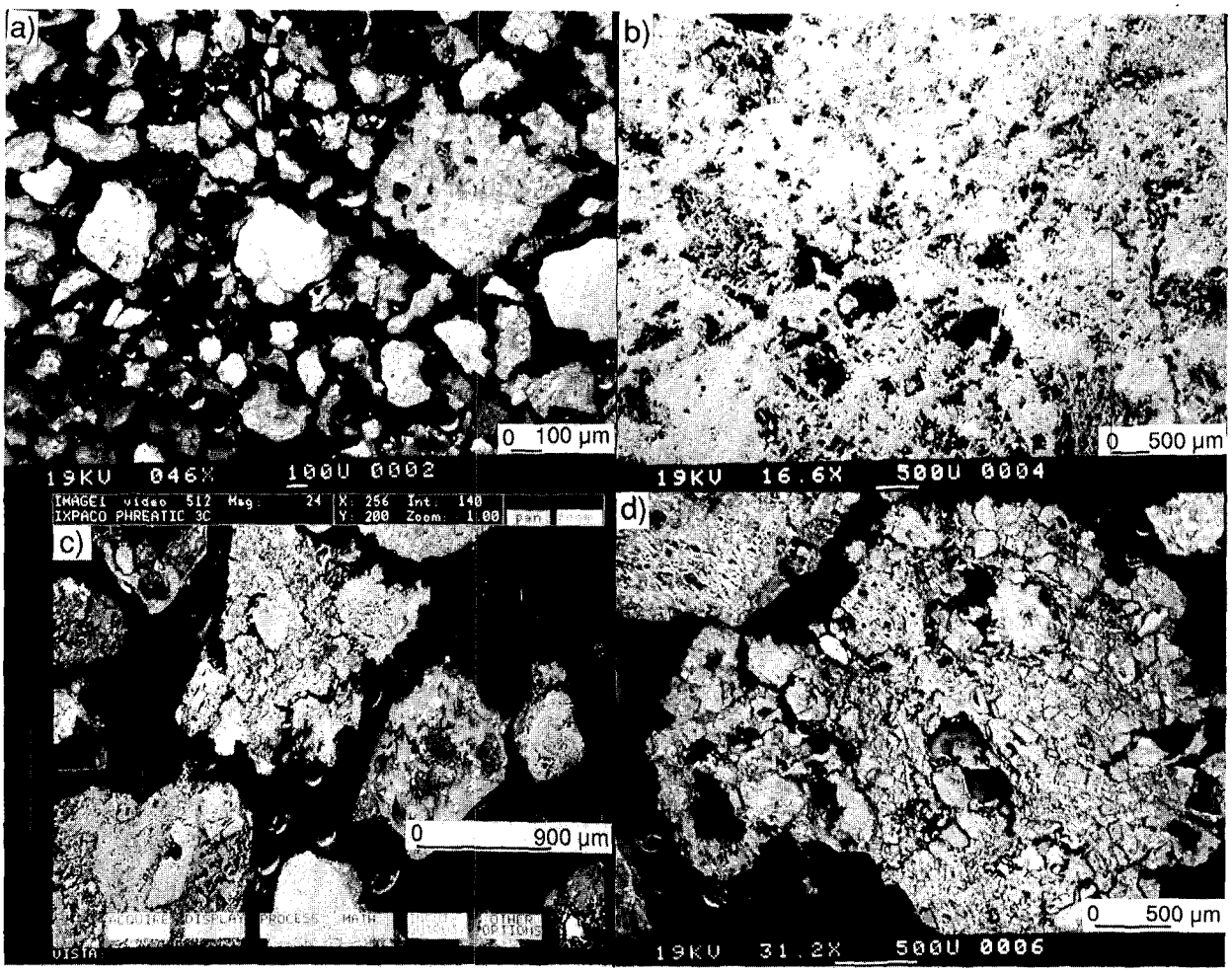

Fig. I.15. SEM images of polished thin sections of the matrix of phreatic breccia from the tuff ring around Laguna Ixpaco: a). Lowermost unit, from eastern crater rim. All of the clasts have been altered to clays, but relict textures reveal a mixture of pumice clasts with vesicularities of around 40-50%, andesitic lithic clasts and plagioclase and pyroxene; b). Upper unit, eastern crater rim. Hydrothermally altered pumice lapillus. Most of this deposit consists of coarse pumice pyroclasts; c). Upper unit northeastern crater rim. Mostly relict pumice pyroclasts; and d). Close-up of pumice pyroclasts from the sample shown in "c".

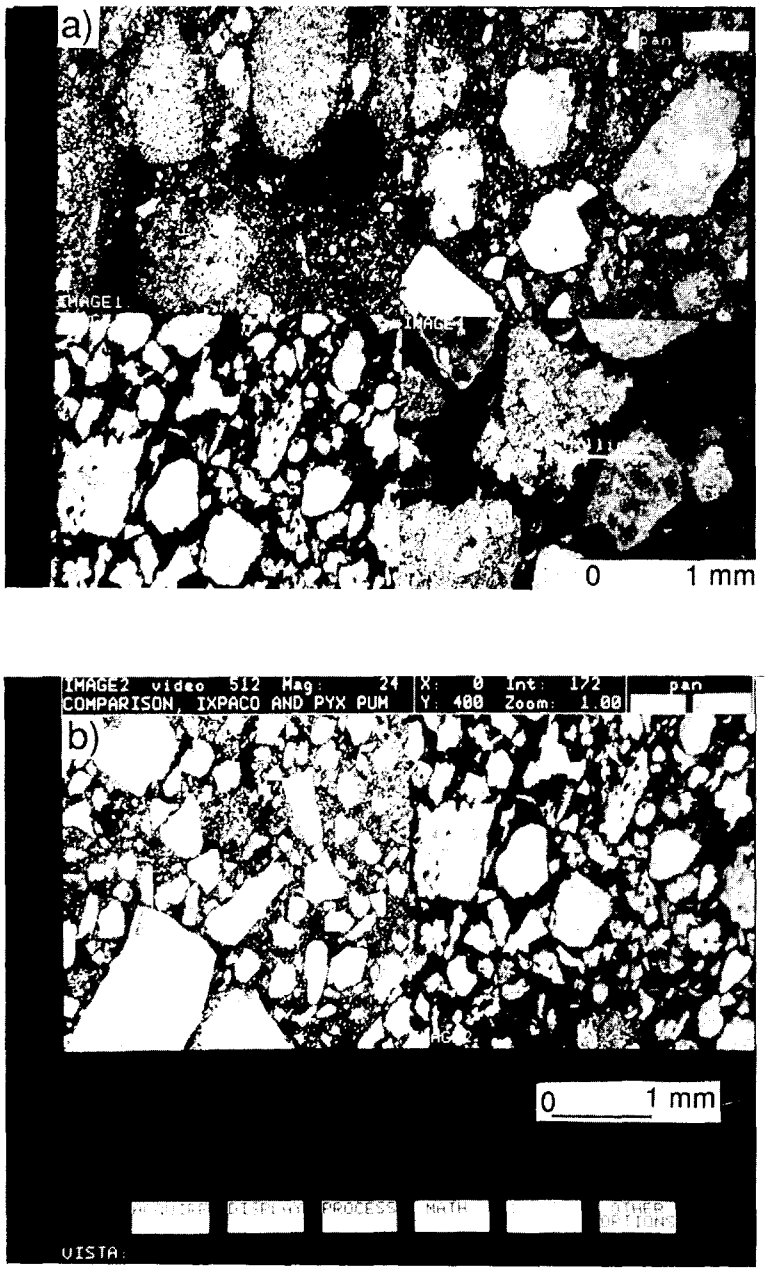

Fig. I.16. Comparison of breccia matrix from the Ixpaco tuff ring with the pyroxene pumice deposits (Qai) and Tecuamburro lithic ash (Qat). SEM views of polished thin sections: a). Lithic ashes from interbeds within lava flows on Tecuamburro (upper two frames), compared with phreatic debris from Ixpaco (lower two frames). These clastic rocks are not similar in texture; and b). Ixpaco debris (right), compared with coarse ash from distal pyroxene pumice deposits (left). The mixture of pumice and phenocrysts and pumice shapes are similar.

Avalanche Deposits From Partial Collapse of Cerro Peña Blanca (Qavpb)

Three lobes of debris avalanche deposits extend north from a nearly vertical scarp on Cerro Peña Blanca, covering an area of about 7 km^2. The hummocky surface and lack of soil on these deposits is evidence for their youth. They overlie the southern rim of the Ixpaco phreatic crater, which has been dated at 2910 ± 70 years. The debris flows have hummocky surfaces littered with blocks of dacitic andesite (containing hornblende, plagioclase, and two pyroxenes) ranging in size from <1 m to >20 m; flow surfaces are clast supported.

An exposure of the eastern margin of the easternmost lobe of the debris flows is shown in Fig. I.17a. The 0.8 m-thick section of breccia is reversely graded, from a matrix-supported base to clast-supported top; clasts range in size from less than 100 μm to many meters long. The matrix is composed of a very poorly sorted mixture of andesitic lithic clasts, mineral clasts and rare pumice grains (Fig. I.17b).

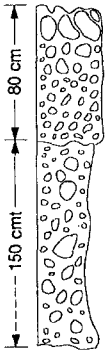

Edge of a massive, hummocky debris flow (deposit from Cerro Pena Blanca). Blocks range in size from 5 cm to many m long. The deposit is monolithologic, consisting of fragmented andesitic lavas. Matrix consists of purple-coarse sand and pebbles of the same rock types.

Massive pumiceous block and ash flow, consisting of pinkish-tan pyroxene pumice. Contains 5% andesitic lithic clasts, many of which are hydrothermally altered.

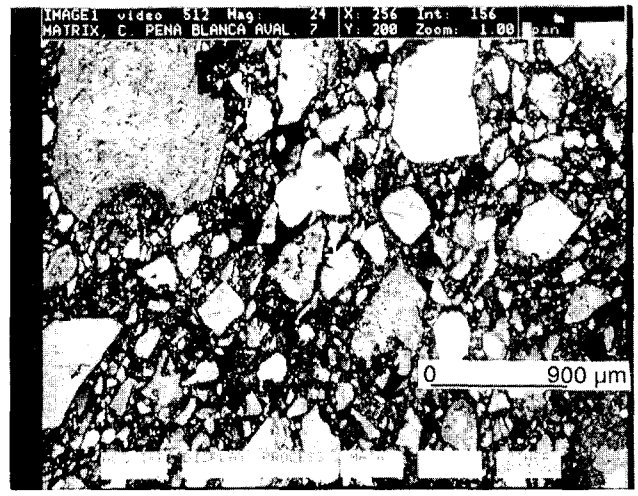

Fig. I.17. a). Stratigraphic section of the edge of an avalanche deposit from Cerro Peña Blanca (Qavpb). b). SEM image of a polished thin section of the matrix from the avalanche deposit. It consists of very poorly sorted andesitic lithic clasts, mineral clasts and rare pumice grains. The pumice was possibly derived from the underlying block and ash flow.

D. STRUCTURAL FRAMEWORK

The geologic map (Fig. I.3) illustrates four structural components within and bounding the Tecuamburro graben and volcanic centers: (1) N-S-trending normal faults that define the graben and offset rocks within it; (2) strike-slip and associated reverse faults of the Jalpatagua fault zone; (3) NW-SE-trending normal faults within the graben; and (4) collapse faults associated with volcanic vent areas.

The Tecuamburro graben belongs to the group of roughly N-S-trending grabens found in southern Guatemala that may be expressions of extension or segmentation within the subducting Pacific plate (Burkhart and Self, 1985). This graben has a well-defined western boundary (normal faults; see Fig. I.3 and cross sections F-F' and G-G' in Appendix A). The eastern margin is less obvious, consisting of a zone of NNE- and N-trending normal faults on the western slopes and summit region of Ixhuatán. Displacements along graben-bounding faults are not known.

The Jalpatagua fault system is a major regional structure that is well defined by satellite imagery, by stratigraphic discontinuities (Carr, 1976), and topographic expression. From Barberena to Oratorio (15 km east of Cuilapa), the fault zone is well defined by steep fault scarps, linear valleys, and sag ponds. Lavas and tuffs along the fault are broken into cataclastic breccias; nonwelded tuffs are sheared and former phenocrysts are present only as rock flour. East of Oratorio, in the Jalpatagua Valley, there is a considerable vertical slip component and a well-defined, 400-m-high scarp, down to the south. The sense of strike-slip movement is generally thought to be right lateral, as defined by drainage channel offset and sense of motion on reverse faults exposed south of the fault. Right-lateral movement along the Jalpatagua fault is also consistent with the model of eastward motion of the Caribbean plate in central Guatemala (Newhall, 1987). The offset of a north-south line of cinder cones across the Jalpatagua fault at Barberena may be interpreted as evidence for left-lateral movement.

NW-trending normal faults are the dominant structures within the Tecuamburro graben. These faults intersect or merge with north-trending normal faults near the western edge of the graben (Fig. I.3). Some of these faults bound large areas of hydrothermal alteration within the andesitic composite cones north of Tecuamburro. Lines of mud volcanoes located 1 km west of Laguna Ixpaco, fissures for hot springs at Colmenares, and lines of vents on the Tecuamburro volcano group of lava domes all reflect this NW-SE structural trend. Faults passing close to the northern boundary of Chupadero crater may serve as a boundary between a hydrothermal system associated with Tecuamburro Volcano/Ixpaco and a possible second system associated with older composite cones located north of Ixpaco (see Chapter III). These faults are exposed along the Río Los Esclavos northeast of the summit of Tecuamburro (Fig. 1.18).

within the northern third of the Tecuamburro graben, high-angle reverse faults are visible along the highway between Cuilapa and Chiquimulilla (Fig. I.19). these are extensions of NNE-trending ridges, which appear to intersect the Jalpatagua fault zone at an acute angle; however, they are buried by younger tuffs and basalt flows near the proposed intersection.

Pueblo Nueva Viñas (Tap), Piedra Grande (QTapg), and Miraflores (Qam and Qavm) are three large composite cone sector collapse craters in the area. Although they are not classified as sector collapse craters here, the northern flanks of the domes of early Tecuamburro (Qat) and Peña Blanca (Qdpb) have collapsed to form extensive debris avalanche deposits.

The most important structural feature related to hydrothermal systems is the Chupadero crater (Fig. I.3). This crater, which is overlain on several sides by younger volcanic deposits, contains the phreatic crater of Laguna Ixpaco and several other sites of fumaroles and boiling springs (see Chapter III for exact locations).

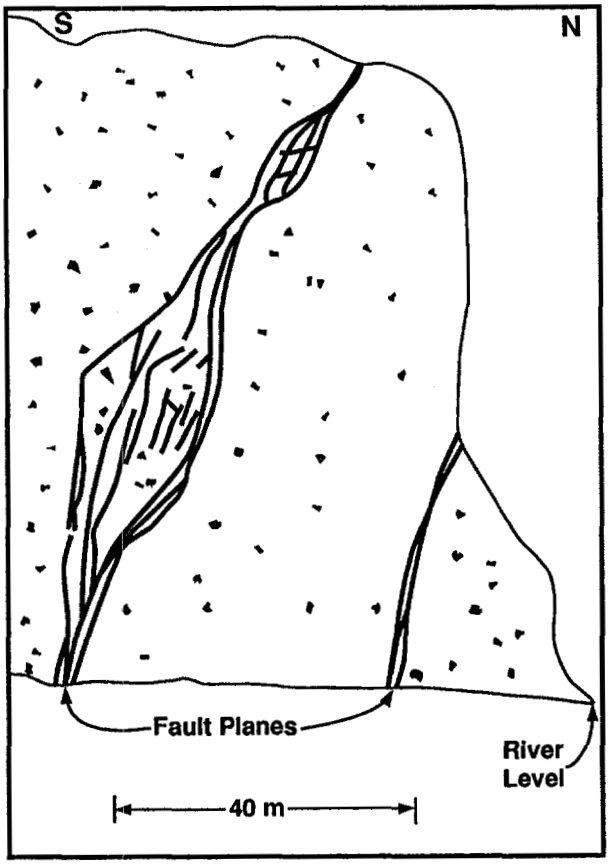

Fig. 1.18. Traces of normal faults along the Río Los Esclavos, northeast of the Tecuamburro summit and east of Chupadero.

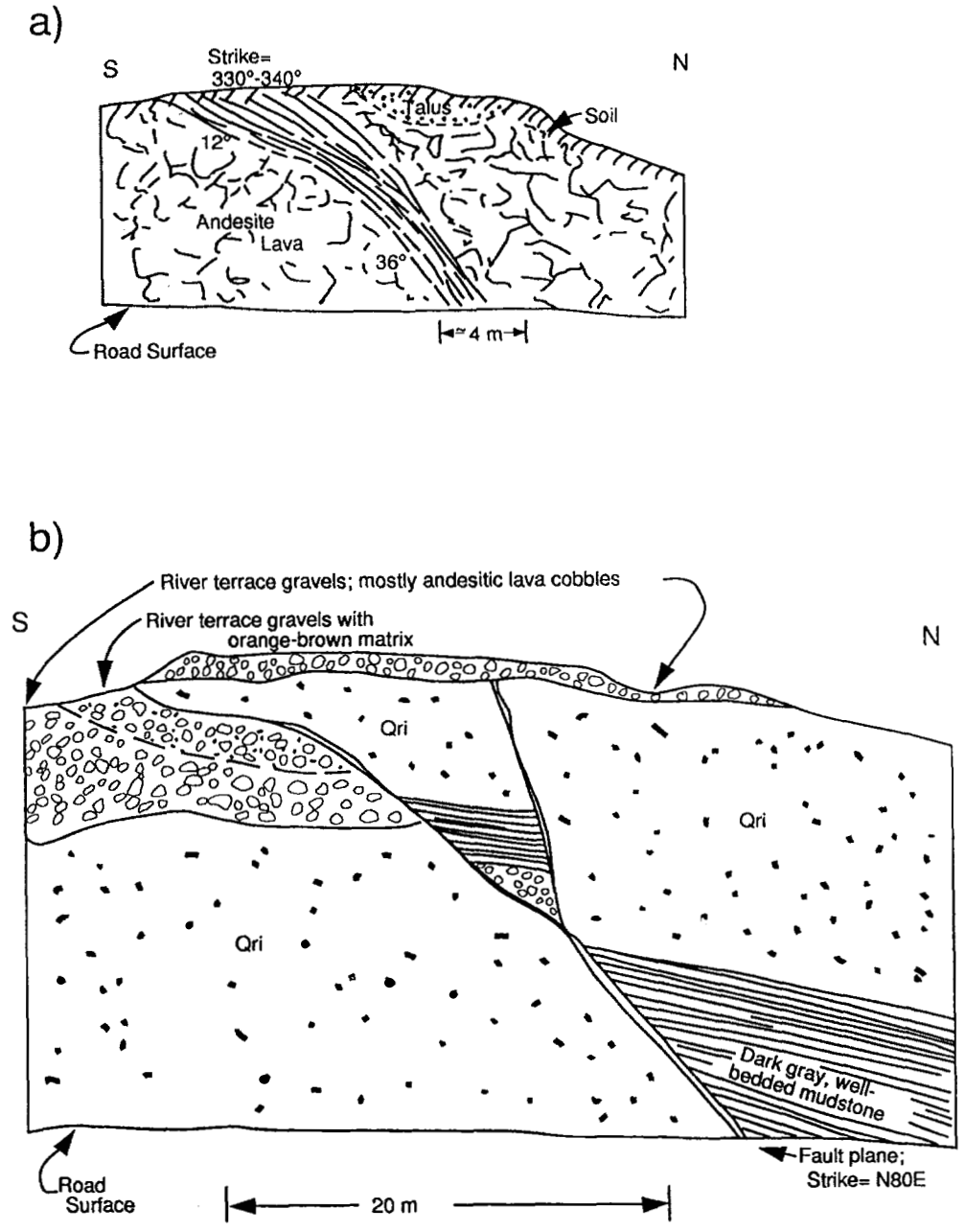

Fig. 1.19. Low-angle reverse faults exposed along Highway 16, near Cuilapa (see Plate 1 for fault locations).

E. DISCUSSION AND CONCLUSIONS

Tecuamburro Volcano lies within a 20-km-wide, N-S trending graben, which we informally call the Tecuamburro graben. The graben is terminated at the strike-slip Jalpatagua fault zone on the north and is buried on the south by Pacific coastal plain sediments. The graben is

flanked on the east and west by the older andesitic to dacitic volcanic complexes of Pueblo Nuevo Viñas and Ixhautan. Graben-bounding faults cut the flanks of these volcanoes, but their principal eruptive centers lie outside the graben.

Structures within the graben include arcuate faults associated with the larger craters, steeply dipping, NW- to north-trending normal faults and moderate- to low-angle reverse faults. Hot springs, boiling springs, and fumaroles are associated with some of the volcanic craters and with the NW-trending faults. Zones of permeability are believed to exist under many of the craters, especially the phreatic crater of Ixpaco, and along some of the NW-trending faults. Careful identification of these structural zones is important in identifying the locations of exploration coreholes.

Volcanic vents and associated eruption products within the Tecuamburro graben are generally younger from the north toward the south. Ages of these volcanoes range from somewhat greater than 1 Ma to less than 38300 years old. Powerful steam explosions that formed the crater containing Laguna Ixpaco occurred as recently as 2910 years ago. Part of the nearby Peña Blanca dacite lava dome collapsed to form a debris avalanche that covers the southeastern rim of the Ixpaco tuff ring; thus the debris avalanche is younger than 2910 years but we do not know if the eruption that formed the Peña Blanca dome is this young. Collapse may have been related to seismic activity or hydrothermal alteration of its core.

Cerro Peña Blanca and adjacent domes (San Francisco, El Soledad, and Tecuamburro) are all less than 38300 years old. We conservatively estimate that 50 km^3 of magma was erupted from closely spaced vents in the southern quarter of the Tecuamburro graben during the past 100000 years, that several km^3 make up the Peña Blanca-La Soledad-Tecuamburro-San Francisco volcanoes and that 0.4 km^3 (minimum) make up the pyroxene pumice deposits.

Simple models of conductive cooling of magma in the crust, constrained by a combination of ages and eruption volume, suggest that a magma body or a group of magma bodies underlie the area of most recent volcanism. If Chupadero crater is the source of the pyroxene pumice deposits and is a small caldera, it is possible that a dacitic magma body is the heat source for Laguna Ixpaco and nearby fumeroles and springs. The dacites of Peña Blanca are among the most silicic rocks of the area, which is also suggestive of a shallow (<10 km), differentiated magma reservoir located below the Tecuamburro-Chupadero area.

The hypothesis that a magmatic crustal heat source is centered in the southern part of the Tecuamburro graben is strongly supported by chemical geothermometers (see Chapter III). The highest calculated temperatures of about 300°C are for gas samples collected at Laguna Ixpaco and at the base of the Peña Blanca dome. Chemical geothermometry for samples collected at hot springs and fumaroles located north, east, and southeast of this group of young volcanoes indicates temperatures of no more than 165°C.

We propose drilling an exploratory corehole beneath the southern part of the graben after considering the multiple lines of evidence for a

crustal heat source centered there. The presence of a young, large phreatic crater at Laguna Ixpaco, fumarole fields near the lake, and the high gas geothermometer temperatures are all indicators of the presence of a hydrothermal system or associated upflow zone within the Chupadero crater. Preliminary electrical resistivity data collected along lines crossing Chupadero crater indicate the presence of a WNW-trending zone of low resistivity that passes through Laguna Ixpaco and a cluster of fumaroles located 1 km WNW of the crater. This conductive zone is parallel to the trend of normal faults within the Tecuamburro graben and may mark a fault zone that serves as a conduit for thermal fluids, beyond a hypothetical zone of hydraulically fractured rocks underlying the Laguna Ixpaco phreatic crater. We recommend that an exploration geothermal gradient corehole be drilled midway between Laguna Ixpaco and a cluster of fumaroles 1 km WNW of Ixpaco.

F. REFERENCES

Beaty, D., W. Beyer, J. Dann, J. Reynolds, D. Hyde, C. Nelson, C. Berquist, D. Dobson, E. Erler, M. Hitzman, and G. Jacobsen, 1980. Mapa Geológico de Guatemala: Cuilapa Sheet. Inst. Geograf. Nac., Guatemala City, 1 sheet 1:50000 scale.

Burkhart, B. and S. Self, 1985. Extension and rotation of crustal blocks in northern Central America and effect on the volcanic arc. Geology, 13, 22-26.

Carr, M., 1976. Underthrusting and Quaternary faulting in northern Central America. Geol. Soc. Am. Bull., 87, 825-829.

Carr, M., 1984. Symmetrical and segmented variation of physical and geochemical characteristics of the Central American volcanic front. J. Volc. Geotherm. Res., 20, 231-252.

Heiken, G. and K. Wohletz, 1987. Tephra deposits associated with silicic domes and lava flows. Geol. Soc. Am. Spec. Pap. 212, 55-76.

Ingamells, C., 1970. Lithium metaborate flux in silicate analysis. Anal. Chimica Acta, 52, 323-334.

Newhall, C., 1987. Geology of the Lake Atitlán region, western Guatemala. J. Volc. Geotherm. Res., 33, 23-55.

Peterson, P. and W. Rose, 1985. Explosive eruptions of the Ayarza calderas, southeastern Guatemala. J. Volc. Geotherm. Res., 25, 289-307.

Reynolds, J., 1987. Timing and sources of Neogene and Quaternary volcanism in south-central Guatemala. J. Volc. Geotherm. Res., 33, 9-22.

Siebert, L., 1984. Large volcanic debris avalanches: characteristics of source areas, deposits and associated eruptions. J. Volcan. Geotherm. Res., 22, 163-197.

Stacy, J., N. Sherril, G. Dalrymple, M. Lanphere, and N. Carpenter, 1978. A computer-controlled five-collector mas spectrometer for precision measurement of argon isotope ratios. US Geol. Surv. Open-file Report 78-701, 3 pp.

Steiger, R. and E. Jager, 1977. Subcommission on geochronology: Convention on the use of decay constants in geo- and cosmochronology. Earth Planet. Sci. Lett., 36, 359-362.

Voight, B., H. Glicken, R. Janda, and P. Douglass, 1981. Catastrophic rockslide debris avalanche of May 18. *In* P. Lipman and D. Mullineaux, eds., The 1980 Eruptions of Mount St. Helens, Washington. US Geol. Surv. Prof. Pap. 1250, 347-377.

White, R. A., E. Sanchez, I. Cifuentes, and D. Harlow, 1980. Preliminary report to the government of Guatemala on the on-going earthquake swarm in the Department of Santa Rosa, Guatemala. US Geol. Surv. Open-file Report, 80-800, 17 pp.

Williams, H. and A. McBirney, 1969. Volcanic history of Honduras. Univ. California Publ. in Geol. Sci., 85: 1-101.

Williams, H., McBirney, A., and Dengo, G., 1964. Geologic Reconnaissance of southeastern Guatemala. Univ. Calif. Pubs. in Geol. Sci., 50, 62 pp.

Wunderman, R. and W. Rose, 1984. Amatitlán, an actively resurging cauldron 10 km south of Guatemala City. J. Geophys. Res., 89, 8525-8539.

II. THE USE OF RADON EMANOMETRY IN THE TECUAMBURRO GEOTHERMAL PROSPECT

(A. I. Adams,[1] K. H. Wohletz,[1] L. W. Maassen,[1] F. E. Goff,[1] and Alfredo Roldán-M.[2])

A. INTRODUCTION

Radon-222 occurs in steam, has a short half-life, is almost inert, and is relatively easy to detect. It is ideal for locating some geologic structures. Radon detectors were emplaced in three lines across the Tecuamburro geothermal prospect of Guatemala. Although several techniques were employed to hide and relocate the detectors, the recovery rates were low on two of the three lines. Radon anomalies along the line from Tecuamburro Volcano to Finca La Pastoría show good correlation with faults, geologic contacts, and with a zone containing steam-condensate thermal waters north of Laguna Ixpaco. The data may also indicate the existence of a hydrogeochemical barrier (aquitard) along the north edge of the postulated liquid-dominated reservoir beneath Laguna Ixpaco.

The use of radon detection as a tool in geothermal exploration has been described by Whitehead (1981), Wollenberg (1976), Thomas et al. (1980), Cox (1981), Cuff (1982) and Gutierrez-Negrin (1985; 1987). Because radon is present in geothermal steam (Belin, 1959; Whitehead, 1981) and is transported in the gas phase to the surface through the path of least resistance (Whitehead, 1981), it can be very useful for locating faults and fractures in geothermal areas (Gutierrez-Negrin 1985; 1987).

At the request of the Instituto Nacional de Electrificación (INDE), Los Alamos and Guatemalan scientists emplaced 264 radon detectors along 3 lines intended to intersect major structures in the Tecuamburro Volcano geothermal area. Line "A" was surveyed with emplacement intervals of 100 m along a north-south transect from the north flank of Tecuamburro Volcano to the Finca La Pastoría area in hopes of detecting major structural boundaries or anomalies associated with the Tecuamburro geothermal reservoir (Fig. II.1). Lines "B" and "C" were surveyed with 30-m emplacement intervals in hopes of detecting structures near Colmenares hot springs and Río Los Esclavos.

---

1. Earth and Environmental Sciences Division, Los Alamos National Laboratory, Los Alamos, NM 87545.
2. Unidad de Desarrollo Geotérmico, Instituto Nacional de Electrificación, Guatemala City, Guatemala.

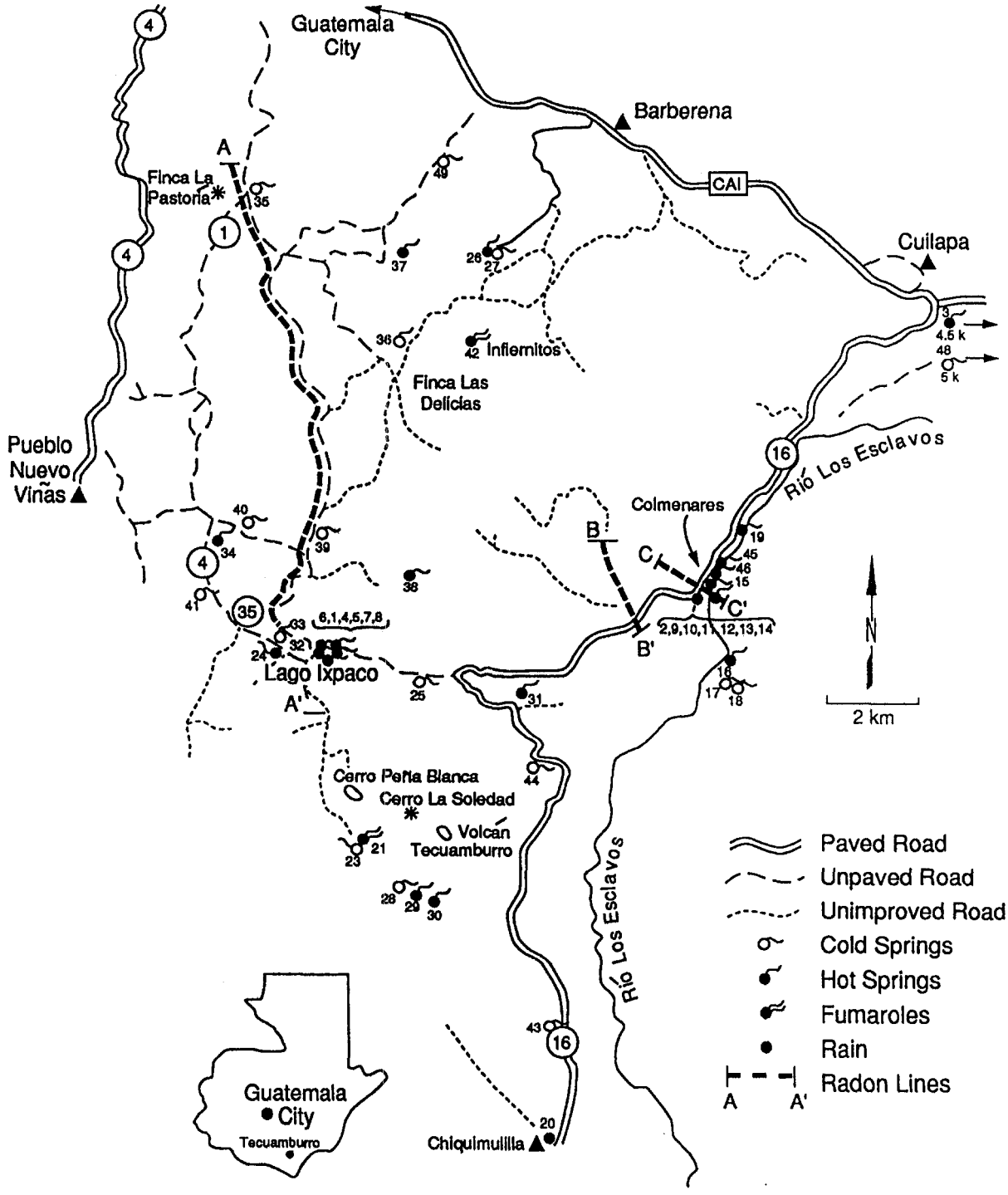

Fig. II.1. Location map of Tecuamburro Volcano region, Guatemala, showing three radon detector traverses.

B. BACKGROUND

Radon is a noble gas that is almost inert, bonding only with fluorine and oxygen. At temperatures above -61.8°C, radon occurs only as a gas in the natural environment (Cotton and Wilkinson, 1972). Rn-222 (the most common isotope) is a daughter product of the decay of U-238 and has a half-life of 3.825 days (Nielson, 1978). Its short half-life makes it ideal for locating geologic structures in a geothermal environment, because the gas can only move short distances from its source. Rn-222 is able to migrate through soil as a gas, and it circulates as dissolved gas in geothermal fluids. In geothermal fluids Rn-222 follows the noncondensable gas phase, separates into vapor as the ascending liquid boils, moves in the vapor to the near surface, and concentrates in residual noncondensable gas as steam decompresses, cools, and condenses (Nielson, 1978). Where faults are active as zones of increased permeability, relatively large amounts of radon gas can migrate to the surface and be detected. However, if the fault is sintered and sealed, it may not allow the gas to migrate and a radon anomaly will not exist.

The radon detector used for this study is a specially treated dielectric material attached to the inside of an inverted cup. The dielectric material is susceptible to radiation damage from alpha particles given off by disintegrating radon atoms. The damage is detected by etching and microscopic examination. The track etch concept (Fleisher et al., 1972) was modified by the Terradex Corporation (Alter and Price, 1974) and provides a passive time-integrated radon concentration measurement (Wollenberg, 1976). The inverted cup is placed in a hole 30-40 cm deep and covered with rock and soil. The thick wall of the cup eliminates any stray alpha particles from entering laterally; therefore, the only radon measured is from the soil or rock directly beneath the inverted cup.

C. EMPLACEMENT

The emplacement and recovery of radon detectors used in geothermal exploration are not trivial. One must be concerned with locating the detectors after a considerable time has elapsed. Much thought went into the development of the emplacement procedures, and our system evolved as we progressed.

We worked in three teams. The first team dug 264 holes, 30-40 cm deep and 10 cm in diameter. The digging team used a 100-m-long rope to measure the distance between holes. The second team labeled the detector serial number and hole number on a small piece of plastic. The cups containing the detectors were buried at the bottom of the hole, and a large nail was placed above the cup about 2-5 cm below the soil surface. The piece of plastic (with serial number and hole number) was placed over the filled hole. A large rock was placed over the plastic and painted a bright

color. The third team checked the plastic label under the rock, cut a blaze mark into a tree or other permanent landmark, drove a nail into the blazed tree pointed roughly in the direction of the hole, painted the nail and blaze, and recorded the hole number, serial number, distance and azimuth of the hole from the landmark.

The following steps were taken to insure location of the burial site:

1.) where it was possible, dug the holes in inconspicuous places;
2.) after emplacement, placed and buried a large ferrous object (in most cases a large nail) in the hole above the cup for later location using a metal detector;
3.) blazed a "permanent landmark" (tree/fence post) with a machete;
4.) drove a large nail into the blaze, pointed in the direction of the hole;
5.) painted the blaze and nail;
6.) measured the distance from the landmark to the center of the hole; and
7.) took a bearing or azimuth with a compass from the nail to the center of the hole.

Our rationale was that, upon returning, we would locate the blazed landmark and nail, find the painted rock, and carefully dig out the detector. If we were unable to locate the painted rock at a given site, we measured the appropriate distance along the azimuth to the hole. If we were unable to locate the hole, we swept the area with a metal detector to locate the ferrous object in the hole. The plastic tag was left over the hole, under the painted rock, to act as camouflage; that is, people passing by would see the painted rock and perhaps investigate. They would find the plastic tag upon removal of the painted rock, which we hoped would satisfy their curiosity.

Unfortunately, upon returning six months later we only found 60% of the detectors although we located over 95% of the holes probably because people recognized the locations and had some use for the plastic cup that contained the detector. In the future we will make the locations less obvious because locating the holes was not as difficult as we had anticipated.

D. DATA

The results of the survey are tabulated in Table II.1 and Fig. II.2.

TABLE II.1. SUMMARY OF RADON VALUES FOR THREE RADON LINES IN THE TECUAMBURRO VOLCANO REGION, GUATEMALA[a]

A-Line	Av Daily[b] Rn Conc (pCi/1)	A-Line	Av Daily Rn Conc (pCi/1)	A-Line	Av Daily Rn Conc (pCi/1)
A-1	453.0	A-59	222.3	A-117	247.8
A-2	268.8	A-60	201.3	A-118	162.5
A-3	126.9	A-61	68.6	A-119	854.1
A-4	113.4	A-62	485.8	A-120	236.0
A-5	239.6	A-63	107.0	A-121	115.5
A-6	181.5	A-64	183.9	A-122	62.7
A-7	N/R	A-65	280.1	A-123	87.8
A-8	458.4	A-66	387.2	A-123A	64.9
A-9	340.8	A-67	169.1	A-124	164.7
A-10	250.6	A-68	510.8	A-125	229.7
A-11	N/R	A-69	357.9	A-126	N/R
A-12	N/R	A-70	111.8	A-127	101.0
A-13	123.2	A-71	217.8	A-128	138.7
A-14	N/R	A-72	324.0	A-129	82.5
A-15	241.6	A-73	345.1	A-130	153.0
A-16	N/R	A-74	128.1	A-131	102.4
A-17	N/R	A-75	82.9	A-132	64.9
A-18	664.7	A-76	210.5	A-133	N/R
A-19	153.0	A-77	63.7	A-134	48.7
A-20	N/R	A-78	86.5	A-135	30.7
A-21	N/R	A-79	117.1	A-136	14.6
A-22	387.2	A-80	217.8	A-137	84.5
A-23	224.2	A-81	446.7	A-138	23.3
A-24	403.7	A-82	314.8	A-139	N/R
A-25	468.7	A-83	379.2	A-140	99.7
A-26	296.6	A-84	358.8	A-141	55.3
A-27	285.6	A-85	325.8	A-142	53.2
A-28	403.7	A-86	286.5	A-143	N/R
A-29	N/R	A-87	208.6	A-144	75.7
A-30	N/R	A-88	249.8	A-145	132.9
A-31	N/R	A-89	106.5	A-146	149.3
A-32	N/R	A-90	527.3	A-147	N/R
A-33	N/R	A-91	306.6	A-148	19.3
A-34	161.0	A-92	277.3	A-149	N/R
A-35	137.2	A-93	338.7	A-150	N/R
A-36	N/R	A-94	493.4	A-151	129.3
A-37	N/R	A-95	216.0	A-152	N/R
A-38	N/R	A-96	130.5	A-153	76.0
A-39	217.8	A-97	131.1	A-154	139.0
A-40	121.2	A-98	92.8	A-155	364.3
A-41	218.7	A-99	195.8	A-156	N/R
A-42	94.7	A-100	396.8	A-157	N/R
A-43	266.1	A-101	96.0	A-158	N/R
A-44	N/R	A-102	621.6	A-159	N/R
A-45	226.0	A-103	493.4	A-160	N/R
A-46	262.4	A-104	633.5	A-161	N/R
A-47	N/R	A-105	116.5	A-162	N/R
A-48	377.3	A-106	95.1	A-163	N/R
A-49	224.1	A-107	N/R	A-164	N/R
A-50	195.9	A-108	372.7	A-165	N/R
A-51	331.7	A-109	413.8	A-166	N/R
A-52	48.4	A-110	441.1	A-167	N/R
A-53	129.3	A-111	N/R	A-168	N/R
A-54	534.1	A-112	235.1	A-169	N/R
A-55	256.0	A-113	230.5	A-170	N/R
A-56	107.2	A-114	86.2	A-171	N/R
A-57	243.3	A-115	179.3	A-172	N/R
A-58	216.8	A-116	473.0	A-173	N/R

[a] Analyses by Tech/Ops Landaur, Inc.
[b] Radon concentration divided by number of days in ground.
N/R = Detector not recovered.

TABLE II.1 (cont)

B-Line	Av Daily Rn Conc (pCi/1)
B-1	144.5
B-2	233.1
B-3	188.6
B-4	N/R
B-5	195.0
B-6	81.3
B-7	215.9
B-8	N/R
B-9	N/R
B-10	165.4
B-11	81.7
B-12	56.5
B-13	283.4
B-14	N/R
B-15	N/R
B-16	N/R
B-17	90.2
B-18	118.1
B-19	60.6
B-20	151.2
B-21	N/R
B-22	N/R
B-23	N/R
B-24	N/R
B-25	N/R
B-26	N/R
B-27	N/R
B-28	N/R
B-29	N/R
B-30	N/R
B-31	N/R
B-32	N/R
B-33	N/R
B-34	34.9
B-35	168.3
B-36	N/R
B-37	N/R
B-38	N/R
B-39	N/R
B-40	N/R

C-Line	Av Daily Rn Conc (pCi/1)
C-1	N/R
C-2	N/R
C-3	N/R
C-4	31.5
C-5	N/R
C-6	N/R
C-7	N/R
C-8	N/R
C-9	N/R
C-10	N/R
C-11	N/R
C-12	N/R
C-13	N/R
C-14	N/R
C-15	58.8
C-16	N/R
C-17	N/R
C-18	N/R
C-19	N/R
C-20	N/R
C-21	N/R
C-22	N/R
C-23	N/R
C-24	N/R
C-25	N/R
C-26	N/R
C-27	N/R
C-28	N/R
C-29	244.2
C-30	N/R
C-31	163.9
C-32	N/R
C-33	192.2
C-34	N/R
C-35	N/R
C-36	158.8
C-37	N/R
C-38	N/R
C-39	N/R
C-40	N/R
C-41	N/R
C-42	N/R
C-43	N/R
C-44	N/R
C-45	N/R
C-46	N/R
C-47	N/R
C-48	N/R
C-49	N/R

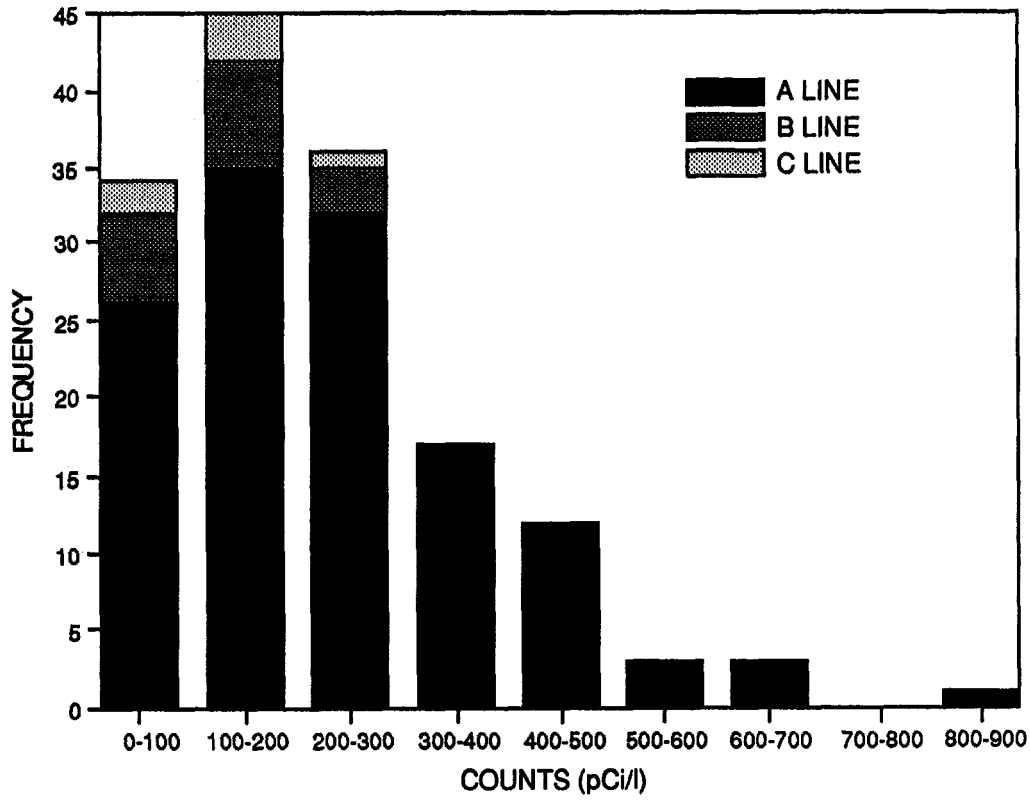

Fig. II.2. Stacked bar graph of three radon detector traverses showing frequency versus counts (pCi/1).

By leaving the detectors in place over a long period of time and then reducing the total counts to the average number of days in place, we reduce the effects of variations in barometric pressure, precipitation, and wind that can cause fluctuations in radon levels. The data points in line "A" are correlated to the geologic structure by a series of structural cross sections along the route of the detector lines (Fig. II.3).

The data are filtered for the cross section; that is, all data points are eliminated below 300 counts (pCi/l) a day. Nielson (1978) uses background levels equivalent to the mean of all points in a survey, which, in our case, is 232 counts (pCi/1) per day. By eliminating all points below 300 counts (pCi/1) per day, the remaining points are considered to be Rn-222 anomalies. Because of the major detector loss on the "B" and "C" lines (60% and 88% lost) and the low values obtained along these lines, the results are not shown on structural sections but are tabulated in Table II.1.

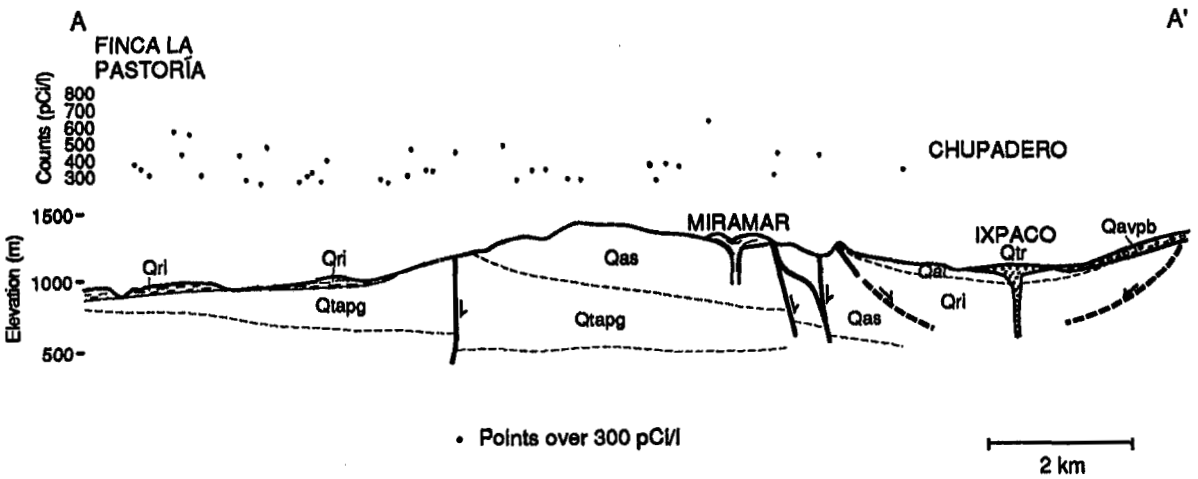

Fig. II.3. Cross section along line A-A' (Fig. II.1) showing radon counts (pCi/l); geology based on map by Duffield et al. (Fig. I.3a).

Qri = hornblende-biotite rhyodacite ignimbrite.
QTapg = pyroxene andesite volcanic complex of Piedra Grande.
Qas = pyroxene andesite lavas and scoria cones of Los Sitios.
Qal = Quaternary alluvium.
Qtr = phreatic tuff ring and enclosed acid lake.
Qavpb = hornblende dacite lava dome of Peña Blanca.

E. RESULTS

The radon anomalies indicate a major structural feature to the north of Laguna Ixpaco that acts as a possible hydrogeochemical barrier (aquitard). This structural feature correlates with a major WNW-trending fault mapped by Duffield et al. (Fig. I.3) and may delineate the northern edge of the liquid-dominated reservoir thought to underlie the Laguna Ixpaco area (Goff et al., in press; Chap. III).

The correlation of radon anomalies with structure (Fig. II.3) shows high radon values at contacts and faults, especially between Laguna Ixpaco and Finca La Pastoría. However, one of the areas of most interest, Laguna Ixpaco, shows no anomalies. This lack of anomalies may be the result of low recovery rates in this area. To the north the radon line closely parallels a large fault and also crosses an area where steam-condensate springs (indicative of steam leakage) are common. These features may explain the high radon values, even though the cross sections do not show many faults in the area (see Fig. I.3.).

Although detector recovery along the "B" and "C" lines was low, there are no anomalous radon values detected in any of the remaining detectors. This would indicate that the lines crossed no major structures, any structures crossed were sealed, or no zones of concealed, subsurface boiling were crossed.

F. REFERENCES

Alter, H. W., and Price, P. B., 1974. Radon detection using track-registration materials. US Patent No. 3,665,194, May 1974.

Belin, R. E., 1959. Radon in New Zealand geothermal regions. Geochim. Cosmochim. Acta, 16, 189-191.

Cotton, F. A., and G. Wilkinson, 1972. *Advanced Inorganic Chemistry.* Interscience, New York, 1145 pp.

Cox, M. E., 1981. Some aspects of geochemical exploration in Hawaii. Proceedings of the New Zealand Geothermal Workshop 1981, pp. 157-162.

Cuff, K. E., 1982. Near surface geochemical investigation in the Las Hornillas fumarolic area, Miravalles Volcano, Costa Rica. Proceedings of the Fourth New Zealand Geothermal Workshop, pp. 461-466.

Fleisher, R. L., H. W. Alter, S. C. Furman, P. B. Price, and R. M. Walker, 1972. Particle track etching. Science, 178, 255-263.

Goff, F., A. H. Truesdell, C. J. Janik, A. Adams, A. Roldán, M., and K. Meeker, 1989. Hydrogeochemical exploration of the Tecuamburro Volcano region, Guatemala. GRC Transactions, 13, 6 pp.

Gutierrez-Negrin, L. C. A., 1985. Radon emanometry in geothermal exploration of volcanic zones. GRC Transactions, 9, 441-445.

Gutierrez-Negrin, L. C. A., 1987. Radon emanometry at the Ceboruco Volcano geothermal zone. GRC Transactions, 11, 159-163.

Nielson, D. E., 1978. Radon emanometry as a geothermal technique: Theory and an example from Roosevelt Hot Spring KGRA Utah. University of Utah Research Institute, Earth Science Laboratory, Report 14, 31.

Thomas, D. M., M. E. Cox, B. R. Lienert, J. P. Kauahikaua, and M. D. Mattice, 1980. Preliminary geothermal assessment surveys of the State of Hawaii. GRC Transactions, 4, 185-188.

Whitehead, N. E., 1981. A test of radon as a prospecting tool in New Zealand. N. Z. J. Sci., 29, 59-64.

Wollenberg, W. A., 1976. Radioactivity of geothermal systems. Proceedings of the Second United Nations Symposium on the Development and Use of Geothermal Resources, San Francisco, pp. 1282-1292.

III. HYDROGEOCHEMICAL EXPLORATION OF THE TECUAMBURRO VOLCANO REGION, GUATEMALA

* Cathy J. Janik,[1] Fraser Goff,[2] Alfred H. Truesdell,[1] Andrew Adams,[2] Alfredo Roldán M.,[3] Kimberly Meeker,[2], P. E. Trujillo Jr.,[2] Dale Counce,[2] and Lynne Fahlquist[1]

A. INTRODUCTION

Chemical and isotopic analyses of thermal and nonthermal waters and gases from springs and fumaroles are used to evaluate the geothermal potential of the Tecuamburro Volcano region, Guatemala. Thermal waters of the acid-sulfate, steam-heated, and neutral-chloride types generally occur in restricted hydrogeologic areas: Tecuamburro-Laguna Ixpaco (acid-sulfate); andesite highland north of Tecuamburro (steam-heated); Río Los Esclavos (neutral-chloride). One small area of neutral-chloride springs east of the village of Los Esclavos is not related to the Tecuamburro geothermal system. Neutral-chloride springs on the Río Los Esclavos east and southeast of Tecuamburro are mixed with various groundwaters and exhibit a maximum ^{18}O enrichment of about 1.5 permil compared to the world meteoric line. Geothermal temperatures calculated from neutral-chloride spring compositions are ≤200°C. In contrast, maximum subsurface temperatures based on gas compositions in the Laguna Ixpaco area are about 300°C. Relation of the neutral-chloride waters to the overall Tecuamburro geothermal system is not entirely resolved but we suggest two hydrogeochemical models. We believe that the first exploration drill hole should be sited within 0.5 km of Laguna Ixpaco to tap the main geothermal reservoir or its adjacent, main upflow zone.

The Tecuamburro Volcano region lies in southeastern Guatemala in the Central American volcanic arc. The region contains volcanic centers of Pleistocene age that are associated with major faults showing Quaternary-age offsets and recent seismic activity. A wide variety of thermal springs and fumaroles occur in the region (Fig. III.1). During July 1988 and February-March 1989, about 100 sample suites of thermal and nonthermal waters and fumarolic gases were collected within a 400-km^2 area (Fig. III.2, Plate 2, and Table III.1, in pocket) near Tecuamburro Volcano. This report presents results of our hydrogeochemical studies of the region. Previous reports on the geothermal potential of the region have been presented by OLADE (1982), Giggenbach (1988), Duffield et al. (1989), and Goff et al. (1989).

---

* **1.** U. S. Geological Survey, 345 Middlefield Rd., Menlo Park, CA 94025. **2.** Earth and Space Sciences Division, Los Alamos National Laboratory, Los Alamos, NM 87545; **3.** Unidad de Desarrollo Geotermico, Instituto Nacional de Electrificacion, Guatemala City, Guatemala

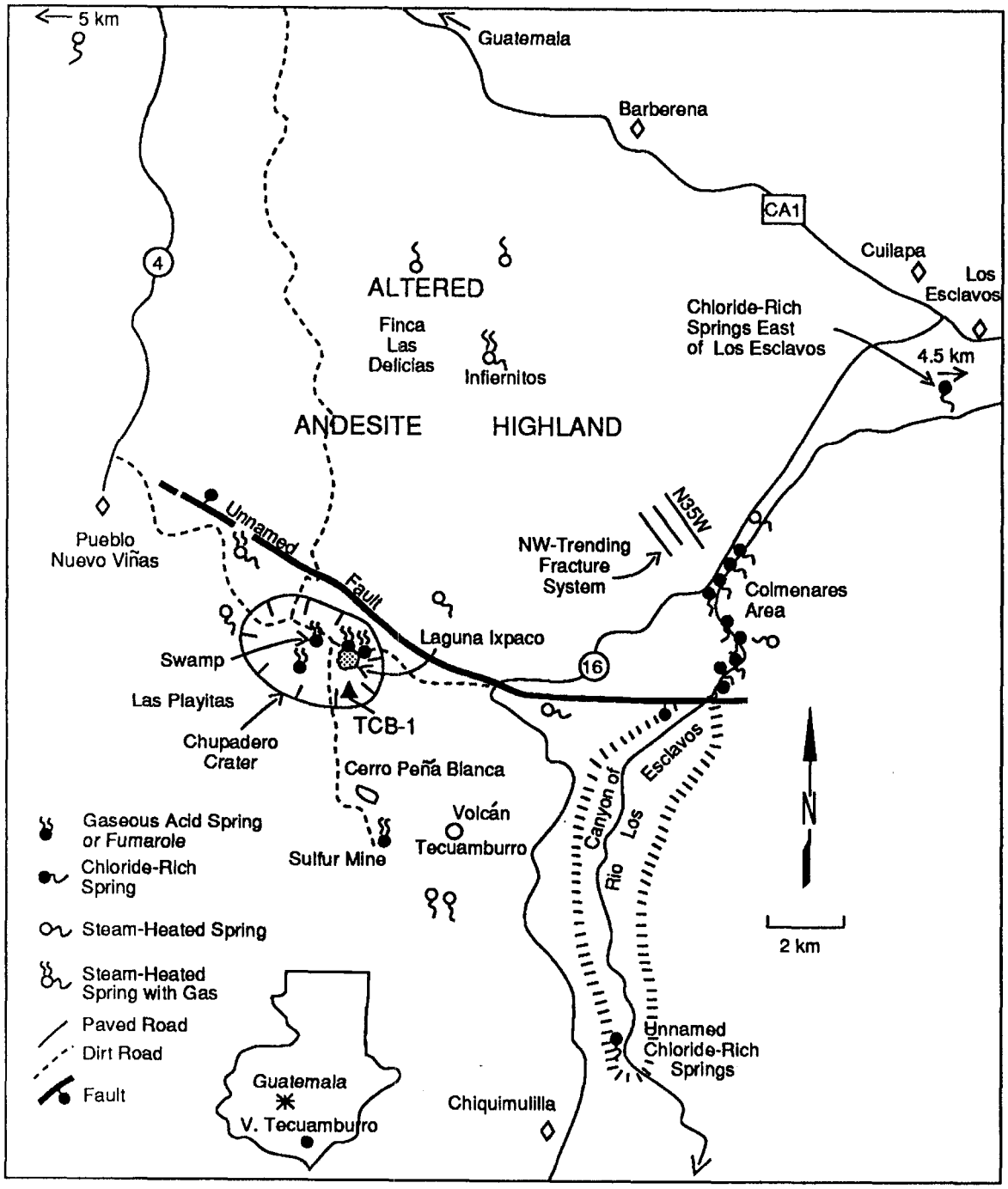

Fig. III.1. Location map of thermal springs and physiographic features, Tecuamburro Volcano region, Guatemala.

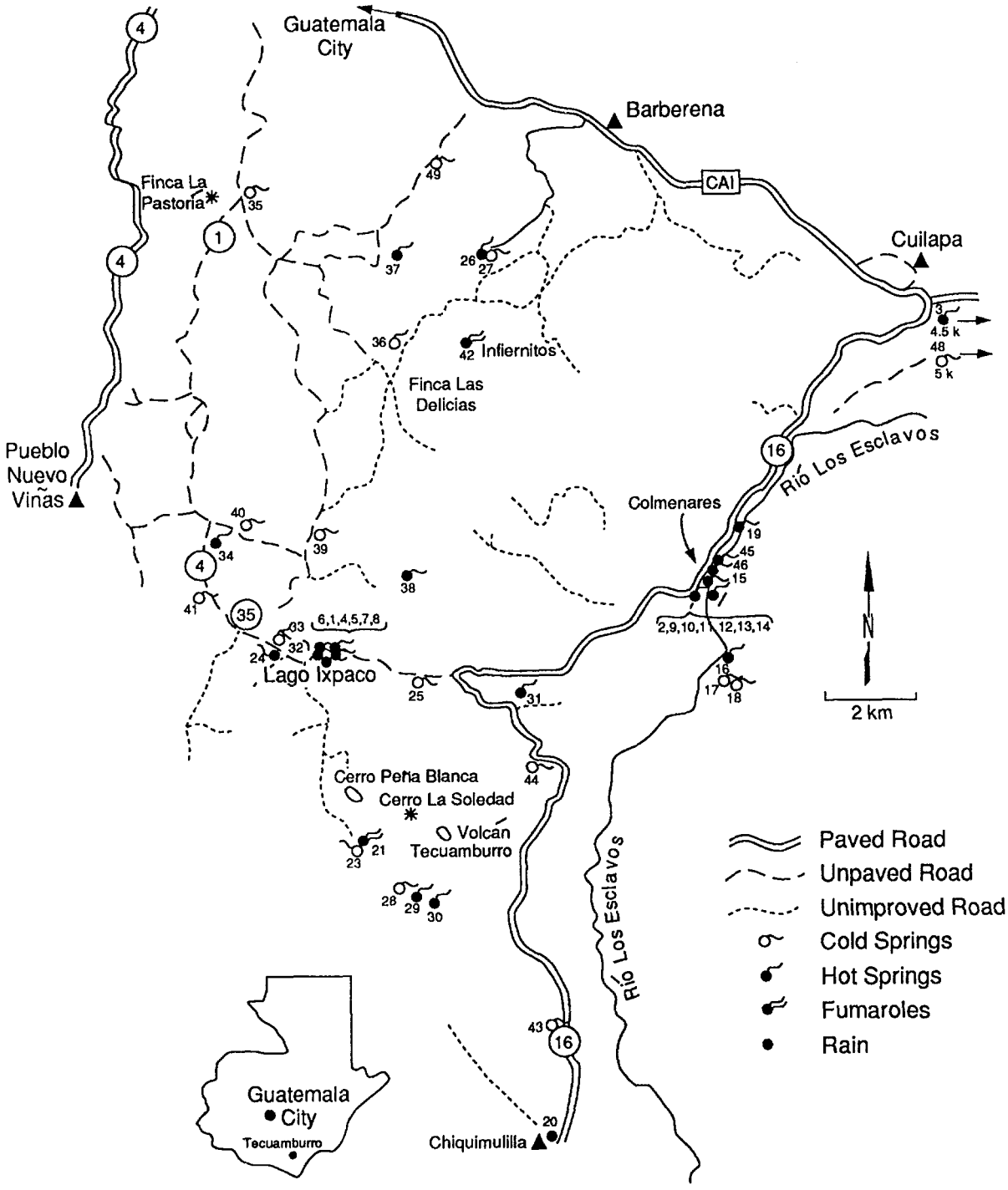

Fig. III.2. Location map of all sampling sites, Tecuamburro Volcano region, Guatemala.

TABLE III.1. CROSS REFERENCE NUMBERING SYSTEM USED FOR LANL/USGS AND INDE SAMPLING SITES, TECUAMBURRO, GUATEMALA (See Fig. III.2 for general locations.)

LANL/USGS Field No.	INDE Field No.	NAME
GT-88-1	TM-13	Site #2 Laguna Ixpaco (Fig. III.3)
GT-88-2		Colmenares Hot Spring (GT-88-13, Fig. III.4)
GT-88-3	TM-1	Warm spring 4.5 km E of Los Esclavos
GT-88-4	TM-13	Site #10 Laguna Ixpaco (Fig. III.3)
GT-88-5	TM-13	Site #8 Laguna Ixpaco (Fig. III.3)
GT-88-6		Site #15 Laguna Ixpaco (Fig. III.3)
GT-88-7		Outflow Laguna Ixpaco
GT-88-8		Large inflow S shore Laguna Ixpaco
GT-88-9	TM-6	Colmenares Hot Spring
GT-88-10		Colmenares "coldest" spring (Fig. III.4)
GT-88-11	TM-5	Colmenares Hot Spring (Fig. III.4)
GT-88-12		Colmenares Hot Spring (Fig. III.4)
GT-88-13		Colmenares Hot Spring (GT-88-2, Fig. III.4)
GT-88-14		Colmenares Hot Spring total outflow (Fig. III.4)
GT-88-15	TM-31	Circa TM-31 hottest spring
GT-88-16	TM-7	Hot spring E side Río Los Esclavos
GT-88-17	TM-34	Finca Agua Tibia
GT-88-18		Large spring 150 m E of TM-34
GT-88-19	TM-19	Warm spring near paved highway
GT-88-20		Rainwater at Chiquimulilla
GT-88-21		Sulfur mine, Tecuamburro
GT-88-22		Sulfur mine, Tecuamburro
GT-88-23		Cold spring at sulfur mine
GT-88-24		Las Playitas
GT-88-25		Cold spring below Chupadero
GT-88-26	TM-17	Warm spring, Finca La Esperanza
GT-88-27	TM-17A	Cold spring, Finca La Esperanza
GT-88-28		Cold spring above TM-12, Finca El Silencio
GT-88-29	TM-12	Large spring Finca El Silencio
GT-88-30	TM-11	Warm spring S side of Tecuamburro
GT-88-31	TM-10	Warm spring at Finca La Morena
GT-88-32	TM-58	Swamp W side Laguna Ixpaco
GT-88-33	TM-58	Swamp W side Laguna Ixpaco
GT-88-34	TM-14a	Finca San Lorenzo
GT-88-35	TM-36	Cold spring Finca La Pastoría
GT-88-36	TM-25	Cold spring Finca Las Delicias
GT-88-37	TM-15,TM-53	Warm spring Finca Bonanza
GT-88-38	TM-33	Hot spring Finca El Chorro
GT-88-39	TM-40	Cold spring
GT-88-40	TM-29	Cold spring Finca San Cayetano

TABLE III.1. (cont)

LANL/USGS Field No.	INDE Field No.	NAME
GT-88-41	TM-26	Warm spring Finca Santa Isabel
GT-88-42	TM-32	Fumarole Infiernitos Finca Las Delicias
GT-88-43		Cold spring by paved road 2-3 km N Chiquimulilla
GT-88-44		Cold spring by paved road 10 km N Chiquimulilla
GT-88-45	TM-2	Hot spring Rio Los Esclavos
GT-88-46	TM-3	Hot spring 80 m downstream from TM-2
GT-88-48		Cold spring 2-3 km E of Los Esclavos on CA#1
GT-88-49		Cold spring near Finca Bonanza
GT-89-53	TM-13	N shore Ixpaco Site #8 (GT-88-5)
GT-89-54	TM-13	N shore Ixpaco Site #10 (GT-88-4)
GT-89-55		Ixpaco inflow (GT-88-8)
GT-89-56		Cold spring W of Chupadero
GT-89-57	TM-7	Hot spring E side Rio Los Esclavos (GT-88-16)
GT-89-58	TM-7	Hot spring Rio Los Esclavos 50 m upstream of 57
GT-89-59	TM-8	Hot spring 30 m downstream of TM-8
GT-89-60		Warm spring E bank of Rio Los Esclavos along cliff
GT-89-61		Hot spring 30 m downstream of GT-60
GT-89-62		Hot spring 100 m downstream of GT-61 E of Rio
GT-89-63	TM-9	Across river from TM-9
GT-89-64		Cold spring W side of Rio Los Esclavos
GT-89-65		Cold spring E wall of canyon of Rio Los Esclavos
GT-89-66		Warm spring at Finca Santa Marta
GT-89-67	TM-29	Cold spring Finca San Cayetano(GT-88-40)
GT-89-68	TM-14A	Finca San Lorenzo (GT-88-34)
GT-89-69	TM-58	Swamp W of Laguna Ixpaco (GT-88-32)
GT-89-70		Las Playitas (GT-88-24)
GT-89-71	TM-2	Hot spring Rio Los Esclavos (GT-88-45)
GT-89-72	TM-3	Hot spring 80 m downstream from (GT-88-46)
GT-89-73	TM-1	Warm spring 4.5 km E of Los Esclavos
GT-89-74	TM-1	Hottest seep at TM-1 area
GT-89-75		Rio Los Esclavos, above to mineral seeps
GT-89-76		Cold spring E of Los Esclavos (GT-88-48)
GT-89-77	TM-12	Finca El Silencio (GT-88-29)
GT-89-78		Cold spring above TM-12, Finca El Silencio (GT-88-28)
GT-89-79		Cold spring at Azufral (GT-88-23)
GT-89-80		Sulfur mine, Tecuamburro (GT-88-21

TABLE III.1. (cont)

LANL/USGS Field No.	INDE Field No.	NAME
GT-89-81	TM-33	Finca El Chorro (GT-88-38)
GT-89-82		Site #8 Laguna Ixpaco
GT-89-83	TM-6	Colmenares (GT-88-9)
GT-89-84	TM-6	Colmenares (GT-88-10)
GT-89-85	TM-6	Colmenares hottest spring (GT-88-12)
GT-89-86		Colmenares outflow (GT-88-14)
GT-89-87	TM-31	Hot spring (GT-88-15)
GT-89-88	TM-19	Warm spring (GT-88-19)
GT-89-90	TM-17	Hot spring Finca La Esperanza (GT-88-26)
GT-89-91	TM-17A	Cold spring (GT-88-27)
GT-89-92	TM-15	Warm spring Finca Bonanza (GT-88-37)
GT-89-93		Cold well, Barberena drinking water
GT-89-94		Cold well in Barberena S side of hwy
GT-89-95		Cold seep near GT-89-97
GT-89-96		Cold spring N of GT-89-95
GT-89-97		Warm spring SSE side of Tecuamburro Volcano
GT-89-98		Cold spring 100 m upstream of GT-89-97
GT-89-99		Rainwater at Hotel San Carlos
GT-89-100	TM-25	Cold spring Finca Las Delicias (GT-88-36)
GT-89-101	TM-32	Fumarole Infiernitos Finca Las Delicias (GT-88-42)
GT-89-102	TM-36	Cold spring Finca La Pastoria (GT-88-35)

B. GEOHYDROLOGY

1. Geologic Setting

The Tecuamburro region occurs in the northwestern corner of the Caribbean plate near the intersection with the North American and Pacific plates (Burkart, 1983; Chap. I). This tectonic regime has undergone considerable Neogene tectonic activity expressed as left-lateral slip along the Polochic-Motagua fault system and as a series of north-trending structural grabens south of this fault system. The Jalpatagua fault zone (north of the Tecuamburro region) and the Tecuamburro graben are typical structural elements within this tectonic regime and are important structural elements to the Tecuamburro geothermal system (Chap. 1). Although there is no known historic seismicity for the Jalpatagua fault zone, a swarm of earthquakes occurred in 1979-1980 that are correlated with motions on the eastern graben fault of the Tecuamburro Graben (White et al., 1980; Chap. I).

The volcanic history of southeastern Guatemala is complex and has been continuous for the last 15 Ma (e.g. Carr et al., 1982; Newhall, 1987; Reynolds, 1987). Although the region is dominated by calc-alkaline andesite and basaltic andesite, major eruptions of basalt, dacite, and rhyolite are interbedded within the andesitic rocks.

Geology of the immediate Tecuamburro area is described by Beaty et al. (1980), Reynolds (1987), and Duffield et al. (this report). Tecuamburro volcano is an andesitic composite cone of late Pleistocene age (0.1 to ≤0.04 Ma). Andesitic domes and flows are interbedded with laharic breccias and landslide debris from episodes of volcanism and sector collapse.

A Pleistocene scoria cone field of predominantly basaltic rocks straddles the Jalpatagua fault zone in the northern part of the region investigated. The cones and flows retain very youthful morphology, and one flow is dated at 0.036 Ma (Duffield et al., this report). On the east and west flanks of the Tecuamburro Graben are Ixhuatán and Pueblo Nuevo Viñas volcanic centers (andesitic) of slightly older age (1 to 2 Ma). Flows and laharic breccias of Ixhuatán andesitic rocks are well exposed in the canyon of the Río Los Esclavos east of Tecuamburro.

2. General Stratigraphy

A generalized regional stratigraphy is shown in Figure III.3 (Bonis et al., 1970; Beaty et al., 1980; Reynolds, 1987; Chap. I). We stress that the depth to and thickness of Mesozoic and Paleozoic rocks is unknown and that the thickness of Tertiary volcanic rocks is highly variable. In addition, there may be local intrusions of Tertiary age that are not represented on this figure (Beaty et al., 1980).

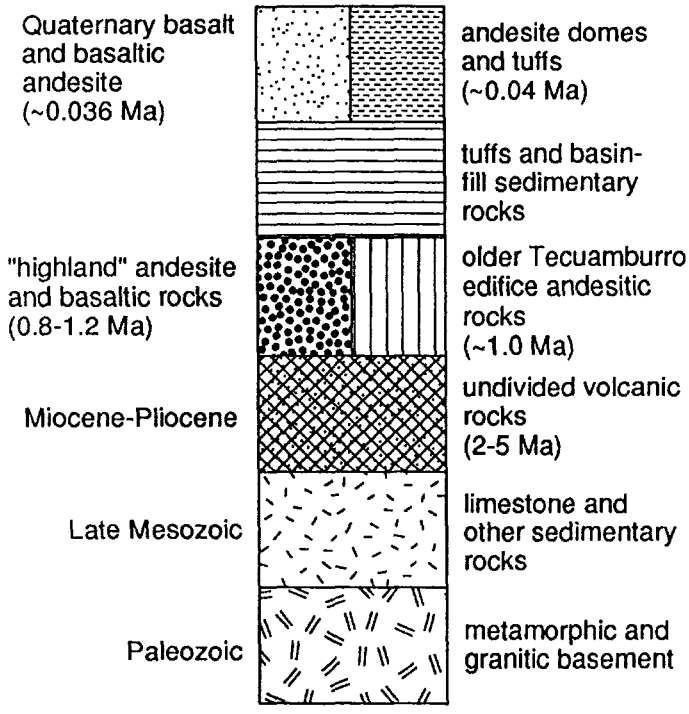

Fig. III.3. Block diagram showing generalized stratigraphic relations of rock units, Tecuamburro Volcano region, Guatemala; all spring and well samples issue from Tertiary to Quaternary volcanic units.

a. Paleozoic Basement. An undivided unit that consists mainly of phyllite, schist, and gneiss is not exposed in the Tecuamburro region but does crop out in a broad east-west belt about 50 km north of Barberena and in an isolated patch about 100 km east of Barberena. Both of the above exposures are south of the Motagua fault zone but their structural relation to younger rocks is not well known.

b. Late Mesozoic Rocks. An undivided unit that consists primarily of Cretaceous carbonate strata is not exposed in the Tecuamburro region, but a 10-km-long exposure occurs about 15 km east of Cuilapa and small outcrops occur about 30 km north of Barberena. Reynolds (1987) claims that these outcrops are part of the Yojoa Group, a widespread limestone-bearing unit exposed through northwestern Guatemala and western Honduras (Carpenter, 1954).

c. Miocene-Pliocene Volcanic Rocks. An undivided unit that consists mainly of andesitic domes, flows, laharic breccias, and rhyolitic ignimbrites is from earlier volcanic activity related to formation of the Central American volcanic arc. K/Ar dates for these rocks in southeastern Guatemala range from about 2 to 15 Ma (Reynolds, 1987). Maximum thickness is unknown but may locally exceed 1000 m.

d. Late Tertiary-Quaternary Volcanic Rocks. Quaternary rocks in the Tecuamburro region are described in detail in Chap. I. Andesitic to basaltic domes, flows, laharic breccias and tuffs of the Tecuamburro Volcano and volcanoes of the andesitic highland are the major units. Some interfingering with andesitic rocks of the Ixhuatán and Pueblo Nuevo Viñas volcanic centers may occur. A valley-fill unit consisting primarily of ignimbrites from an unknown source fills the valleys west and north of the andesitic highland. Basaltic cinder cones and flows straddle the Jalpatagua fault zone. Terrace gravels and alluvium border the Río Los Esclavos. Maximum thickness of andesitic rocks at Tecuamburro Volcano exceeds 1000 m.

3. Heat Flow

No heat flow data are available for Guatemala. Heat flow has been measured in the Cordillera de Guanacaste of Costa Rica, at the southern end of the Central American volcanic arc (Blackwell et al., 1977). Background heat flow in the Cordillera, composed mostly of Pliocene and Pleistocene andesitic stratovolcanoes and subordinate silicic calderas, is about 60 mW/m^2, which is equivalent to 1.5 heat flow units (HFU). This value is common for island arc settings, where rainfall and the presence of porous volcanic sequences favor downward circulation of cool meteoric water that suppresses regional heat flow.

In contrast, a heat flow of 550 mW/m^2 (13 HFU) is associated with the hydrothermal system at Volcán Miravalles, Costa Rica (Blackwell et al., 1977). Similar thermal gradient anomalies are observed for the hydrothermal-convective systems at Momotombo, Nicaragua (Lopez et al., 1980), at Ahuachapán, El Salvador (Vides, 1976), at Amatitlán, Guatemala

(Tobias, 1987) and at Zunil, Guatemala (MK-Ferguson, 1988). Like Tecuamburro, each of these sites lies adjacent to major, late Quaternary andesite stratovolcanoes and/or calderas. Shallow temperature gradients at these locations commonly exceed 500°C/km.

Heat flow associated with hydrothermal systems in the back-arc tectonic environment of Honduras can exceed 250 mW/m^2 (Meert and Smith, in press). Regional heat flow in the back arc environment was estimated at about 120 mW/m^2 by Goff et al. (1987), using an empirical relation between silica content of cool groundwaters and heat flow developed by Swanberg (1979). This relation is based on the solubility of quartz. Unfortunately, the Tecuamburro region is characterized by relatively young volcanic rocks containing abundant amorphous silica, whereas rocks in Honduras are mostly schist, gneiss, sandstone, shale, conglomerate, limestone, and older volcanic deposits in which the silica exists mainly as quartz/chalcedony. Therefore, background silica concentrations in cool groundwaters in the Tecuamburro region are nearly twice as high as those in Honduras (76 versus 43 mg/kg). Calculated regional heat flow using the data in Table III.2 and equations of Swanberg (1979) is ~165 mW/m^2 or nearly 4 HFU, a value much higher than is reasonable for an area of such high rainfall and rugged topography. Although exceptionally high heat flow must occur near thermal springs and fumaroles, we would expect regional values to be more like those determined by Blackwell et al. (1977) in the Costa Rican volcanic chain; about 60 mW/m^2.

4. Thermal Features

The main area of geothermal exploration lies within the 20-km-wide Tecuamburro Graben extending from the volcano north to the WNW-trending Jalpatagua fault zone. Between this fault zone and the volcano, and within the structural graben lies a broad highland of andesitic and basaltic rocks comprising several volcanic centers that were active from at least 1.2 to 0.8 Ma (Chap. I). Local zones of intense hydrothermal alteration are evident in these rocks. The highland is characterized by steam-heated hot springs of which Fumarole Infirnitos (Figs. III.1 and III.2) is the only one that is boiling.

The altered basaltic rocks of Fumarole Infirnitos are laced with calcite veins containing abundant pyrite and up to 40 ppm Cu and 70 ppm Zn. Four U-Th disequilibrium dates on one calcite vein sampled within the hot spring area have an isochron age of 136 ± 22 ka (T. Ku, University of Southern California, personal communication, 1989). Because the present steam-heated waters are very dilute and not depositing calcite, this age represents an earlier hydrothermal event in the area.

Areas of acid-sulfate hot springs and fumaroles are found near the summit and on the northern flank of Tecuamburro Volcano. An abandoned sulfur mine in the summit area contains active, H_2S-rich fumaroles. About 6 km north of the mine, near the base of the Tecuamburro domes, is a 2910 ± 70-year-old phreatic crater about 500 m in diameter that contains an acid lake (Laguna Ixpaco; pH=3). Vigorous

TABLE III.2. SELECTED PHYSICAL, CHEMICAL, AND ISOTOPIC DATA FOR 30 COLD WATERS OF THE TECUAMBURRO VOLCANO REGION, GUATEMALA

Sample No.	Name	Measured Temp. (°C)	SiO_2 (mg/kg)	Cl (mg/kg)	δD (‰)	$\delta^{18}O$ (‰)	^3H (T.U.)	Rock Type
GT88-8	Inflow to Laguna Ixpaco	22.1	67	1.9	-60.3	-8.90	4.53	Andesite
GT89-55	Inflow to Laguna Ixpaco	20.0	81	2.5			--	Andesite
GT89-23	Cold spring near summit of Tecuamburro	20.0	48	2.5	-59.5	-8.49	5.55	Andesite
GT89-79	Cold spring near summit of Tecuamburro	17.5	53	1.7			5.53	Andesite
GT89-25	Spring below Chupadero	22.3	79	2.5	-62.5	-4.74	7.41	Andesite
GT89-56	Spring west of Chupadero	22.2	82	5.7			5.24	Andesite
GT89-27	Cold spring at Finca La Esperanza	21.3	68	1.4	-49.2	-7.19	--	Andesite
GT89-91	Cold spring at Finca La Esperanza	17.2	88	1.0			--	Andesite
GT89-28	Cold spring above Finca El Silencio	24.1	74	1.2	-51.8	-7.88	--	Andesite
GT89-78	Cold spring above Finca El Silencio	25.1	83	1.5			6.15	Andesite
GT89-35	Cold spring north of Finca La Pastoría	23.4	90	4.3	-46.9	-6.93	8.29	Rhyo. Tuff
GT89-102	Cold spring north of Finca La Pastoría	23.5	102	4.8			--	Rhyo. Tuff
GT89-36	Cold spring, Finca Las Delicias	22.2	33	1.6	-51.9	-7.84	7.11	Basalt
GT89-100	Cold spring, Finca Las Delicias	20.7	36	1.5			6.94	Basalt
GT89-39	Unnamed cold spring	20.4	64	14.4[a]	-52.9	-7.72	4.51	Andesite
GT89-40	Cold spring at Finca San Cayetano	25.3	88	0.6			2.85	Andesite
GT89-67	Cold spring at Finca San Cayetano	22.4	90	0.8	-53.5	-7.91	--	Andesite
GT88-43	Unnamed cold spring	24.8	85	1.5	-54.4	-7.75	--	Andesite
GT88-44	Unnamed cold spring	24.7	53	25.3[b]	-48.6	-7.04	--	Andesite
GT88-48	Cold spring east of Los Esclavos	22.7	57	2.3	-44.7	-6.82	3.50	Andesite
GT89-76	Cold spring east of Los Esclavos	21.1	78	1.0			--	Andesite
GT89-49	Unnamed cold spring	22.8	99	28.5[c]	-40.1	-5.97	--	Rhyo. tuff
GT89-64	Cold spring, Río Los Esclavos	25.0	95	3.0			--	Andesite
GT89-65	Cold spring, above Río Los Esclavos	20.8	98	1.4			6.20	Andesite
GT89-75	Río Los Esclavos above TM-1	30.0	61	14.4[d]			--	Varied
GT89-93	Cold well, Barberena	21.9	70	2.5			--	Basalt
GT89-94	Cold well, Barberena	21.7	93	15.7[e]			6.62	Basalt
GT89-98	Cold spring, Río Los Esclavos	27.8	94	1.9			--	Andesite
GT88-20	Rain, Chiquimulilla	~20.0	--	--			3.52	--
GT89-99	Rain, Los Esclavos	~20.0	<1	2.7	-14.5	-2.67	3.07	--
	AVERAGE	22.3±2.4[f]	76±19[f]	2.1±1.3[g]				

[a] Contains 163 mg/kg NO_3 from fertilizing operations, Cl value in doubt.
[b] Contains 599 mg/kg NO_3 from fertilizing operations; Cl value in doubt.
[c] Contains 342 mg/kg NO_3 from fertilizing operations; Cl value in doubt.
[d] Cl value anomalous possibly due to sewage, evaporation, unknown hot springs, or ?
[e] Cl value anomalous from chlorination for drinking.
[f] Average value does not include GT89-75, GT88-20, or GT89-99.
[g] Average value does not include GT88-20, GT88-39, GT88-44, GT88-49, GT89-75, GT89-94, or GT89-99.

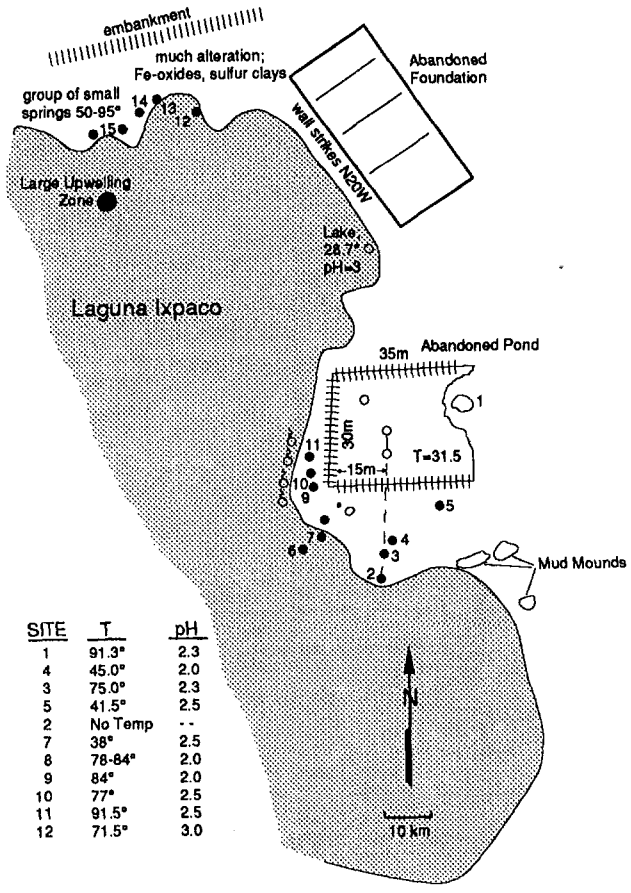

Fig. III.4. Location map of thermal features, Laguna Ixpaco, Tecuamburro Volcano region, Guatemala.

acid-sulfate hot springs and mud pots are located around the northern shore, and a large zone of upwelling gas is visible about 20 m offshore (Fig. III.4). Two small areas of low-temperature acid springs are located about 1 to 1.5 km west of Laguna Ixpaco (swamp and Las Playitas, Fig. III.1)

We have examined three areas of neutral-chloride hot springs in the Tecuamburro region. The most impressive area (35° to 97°C springs) occurs near Colmenares along a 7-km stretch of the Río Los Esclavos northeast of Tecuamburro Volcano. At Colmenares proper (Fig. III.5) is a cluster of springs issuing from andesitic alluvium about 150 m west of the river. Within this cluster are springs ranging from 50° to 94°C, and the total discharge is 0.04 m^3/s. Another cluster of springs issues from alluvium on the west bank of the river just north of Colmenares proper and a third cluster of springs issues from fractured andesitic laharic breccias 0.5 km farther north. More neutral-chloride springs issue from terrace gravels and andesitic rocks on both sides of the river south of Colmenares.

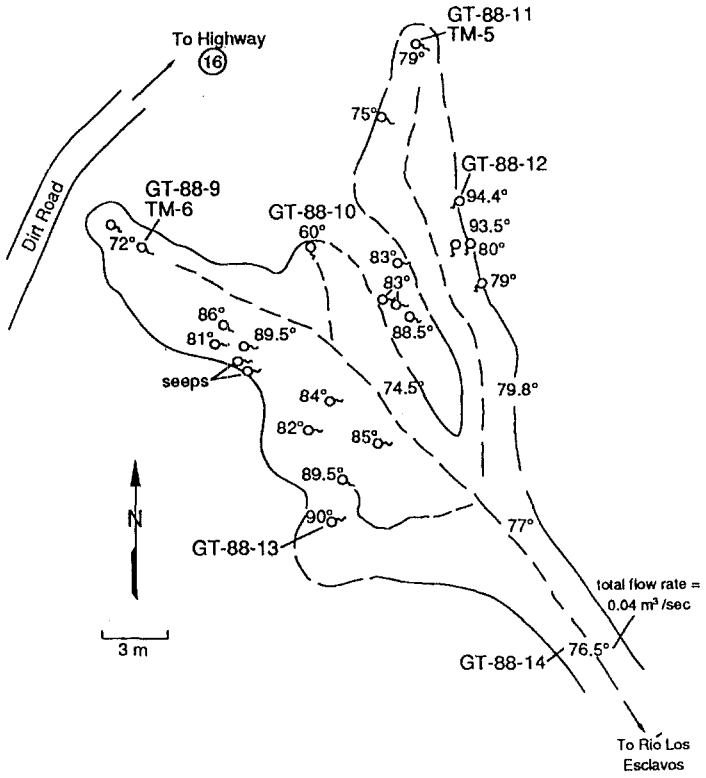

Fig. III.5. Location map of thermal features, Colmenares site, Tecuamburro Volcano region, Guatemala.

The Colmenares group comprises approximately 60 springs and seeps in total. Where the relation of springs to "bedrock" is visible, all springs issue from fractured andesitic rocks and the fractures are generally oriented in a N10W to N40W direction. The southern boundary of the Colmenares Group occurs where the Río Los Esclavos crosses a major E-W-trending fault zone (Fig. III.1). At this location, the fault is a normal fault with down to the south displacement. The northern boundary of the group is not structurally defined in outcrop.

A second area of neutral-chloride springs (30° to 42°C) occurs about 4.5 km east of the village of Los Esclavos. The springs discharge from a gravel bar and along a small bench of andesite on the north side of the Río Los Esclavos over a distance of about 200 m.

A few neutral-chloride springs (≤39°C), located about 3 km northeast of Chiquimulilla, issue from alluvium and andesitic rocks on the west bank of the Río Los Esclavos. An altered zone of laharic breccia beneath terrace gravels is exposed on the western wall of the canyon about 0.5 km south of the hot spring. The zone is 15 m high and 30 m wide and contains sulfur, sulfate salts, and clays. No spring or fumarole was found in this zone in March 1989. No other thermal features were found in the canyon of the Río Los Esclavos east of Tecuamburro Volcano. Clearly, the river controls the discharge elevation of all neutral-chloride springs in the region. Very weak gas emanations are visible in some neutral-chloride springs at each location.

C. GEOCHEMISTRY

1. Models for Volcanic Geothermal Systems

Various conceptual hydrologic-geochemical models have been proposed for geothermal systems based on surface and drillhole rock and fluid chemistry, exposed fossil hydrothermal systems, and chemical theory. These models suffer from decreasing availability of information with increasing depth in the system, but they present generalizations from a number of better known geothermal systems that are likely to be useful at Tecuamburro. Physical hydrologic models of heat transfer in geothermal systems have been discussed by Elder (1981) and many others. We are more interested in geochemical models because essentially all of our data are chemical. Several authors have discussed origin of particular water types in geothermal systems (e.g., White, 1957; Ellis, 1970; Mahon, 1970) but the most useful syntheses of these ideas are from Henley and Ellis (1983) and (particularly for the deeper zones) Giggenbach (1981) and Giggenbach et al. (1989). Figures III.6 and III.7 are from Henley and Ellis (1983) and Figures III.8 and III.9 are from Giggenbach (1981, 1989). These show fluid flows, temperatures and water types of geothermal systems related to caldera-type volcanism and to andesitic stratovolcanoes.

Caldera-related geothermal systems are well known from extensive exploration and production drilling at Wairakei and Broadlands, New Zealand, and from research drilling and extended geological and geochemical studies at Yellowstone Park and the Valles caldera, USA (White et al., 1975; Nielson et al., 1988). Deep neutralization of acid volcanic gases and extensive mixing with meteoric waters produce a plume of neutral high-chloride water with high K and SiO_2 in the center of the system (Fig. III.8). This type of water has also been proposed to originate from leaching of soluble constituents from volcanic rocks by heated meteoric waters. This water is characteristic of most exploited, high-temperature, hot water geothermal systems.

Most variations in geothermal waters result from processes taking place in the upper 1-3 km as shown in Fig. III.6. The upflowing water starts to boil when pressures decrease, forming steam that contains CO_2, H_2S, and other gases. Part of this steam condenses into shallow groundwaters, and CO_2 reacts with rocks to form $NaHCO_3$ "steam-heated" groundwaters. Only a small amount of H_2S is oxidized to SO_4 by aerated groundwater, and most reacts with Fe in rock to form pyrite. When the steam condenses at the surface (in the unsaturated zone), H_2S reacts with oxygen in air to form sulfuric acid. This acid reacts with rock and is partially neutralized to form "acid-sulfate" spring waters with metals and silica leached locally. Neutral chloride waters mixed near the surface with meteoric waters may emerge as diluted chloride springs. The neutral-chloride spring waters and these diluted chloride springs carry the most chemical information about subsurface conditions.

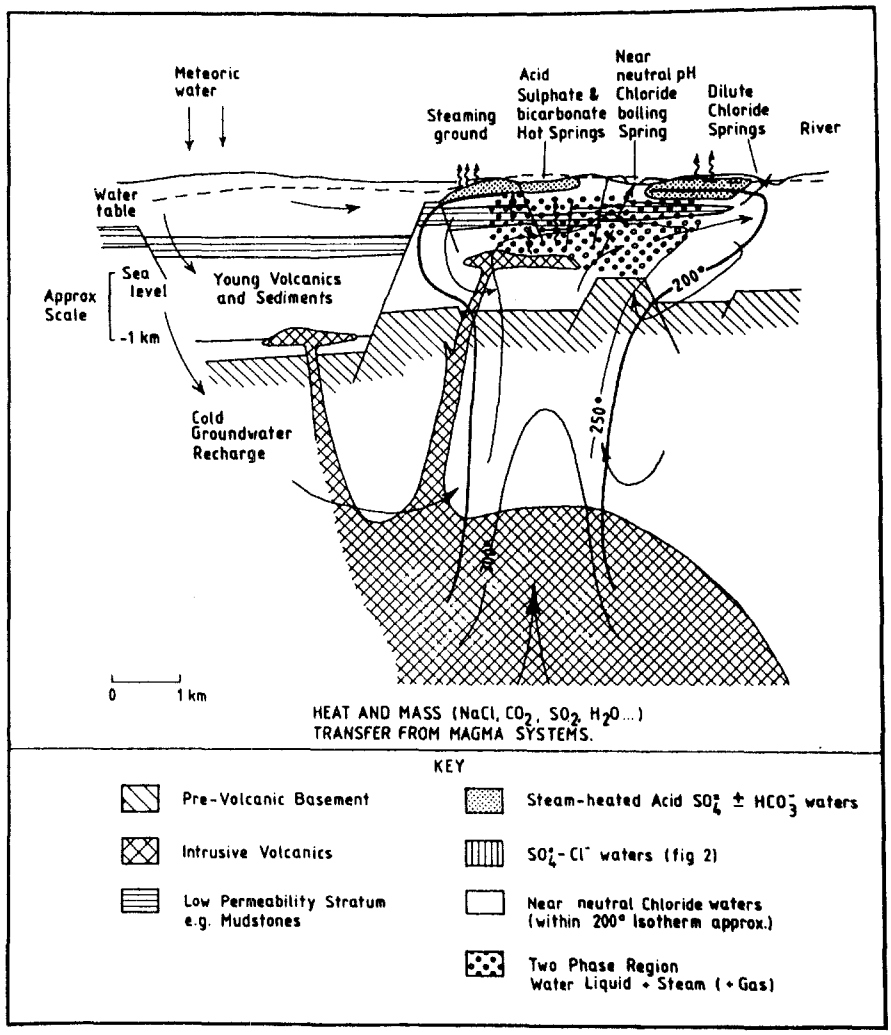

Fig. III.6. Schema of the main features of a geothermal system typical of those in silicic volcanic terranes. The system is supplied by groundwater, in this case derived from meteoric water. Heat, together with some gases, chloride, water, and some other solutes, is assumed to be supplied by a deeply buried magmatic system and results in a convecting column of near-neutral pH chloride water with two phase conditions in the upper part of the system. Steam-separation processes give rise to fumaroles and steam absorption by groundwater, with oxidation of H_2S at the water table, gives rise to isotopically enriched steam-heated, acid-sulfate, and bicarbonate waters. Mixing may occur between the deeper chloride waters, steam-heated waters, and fresh groundwater to give a range of hybrid waters. Outflows from the deep chloride system occur either as boiling alkaline springs often associated with silica terraces, or after mixing with cold groundwaters, as near-neutral pH relatively dilute chloride springs (from Henley and Ellis, 1983).

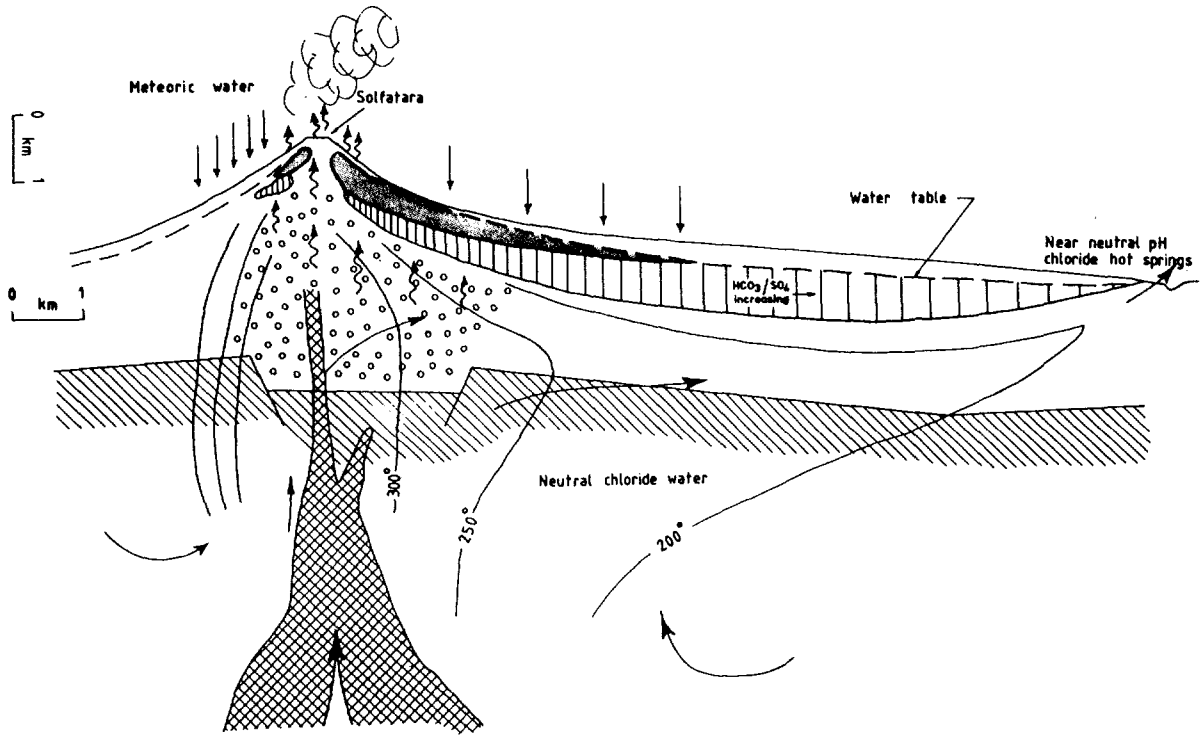

Fig. III.7. Schema of a geothermal system typical of active island-arc andesite volcanoes. Lower permanent water tables in tropical regions and the high relief of the volcanic structures result in a scarcity of chloride water discharges except at some distance from the upflow center. The latter may be revealed by fumaroles, intense rock alteration, and steam-heated, often perched, aquifers. Near-surface condensation of volcanic gases and oxidation result in acid-sulfate waters in the core of the volcano, and an acid crater lake may also form (from Henley and Ellis, 1983).

Geothermal systems related to active andesitic volcanoes are more complex (Figs. III.7 and III.9). The central conduit of these volcanoes may remain very hot and prevent access of meteoric water, with ascending fluids forming high-temperature summit fumaroles carrying steam with HCl and SO_2. These gases are compatible only with highly acidic waters not found at shallow depths in a caldera geothermal system. Neutral high-chloride reservoir waters of volcano-related geothermal systems are displaced laterally from the hot, acidic core to locations where reaction with rock has neutralized acids and temperatures are low enough for liquid to be present. These relations are seen in the proposed model for Nevado del Ruiz Volcano, Colombia (Fig. III.9); Nevado del Ruiz is much larger and more mature than Tecuamburro, but can be used as a similar model system. Topography and near surface meteoric water may prevent surface discharge of neutral high-chloride water except as diluted springs at a distance from the volcano (Fig. III.7). Long passage

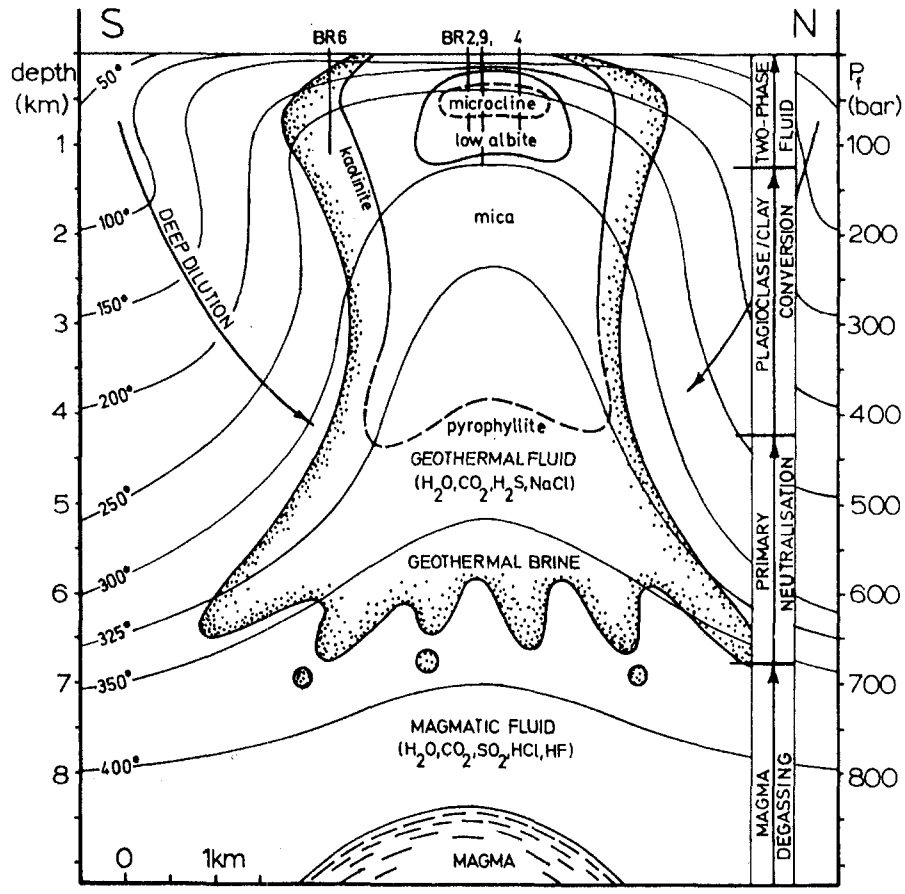

Fig. III.8. Schematic cross section of a caldera-hosted geothermal system of the Broadlands type. CO_2, H_2S and the other constituents of the geothermal fluid are assumed to be largely derived through interaction of gases (H_2O, CO_2, SO_2, HCl, HF) released from a magma located at an arbitrary depth of around 8 km with deeply circulating groundwaters and rock (from Giggenbach, 1981).

through cooler rocks is likely to cause reequilibration of geothermometer temperatures, and (unlike dilute chloride spring waters in caldera systems with short flow paths cooled only by mixing) these waters may not be useful for indicating conditions in the main reservoir. In these systems only steam moves rapidly from the reservoir fluid to the surface, and only gases in the steam may be useful in geothermometer calculations.

The models shown for stratovolcano-related systems depend on the intensity of the volcanic activity and maturity of the composite cone. If the activity is not sufficiently intense to maintain high-temperature fumaroles with acid gases, the geothermal reservoir (with neutral waters) may be closer to the center of the edifice; if the activity is greater, it may

occur farther away. In addition the zones may be asymmetric or tilted, depending on geologic factors. Thus the models give only general guidance to the exploration of any particular system.

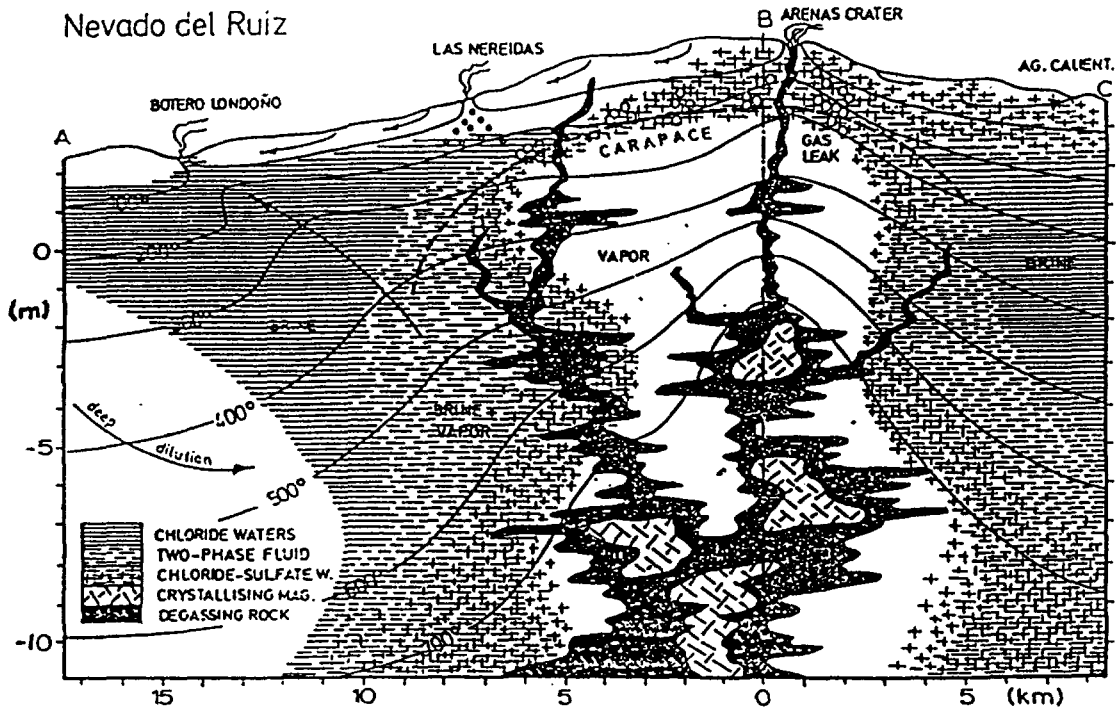

Fig. III.9. Tentative cross section through Nevado del Ruiz volcanic structure showing potential distribution of fluids compatible with geochemical findings. The Ruiz model has never been tested by drilling (from Giggenbach et al., 1989).

It is important to distinguish fluids produced from the geothermal system and those from the volcanic system. All fumaroles are not the same. Surface temperatures >200°C are characteristic of volcanic fumaroles, and volcanic steam originating directly from a magma body contains carbon and sulfur gases in their various oxidation states (CO_2, CO, SO_2, H_2S) together with HCl, HF, and H_2. High CO_2 and H_2S, the absence of SO_2, HCl, and HF, and surface temperatures <160°C (more often near local boiling temperature) are characteristic of geothermal fumaroles. Neutral, high-chloride, high-SiO_2 (compared with meteoric waters) spring waters cannot be solely of volcanic origin and must indicate some sort of high-temperature geothermal reservoir.

2. Fluid Chemistry and Stable Isotope Compositions

Approximately 100 thermal and nonthermal water samples and 20 gas samples from springs and fumaroles were chemically and isotopically analyzed for our geochemical investigation of the Tecuamburro Volcano region. Most sampling locations are shown on Fig. III.2 (all are shown on the large map, plate 2, in pocket), and a description of each site (including field measurements and flow data) is given in Appendix C,

Table C-1. Complete chemical analyses (major and trace element) and isotopic measurements are given in Tables C-2, C-3 and C-4. The LANL/USGS numbering system used to identify sampling sites differs from that used by INDE; the sites and samples are cross referenced in Table III.1.

As mentioned above in the general description of thermal features, three types of thermal waters discharge in the Tecuamburro region: steam-heated, acid sulfate, and neutral chloride. These waters are chemically distinct (Table III.3) and occur in separate geographical areas. The springs in Colmenares can be subdivided into northern and southern groups. The main chemical differences between these water types are illustrated by Schoeller diagrams of representative analyses (Fig. III.10).

Figure III.10a shows neutral-chloride waters as found in four areas of the Tecuamburro region. The detailed differences are discussed later but note that Na and Cl are usually the major constituents at northern and southern areas of Colmenares (lines 1 and 2); these analyses show $Na>Ca>K>Li\sim Mg>NH_4$ among the cations and $Cl>SO_4\sim HCO_3>F$ among the anions. Springs east of Los Esclavos and SSE of Tecuamburro Volcano (lines 3 and 4) differ in having higher Mg, HCO_3, and K, with lower F. All of these waters have between 6.6 and 8.2 pH (except one with 5.7) and are relatively concentrated, with total dissolved solids (TDS) of between 1000 and 2900 mg/kg (one sample is lower).

Acid-sulfate, steam-heated and cold meteoric water analyses are shown in Fig. III.10b. Acid-sulfate waters have 270-5800 mg/kg TDS. Steam-heated and cold meteoric waters are usually dilute, with steam-heated waters having 200-1000 mg/kg TDS and cold waters having 100-450 mg/kg TDS and low Cl (Table III.3). Individual cations (except NH_4) are not so clearly differentiated, with $Ca\geq Na?Mg?K>>NH_4$. Anions show large differences, with $SO_4>>Cl>F$ and HCO_3 missing for acid-sulfate waters (line 1). $HCO_3>SO_4>Cl>F$ for steam-heated (line 2) and cold (line 3) waters. Note on Fig. III.10b that concentrations below detection do not appear because of the logarithmic scale. The line for acid-sulfate water is discontinuous because HCO_3 is below detection. The cold-water line is discontinuous because F and B are below detection. The SiO_2 concentration of cold water is shown as a dot.

Other diagrams indicate differences in water compositions through the comparison of constituent pairs. Sodium and total HCO_3 (Fig. III.10c) show the generally dilute character of acid-sulfate, steam-heated, and cold waters that plot near the origin with zero HCO_3 for acid-sulfate waters. The neutral chloride waters are distinguished by differences in HCO_3.

TABLE III.3. CHEMICAL AND ISOTOPIC ANALYSES OF WATERS IN THE REGION OF TECUAMBURRO VOLCANO, GUATEMALA
(Concentrations in mg/kg and permil SMOW.)

Sample No.	Date	Temp	pH-1	Li	Na	K	Mg	Ca	Cl	HCO_3	CO_3	SO_4	SiO_2	B	dDwatS	dOwatS	dOwat	$dOSO_4$
Neutral-Chloride Springs																		
Colmenares, Northern Area																		
GT-88-2	88/03/17	90.0	6.70	1.89	609	23.0	1.15	59.3	787	127	–	256	88	12.6	–	–	–	–
GT-88-13	88/07/08	90.4	7.46	1.62	591	22.4	1.08	59.8	801	142	–	249	89	17.5	–	–	–	–
GT-88-9	88/07/08	70.0	7.64	1.91	598	24.8	1.30	55.2	796	156	–	236	95	17.1	-51.9	-6.45	-6.47	3.01
GT-89-83	89/03/04	82.4	7.74	1.86	578	24.0	1.53	58.0	771	101	25.2	235	92	17.0	-50.6	-6.81	-6.85	2.81
GT-88-10	88/07/08	60.0	7.25	1.04	334	13.8	2.73	35.9	377	239	–	124	90	8.9	-51.7	-7.15	-7.23	3.12
GT-89-84	89/03/04	65.4	7.30	1.07	339	14.6	4.66	47.2	423	165	–	138	92	9.6	-51.1	-7.11	–	–
GT-88-11	88/07/08	78.2	7.38	1.46	464	18.8	2.34	50.1	608	169	–	190	87	13.1	–	–	–	–
GT-88-12	88/07/08	94.3	7.22	1.99	610	24.0	1.10	66.1	811	147	–	259	90	17.5	-49.4	-6.56	-6.85	3.66
GT-89-85	89/03/04	95.8	7.78	1.99	612	23.0	1.28	61.2	810	74	27.6	270	95	18.1	-50.0	-6.74	-675	2.77
GT-88-14	88/07/08	77.2	7.67	1.60	543	22.0	1.48	55.4	735	164	–	225	92	15.8	–	–	–	–
GT-89-86	89/03/04	75.0	7.84	1.67	516	20.2	1.84	55.0	681	96	26.4	217	92	15.7	–	–	–	–
GT-88-15	88/07/08	82.5	7.33	1.84	601	22.4	1.04	60.1	795	142	–	258	94	12.3	-50.1	-6.68	–	–
GT-89-87	89/03/04	92.4	7.69	1.89	579	21.8	1.16	60.0	772	84	25.2	256	95	17.4	-50.2	-6.84	-6.80	2.82
GT-88-45	88/07/16	96.2	7.35	1.86	604	25.2	1.18	69.0	817	144	–	280	95	17.6	-53.9	-6.72	-6.69	3.64
GT-89-71	89/02/25	96.5	7.63	2.02	671	25.4	1.46	67.2	815	131	–	275	107	18.7	-48.1	-6.68	-6.73	2.96
GT-88-46	88/07/16	88.8	7.29	1.55	504	22.4	1.25	56.1	709	159	–	235	99	16.4	-48.0	-6.52	–	–
GT-89-72	89/02/25	87.4	7.66	1.83	587	23.4	1.62	60.9	730	145	–	246	102	16.7	-49.9	-6.88	-6.70	2.93
Colmenares, Southern Area																		
GT-88-16	88/07/08	83.7	7.60	1.11	444	6.6	0.20	47.3	546	69	–	293	72	8.9	-51.5	-6.83	-6.96	4.25
GT-89/57	89/02/22	80.2	8.07	1.06	417	8.3	0.28	43.4	488	68	–	283	72	9.1	-49.9	-7.15	-7.06	4.15
GT-89-58	89/02/22	86.2	8.11	1.16	457	10.0	0.26	49.0	542	51	–	311	73	12.6	-47.2	-6.99	-6.98	4.20
GT-89-59	89/02/22	85.0	8.01	1.21	485	10.2	0.48	51.2	575	54	–	307	88	12.0	-48.9	-6.66	-6.96	4.23
GT-89-60	89/02/22	36.0	7.51	0.12	62	5.2	7.30	24.2	62	137	–	32	83	1.4	-53.8	-8.08	–	–
GT-89-61	89/02/22	53.5	7.48	0.59	255	7.8	3.80	34.8	296	110	–	145	88	6.9	-51.6	-7.32	–	–
GT-89-62	89/02/22	85.0	8.17	1.24	508	10.0	0.24	59.6	623	35	–	293	70	14.6	-52.6	-7.01	-6.95	3.74
GT-89-63	89/02/23	85.2	8.10	1.24	511	10.6	0.38	60.0	639	44	–	302	74	15.2	-49.5	-6.92	-7.06	3.82
E of Los Esclavos																		
GT-88-3	88/03/21	37.0	5.70	0.98	381	25.0	39.6	67.9	335	849	–	109	117	3.1	–	–	–	–
GT-89-73	89/03/21	37.5	6.75	1.20	443	32.4	39.5	66.7	347	885	–	117	140	3.4	-47.4	-7.16	-7.13	2.33
GT-89-74	89/03/21	41.8	6.69	1.89	680	44.0	52.0	84.0	530	1220	–	178	139	5.4	-49.0	-7.30	-7.30	1.99
SSE of Tecuamburro Volcano																		
GT-89-97	89/03/07	39.2	8.15	0.58	436	37.6	64.5	79.3	519	763	–	121	141	11.0	-51.8	-7.29	-7.32	7.01

TABLE III.3. (cont)

Sample No.	Date	Temp	pH-1	Li	Na	K	Mg	Ca	Cl	HCO_3	CO_3	SO_4	SiO_2	B	dDwatS	dOwatS	dOwat	$dOSO_4$
Acid-Sulfate Springs																		
GT-88-1	88/03/18	88.0	2.95	<0.02	13.1	9.0	26.6	32.4	2.3	–	–	355	213	0.02	–	–	–	–
GT-88-4	88/07/07	77.0	2.27	0.09	70.0	6.2	87.4	180	<0.4	–	–	3560	288	0.31	-21.9	2.55	–	–
GT-89-54	89/02/21	85.2	2.45	0.05	48.0	2.1	62.0	103	<1.0	–	–	2180	288	0.16	–	–	–	–
GT-88-5	88/07/07	85.0	2.32	0.03	26.0	8.1	30.6	64.2	0.2	–	–	1285	190	0.18	-31.2	-0.76	–	–
GT-89-53	89/02/21	93.5	2.39	0.06	17.8	9.5	23.7	38.6	1.3	–	–	913	201	<0.05	-26.5	-0.54	–	–
GT-88-6	88/07/07	71.5	2.42	<0.02	7.5	9.1	7.2	21.8	2.7	–	–	427	92	<0.02	-41.0	-4.58	–	–
GT-88-7	88/07/07	27.8	2.50	0.02	8.0	9.9	7.2	22.4	2.6	–	–	400	70	z0.02	-39.2	-4.29	–	4.89
GT-88-24	88/07/09	32.4	2.11	0.06	82.0	9.0	50.8	214	8.7	–	–	5200	202	0.20	-44.7	-5.64	–	–
GT-89-70	89/02/25	20.1	2.71	<0.01	28.0	4.7	29.3	62.2	7.8	–	–	638	180	<0.05	–	–	-6.10	0.18
GT-88-32	88/07/12	23.5	2.91	<0.01	17.6	7.0	16.1	46.7	2.8	–	–	412	102	0.03	–	–	–	–
GT-89-69	89/02/25	25.5	2.97	<0.01	27.0	3.2	29.2	76.2	1.4	–	–	456	118	<0.05	–	–	-6.69	1.37
GT-88-37	88/07/13	34.8	3.33	<0.01	8.9	4.3	6.1	27.6	1.2	–	–	149	75	<0.02	-53.6	-7.81	-7.87	3.20
GT-89-92	89/03/07	35.5	3.65	0.01	9.5	4.3	6.6	27.5	1.7	–	–	149	79	<0.05	-49.2	-7.68	–	2.81
Steam-Heated Springs																		
GT-88-17	88/07/08	34.6	6.89	0.01	16.2	5.8	6.7	21.4	2.3	156	–	2	91	<0.02	-59.2	-8.26	-8.35	–
GT-88-18	88/07/08	32.7	6.83	<0.01	13.7	4.6	6.8	20.9	1.2	159	–	1	91	<0.02	-53.4	-7.82	–	–
GT-88-19	88/07/08	40.2	6.92	0.02	22.0	6.9	4.8	30.3	4.0	168	–	4	115	<0.02	-53.6	-7.49	–	–
GT-89-88	89/03/04	42.0	7.59	0.02	22.5	7.1	5.3	31.1	6.1	162	–	7	123	<0.05	-54.1	-7.43	–	–
GT-88-26	88/07/11	37.4	5.75	<0.01	11.8	3.5	4.8	15.8	0.5	44	–	69	63	<0.02	-54.6	7.92	-7.87	10.92
GT-89-90	89/03/07	37.9	5.82	0.01	11.9	3.5	5.0	16.2	0.6	29	–	72	67	<0.05	-55.5	-7.95	-7.99	10.45
GT-88-29	88/07/11	58.1	6.42	0.02	62.0	9.1	31.8	115	4.1	195	–	376	200	0.09	-58.0	-8.58	-8.44	4.11
GT-89-77	89/03/03	58.0	6.40	0.01	56.0	8.1	28.8	104	3.9	206	–	324	184	<0.05	-56.7	-8.56	-8.59	3.42
GT-88-30	88/07/11	42.0	6.47	0.03	58.0	8.8	24.0	86.8	2.5	213	–	249	150	0.12	-58.0	-8.60	-8.66	3.91
GT-88-31	88/07/12	34.5	6.83	0.01	41.0	9.0	37.2	59.4	3.6	356	–	117	120	0.09	-61.7	-8.79	-8.97	2.40
GT-88-34	88/07/12	42.0	6.19	0.01	39.0	7.2	8.7	43.1	1.3	186	–	109	55	0.02	-55.7	-8.26	-8.19	7.24
GT-89-68	89/02/25	40.8	6.45	<0.01	38.2	7.4	10.2	46.5	2.0	183	–	104	58	<0.05	-53.6	-8.15	-8.16	–
GT-88-38	88/07/14	51.6	4.96	<0.01	25.0	9.0	5.7	22.8	1.1	30	–	165	85	0.03	-56.6	-8.40	-8.45	6.41
GT-89-81	89/03/04	52.4	4.85	0.06	23.9	8.8	6.0	22.4	1.1	21	–	162	88	<0.05	-60.2	-8.02	-8.53	5.74
GT-88-41	88/07/14	33.8	6.16	<0.01	32.0	3.4	19.9	50.3	2.5	164	–	156	75	0.08	-54.5	-8.09	-8.20	8.14
GT-88-42	88/07/15	96.6	7.17	<0.01	1.5	0.8	19.8	194	5.5	276	–	328	25	<0.02	-57.6	-7.25	-7.50	-5.49
GT-89-101	89/03/08	97.0	6.95	<0.01	1.4	4.0	43.4	480	2.6	204	–	1157	21	<0.05	-35.0	+0.03	-0.07	–

TABLE III.3. (cont)

Sample No.	Date	Temp	pH-1	Li	Na	K	Mg	Ca	Cl	HCO_3	CO_3	SO_4	SiO_2	B	dDwatS	dOwatS	dOwat	$dOSO_4$
Cold Meteoric Waters																		
GT-88-8	88/07/07	22.1	6.43	0.01	9.5	3.0	6.1	20.6	1.9	117	–	13.2	67	<0.02	-60.3	-8.90	–	–
GT-89-55	89/02/21	20.0	7.29	<0.01	10.6	3.1	7.4	25.4	2.5	98	–	21.1	81	<0.05	-60.5	-9.04	–	–
GT-88-20	88/07/08	–	–	–	–	–	–	–	–	–	–	–	–	–	-14.5	-2.67	–	–
GT-88-23	88/07/09	20.0	6.13	0.01	5.5	2.1	2.2	10.9	2.5	49	–	12.5	48	<0.02	-59.5	-8.49	–	–
GT-89-79	89/03/01	17.5	6.69	0.01	5.9	1.9	2.2	9.6	1.7	37	–	17.7	53	<0.05	-62.3	-9.50	–	–
GT-88-25	88/07/09	22.3	6.54	<0.01	14.6	2.5	5.2	53.4	2.5	152	–	110	79	<0.02	-62.2	-9.01	–	–
GT-88-27	88/07/11	21.3	6.44	<0.01	7.8	2.3	3.8	10.7	1.4	88	–	1.6	68	<0.02	-49.2	-7.19	–	–
GT-89-91	89/03/07	17.2	7.73	<0.01	12.0	2.9	7.1	16.6	1.0	53	27.6	13.2	88	<0.05	-50.8	-7.45	–	–
GT-88-28	88/07/11	24.1	6.58	<0.01	10.1	2.7	7.1	28.3	1.2	159	–	3.0	74	<0.02	-51.8	-7.88	–	–
GT-89-78	89/03/01	25.1	7.05	<0.01	9.6	1.8	6.4	22.8	1.5	115	–	4.2	83	<0.05	-50.6	-8.06	–	–
GT-88-35	88/07/13	23.4	6.39	0.01	10.6	11	3.1	8.3	4.3	76	–	3.1	90	<0.02	-46.9	-6.93	–	–
GT-89-102	89/03/08	23.5	6.80	0.01	9.5	12	3.1	9.0	4.8	78	–	3.5	102	<0.05	-46.2	-6.87	–	–
GT-88-36	88/07/13	22.2	6.75	<0.01	2.9	1.0	4.8	70.2	1.6	242	–	4.3	33	<0.02	-51.9	-7.84	–	–
GT-89-100	89/03/08	20.7	7.26	<0.01	3.1	1.5	5.0	68.9	1.5	240	–	6.8	36	<0.05	-51.6	-7.60	–	–
GT-88-39	88/07/14	20.4	6.11	<0.01	9.7	3.6	16.3	41.3	14.4	56	–	8.7	64	<0.02	-52.9	-7.72	–	–
GT-88-40	88/07/14	25.3	6.51	<0.01	9.7	2.7	8.5	16.3	0.6	149	–	1.5	88	<0.02	-53.5	-7.91	–	–
GT-89-67	89/02/25	22.4	7.30	<0.01	9.7	2.9	8.9	16.0	0.8	128	–	2.1	90	<0.05	-52.8	-7.93	–	–
GT-88-43	88/07/16	24.8	6.45	<0.01	17.6	3.2	11.1	35.6	1.5	122	–	75.0	85	<0.02	-54.4	-7.75	–	–
GT-88-44	88/07/16	24.7	6.06	<0.01	9.5	5.0	48.2	160	25.3	54	–	80.4	53	<0.02	-48.6	-7.04	–	–
GT-88-48	88/07/16	22.7	6.28	<0.01	5.8	4.0	3.7	15.6	2.2	78	–	2.7	57	<0.02	-46.3	-6.82	–	–
GT-89-76	89/03/01	21.1	7.40	<0.01	9.6	2.6	8.9	27.4	1.0	161	–	1.6	78	<0.05	-48.2	-7.27	–	–
GT-88-49	88/07/16	22.8	6.07	<0.01	17.8	3.2	57.0	52.0	28.5	39	–	72.4	99	<0.02	-41.0	-6.00	–	–
GT-89-56	89/02/21	22.2	7.53	<0.01	17.4	2.7	16.2	59.5	5.7	126	–	128	82	<0.05	-60.4	-8.97	–	–
GT-89-64	89/02/23	25.0	7.94	0.02	14.2	3.0	11.1	25.8	3.0	166	–	4.6	95	<0.05	-49.1	-7.19	–	–
GT-89-65	89/02/24	20.8	7.55	<0.01	10.6	0.8	6.5	13.7	1.4	107	–	3.7	98	<0.05	-48.6	-7.40	–	–
GT-89-75	89/03/01	30.0	7.27	0.04	21.3	5.2	6.1	16.2	14.4	121	–	8.8	61	<0.05	-47.8	-6.94	–	–
GT-89-93	89/03/06	21.9	8.00	0.01	10.8	3.2	8.1	21.4	2.5	37	42.0	6.6	70	<0.05	–	–	–	–
GT-89-94	89/03/06	21.7	7.10	<0.01	10.8	2.9	12.7	26.5	15.7	142	–	4.6	93	<0.05	-48.8	-7.27	–	–
GT-89-98	89/03/07	27.8	6.96	0.01	14.7	2.6	10.6	24.3	1.9	138	–	29.7	94	<0.05	-47.6	-7.15	–	–
GT-89-99	89/03/07	–	5.36	<0.02	3.1	0.7	0.3	1.0	2.7	98	–	1.7	<1	<0.05	-16.4	-3.57	–	–

Notes: Chemical analyses by P. E. Trujillo and D. Counce.
dDwatS and dOwatS deuterium and oxygen-18 analyses by the Stable Isotope Laboratory, I.S.E.M. at Southern Methodist University, Dallas, Texas.
dOwat oxygen-18 analyses of water by P. Gemery and C. Janik; $dOSO_4$ oxygen-18 analyses of dissolved sulfate by J. Clark, C. Janik, and L. Fahlquist.
pH-1 measured in laboratory.
Temp measured in degrees C.

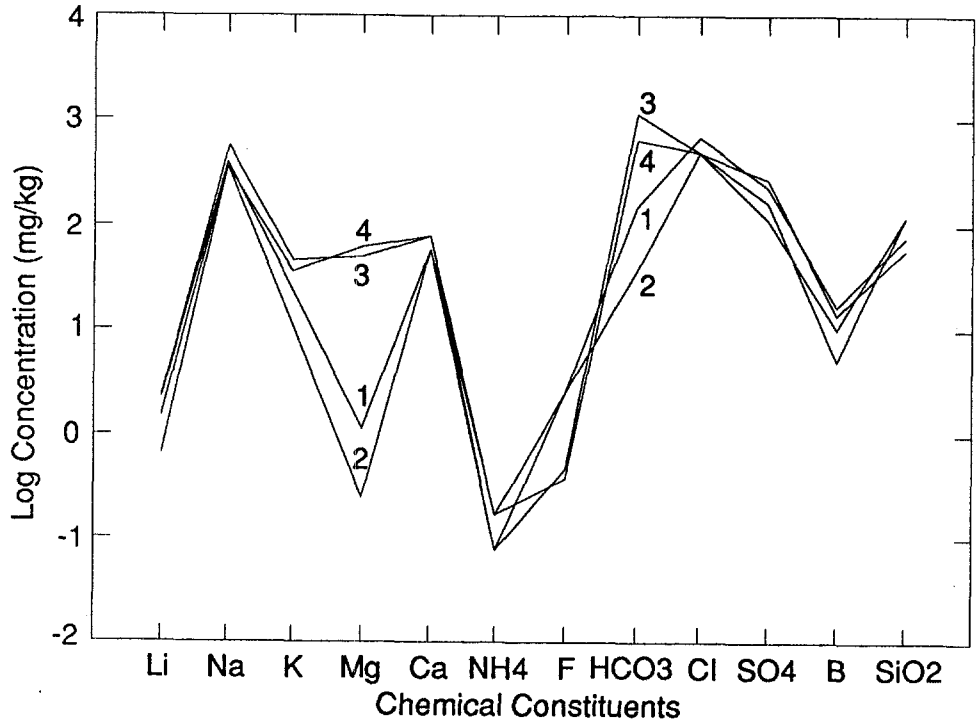

Fig. III.10a. Schoeller diagram of neutral-chloride waters, Tecuamburro region, Guatemala. Lines 1 and 2 represent waters of the Colmenares group, whereas lines 3 and 4 represent the waters east of Los Esclavos and SSE of Tecuamburro Volcano, respectively.

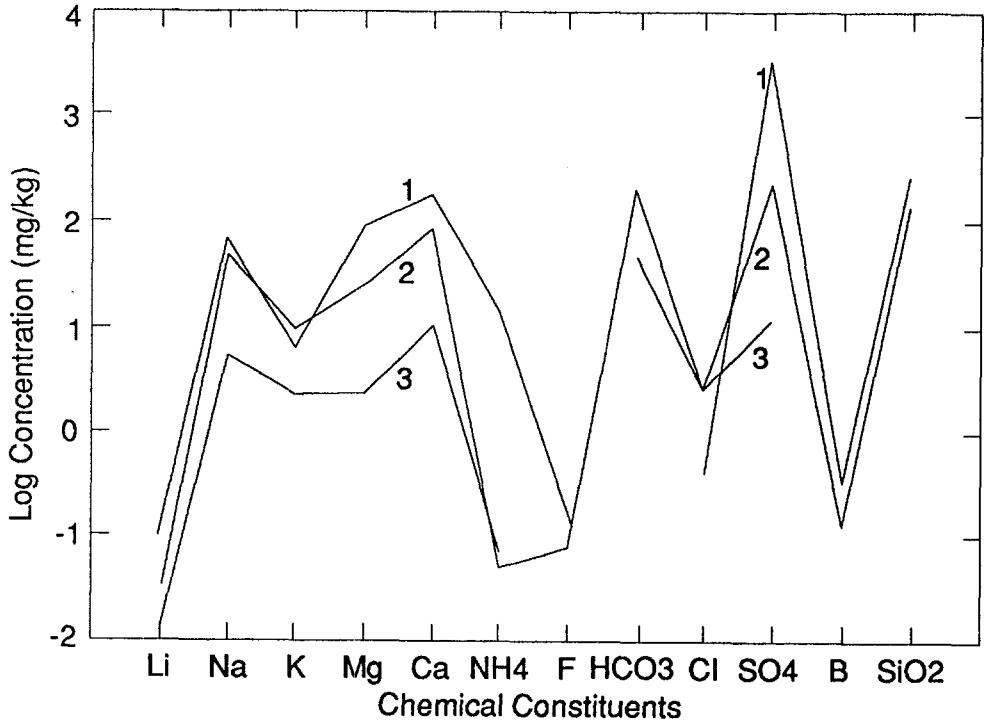

Fig. III.10b. Schoeller diagram of acid-sulfate, steam-heated, and cold meteoric waters, Tecuamburro region, Guatemala. Line 1 represents acid-sulfate waters, line 2 represents steam-heated waters, and line 3 represents cold meteoric waters.

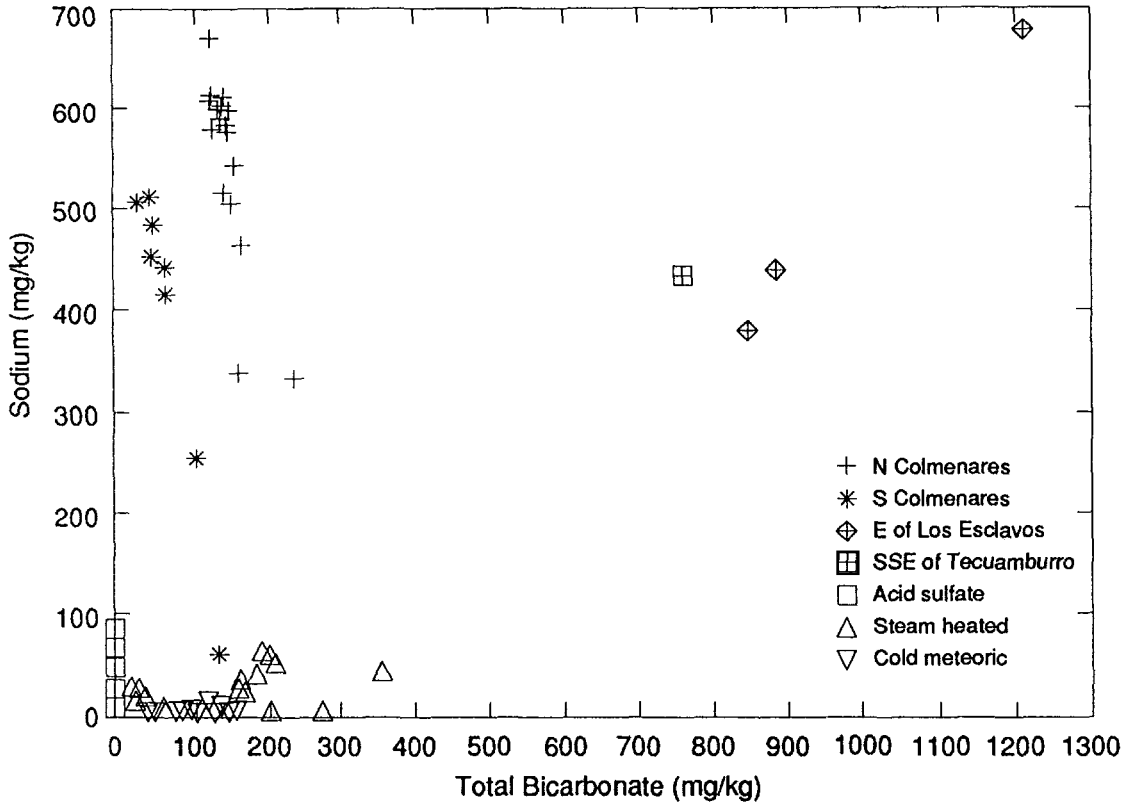

Fig. III.10c. Plot of sodium versus total bicarbonate. Symbols used in geochemical plots: plus=neutral-chloride springs in northern Colmenares area; asterisk=neutral-chloride springs in southern Colmenares area; square=acid sulfate springs; triangles=steam-heated springs; inverted triangle=cold meteoric waters; diamond with plus inside=east of Los Esclavos; square with plus inside=SSE of Tecuamburro Volcano.

Steam-heated waters occur primarily in the altered andesitic highland north of Tecuamburro Volcano. Compositionally, they are relatively dilute with low concentrations of Cl and trace elements commonly associated with high-temperature fluid/rock equilibrium (e.g., As, B, Br, and Li). Isotopically they plot on or near the world meteoric line (Fig. III.11) and have variable tritium contents (Fig. III.12). Gases from these springs are relatively low in H_2S and relatively high in the air components N_2, O_2, and Ar (Table III.3). Thus "steam-heated" waters are composed primarily of near-surface groundwaters of varying age heated by condensation of steam from a boiling reservoir below and/or by high subsurface heat flow.

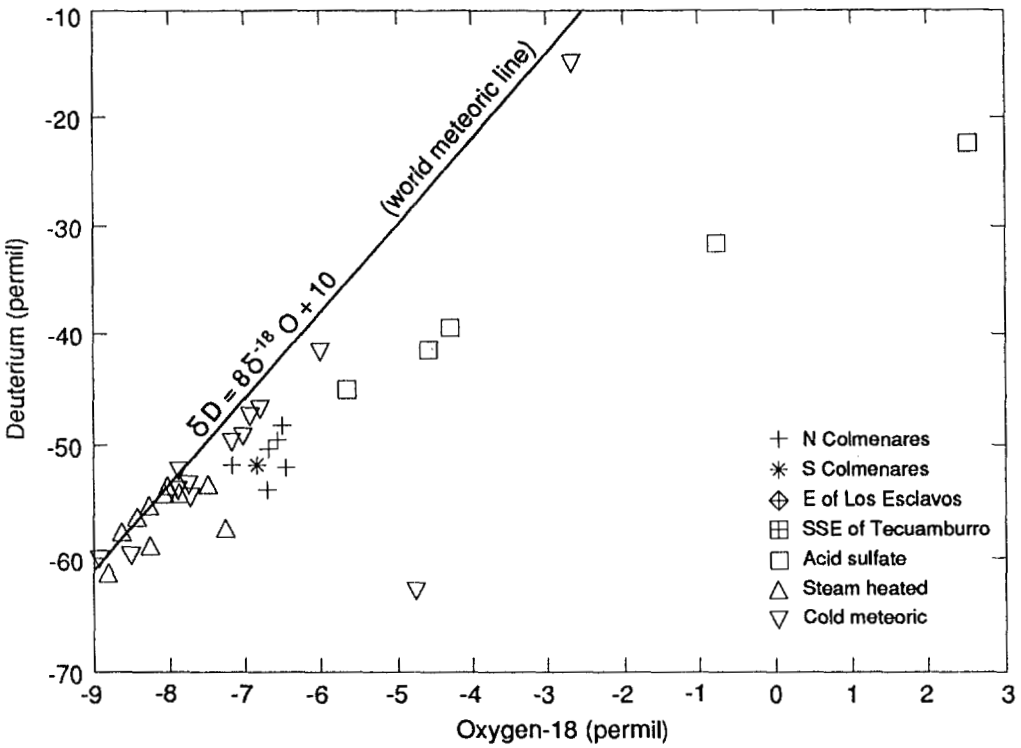

Fig. III.11. Plot of deuterium versus oxygen-18.

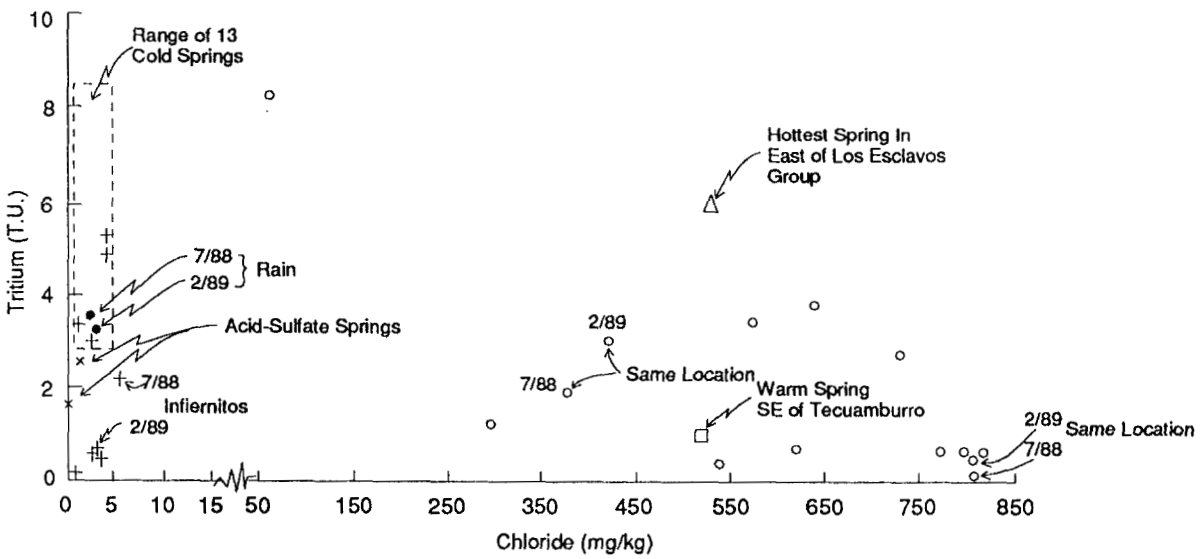

Fig. III.12. Plot of tritium versus chloride. Circles are neutral chloride springs of the Colmenares groups, the square is a neutral chloride spring SE of Tecuamburro, the triangle is a neutral chloride spring east of Los Esclavos, pluses are steam-heated springs, Xs are acid-sulfate springs, and dark circles are rainwater.

Acid-sulfate springs occur only adjacent to Laguna Ixpaco and at two small sites to the west. Compositionally, they are relatively low in pH (≤3), they have very high sulfate concentrations, moderate concentrations of volatile to partly volatile components such as B and NH_4, and low

concentrations of Cl, Li, Br, and As. Contents of Ca+Mg are greater than Na+K. Isotopically, acid-sulfate springs exhibit a typical evaporation trend of increasing ∂D and $\partial^{18}O$ and have tritium contents of 1 to 3 T.U., indicating that a large fraction of the water is young meteoric water (probably shallow groundwater). Presumably, the volatile components and steam originate from a high temperature reservoir boiling at depth.

Acid-sulfate springs in the Laguna Ixpaco area are associated with fumaroles and gas seeps with very high concentrations of H_2S (Table III.4). Gas seeps west of Laguna Ixpaco have similar CO_2/H_2S ratios, but H_2 values are considerably lower and CH_4 values are slightly higher. Gases of similar composition issue from low-pressure fumaroles at the sulfur mine near the summit of Tecuamburro Volcano; these fumaroles are not associated with permanent acid springs. All of these gases have nearly the same relative concentrations of N_2, He, and Ar, indicating a common parent fluid. The high relative N_2 concentration suggests a magmatic gas contribution is present.

As of this writing, we only have comprehensive stable isotopic data for neutral-chloride springs of the Colmenares Group. Springs in this group form a cluster of points shifted about 1 to 1.5 permil to the right of the world meteoric line. Curiously, the Colmenares points are shifted to the right with respect to cold springs such as Finca Las Delicias in the andesite highland (Fig. III.11). suggesting recharge from this area. The isotope data do not suggest recharge of the Colmenares springs from a source at Tecuamburro Volcano.

The single chloride-rich spring sampled SSE of Tecuamburro Volcano plots on the same B versus Cl mixing trend as Colmenares waters (Fig. III.13) and has a few other chemical similarities to Colmenares waters (e.g., As/Cl and Br/Cl). The "SSE spring" is different from Colmenares waters in contents of SiO_2, Mg, HCO_3, and Na/K ratio. At this time, it is impossible for us to conclude if the two locations are hydrologically connected and chemically related. The spatial separation of the two sites and the abrupt hydrologic control of Colmenares springs by the east-west fault shown in Fig. III.1 would argue that the sites are hydrologically separated.

Neutral-chloride springs issuing east of Los Esclavos are compositionally different from Colmenares waters in ratios of B/Cl (Fig. III.13), Li/Cl, As/Cl, and Na/K and in contents of SiO_2, Mg, and HCO_3. The Los Esclavos springs are also composed of at least 50% young meteoric water, determined from their high tritium content (~6 T.U.). The springs east of Los Esclavos and those at Colmenares cannot be part of a single geothermal system.

Neutral-chloride springs have relatively high concentrations of Cl, As, B, Br, and Li, but they have only moderate concentrations of SO_4 and HCO_3 compared with neutral-choride fluids from drilled, high-temperature geothermal fields (Fournier, 1981). The Tecuamburro examples contain only modest concentrations of SiO_2 ($\leq$150 mg/kg) and relatively high concentrations of Ca+Mg, suggesting either moderate temperatures of subsurface equilibration (<180°C) or mixing with cool

TABLE III.4. GAS DATA FROM FUMAROLES AND THERMAL SPRINGS IN THE REGION OF TECUAMBURRO VOLCANO, GUATEMALA (Concentrations in mol% and permil PDB.)

Sample No.	Date	Temp	CO_2	H_2S	H_2	CH_4	NH_3	N_2	He	Ar	O_2	^{13}C-CO_2	T-DP
Neutral-Chloride Springs													
GT-89-71	89/03/06	96.9	27.57	0.0759	0.0146	0.2609	ND	69.67	0.0445	1.036	1.485	-6.5	100
GT-89-97	89/03/07	34.3	91.96	0.0211	0.00072	0.0451	ND	7.669	0.00093	0.1076	0.1784	-5.5	114
Acid-Sulfate Springs													
GT-88-4	88/07/07	77.0	87.99	7.860	0.9057	0.0121	0.0044	3.196	0.00023	0.0144	0.0021	-3.2	298
GT-89-54	89/02/21	85.2	86.94	9.353	0.7588	0.0102	ND	2.905	ND	0.0085	0.0026	-3.5	297
GT-88-5	88/07/07	85.0	87.12	9.381	0.6155	0.0087	ND	2.836	0.00021	0.0116	ND	-3.0	292
GT-89-53	89/92/21	93.5	87.59	9.133	0.6565	0.0092	0.0014	2.582	0.00022	0.0079	ND	-3.1	293
GT-88-6	88/07/07	71.5	88.06	8.843	0.1109	0.0086	ND	2.924	0.00035	0.0150	0.0020	-3.4	238
GT-88-24	88/07/09	33.0	89.60	7.218	0.00196	0.0288	0.0021	3.133	0.00034	0.0069	ND	-3.0	192
GT-89-70	89/02/25	20.1	88.26	8.180	0.00040	0.0323	ND	3.515	0.00039	0.0059	0.0012	-4.8	159
GT-88-32	88/07/12	28.0	88.40	8.157	0.00055	0.0299	0.0009	3.384	0.00059	0.0130	ND	-3.6	166
GT-89-69	89/02/25	25.5	88.57	8.320	0.00041	0.0290	ND	3.061	0.00034	0.0074	0.0015	-4.7	160
GT-88-33	88/07/12	--	87.78	7.069	0.00064	0.0427	0.0018	5.077	0.00056	0.0245	ND	-2.9	165
Fumaroles, Sulfur Mine Near Tecuamburro Summit													
GT-88-21	88/07/09	94.9	86.22	10.65	0.00145	0.0086	0.0018	3.076	0.00035	0.0129	ND	-2.7	199
GT-89-80	89/03/03	95.0	85.35	11.58	0.00196	0.0051	ND	3.036	0.00036	0.0169	0.0012	-3.0	212
Steam-Heated Springs													
GT-88-34	88/07/12	42.0	78.41	1.721	0.00084	0.9760	0.0031	18.73	0.00188	0.223	ND	-4.9	140
GT-89-68	89/02/25	40.8	83.10	0.2505	0.00132	0.9556	ND	15.49	0.00130	0.188	0.0050	-4.6	130
GT-88-42	88/07/15	98.6	95.37	0.2120	0.0550	0.0464	0.0221	4.230	0.00102	0.0330	0.0282	-2.6	163
GT-89-101	89/03/08	97.0	95.36	0.1485	0.0548	0.0406	0.0034	4.223	0.00182	0.0388	0.1428	-2.9	160

Notes: Analyses by C. Janik and L. Fahlquist.
T-DP = Empirical gas geothermometer temperatures (D'Amore and Panichi, 1980) in degrees C.
ND = Not Detected.

dilute waters. A plot of B versus Cl (Fig. III.13) reveals that mixing is an important hydrologic process for the large group of springs in the Colmenares area. This plot also shows that although most Colmenares springs have a constant B/Cl ratio, which indicates mixing, all springs east of Los Esclavos and some Colmenares springs have lower ratios, suggesting evolution differences.

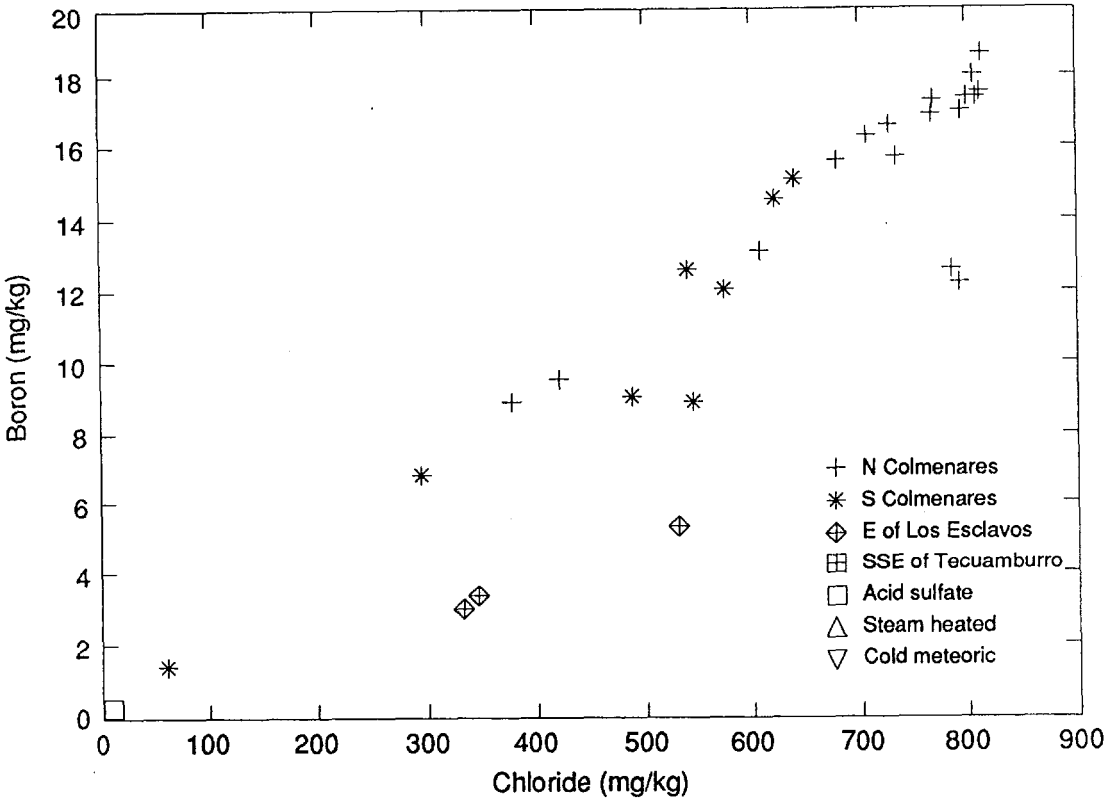

Fig. III.13. Plot of boron versus chloride.

Figure III.14, a plot of Li versus Cl, also indicates mixing. In this plot most analyses fall along a mixing line, with similar Li/Cl ratios; waters from east of Los Esclavos plot above the line (higher Li/Cl ratios) and water from SSE of Tecuamburro Volcano plot below the line (lower Li/Cl). Different rock types or different equilibration temperatures could explain these differences. Also note that Li concentrations are lower than those of B and may have more analytical variation.

The cool fluids that mix with Colmenares thermal waters have interesting geochemistry. If we examine a plot of $\partial^{18}O$ versus Cl (Fig. III.15), we see that neutral-chloride waters of all types display a rather restricted range in $\partial^{18}O$ even though Cl varies dramatically; this requires that the cool mixing fluids originate from one general source area. Because Colmenares fluids discharge along a 7-km-long stretch of the Río Los Esclavos, the "aquifer" responsible for mixing must also be extensive. On the other hand, tritium variations in the mixed waters are dramatic (Fig. III.12), suggesting that the aquifer is not homogeneous with respect

to age. The plot of Na versus HCO_3 (Fig. III.10c) indicates that the mixing fluid might be relatively HCO_3-rich, and similar to many steam-heated waters of the andesitic highland northwest of Colmenares. Although not all stable isotopic analyses have been completed, the data in hand indicate that recharge to hot Colmenares fluids and the source of the cool "aquifer" responsible for mixing both originate in the andesitic highlands.

The neutral-chloride springs in the Colmenares area can be divided into two groups, northern and southern. The southern springs have significantly lower concentrations of K and Mg, and different flow paths, types of mixing processes, and reequilibration histories. All springs in the Colmenares area issue from fractured andesitic rocks (laharic breccias and lava flows) or from alluvium along the river. Chemical differences in spring waters cannot be caused by differences in rock types.

All gases collected from the Tecuamburro region thus far have $\partial^{13}C$-CO_2 values between -2.6 and -4.9 permil. These values are heavier than those thought to be derived solely from CO_2 in volcanic/mantle sources (-5 to -8 permil) but are similar to values found from marine limestones (Hoefs, 1973). Mesozoic limestones are abundant in Central America north and east of Tecuamburro and a few scattered outcrops of limestone are found south of the Jalpatagua fault zone east of Tecuamburro. Thus, it appears that much of the CO_2 in the geothermal prospect region is derived by thermal decarbonation of limestones in "basement" rocks buried by Tertiary volcanic rocks.

3. Tritium

Tritium, a radioactive form of hydrogen present in water in small concentrations, is useful in determining the relative ages of groundwaters because it has a short half-life (12.43 years) and because it was produced in large amounts during atmospheric nuclear tests of the 1950's and early 1960's

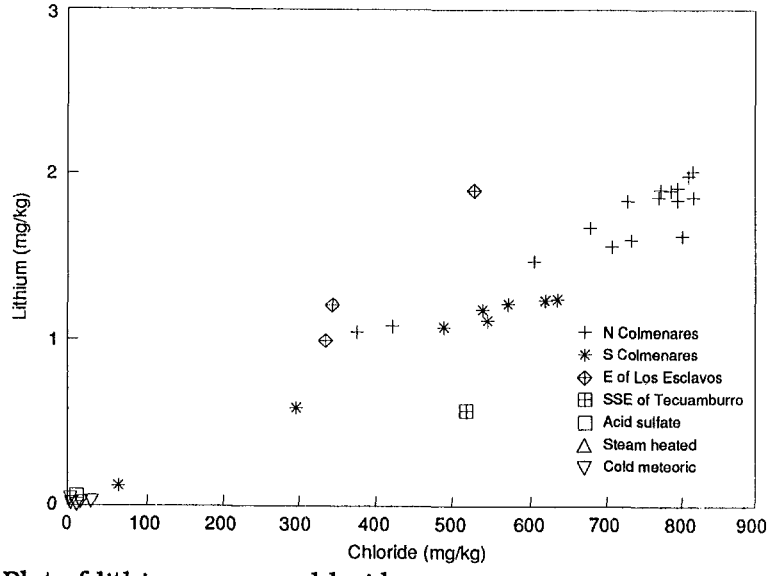

Fig. III.14. Plot of lithium versus chloride.

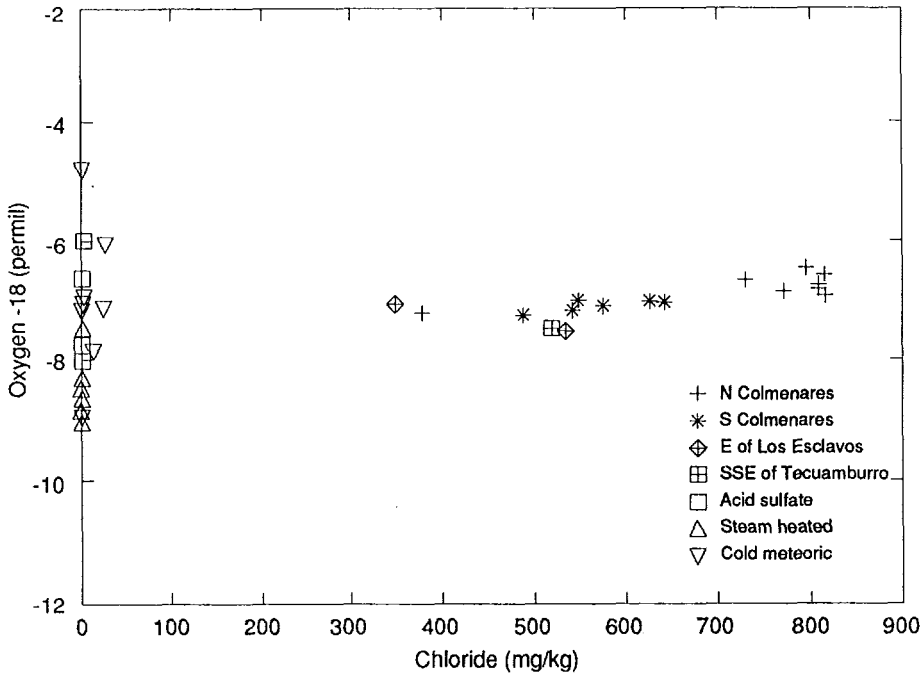

Fig. III.15. Plot of oxygen-18 versus chloride.

(Fontes, 1980). As a result of these tests, atmospheric tritium levels peaked in 1963 and have decreased steadily since. Tritium levels vary greatly by latitude. In 1963 atmospheric tritium in precipitation in the southwestern United States averaged 2800 tritium units (T.U.) (Vuataz and Goff, 1986), whereas in Veracruz, Mexico, it reached a maximum of only 65 T.U. (IAEA data are referenced in Goff et al., 1987). Atmospheric tritium also varies seasonally, with the highest levels occurring in the summer months and the lowest levels in the winter months. For example, at San Salvador, El Salvador, the tritium level in precipitation during August 1972 was 16.7 T.U. and in November of that year it was only 4 T.U.

For our investigations, 16 samples of cold water (12 springs, 2 rain, 1 stream, 1 well) from the Tecuamburro region were analyzed for tritium content (Table III.2). Background levels of present (1988-1989) precipitation are estimated using the rain samples (collected in different seasons) that contain 3.5 and 3.1 T.U. These values agree well with concentrations measured in rainwater from Tegucigalpa, Honduras in October, 1985 (2.6 and 3.4 T.U.). Values of cold waters higher than 4 T.U. must reflect slightly older precipitation that entered the groundwater system several years ago when atmospheric tritium levels were higher. Thermal springs having tritium values of approximately 0.5 T.U. must be composed primarily of older waters that infiltrated before the start of widespread nuclear testing (ca 1953).

Relative ages and mixing processes in thermal waters are shown by a plot of tritium versus chloride (Fig. III.12). Cold groundwaters tend to have the lowest chloride and highest tritium. Steam-heated waters have the same range of chloride but a lower range of tritium values. Some

steam-heated waters such as Finca El Chorro (0.14 T.U. in July 1988; 1.0 T.U. in February and March, 1989) sometimes contain a large proportion of old water, but substantial seasonal variations in tritium contents indicate connection to a shallow groundwater system. Other steam-heated waters such as Finca El Silencio (4.85 T.U.) are composed primarily of shallow groundwater.

Acid-sulfate waters are generally composed of steam from a boiling reservoir at depth mixed with near-surface groundwater. Values of 1.7 and 2.9 T.U. obtained from two different acid-sulfate springs at Laguna Ixpaco are consistent with this origin.

Neutral-chloride waters in the Tecuamburro region have a larger range of tritium and chloride values. The springs with the highest chloride concentrations (Colmenares area) have the lowest tritium (≤0.5 T.U.). In contrast to simple mixing suggested by the boron versus chloride plot (Fig. III.13), the tritium-chloride relations show that shallow groundwater of varying ages are involved in mixing. One warm spring in the southern end of the Colmenares group contains over 8 T.U., indicating mixing with groundwater of intermediate age containing elevated tritium. A similar mixing process must be occurring in the group of neutral-chloride springs east of Los Esclavos because the highest temperature spring (41°C) contains about 6 T.U. On the other hand, the warm, neutral-chloride spring southeast of Tecuamburro appears to be a mixture of geothermal water and older groundwater because it contains only 1.0 T.U.

If we assume that Colmenares fluids with the highest chloride contents are representative of relatively undiluted geothermal fluids (≤0.5 T.U.) from a deep reservoir, it is possible to estimate the mean residence time of water in the same reservoir of Colmenares using methods outlined in Goff et al. (1987, p. 18; adapted from Pearson and Truesdell, 1978). Assuming the geothermal reservoir is well mixed, Table III.5 lists mean residence times of water in aquifers of varying tritium contents for a sequence of sampling years. For a value of ≤0.5 T.U. collected in 1988-1989, the mean residence time is ~350 years.

4. Geothermometry

One method of investigation used to explore for geothermal energy, is the application of fluid geothermometers to hot spring discharges to estimate subsurface temperatures. Geothermometers depend on temperature-sensitive reactions between fluids and rocks or reactions within the fluid. These reactions must be sufficiently slow so that evidence of equilibration temperature remains "frozen in" as fluids rise to the surface. The most successful geothermometers depend on (1) solution of silica minerals, (2) cation exchange with feldspars, micas, and possibly clays, (3) equilibria of gases with rock minerals, and (4) isotopic fractionation between fluid constituents. Geothermometers used in this report are listed in Table 6; their application has been reviewed by White (1970), Truesdell (1976), Fournier (1981), and Henley et al. (1984) among others.

TABLE III.5 TRITIUM CONCENTRATION AND RESIDENCE TIMES FOR SELECTED BASE YEARS IN CENTRAL AMERICA, WELL-MIXED CASE (from Goff et al., 1988).

Residence Time	Tritium Concentration (T.U)							
τ(yr)	1985	1986	1987	1988	1989	1990	1995	2000
1.0	1.70	1.46	1.25	1.07	0.92	0.79	0.37	0.17
2.0	1.91	1.63	1.40	1.20	1.03	0.88	0.41	0.19
3.0	2.19	1.88	1.61	1.38	1.18	1.01	0.47	0.22
4.0	2.58	2.21	1.89	1.61	1.28	1.18	0.55	0.25
5.0	3.02	2.59	2.22	1.90	1.63	1.40	0.65	0.30
7.5	4.01	3.49	3.04	2.64	2.30	1.99	0.98	0.47
10.0	4.63	4.09	3.61	3.19	2.81	2.48	1.30	0.67
12.5	4.91	4.40	3.93	3.51	3.13	2.79	1.55	0.85
15.0	5.00	4.51	4.07	3.66	3.30	2.97	1.73	0.99
17.5	4.96	4.51	4.09	3.71	3.36	3.05	1.84	1.09
20.0	4.86	4.44	4.05	3.69	3.37	3.06	1.90	1.16
22.5	4.72	4.33	3.97	3.63	3.33	3.04	1.93	1.21
25.0	4.57	4.20	3.86	3.55	3.26	2.99	1.93	1.23
27.5	4.40	4.07	3.75	3.46	3.18	2.93	1.92	1.24
30.0	4.24	3.93	3.63	3.35	3.10	2.86	1.90	1.24
40.0	3.66	3.41	3.17	2.95	2.74	2.55	1.75	1.19
50.0	3.18	2.98	2.78	2.60	2.43	2.27	1.59	1.11
75.0	2.38	2.24	2.10	1.98	1.86	1.74	1.26	0.90
100.0	1.89	1.78	1.68	1.58	1.49	1.40	1.03	0.75
150.0	1.33	1.26	1.19	1.13	1.06	1.01	0.75	0.56
200.0	1.03	0.98	0.92	0.87	0.83	0.78	0.59	0.44
300.0	0.71	0.67	0.64	0.60	0.57	0.54	0.41	0.31
400.0	0.54	0.51	0.48	0.46	0.44	0.41	0.31	0.24
500.0	0.43	0.41	0.39	0.37	0.35	0.33	0.25	0.19
750.0	0.29	0.28	0.26	0.25	0.24	0.23	0.17	0.13
1000.0	0.22	0.21	0.20	0.19	0.18	0.17	0.13	0.10
1500.0	0.15	0.14	0.13	0.13	0.12	0.11	0.09	0.07
2000.0	0.11	0.11	0.10	0.10	0.09	0.09	0.07	0.05
3000.0	0.07	0.07	0.07	0.06	0.06	0.06	0.04	0.03
4000.0	0.06	0.05	0.05	0.05	0.05	0.04	0.03	0.03
5000.0	0.04	0.04	0.04	0.04	0.04	0.03	0.03	0.02
7500.0	0.03	0.03	0.03	0.03	0.02	0.02	0.02	0.01
10000.0	0.02	0.02	0.02	0.02	0.02	0.02	0.01	0.01
15000.0	0.01	0.01	0.01	0.01	0.01	0.01	0.01	0.01

Silica geothermometers depend on saturation with silica minerals (usually quartz at temperatures above 140°C and chalcedony at lower temperatures) and equilibrate rapidly at moderate to high temperatures. These geothermometers are fully equilibrated in most geothermal reservoirs. They are, however, affected by dilution and reequilibration during ascent of fluids to the surface. Silica geothermometers applied to spring samples usually do not indicate temperatures above about 220°C because solutions saturated with quartz at or above this temperature rapidly precipitate amorphous silica during ascent and cooling to surface temperatures.

Cation geothermometers include the K/Mg (Giggenbach et al., 1983; Giggenbach, 1986), Na/K (Ellis and Mahon, 1964; White, 1970: Truesdell, 1976; Fournier, 1981), and Na/Li (Fouillac and Michard, 1981) ratios and the Na-K-Ca function (Fournier and Truesdell, 1973). These geothermometers equilibrate only in the presence of feldspars or other alumino-silicate minerals. Their rate of reequilibration during ascent depends on the cation concentrations (dilute solutions equilibrate more rapidly than concentrated ones), the flow rate and temperature during ascent, and the minerals encountered during ascent (if the upflow channels are lined with silica minerals, cation reequilibration is greatly slowed or prevented). In general, the K/Mg geothermometer is

the fastest to reequilibrate at lower temperatures; the Na/Li geothermometer reequilibrates slowly during ascent and may not be fully equilibrated in reservoirs whose temperatures are below 250 to 300°C. The Na/K White-Ellis equation generally yields lower temperatures than the Fournier equation, and together they bracket Na/K geothermometer temperatures.

Geothermometers based on Na/K ratios are generally similar to the Na-K-Ca geothermometer but can be applied only to low-Ca waters. For high-Ca waters Na/K geothermometers give unreasonably high temperatures. Na/K geothermometers have the advantage of being little affected by dilution so long

TABLE III.6. EQUATIONS EXPRESSING THE TEMPERATURE DEPENDENCE OF SELECTED GEOTHERMOMETERS (C is the concentration of dissolved silica.)

Geothermometer	Equation (Dissolved Components in mg/l; Gas Components in vol%)	Restrictions
Quartz (no steam loss)	$T°C = \frac{1309}{5.19 - \log C} - 273.15$	T = 0-250°C
Chalcedony	$T°C = \frac{1032}{4.69 - \log C} - 273.15$	T = 0-150°C
Na/K (White and Ellis)	$T°C = \frac{855.6}{\log (Na/K) + 0.8573} - 273.15$	T ≥ 150°C
Na/K (Fournier)	$T°C = \frac{1217}{\log (Na/K) + 1.483} - 273.15$	T ≥ 150°C
Na-K-Ca	$T°C = \frac{1647}{\log (Na/K) + \beta \{ \log (\sqrt{Ca}/Na) + 2.06 \} + 2.47} - 273.15$	T <100°C, β=4/3 T ≥100°C, β=1/3
Na-Li [a]	$T°C = \frac{1000}{\log (Na/Li) + 0.38} - 273.15$	T = 0-300°C(?) and Cl <7000 mg
K-Mg	$T°C = \frac{4410}{\log (Mg/K^2) + 13.95} - 273.15$	T ≥100°C
$\delta^{18}O(SO_4^{2-}\text{-}H_2O)$	$T°C = \left[\frac{2.88 \times 10^6}{1000 \ln\alpha + 4.1}\right]^{1/2} - 273.15$ where $\alpha = \frac{1000 + \delta^{18}O\ (SO_4)}{1000 + \delta^{18}O\ (H_2O)}$	T = 100-300°C(?)

TABLE III.6. (cont)

Gas (CO_2-H_2S-CH_4-H_2) $T°C = \frac{24775}{\alpha + \beta + 36.05} - 273.15$ T = 100-300°C

$$\alpha = 2 \log \frac{CH_4}{CO_2} - 6 \log \frac{H_2}{CO_2} - 3 \log \frac{H_2S}{CO_2} \quad \text{and}$$

$$\beta = 7 \log P_{CO_2}$$

$$\beta \begin{cases} = 7 \text{ if } CO_2 < 75 \text{ vol\%; } P_{CO_2} = 0.1 \text{ atm} \\ = 0 \text{ if } CO_2 > 75 \text{ vol\%; } CH_4 < 2H_2; H_2S < 2H_2; P_{CO_2} = 1 \text{ atm} \\ = -7 \text{ if } CO_2 > 75 \text{ vol\%; } CH_4 > 2H_2; H_2S > 2H_2; P_{CO_2} = 10 \text{ atm} \end{cases}$$

[a] Components in minols.

as the thermal water is much more concentrated than the diluting water and reequilibriation does not occur as a result of mixing. In general, the Na-K-Ca geothermometer gives satisfactory results with the widest range of water types. It does not have a sharp upper temperature limit (like silica) but may partially reequilibrate in passage from higher-temperature reservoirs to the surface unless flow is extremely rapid within inert upflow channels and there is no significant precipitation of calcite (and loss of Ca) caused by boiling. Waters that lose heat by conduction during moderately slow flow through silica-lined conduits and do not boil may also arrive at the surface unchanged in Na-K-Ca temperature. Waters containing high Mg may give high-temperature indications and require an Mg correction (Fournier and Potter, 1979), but Mg is generally low in waters with temperatures above 200°C. The Mg correction should be used with caution because it is not reasonable to correct for Mg that enters thermal waters through mixing.

If cold, dilute water mixes with thermal fluid during ascent to the surface, it may prevent or reduce reequilibration and preserve evidence of deep temperatures. Several "mixing models" have been suggested by Fournier and Truesdell (1974) and Truesdell and Fournier (1976, 1977). Although useful formulas are available, these mixing models can most easily be used graphically. For warm (not boiling) spring waters and cold

waters, the enthalpy and silica contents may be considered to be conservative components, and a mixing line can be drawn between representative points. This mixing line may be extrapolated to the solubility curve of the silica mineral (usually quartz) that is thought to control concentrations of dissolved silica in the reservoir. The enthalpy at the intersection of the mixing line and the solubility curve indicates the reservoir temperature. This mixing model assumes no loss or gain of silica or heat either before or after mixing. Equilibration after mixing is assumed not to have occurred because the temperature is low and the reaction rate is very slow. Conductive cooling commonly occurs after mixing, and the temperature indicated is then too high. This method should be used only for springs with high discharge volumes in which conductive cooling is unlikely. This method should also be used if cation geothermometer temperatures are much higher than quartz solublity temperatures.

The most widely applied isotope geothermometer involves fractionation of oxygen between water and dissolved sulfate (McKenzie and Truesdell, 1977). This geothermometer completely equilibrates in geothermal reservoirs whose temperatures are above 150°C and only slightly reequilibrates in spring waters ascending at average velocities. Corrections must be made, however, for mixing with H_2O or SO_4 of different origin and for isotopic changes in water oxygen caused by boiling. The changes in water isotopes caused by boiling depend on the amount of boiling and the temperature of steam separation. The maximum effect occurs if cooling is entirely by boiling and all steam separates at the surface (adiabatic cooling); there is less effect if steam separates as it is formed (continuous separation); and, of course, there is no isotopic change if the water cools conductively without steam loss (conductive cooling). This geothermometer may indicate temperatures somewhat higher than those found upon drilling.

Gas geothermometers are generally difficult to apply to hot spring and fumarole gases because most of the pertinent equilibria are pressure sensitive and competing gas reactions differ greatly in reaction rate. Gas pressures cannot be calculated without knowledge of the gas/total water ratio, which is usually unavailable for hot spring discharges. Despite these difficulties the empirical D'Amore-Panichi (1980) geothermometer has been surprisingly successful in a wide variety of systems.

Gases from acid-sulfate springs and from the sulfur mine (near Peña Blanca) yield estimated subsurface temperatures of 160° to 300° C. Gases from Laguna Ixpaco, the most vigorous area of fumarolic activity, consistently yield the highest temperatures (Table III.4). Gases from lower pressure vents with small gas volumes yield lower temperature values, possibly because of chemical alteration of gas composition in the near-surface environment.

Steam-heated waters north of Tecuamburro are not suitable for geothermometry because of their relatively low equilibration temperature in the near-surface environment. Subsurface temperatures estimated from gas geothermometry at two sites of steam-heated springs suggest

that a source of steam at 140° to 165° C may underlie the altered andesitic highland.

Geothermometer temperatures calculated from analyses of neutral-choride waters in the Tecuamburro region are given in Table III.7. Calculated reservoir temperatures for the neutral-chloride springs of the Colmenares Group range from 130 to165°C, with springs in the southern area giving temperatures approximately 20°C lower than the springs in the north. Estimates based on the quartz geothermometer (124° to 134° C) are lowest, reflecting the fact that these springs are mixed. Cation geothermometers yield a very tight range of 145 to150°C. Estimates based on the ^{18}O-SO_4 geothermometer are slightly higher. Calculated reservoir temperatures for the other two sites of neutral-chloride springs show more extreme variations than Colmenares waters; the lone sample from the "SSE spring" yields the highest estimated reservoir temperature (160 to 205°C).

Silica-spring temperature relations for the Tecuamburro region are shown in Fig. III.16, which is a plot of solubility curves for amorphous silica, chalcedony, and quartz. Precipitation of amorphous silica is rapid and, unless silicates are being actively dissolved, little supersaturation occurs; this is possible for the two cool, acid-sulfate waters. Cold water silica contents are variable but cover the range of the Colmenares neutral-chloride waters so that dilution of the Colmenares waters with cold water might not change SiO_2 concentrations. This is probably the origin of the flat mixing line shown for northern Colmenares samples.

TABLE III.7. CHEMICAL AND ISOTOPIC GEOTHERMOMETER TEMPERATURES FOR NEUTRAL-CHLORIDE WATERS

Sample No.	Date	Temp	TQC	TCH	TNK-WE	TNK-F	T_{13}	TNaLi	TKMg	TSO_4 (cond)	TSO_4 (csl)
Colmenares, Northern Area											
GT-88-2	88/03/17	90.0	131	101	102	146	144	149	118	–	–
GT-88-13	88/07/08	90.4	131	102	102	146	144	140	118	–	–
GT-88-9	88/07/08	70.0	135	106	109	152	149	151	118	187	172
GT-89-83	89/03/04	82.4	133	104	109	152	148	152	115	184	172
GT-88-10	88/07/08	60.0	132	103	109	151	143	149	(91)	173	159
GT-89-84	89/03/04	65.4	133	104	112	154	143	150	(86)	–	–
GT-88-11	88/07/08	78.2	130	101	107	150	144	150	102	–	–
GT-88-12	88/07/08	94.3	132	103	105	148	145	153	120	171	162
GT-89-85	89/03/04	95.8	135	106	102	145	144	153	116	186	176
GT-88-14	88/07/08	77.2	133	104	107	150	146	145	113	–	–
GT-89-86	89/03/04	75.0	133	104	105	148	144	152	107	–	–
GT-88-15	88/07/08	82.5	134	105	101	145	143	148	118	–	–
GT-89-87	89/03/04	92.4	135	106	102	146	143	153	116	185	174
GT-88-45	88/07/16	96.2	135	106	109	152	147	149	120	173	165
GT-89-71	89/02/25	96.5	141	114	102	146	145	147	117	184	173
GT-88-46	88/07/16	88.8	137	109	114	156	149	148	116	–	–
GT-89-72	89/02/25	87.4	139	110	106	149	146	150	113	185	173
Averages			134 ± 3	105 ± 3	106 ± 4	149 ± 3	145 ± 2	149 ± 3	115 ± 5	181 ± 7	170 ± 6
Colmenares, Southern Area											
GT-88-16	88/07/08	83.7	120	90	(45)	(94)	(103)	133	107	160	152
GT-89-57	89/02/22	80.2	120	90	61	109	114	135	108	160	151
GT-89-58	89/02/22	86.2	121	90	67	114	118	134	115	161	153
GT-89-59	89/02/22	85.0	131	101	64	112	117	133	107	161	152
GT-89-60	89/02/22	36.0	128	98	(169)	(202)	(153)	(116)	(56)	–	–
GT-89-61	89/02/22	53.5	131	101	(88)	(133)	(126)	128	(73)	–	–
GT-89-62	89/02/22	85.0	119	88	61	109	114	131	116	168	159
GT-89-63	89/02/23	85.2	122	91	64	111	116	131	111	165	156
Averages			124 ± 5	94 ± 5	63 ± 3	111 ± 2	116 ± 2	132 ± 2	111 ± 4	163 ± 3	154 ± 3
E of Los Esclavos											
GT-88-3	88/03/21	37.0	146	119	146	183	162	135	73	–	–
GT-89-73	89/03/01	37.5	157	132	156	192	170	139	79	187	167
GT-89-74	89/03/01	41.8	157	131	145	182	169	141	83	190	170
Averages			153 ± 5	127 ± 6	149 ± 5	186 ± 5	167 ± 4	138 ± 3	78 ± 4		
SSE of Tecuamburro Volcano											
GT-89-97	89/03/07	39.2	157	132	172	205	177	92	77	122	113

Notes: Quartz solubility data from Fournier and Potter (1982); other silica data from Fournier (1981).
Temperatures in degrees C.

TQC	Quartz saturation with conductive cooling.
TCH	Chalcedony saturation.
TNK-WE	Na/K (Truesdell, 1976, using data of White and Ellis).
TNK-F	Na/K (Fournier, 1979).
T_{13}	Na-K-Ca using $\beta = 1/3$ (Fournier and Truesdell, 1973).
TNaLi	Na/Li (Fouillac and Michard, 1981).
TKMg	K/Mg (Giggenbach et al., 1983; Giggenbach, 1986).
TSO_4 (cond)	O-18 in H_2O and dissolved SO_4 (McKenzie and Truesdell, 1977) cond based on conductive cooling.
(csl)	csl based on continuous steam loss.

Averages exclude data in parentheses.

Waters from southern Colmenares apparently equilibrated at lower temperatures and those from east of Los Esclavos and SSE of Tecuamburro Volcano at higher temperatures. These last waters are near saturation with amorphous silica and could have precipitated silica during ascent to the surface or as a result of surface evaporation. The figure does not indicate whether the Colmenares waters equilibrated with quartz or chalcedony, but the correspondence of cation geothermometer temperatures with quartz saturation temperatures suggests quartz.

These same data, for neutral-chloride springs only, are shown in Fig. III.17 as quartz saturation temperatures calculated assuming conductive cooling during ascent to the surface. Cooling by mixing with cold waters of similar silica content would yield the same flat temperature line. The neutral-chloride springs east of Los Esclavos and SSE of Tecuamburro Volcano indicate temperatures of quartz saturation near 160°C, the more concentrated northern Colmenares waters show 135°C, and southern Colmenares waters show 120°C.

Cation (Na-K-Ca) geothermometer temperatures (Fig. III.18) look similar to the quartz temperatures. The same trends and groupings occur but temperatures are 145°C for northern Colmenares, 115 to 125° C for southern Colmenares, and 160 to175°C for the other areas. The Na-K-Ca temperatures are not greatly affected by mixing as shown by nearly constant values for northern Colmenares.

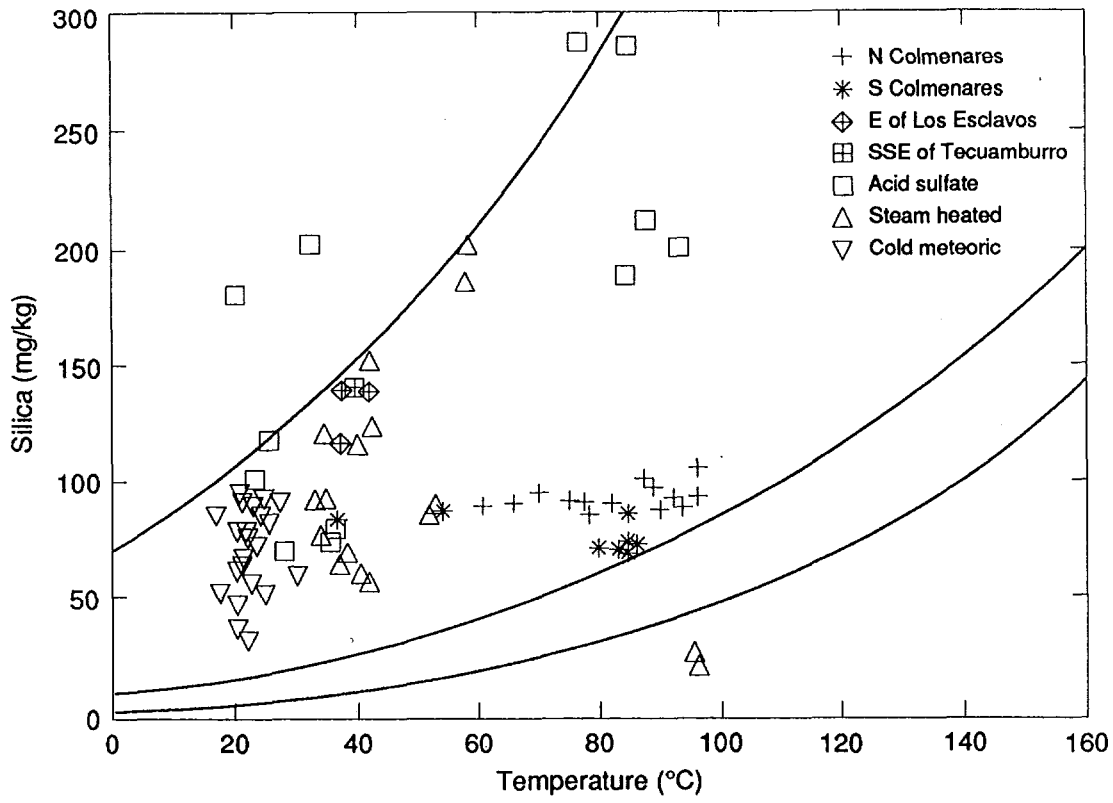

Fig. III.16. Plot of silica versus temperature.

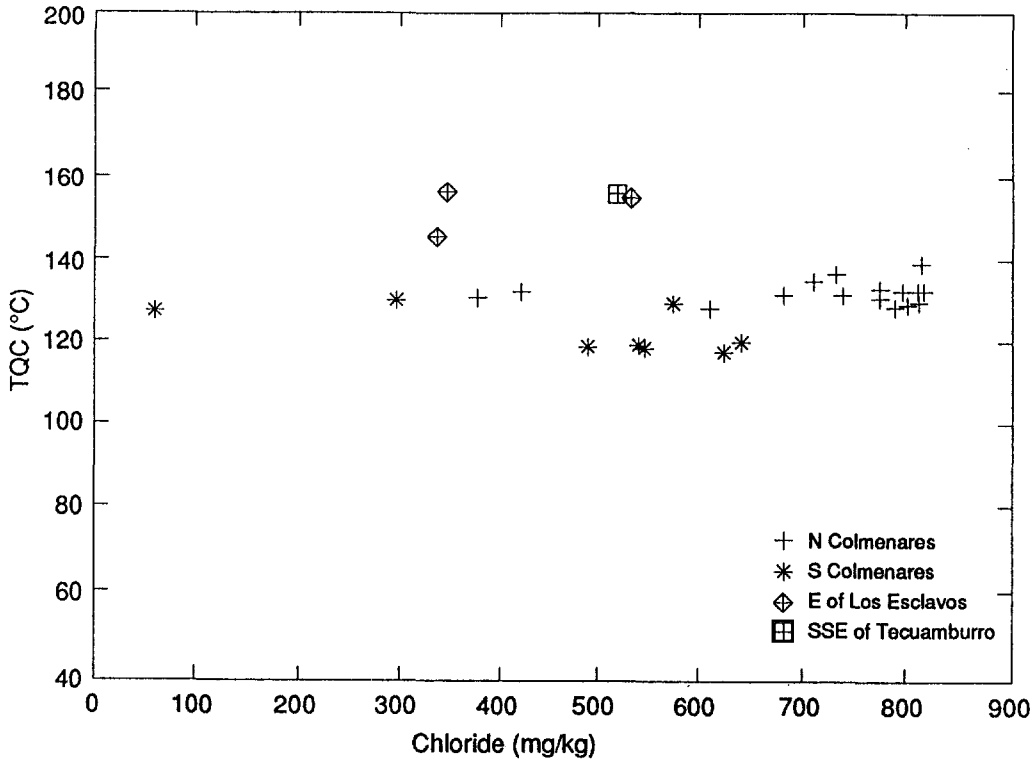

Fig. III.17. Plot of temperature (based on solubility of quartz, conductive cooling) versus chloride.

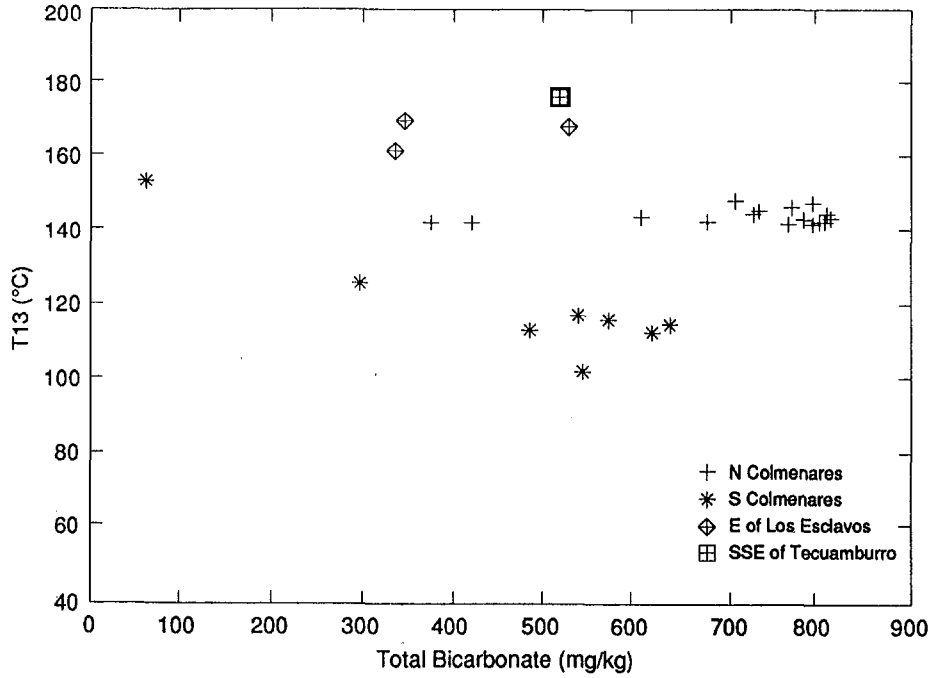

Fig. III.18. Plot of temperature (based on the Na-K-Ca, β=1/3 geothermometer) versus chloride.

Because all neutral-chloride springs show evidence of mixing, it is no surprise that estimates based on quartz are less than cation estimates. If we assume that waters are of the Colmenares Group and the "SSE spring" is derived from a 300°C reservoir underlying the Tecuamburro-Laguna Ixpaco area, then cation ratios, particularly Na/K, have reequilibrated drastically as waters have moved from the reservoir to the hot spring sites.

Based on the geothermometer temperatures, no reservoirs of high temperature underlie the neutral-choride spring sites. Only the Laguna Ixpaco area appears to have the estimated subsurface temperature and other geothermal characteristics suitable for exploration drilling.

D. RESERVOIR MODEL

We present two reservoir models at this time, but neither model affects our choice of location for a first exploration well (discussed below). In the first model (Fig. III.19a), we assume that a liquid-dominated reservoir of about 300°C beneath the Laguna Ixpaco area is overlain by a vapor-dominated zone not more than a few hundred meters thick. This reservoir feeds a large fan of lateral flow systems of hot, chloride-rich water to the north, east, and south. These flow systems are isolated by a combination of structural and stratigraphic controls such that the flow systems feeding the Colmenares group and the "SSE spring" have different evolutionary paths. Mixing and reequilibration with rock along the flow paths cause the estimated subsurface reservoir temperatures to be lower than true reservoir temperatures.

In the second model (Fig. III.19b), we assume that two reservoirs exist within the Tecuamburro region; one beneath the Laguna Ixpaco area and one beneath the altered andesite highland near Infirnitos. The two reservoirs are separated from each other by the major east-west fault shown in Fig. III.1. The Ixpaco reservoir has a temperature of about 300°C and feeds the "SSE spring" by a lateral flow system (that undergoes reequilibration). The Infernitos reservoir has a temperature of about 165°C and feeds the Colmenares group by a second lateral flow system. Three geologic arguments support such a model: 1) the entire region (not just the Tecuamburro area) is tectonically active, has high heat flow, and has late Pleistocene volcanism; 2) a major structural boundary confines fluid flow on the south side of the Colmenares group; and 3) Colmenares-group springs issue from major fractures in andesite along the west bank of Río Los Esclavos trending in a N35W direction toward Infirnitos.

Neutral-chloride springs east of Los Esclavos are not part of the Tecuamburro "reservoir." They are related to fluid flow and heating adjacent to or within the Jalpatagua fault zone and its nearby cluster of basaltic cinder cones.

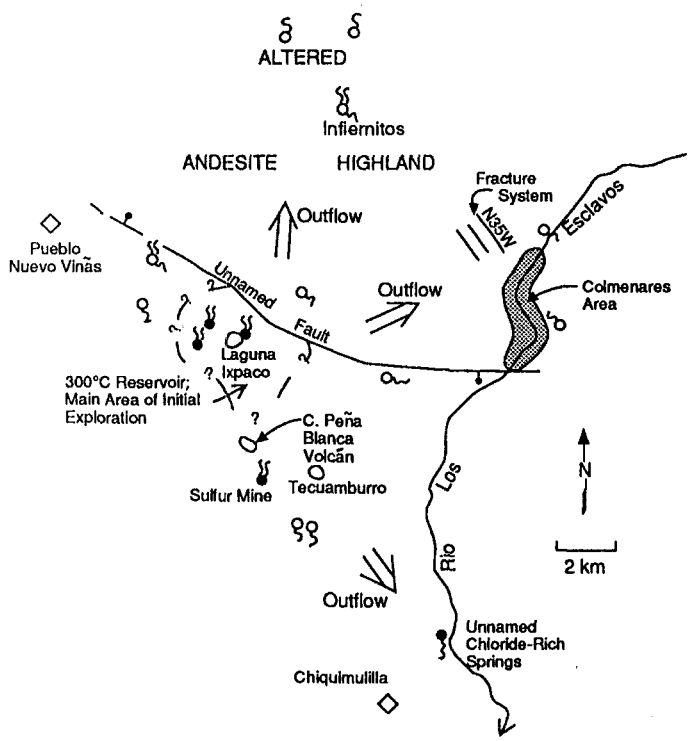

Fig. III.19a. Diagram of Tecuamburro geothermal area, assuming one large geothermal system located beneath Tecuamburro Volcano and Laguna Ixpaco (Chupadero crater).

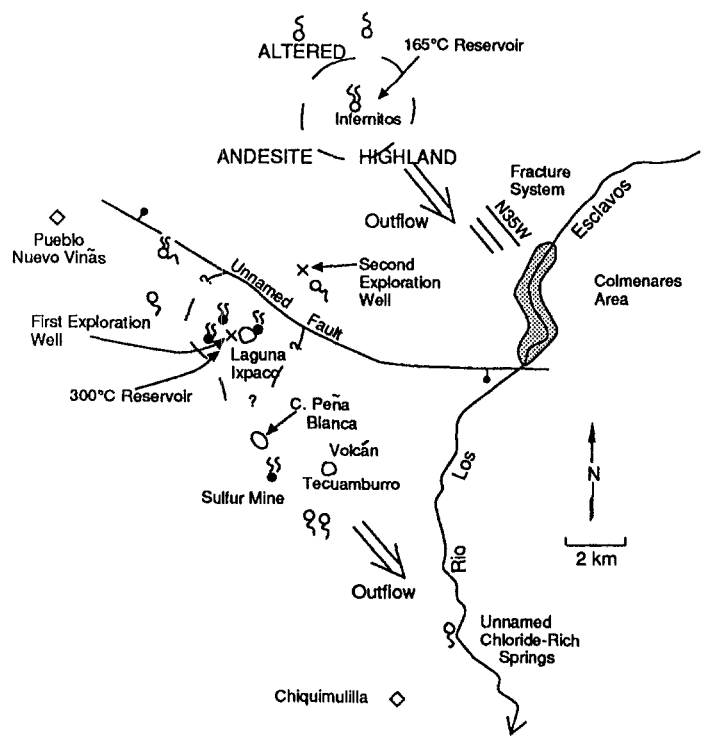

Fig. III.19b. Diagram of Tecuamburro geothermal area, assuming two separate but adjacent systems, separated by a major NW-SE-trending fault zone.

E. EXPLORATION WELLS

We have selected two sites for exploration drilling to verify temperatures and to test our models. Regardless of the model, the first well should be drilled very close to Laguna Ixpaco to a depth of at least 700 m to test temperatures, stratigraphy, and fluid types. If the first well is successful, a second well should be drilled to a depth of 700 m just north of Laguna Ixpaco and the E-W-trending fault to test whether or not there is one geothermal system with outflow in many directions or two separate systems.

F. REFERENCES

Beaty, D., W. Beyer, J. Dann, J. Reynolds, D. Hyde, C. Nelson, C. Bergquist, D. Dobson, E. Erler, M. Hitzman, and G. Jacobsen, 1980. Cuilapa Sheet, Mapa Geológico de Guatemala, Inst. Geográfico Nacional, Guatemala, C. A., 1 sheet, 1:50,000 scale.

Blackwell, D. D., E. Granados, and J. B. Koenig, 1977. Heat flow and geothermal gradient exploration of geothermal areas in the Cordillera de Guanacaste of Costa Rica: Geoth. Res. Counc. Transactions, *1*, 17-18.

Bonis, S., O. H. Bohnenberger, and G. Dengo, 1970. Mapa geológico de la Republica de Guatemala, Inst. Geográfico Nacional, Guatemala, C. A., 6 sheets, 1:500,000 scale.

Burkart, B., 1983. Neogene North American-Caribbean plate boundary across northern Central America: Offset along the Polochic Fault: Tectonophysics, *99*, 251-270.

Carpenter, R. H., 1954. Geology and ore deposits of the Rosario Mining District and the San Jauncito Mountains, Honduras, Central America: Geol. Soc. Amer. Bull., *65*, 23-28.

Carr, M. J., W. I. Rose, and R. E. Stoiber, 1982. Central America andesites, in R. S. Thorpe (ed.), *Andesites: Orogenic andesites and related rocks*, John Wiley & Sons, New York, N. Y.,149-166.

D'Amore, F. and C. Panichi, 1980. Evaluation of deep temperatures of hydrothermal systems by a new gas geothermometer: Geochim. Cosmochim. Acta, *44*, 549-556.

Duffield, W., G. Heiken, K. Wohletz, L. Maassen, G. Dengo, and E. McKee, 1989. Geology and geothermal potential of the Tecuamburro Volcano area of Guatemala, Geoth. Res. Counc.Transactions, *13*, 8.

Elder, J., 1981. *Geothermal Systems.* Academic Press, San Francisco, 508 pp.

Ellis, A. J., 1970. Quantitative interpretation of chemical characteristics of hydrothermal systems, in Proceedings of the United Nations Symposium on the Development and Utilization of Geothermal Resources, Pisa, 1970, Geothermics Special Issue 2, 516-528.

Ellis, A.J. and W. A. J. Mahon, 1964. Natural hydrothermal systems and experimental hot-water/rock interactions. Geochim. Cosmochim. Acta, *28*, 1323-1357.

Fontes, J. Ch., 1980. Environmental isotopes in groundwater hydrology, *in* P. Fritz and J. Ch. Fontes (eds.), *Handbook of Environmental Isotope Geochemistry, v. 1A; The Terrestial Environment*, Elsevier, Amsterdam, 75-140.

Fouillac, C. and G. Michard, 1981. Sodium-lithium ratios in water applied to geothermometry of geothermal reservoirs. Geothermics, *10*, 55-70.

Fournier, R.O., 1979. A revised equation for the Na/K geothermometer. Geother. Resourc. Counc. Transactions, *3*, 221-224.

Fournier, R.O., 1981. Application of water geochemistry to geothermal exploration and reservoir engineering. *In* L. Rybach and L. J. P. Muffler (eds.), *Geothermal Systems: Principles and Case Histories.* John Wiley and Sons, New York, pp. 109-143.

Fournier, R.O. and R. W. Potter, 1979. Magnesium correction to the Na-K-Ca chemical geothermometer. Geochim. Cosmochim. Acta, *43*, 1543-1550.

Fournier, R.O. and R. W. Potter, 1982. An equation correlating the solubility of quartz in water from 25°C to 900°C at pressures up to 10,000 bars. Geochim. Cosmochim. Acta, 46, 1969-1974.

Fournier, R.O. and A. H. Truesdell. 1973. An empirical Na-K-Ca geothermometer for natural waters: Geochim. Cosmochim. Acta, *37*, 1255-1275.

Fournier, R.O. and A. H. Truesdell, 1974. Geochemical indicators of subsurface temperature-Part 2. Estimation of temperature and fraction of hot water mixed with cold water. J. Res. U.S. Geol. Surv., *2*, 263-269.

Giggenbach, W.F., 1981. Geothermal mineral equilibria. Geochim. Cosmochim. Acta, *45*, 393-410.

Giggenbach, W.F., 1986. Graphical techniques for the evaluation of water/rock equilibration conditions by use of Na, K, Mg and Ca contents of discharge waters: Proceedings of the Eighth New Zealand Geothermal Workshop, pp. 37-43.

Giggenbach, W. F., 1988. Report on the isotopic and chemical composition of water and steam discharges from the Zunil, Tecuamburro and Moyuta geothermal fields, Guatemala. Unpublished Report, Chem. Div. DSIR, Peton, New Zealand, 42 pp.

Giggenbach, W. F., P. N. Garcia P, C. A. Londoño, V. L. Rodriguez, G. N. Rojas, and M. L. Calvache, 1989. The chemistry of fumarolic vapor and thermal spring discharges from the Nevado del Ruiz Volcano, Columbia. Unpublished report.

Giggenbach, W.F., R. Gonfiantini, B. L. Jangi, and A. H. Truesdell, 1983. Isotopic and chemical composition of Parbati Valley geothermal discharges, N.W. Himalayas, India. Geothermics, *12*, 199-222.

Goff, F., A. Truesdell, C. Grigsby, C. Janik, L. Shevenell, J. Parades, J. Gutierrez, P. Trujillo, and D. Counce, 1987. Hydrogeochemical investigation of six geothermal sites in Honduras, Central America. Los Alamos National Laboratory, Report LA-10785-MS.

Goff, F., A. Truesdell, L. Shevenell, C. Janik, C. Grigsby, R. Parades, P. Trujillo, D. Counce, J. Gutierrez, A. Adams, F. Urbani, and R. Perdomo, 1988, Hydrogeochemical report of the second Honduras sampling trip, January-February, 1986. Unpub. Rept. Los Alamos National Laboratory (obtain from Goff), 105 pp.

Goff, F., A. H. Truesdell, C. Janik, A. Adams, A. Roldán-M. and K. Meeker, 1989. Hydrogeochemical exploration of the Tecuamburro Volcano region, Guatemala. Geoth. Res. Counc. Transactions, *13*, 6 pp.

Henley, R. W. and A. J. Ellis, 1983. Geothermal systems ancient and modern, a geochemical review. Earth Science Reviews, *19*, 1-50.

Henley, R.W., A. H. Truesdell, and P. B. Barton, 1984. Fluid-mineral equilibria in hydrothermal systems: Rev. Econ. Geol., *1*, 267 pp.

Hoefs, J. 1973. *Stable Isotope Geochemistry.* Springer-Verlag, New York, 140 pp.

Lopez, C., B. Hoyt, and Y. Eckstein, 1980. Subsurface temperature distribution and structure of geothermal reservoir at Momotombo, Nicaragua. Geoth. Res. Counc. Transactions, 4, 459-462.

Mahon, W. A. J., 1970. Chemistry in the exploration and exploitation of hydrothermal systems. *In* Proceedings of the United Nations Symposium on the Development and Utilization of Geothermal Resources, Pisa, 1970: Geothermics Special Issue 2, 1310-1322.

McKenzie, W.F. and A. H. Truesdell, 1977. Geothermal reservoir temperatures estimated from the oxygen isotope compositions of dissolved sulfate and water from hot springs and shallow drill holes. Geothermics, 5, 51-61.

Meert, J., and D. Smith, in press. Heat flow at the Platanares, Honduras geothermal site. J. Volcan. Geotherm. Res.

MK-Ferguson, Co., 1988. Mision de Enfoque Report: Geothermal Power Plant; Zunil I, Quetzaltenango, Unpublished Consulting Report, MK-Ferguson, Co., Boise, Idaho, 112 pp.

Newhall, C. G., 1987. Geology of the Lake Atitlán region, western Guatemala. Jour. Volcan. Geotherm. Res., 33, 23-55.

Nielson, D., J. Hulen, F. Goff, and J. Gardner, 1988. Scientific exploration of an active magma-hydrothermal system in the Valles caldera, New Mexico, through drilling. *in* Boden, A. and Eriksson, K. (eds), *Deep Drilling in Crystalline Bedrock*, Vol. w, Springer-Verlag, N. Y., pp. 361-380.

OLADE, 1982. Estudio de Reconocimiento de los recursos geotermicos de la Republica de Guatemala. Rapport du B. R. G. M., 82 SGN 021 GTH.

Pearson, F. J. and A. H. Truesdell, 1978. Tritium in the waters of Yellowstone National Park: U.S. Geol. Surv. Open-file Report 78-701.

Reynolds, J. H., 1987. Timing and sources of Neogene and Quaternary volcanism in south-central Guatemala. Jour. Volcan. Geotherm. Res., 33, 9-22.

Swanberg, C. A., 1979. Chemistry of thermal and nonthermal groundwaters in the Rio Grande rift and adjacent tectonic provinces. *In* R. E. Riecker (ed.) *Rio Grande Rift: Tectonics and Magmatism.* Amer. Geophys. Union. Wash. D. C., pp. 279-288.

Tobias, E., 1987. Proyecto Geothermico Amatitlán; estudio de prefactibilidad. Unpublished report, Inst. Nacional de Electrificacion, Guatemala, C. A., 62 pp. w/appendices.

Truesdell, A.H., 1976. Summary of section III, geochemical techniques in exploration, in Proceedingsof the Second United Nations

Symposium on the Development and Use of Geothermal Resources, San Francisco, California, 1975, *1*, liii-lxxix.

Truesdell, A.H. and R. O. Fournier, 1976. Calculation of deep temperatures in geothermal systems from the chemistry of boiling spring waters of mixed origin. in Proceedings of the Second United Nations Symposium on the Development and Use of Geothermal Resources. U.S. Government Printing Office, Washington, D.C., *1*, 837-844.

Truesdell, A.H. and R. O. Fournier, 1977. Procedure for estimating the temperature of a hot-water component in a mixed water by using a plot of dissolved silica versus enthalpy. J. Res. U.S. Geol. Surv., *5*, 49-52.

Vides, A., 1976. Recent studies of the Ahuachapán geothermal field. in Proceedings, of the Second United Nations Symposium on the Development and Use of Geothermal Resources: U.S. Gov't Printing Office, Washington D. C.,*3*, 851-1854.

Vuataz, F.-D., and F. Goff, 1986. Isotope geochemistry of thermal and nonthermal waters in the Valles caldera, Jemez Mountains, New Mexico. J. Geophys. Res., *91*, 1835-1853.

White, D.E., 1957. Thermal waters of volcanic origin. Bull. of the Geol. Soc. Am., *68*, 1637-1658.

White, D.E., 1970. Geochemistry applied to the discovery, evaluation, and exploitation of geothermal energy resources: Rapporteur's Report, in Proceedings of the United Nations Symposium on the Development and Utilization of Geothermal Resources, Pisa, 1970: Geothermics Special Issue *2*, 58-80.

White, D. E., R. O. Fournier, P. Muffler, and A. H. Truesdell, 1975. Physical results of research drilling in thermal areas of Yellowstone National Park, Wyoming. U. S. Geol. Surv. Prof. Paper *892*, 70 pp.

White, R. A., E. Sanchez, I. L. Cifuentes, and D. H. Harlow, 1980. Preliminary report to the government of Guatemala on the on-going earthquake swarm in the Department of Santa Rosa, Guatemala, U. S. Geol. Surv. Open-file Rept., *80-800*, 17 pp.

IV. ELECTRICAL GEOPHYSICAL STUDIES OF THE TECUAMBURRO GEOTHERMAL AREA, GUATEMALA

(D. B. Hoover[1] and H. A. Pierce[1])

A. INTRODUCTION

The Tecuamburro geothermal area located in the Department of Santa Rosa lies approximately 50 km southeast of Guatemala City. Thermal manifestations and extensive regions of hydrothermal alteration cover an area of ~200 km^2 within the Tecuamburro geothermal area which is situated generally on the north side of Tecuamburro volcano. The geothermal area is bounded on the east and west sides by north-trending normal faults that define the 20-km-wide Tecuamburro graben in which the geothermal area lies. The graben is bounded on the north by the WNW-trending Jalpatagua fault.

Geological and geochemical studies had earlier identified the Chupadero crater region within the Tecuamburro geothermal areas as a most promising high-temperature geothermal resource (Chap. I). The Chupadero crater is at the northern flank of Tecuamburro volcano and measures about 4 km across. Nested within it is the 0.5-km-wide Ixpaco phreatic crater dated at 2900 years.

Electrical geophysical studies of the Chupadero Crater region were made to assist in selecting exploration drilling sites to test the geothermal system.

B. GEOPHYSICAL METHODS

Both audio-magnetotelluric (AMT) soundings and multifrequency telluric traverses, the two principal electrical methods employed in this study, use natural electromagnetic (EM) signals, which in this study's frequency range (7.5 to 14 000 Hz) originate from distant lightning storms. The USGS has employed the AMT method extensively in geothermal investigations (Hoover et al., 1978). The principal advantages of the AMT method are its relative low cost and better lateral resolution compared with conventional DC soundings and its ability to obtain soundings in difficult terrain where it is impractical to lay out the long lines required for DC soundings. For example, typically we use a 25-m dipole and obtain information to 1 km or more (see discussion below on exploration depth), whereas DC methods require about 4 km of line to sound to 1 km. The principal disadvantage of natural-source EM methods arises from the low signal levels that contribute to scatter in the data. The advantages of AMT when working in difficult terrain have been discussed by Hoover et al. (1984).

---

1. US Geological Survey, Denver, CO 80225

The USGS has used natural-source telluric methods for many years in geothermal studies to define lateral electrical boundaries and large throughgoing faults. In the past, most of the telluric work used a single frequency of 0.033 Hz (30 second period). This very low frequency gives great depth of exploration, but data acquisition is slow and definition of near-surface effects tends to be lost. Recently we developed a multifrequency telluric receiver for use in the AMT frequency range. Multiple frequencies that cover a large range provide a unique means for measuring variations in the earth's resistivity structure, both laterally and as a function of depth.

Telluric measurements, by themselves, provide only a measure of relative resistivity variations along a profile. Thus there is no absolute measurement of apparent resistivity and no way of referencing one profile to another in an absolute sense. This problem can be somewhat overcome by measuring an AMT sounding on one dipole of a traverse. If one them assumes that the traverse is normal to the electrical structure, he can calculate the resistivity along the traverse and reference parallel traverses to each other. Because resistivity is not a scalar function of position (it varies with the measurement direction), telluric traverses run at large angular differences will not tie in areas where structures are complex.

The angular variations in apparent resistivity about a measurement point in structurally complex areas will describe an ellipse if the magnitude of the apparent resistivity is plotted as a function of measurement direction. Thus, resistivities measured along a traverse in the direction of the minor axis of the ellipse will not be the same as those measured, at the same position on a traverse normal to the minor axis. Therefore, one should not attempt to contour apparent resistivities using traverses run at large angles to each other. In areas as structurally complex as Tecuamburro, such conditions would be expected.

Telluric methods take measurements on a three-electrode in-line array that comprises two equal dipoles with a common center electrode (Fig. IV.1) pair of matched narrow-band tunable voltmeters connects to each dipole, and measures the ratio of the voltage of one dipole to the other as a function of frequency. For a homogeneous half-space, or for a horizontally stratified earth; the voltage measured in each dipole would be the same. In the presence of a lateral boundary, the voltages would be different. For a dipole array normal to the boundary, the voltage ratio would be proportional to the square root of the transverse mode resistivity.

After making one set of measurements, the dipole array is advanced one dipole length in-line, and makes another set of measurements. This process is repeated over the desired traverse. Because the voltage on each new dipole is referenced to the previous dipole, the relative voltage of each dipole may be calculated referenced to the first or any dipole along the traverse.

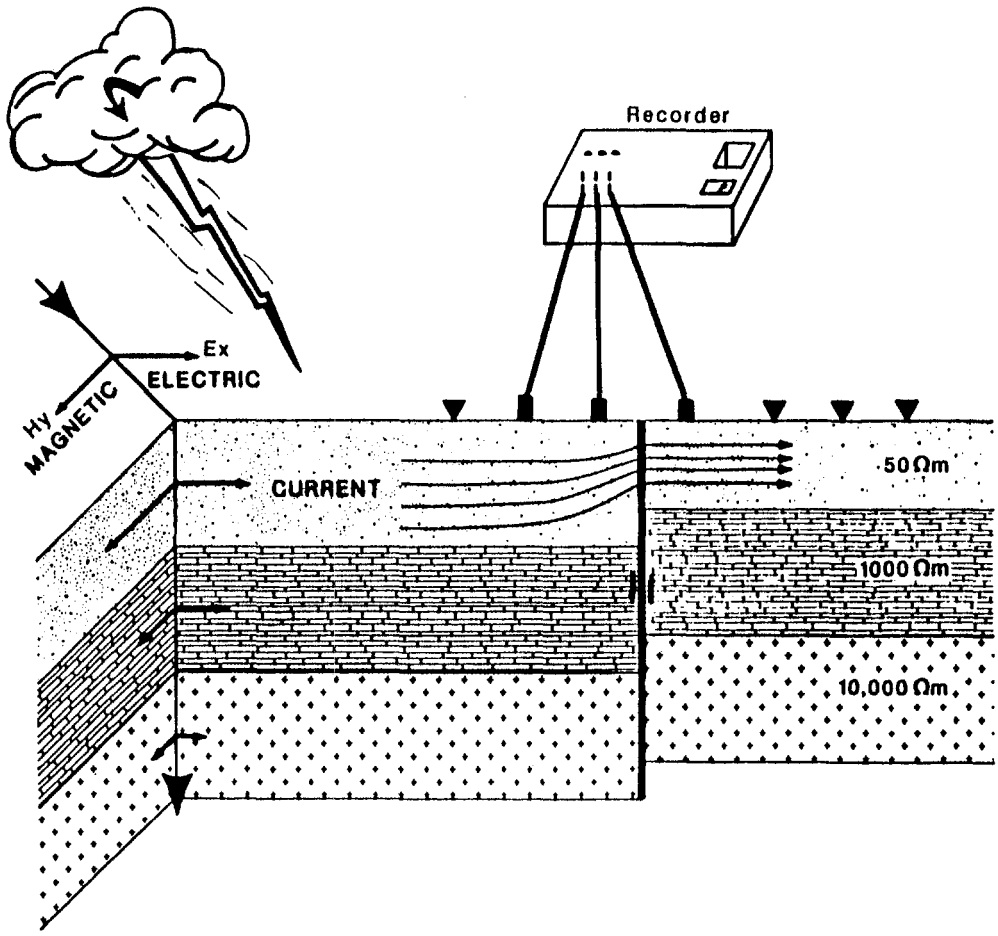

Fig. IV.1 Cartoon illustrating the telluric method where the source energy is derived from distant lightning sources.

Because the measurements are simple and quick, we measure the self-potential (SP) on each dipole at each station, and the AC voltage, using a common multimeter. For the SP measurements this provides two independent profiles except for the last dipole on each end of the traverse. This leapfrog method of SP measurement is not the most desirable because errors may accumulate, as is evident in some of the data presented. However, we can evaluate the effects of drift and random measurement error, having two independent measurements.

Measurement of the unfiltered AC voltage with a multimeter normally measures the dominant 60-Hz, and in part 180-Hz, signals present in the ground, which may be much stronger than the natural signals measured by the telluric receiver. These measurements can then be treated in the same manner as telluric signals because the source amplitude is generally not constant with time. Typically, the unfiltered AC voltages will not only reflect changes similar to those observed at frequencies near 60 Hz but also show a rapid decrease in amplitude as a traverse moves away from power line sources.

In the Chupadero crater region, several power lines were encountered that posed problems probably related to local inbalances in the distribution system and some power return through the ground. In a few cases, data taken at frequencies near the 60-Hz power line frequency on dipoles crossed by the power lines were seriously biased. However, the higher and lower frequencies measured at these sites do not appear to be significantly affected. For example, on telluric line 1 at dipole 2.50-2.75 km in the middle of Ixpaco village, a large peak is seen on the 75- and 450-Hz profiles where a power line is crossed. Because of the proximity and number of power lines in the survey area, the unfiltered AC data have not been plotted but are tabulated in Appendix D.

The depth of exploration for these natural-source methods is a function of frequency and earth resistivity. Exploration depth is often claimed to be equal to the skin depth of the EM wave, which for a half-space is (1) $\delta = 503\sqrt{\rho / f}$ in meters, where ρ is the resistivity in ohm-meters and f is the frequency. This really overstates the practical exploration depth. The relationship for maximum exploration depth we use is (2) $355\sqrt{\rho / f}$ in meters. This relationship can be understood by referring to the sounding graph shown in Fig. IV.2. The diagonal lines represent constant depth lines from Eq. (2) and are the asymptotic values for a sounding curve if a perfect conductor were present at the given depth. This graph shows the log of the apparent resistivity on the ordinate and of the period on the abscissa. Because we calibrate our system in terms of frequency, the abscissa is scaled in the equivalent frequency rather than period. This plotting procedure produces sounding curves similar to those used in DC sounding methods where depth increases to the right.

The data presented in Fig. IV.2 are for dipole 0.25-0.50 km on Ixpaco telluric line 4. The high-frequency data show near-surface resistivities are in the range of 100 to 60 ohm-m, and the lower frequencies show the sounding decreasing to 6.0 ohm-m at 7.5 Hz. The transition from ~60 to 4.5 ohm-m occurs along a diagonal line equivalent to a depth line of 300 m, which indicates the depth to the top of a conductive unit at this site.

C. PRESENTATION OF DATA

Fig. IV.3 shows the location of all telluric traverses measured in this survey. The base map used is the Chupadero crater portion of the Cuilapa 1:50 000 topographic quadrangle of the Instituto Nacional de Geográfico, enlarged to a scale of 1:25 000. Three telluric lines, numbers 1, 2, and 3 were oriented in an east-west direction and were 4.75 km, 2.75 km, and 3.25 km long, respectively. In addition to identifying areas of anomalous resistivities, these lines identified possible NS-trending structural features in the Chupadero crater that might relate to the Tecuamburro graben. Five other lines, numbers, 4, 5, 6, 7, and 8, were positioned in a northeast orientation normal to the other principal structural trend in the region.

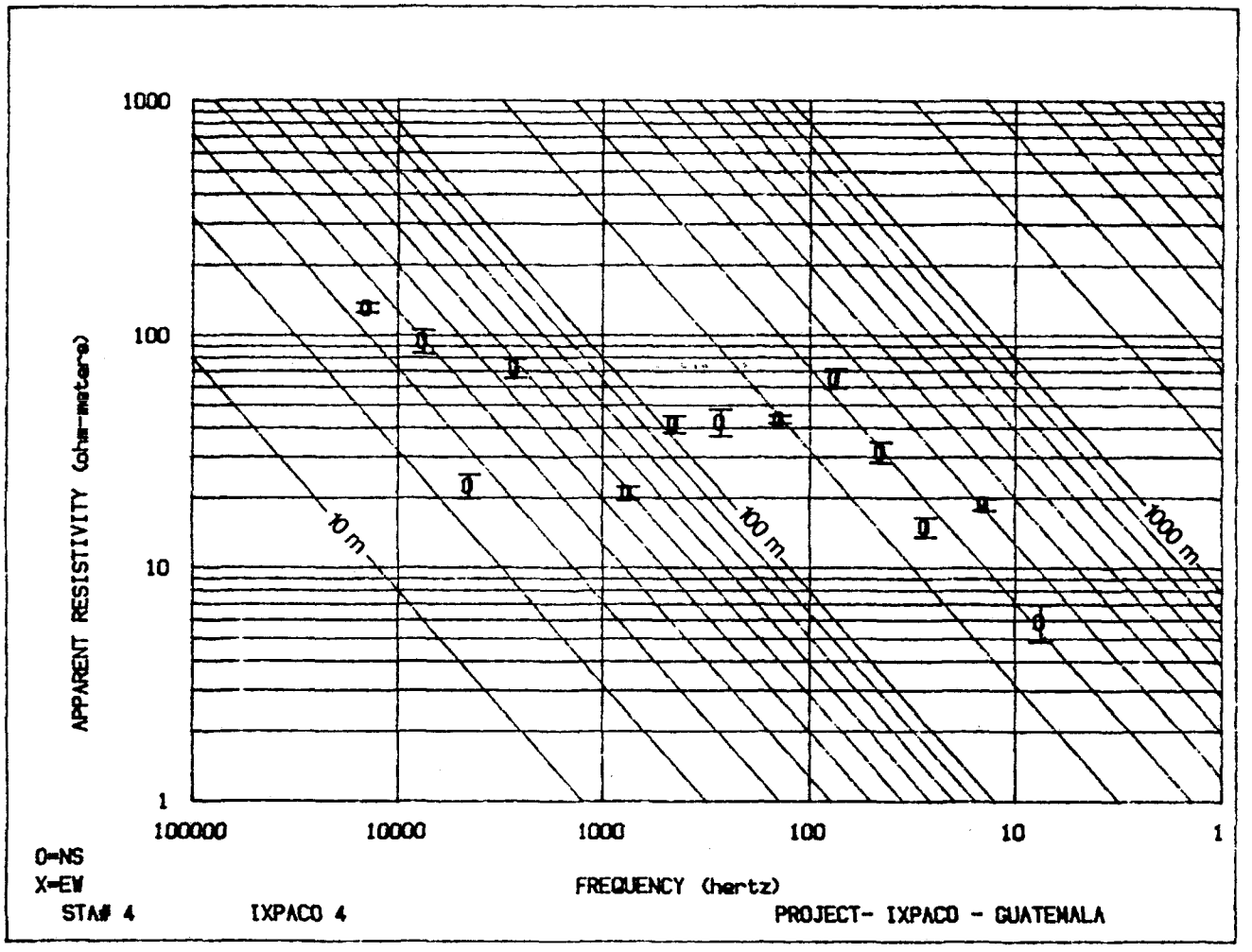

Fig. IV.2. AMT sounding on dipole 250-500 m of Ixpaco line 4. Data point shown by a 0, and I shows the error bars. Diagonal lines on a logarithmic scale indicate the depth of investigation as a function of resistivity and frequency.

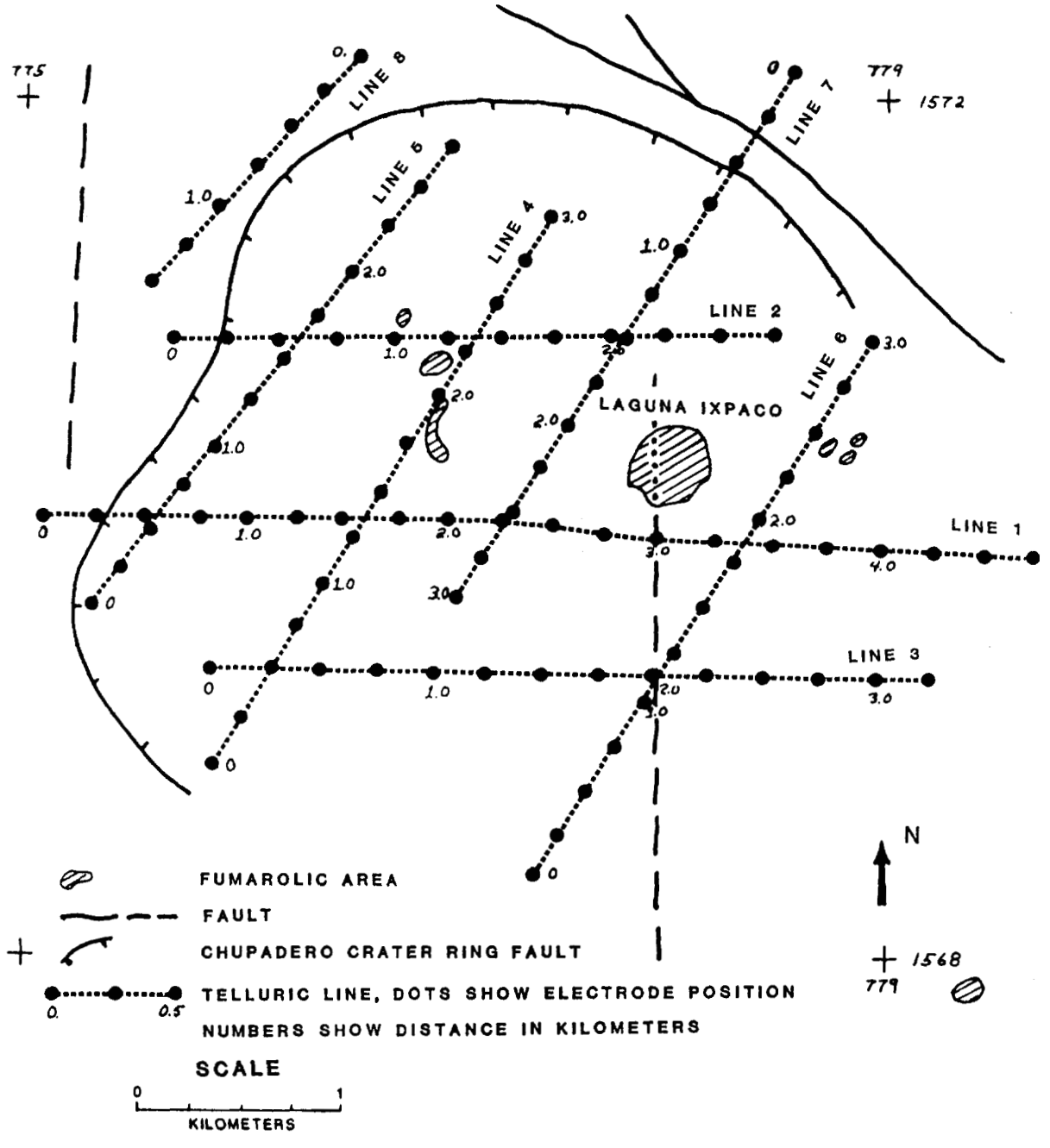

Fig. IV.3. Map showing the Chupadero crater ring fracture, faults, and fumaroles in the Ixpaco area in relation to the telluric traverse. Dashed lines show faults from the Cuilapa geologic map Inst. Geogr. Nacional (1980), and solid lines show faults from Duffield (pers. commun.).

These lines were 3,0, 2.75, 3.0, 3.0, and 1.5 km long, respectively. On all lines the dipole length was 250 m, and data were taken at frequencies of 7.5, 27, 75, 450, and 14 000 Hz. On all lines electrode positions are given in terms of distance from the initial starting position on the end of each line.

An AMT sounding was made on one 250-m dipole of each traverse. Table IV.1 gives the dipole on which these measurements were performed. Figures IV.4 through IV.11 show the sounding data. The soundings show that, in general, resistivities range between 100 and 10 ohm-m in the Chupadero crater area, which is consistent with vertical electrical soundings (VES) performed by INDE in the area. From Eq. (2), the maximum exploration depth range at 7.5 Hz for a 10 and 100 ohm-m earth is 400 and 1200 m, respectively.

These soundings yield resistivity data on each of the telluric lines so that, for all subparallel lines, contour maps of the data may be made (see Slankis et al., 1972). A series of continuous profiles employing a plane-wave energy source provides much more detail about vertical structures in complex areas than a similar number of DC electrical soundings.

Figures IV.12 through IV.19 present telluric data for the eight lines as plots of relative voltage versus dipole position. Because the measured voltage represents the integral of the natural electric field strength over the dipole length, the value is plotted a the midpoint between electrode positions. Curves for each frequency are offset an arbitrary amount, generally two times, so as to avoid overlapping of curves. The highest frequency, 14 000 Hz (curve 5), is uppermost and the lowest frequency, 7.5 Hz (curve 1), is at the bottom. Thus the top curve shows shallow features, roughly 10- to 30-m maximum depth, and each lower curve represents an increasing depth of exploration. This nesting of curves thus shows variations of electrical properties both laterally and with depth.

Figures IV.20 through IV.27 show plots of the SP on each line.

TABLE IV.1. DIPOLE LOCATIONS OF AMT SOUNDINGS

Line No.	Dipole (m)
1	4750-4775 m
2	500-750 m
3	0-250 m
4	250-500 m
5	0-250 m
6	0-250 m
7	0-250 m
8	0-250 m

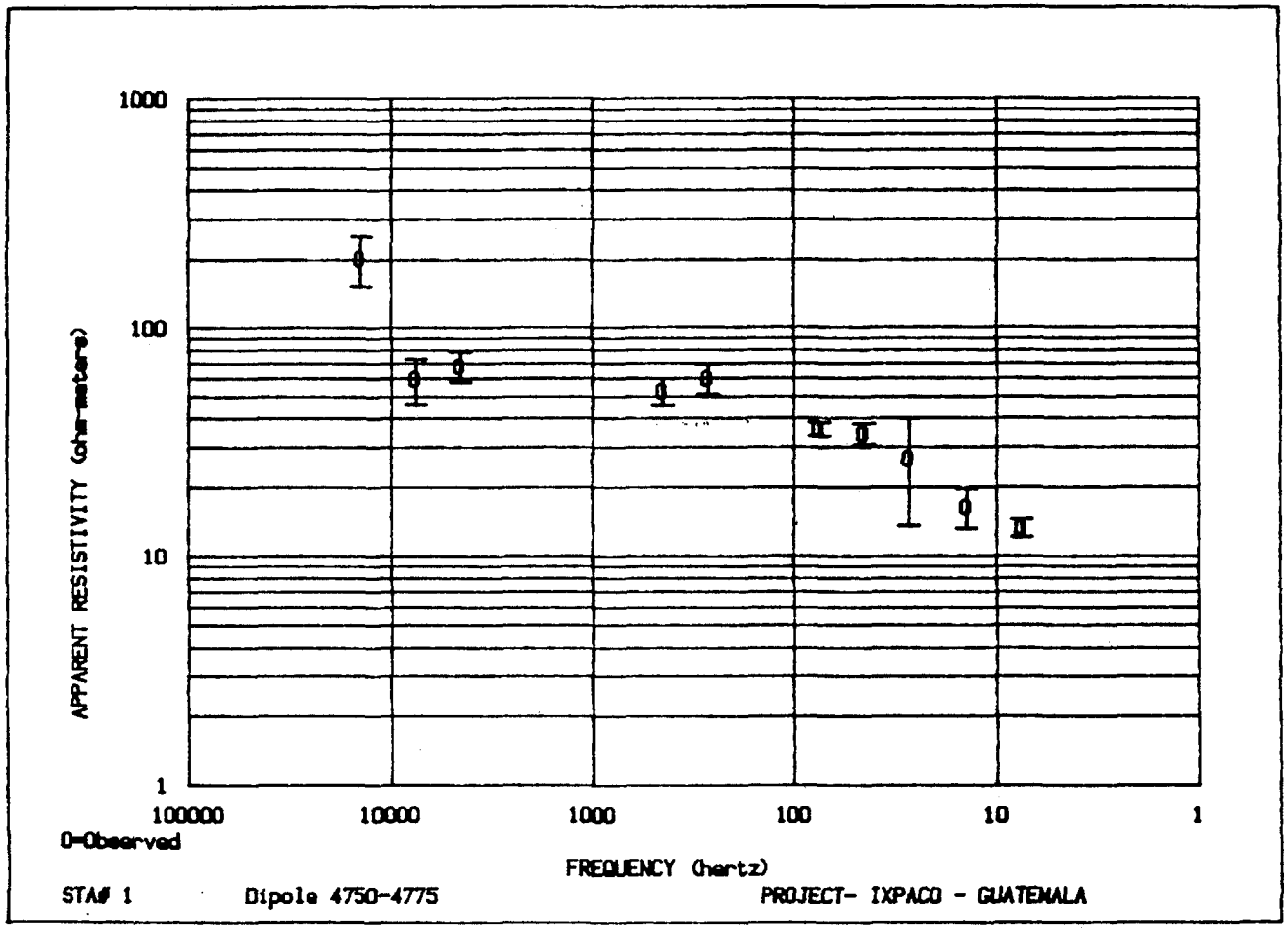

Fig. IV.4. AMT sounding on dipole 4750-4795 m of Ixpaca line 1. Data point shown by a 0, and I shows the error bars.

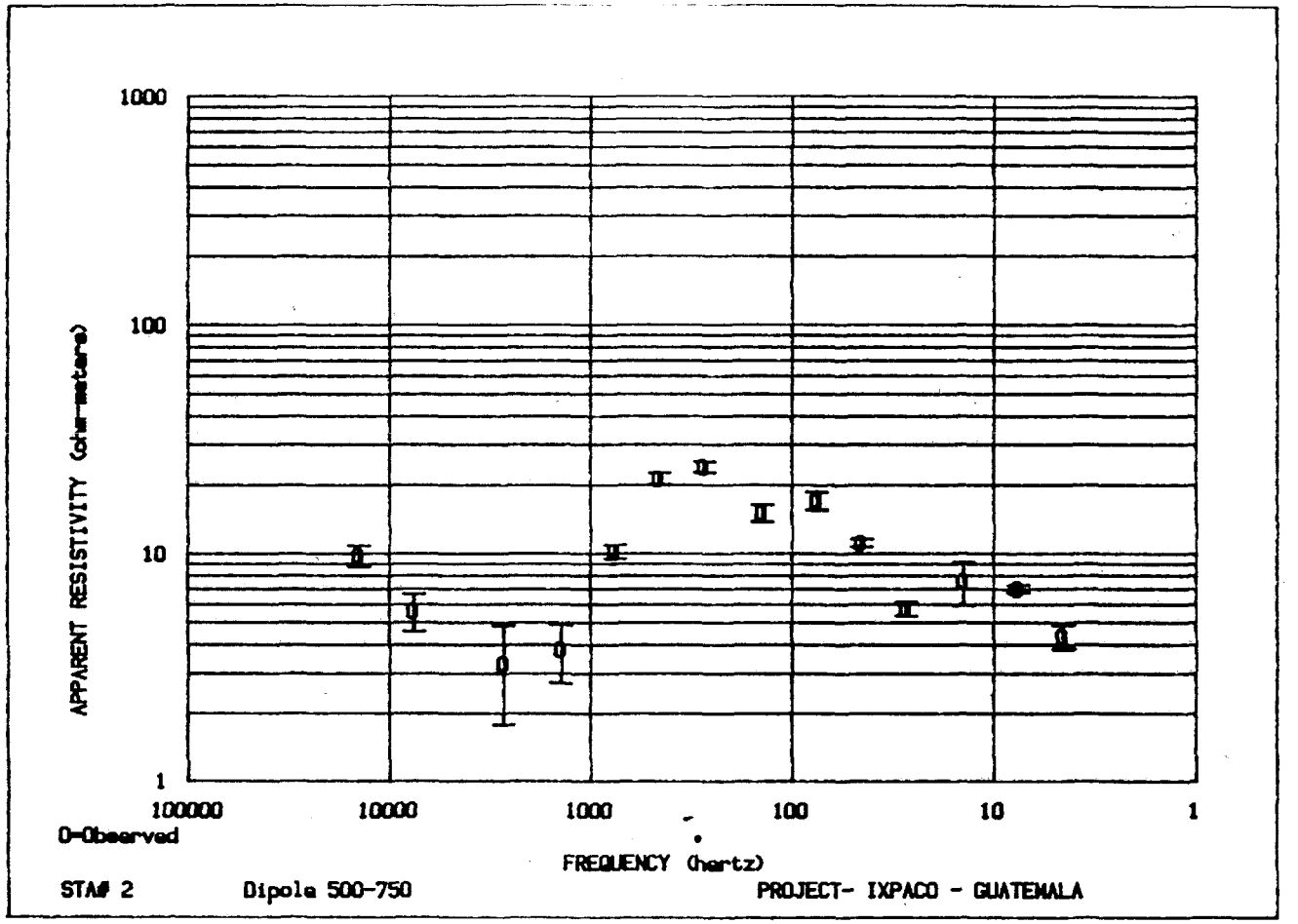

Fig. IV.5. Amt sounding on dipole 500-750 m of Ixpaca line 2. Data point shown by a 0, and I shows the error bars.

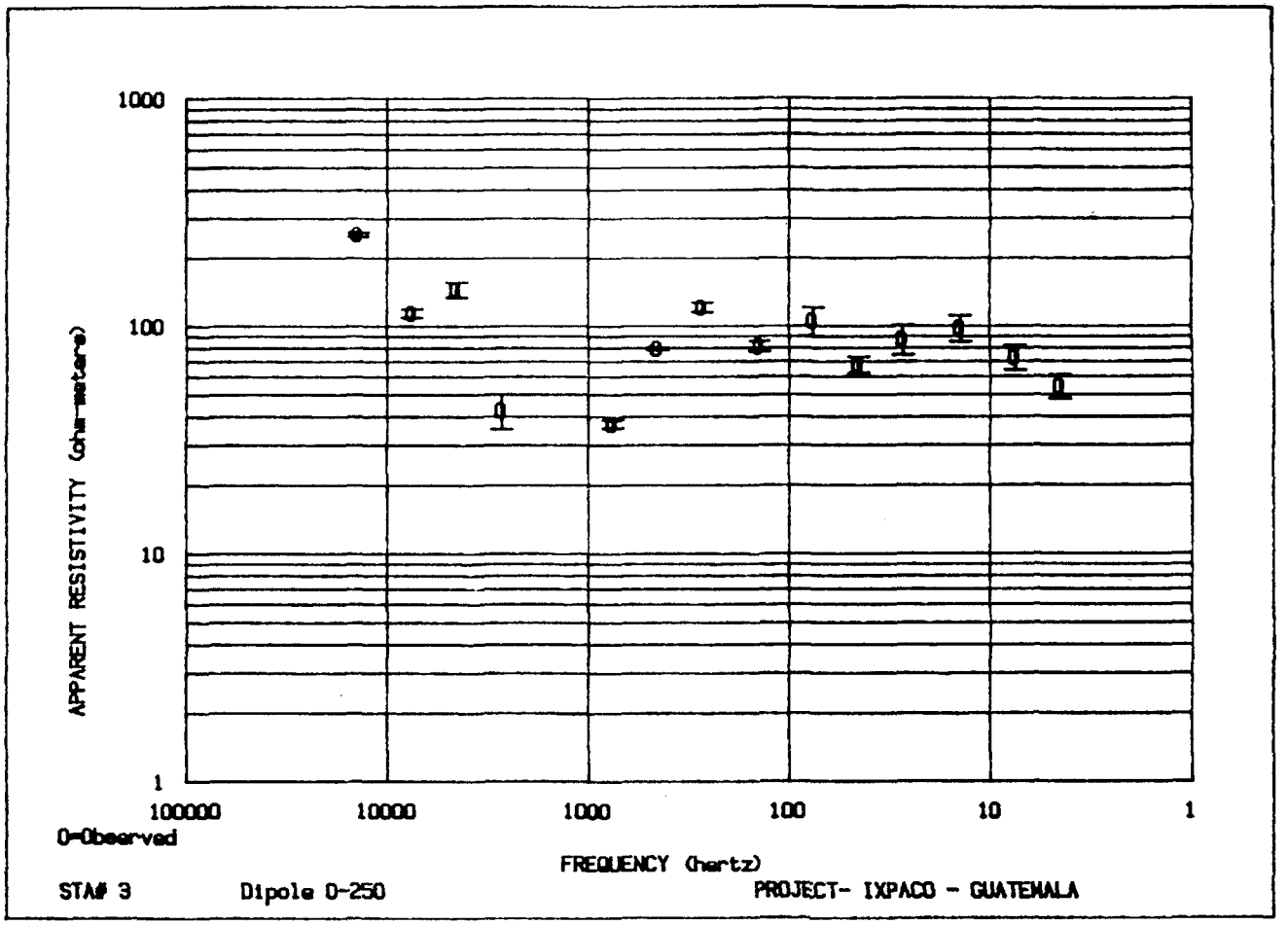

Fig. IV.6. AMT sounding on dipole 0-250 m of Ixpaca line 3. Data point shown by a 0, and I shows the error bars.

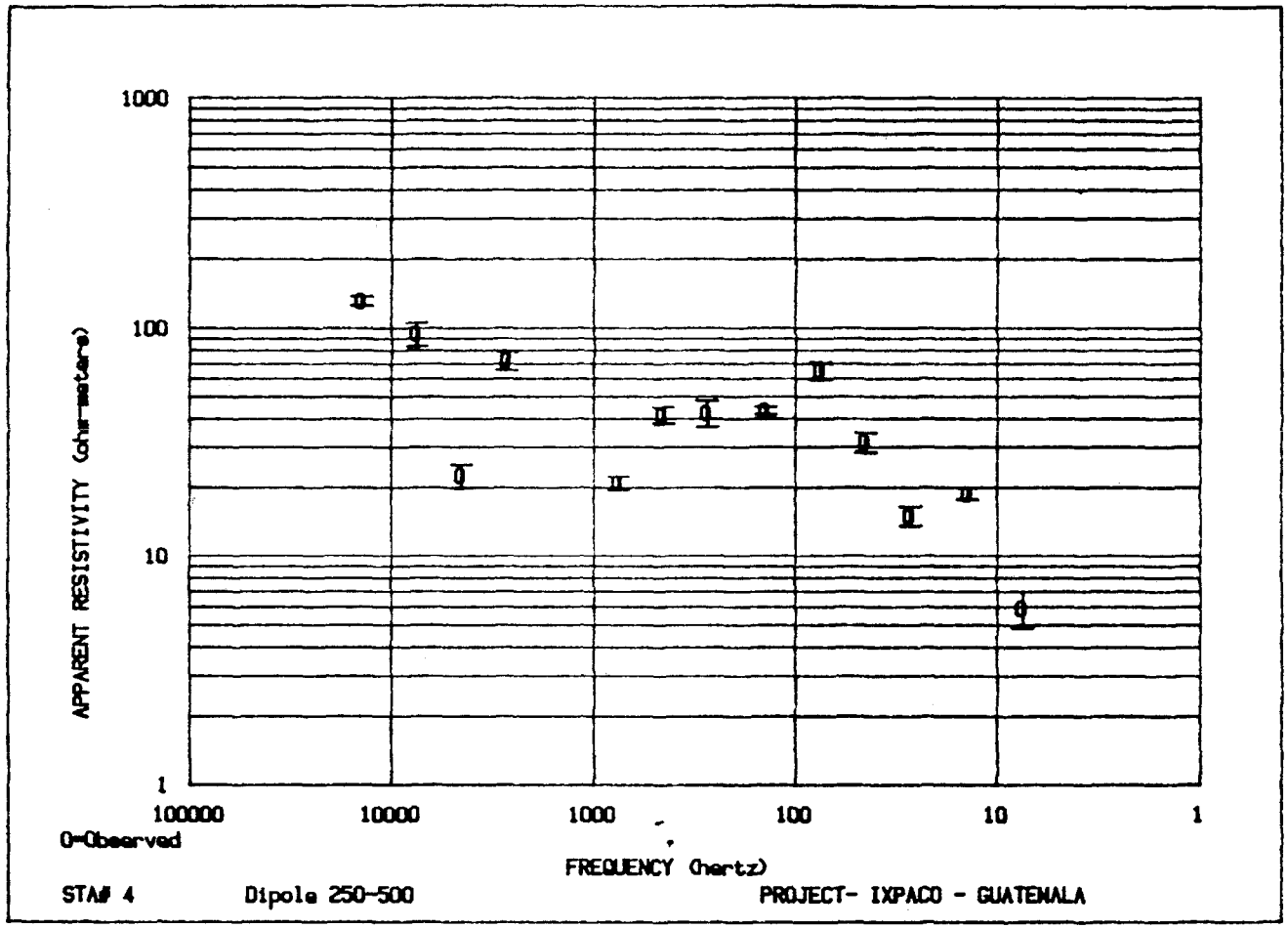

Fig. IV.7. AMT sounding on dipole 250-500 m of Ixpaca line 4. Data point shown by a 0, and I shows the error bars.

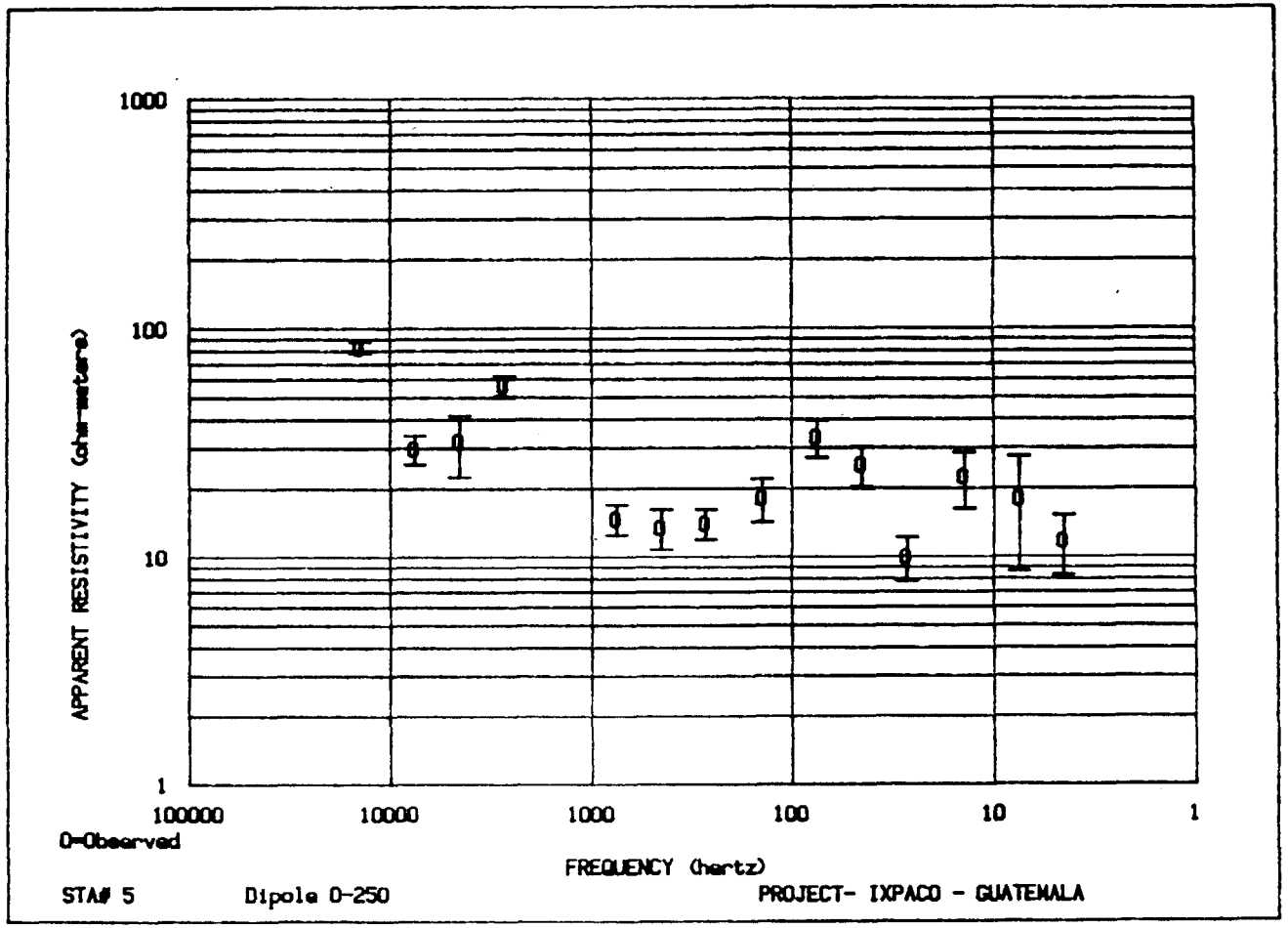

Fig. IV.8. AMT sounding on dipole 0-250 m of Ixpaca line 5. Data point shown by a 0, and I shows the error bars.

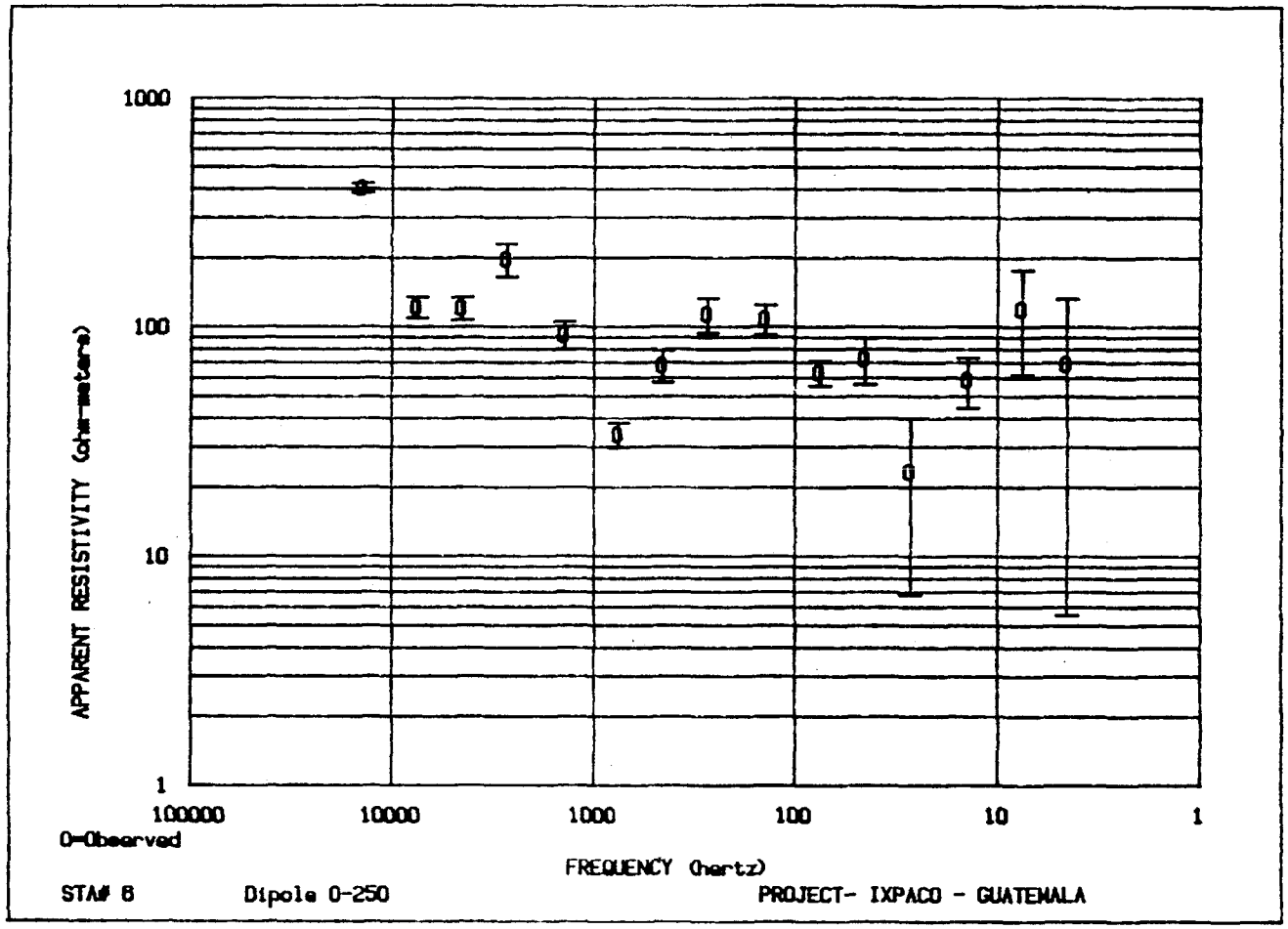

Fig. IV.9. AMT sounding on dipole 0-250 m of Ixpaca line 6. Data point shown by a 0, and I shows the error bars.

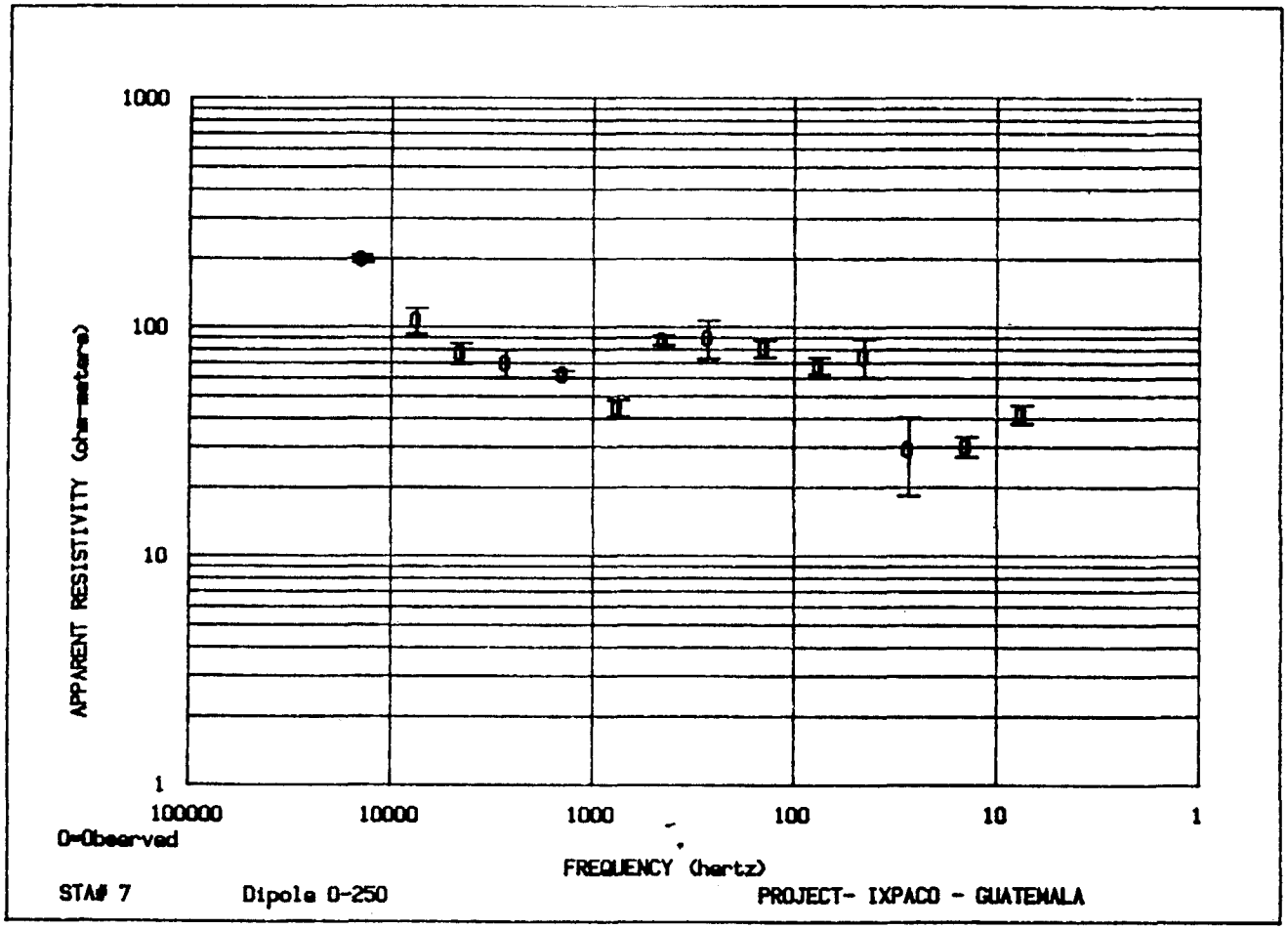

Fig. IV.10. AMT sounding on dipole 0-250 m of Ixpaca line 7. Data point shown by a 0, and I shows the error bars.

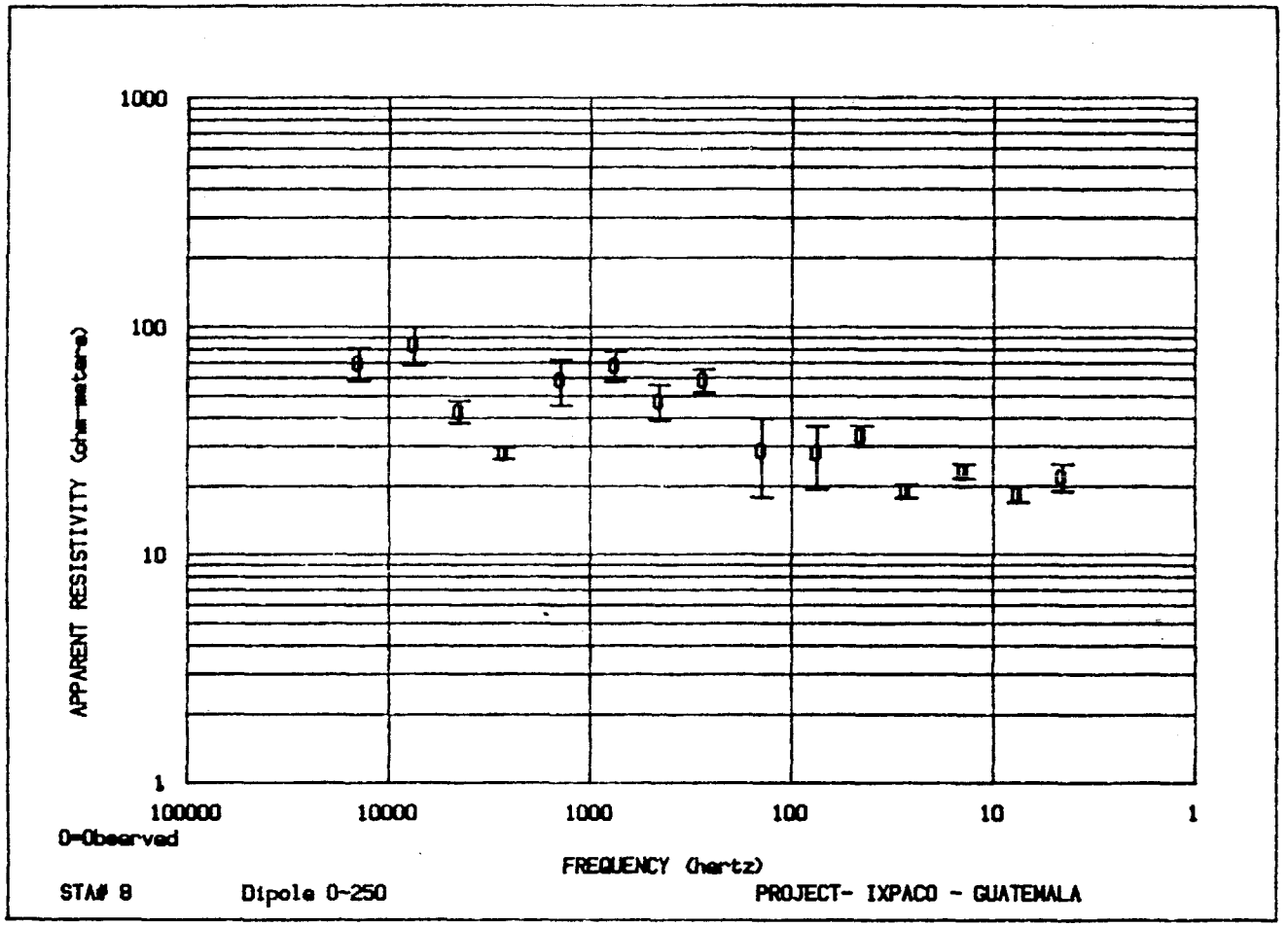

Fig. IV.11. AMT sounding on dipole 0-250 m of Ixpaca line 8. Data point shown by a 0, and I shows the error bars.

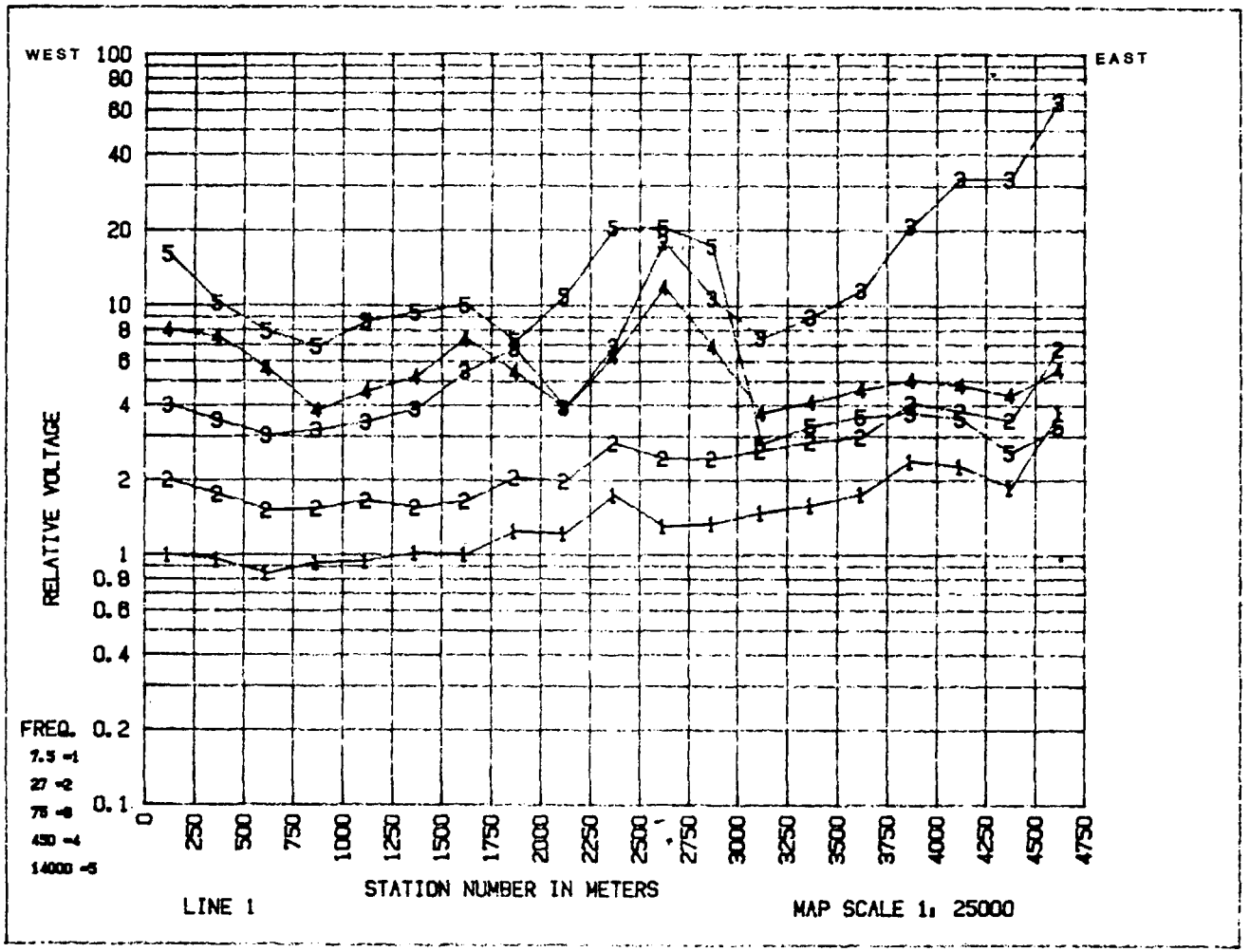

Fig. IV.12. Multifrequency telluric data for Chupadero line 1. For 7.5 Hz the ordinate shows the ratio of the telluric voltage at any dipole, to the voltage on the initial dipole (0-250 m). Because only changes in voltage are important geologically the higher frequency curves have been shifted vertically for ease of viewing.

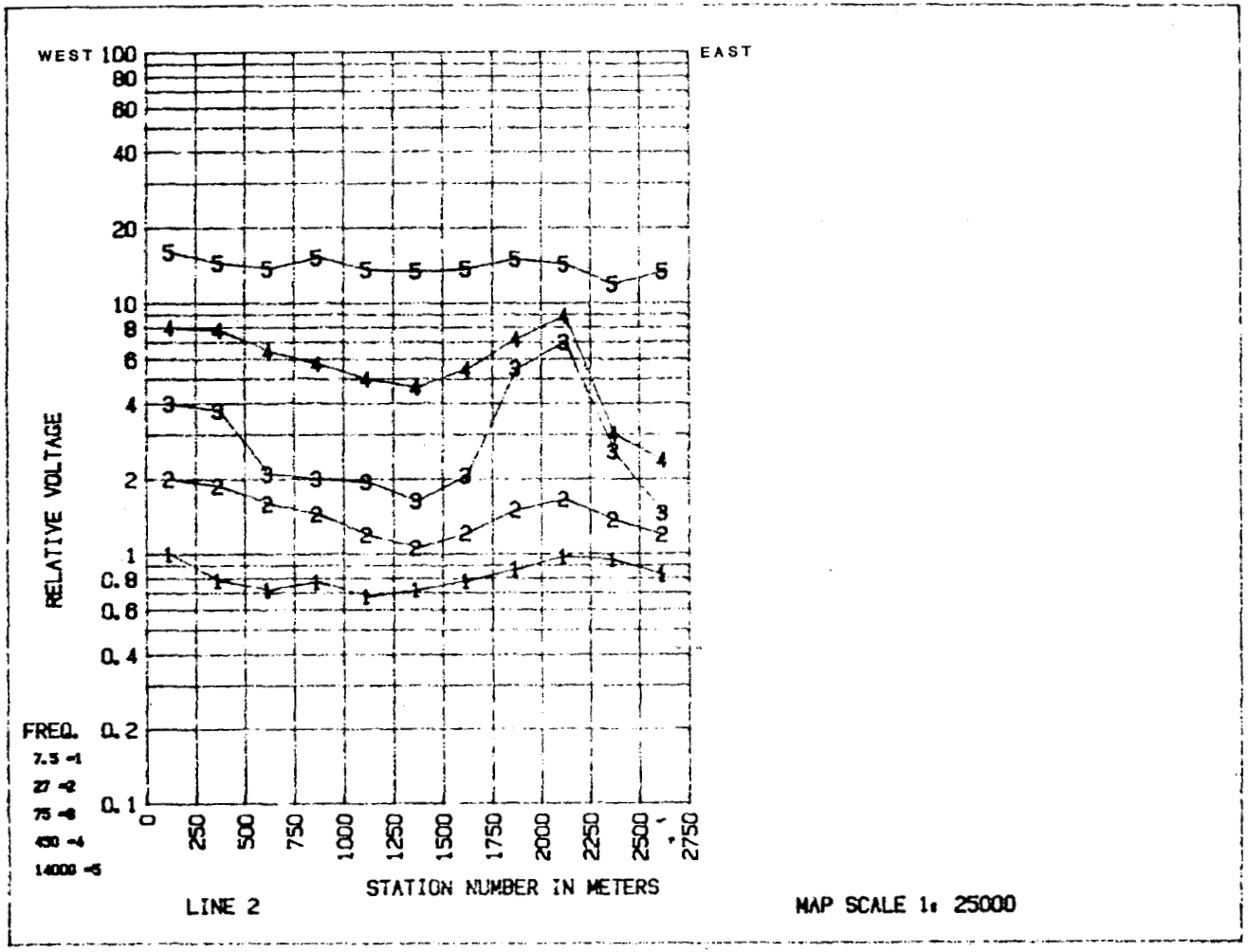

Fig. IV.13. Multifrequency telluric data for Chupadero line 2. For 7.5 Hz the ordinate shows the ratio of the telluric voltage at any dipole, to the voltage on the initial dipole (0-250 m). Because only changes in voltage are important geologically, the higher frequency curves have been shifted vertically for ease of viewing.

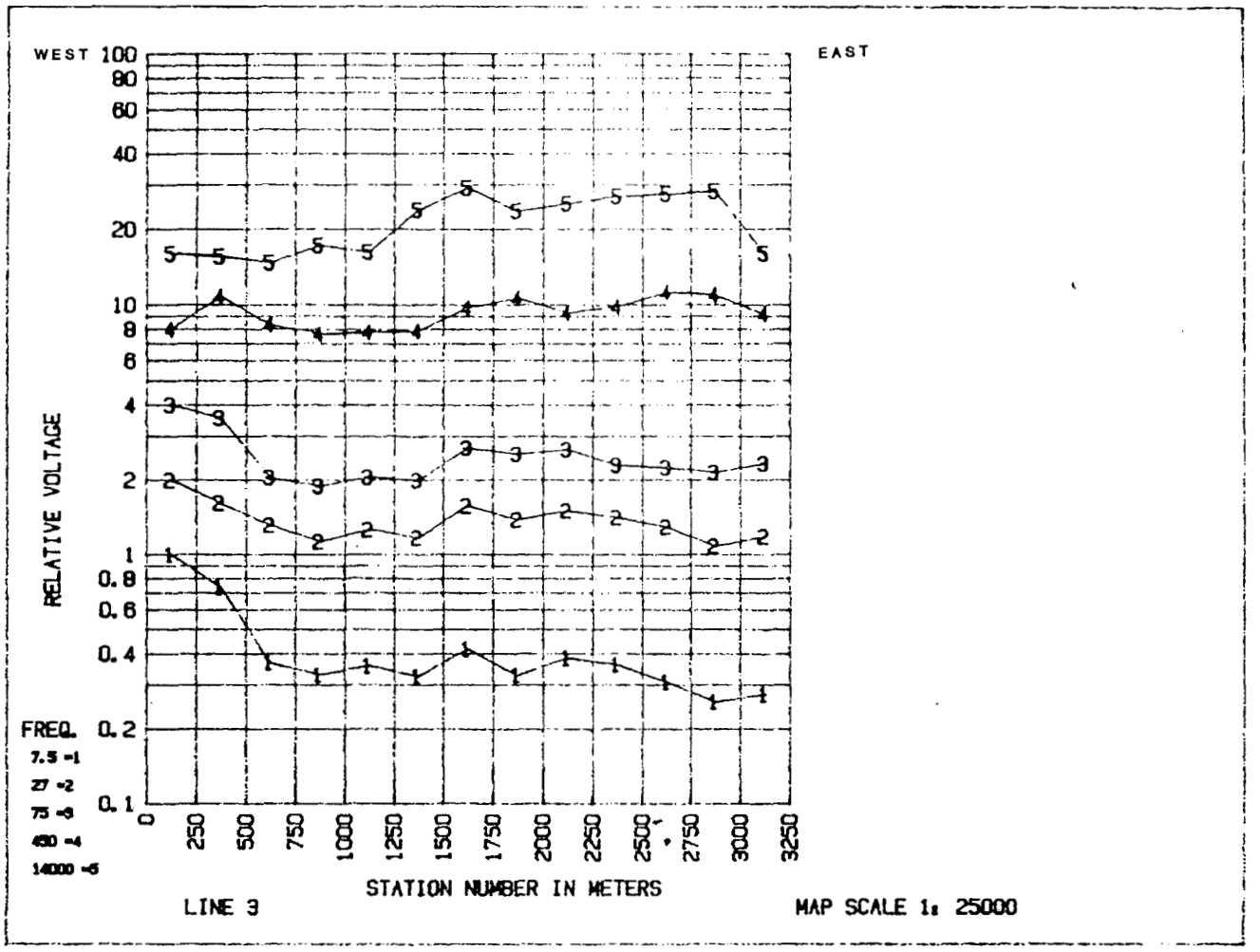

Fig. IV.14. Multifrequency telluric data for Chupadero line 3. For 7.5 Hz the ordinate shows the ratio of the telluric voltage at any dipole, to the voltage on the initial dipole (0-250 m). Because only changes in voltage are important geologically, the higher frequency curves have been shifted vertically for ease of viewing.

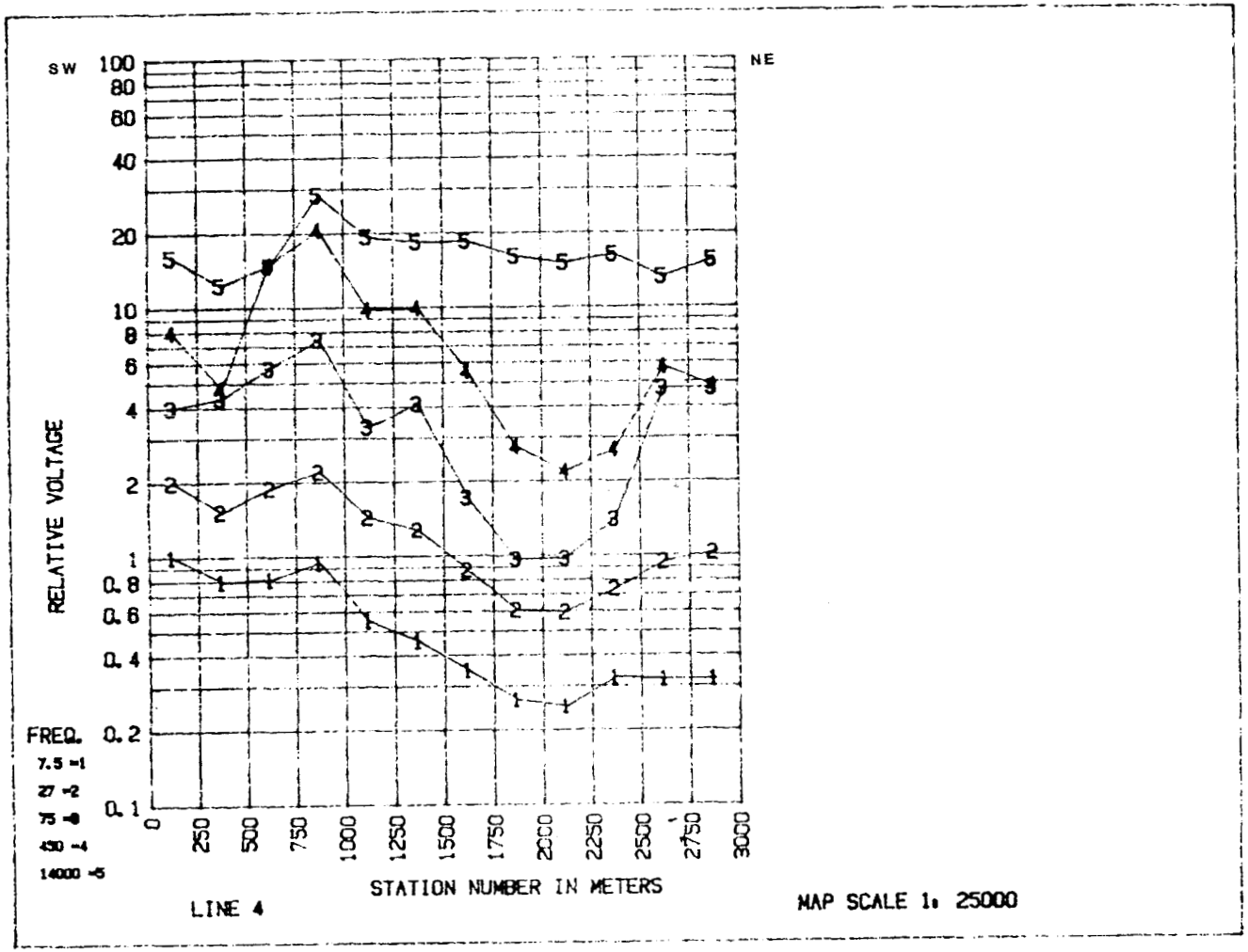

Fig. IV.15. Multifrequency telluric data for Chupadero line 4. For 7.5 Hz the ordinate shows the ratio of the telluric voltage at any dipole, to the voltage on the initial dipole (0-250 m). Because only changes in voltage are important geologically, the higher frequency curves have been shifted vertically for ease of viewing.

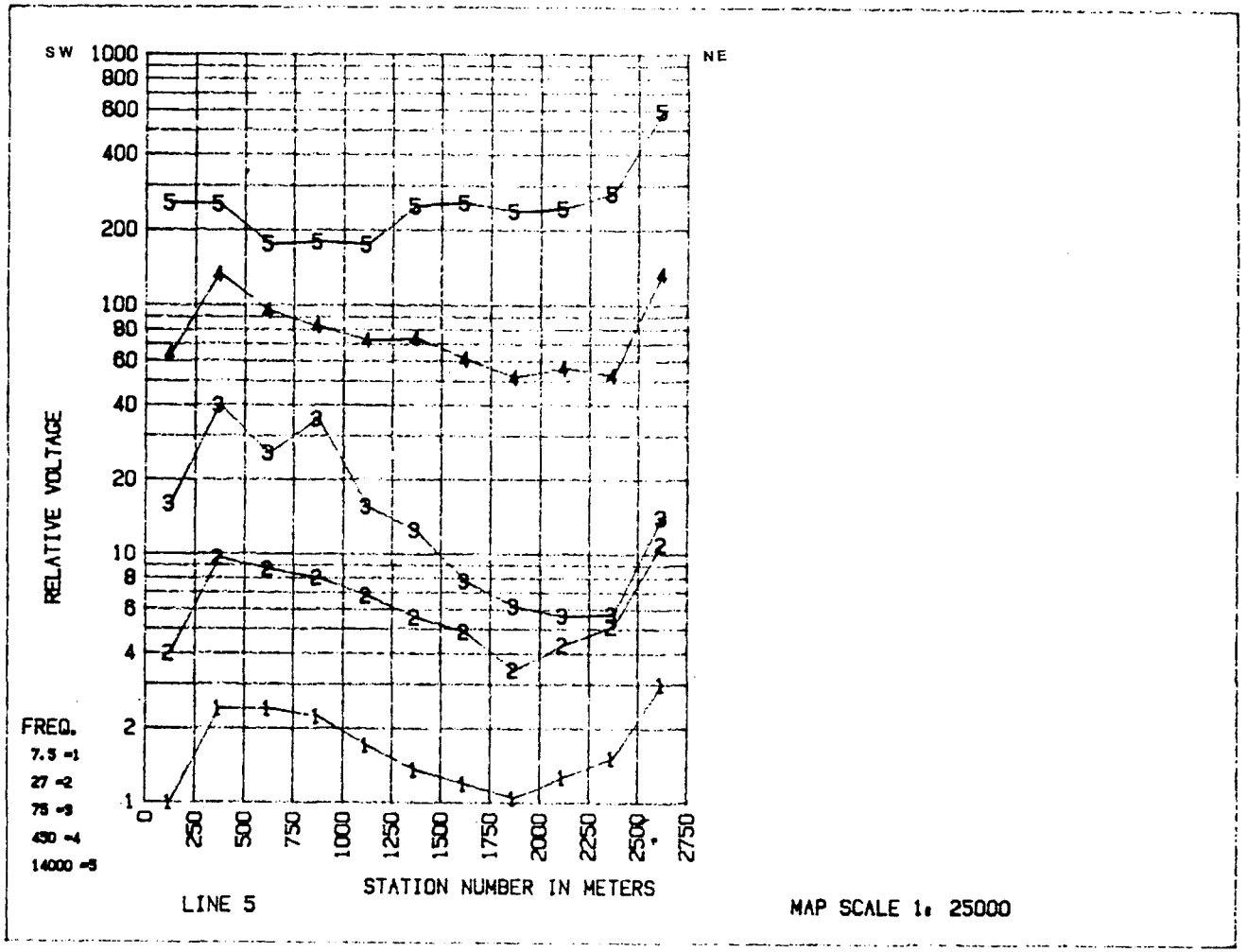

Fig. IV.16. Multifrequency telluric data for Chupadero line 5. For 7.5 Hz the ordinate shows the ratio of the telluric voltage at any dipole, to the voltage on the initial dipole (0-250 m). Because only changes in voltage are important geologically, the higher frequency curves have been shifted vertically for ease of viewing.

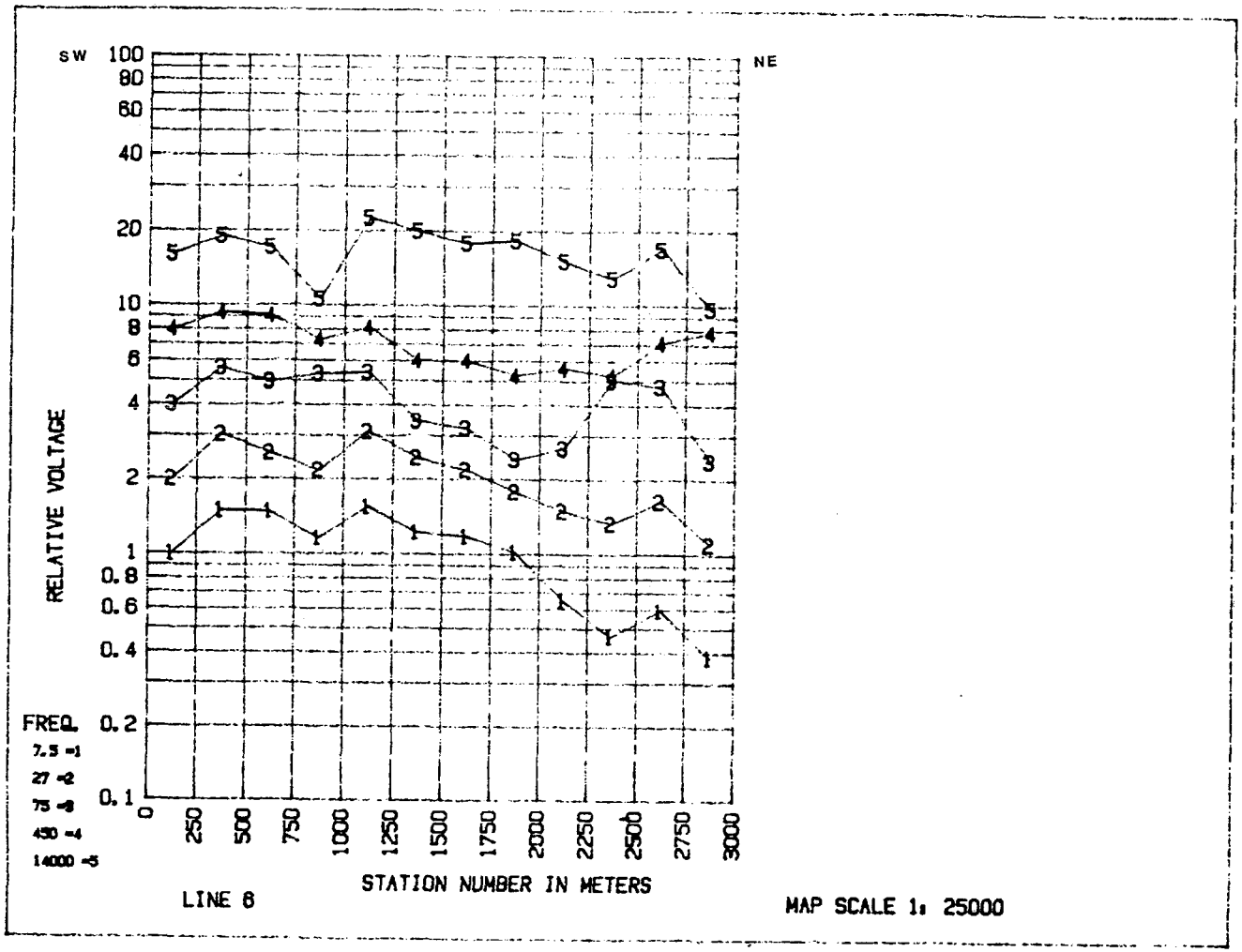

Fig. IV.17. Multifrequency telluric data for Chupadero line 6. For 7.5 Hz the ordinate shows the ratio of the telluric voltage at any dipole, to the voltage on the initial dipole (0-250 m). Because only changes in voltage are important geologically, the higher frequency curves have been shifted vertically for ease of viewing.

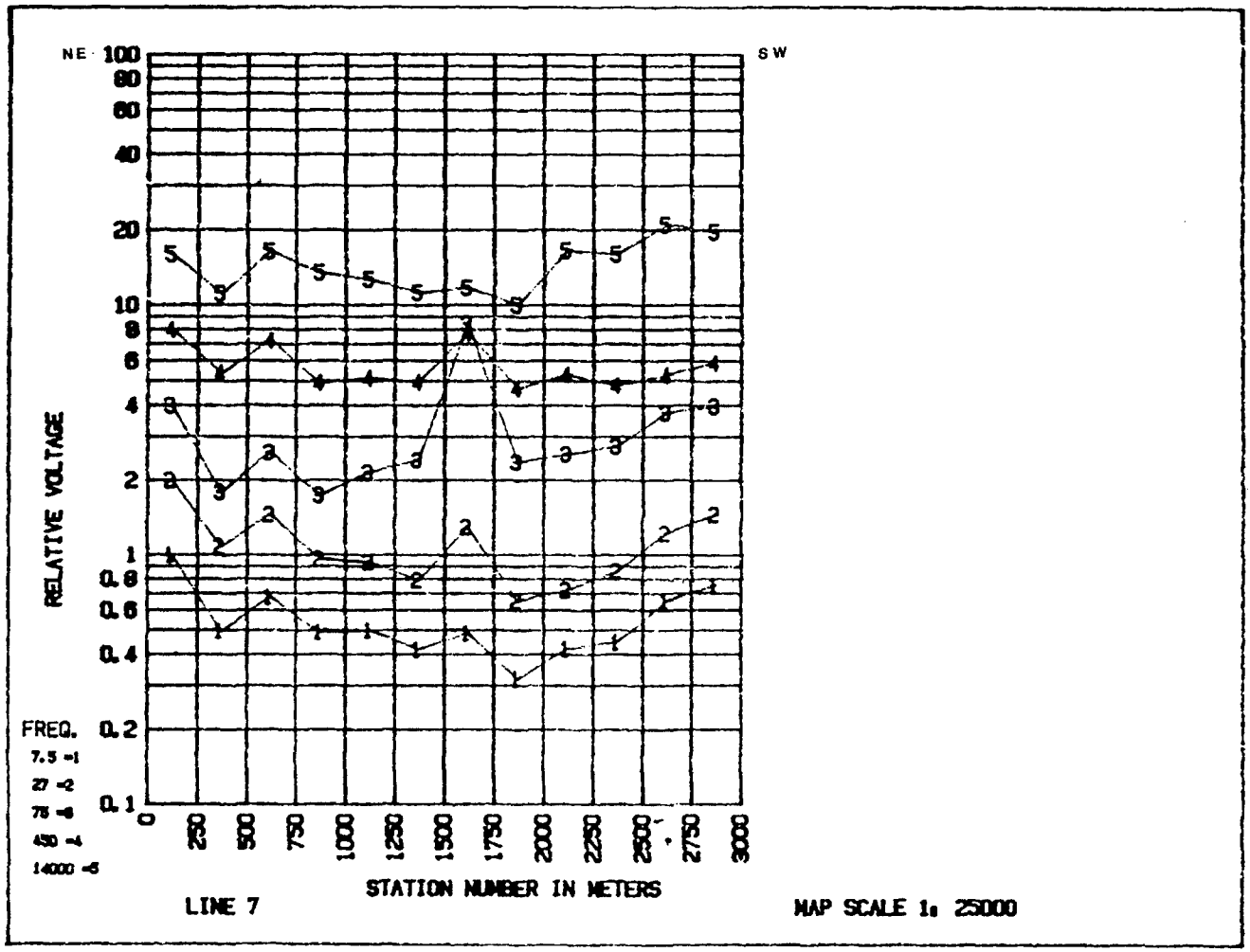

Fig. IV.18. Multifrequency telluric data for Chupadero line 7. For 7.5 Hz the ordinate shows the ratio of the telluric voltage at any dipole, to the voltage on the initial dipole (0-250 m). Because only changes in voltage are important geologically, the higher frequency curves have been shifted vertically for ease of viewing.

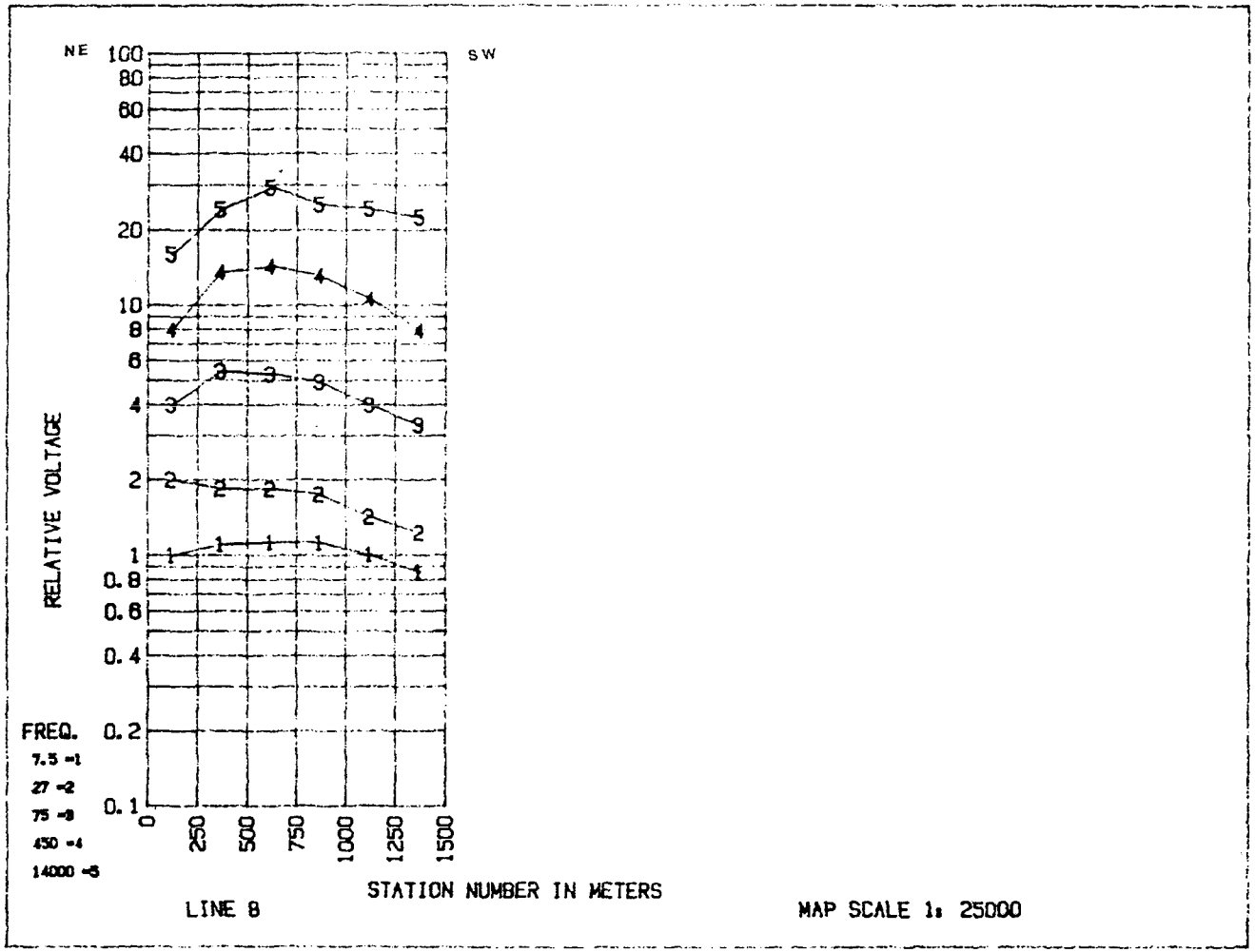

Fig. IV.19. Multifrequency telluric data for Chupadero line 8. For 7.5 Hz the ordinate shows the ratio of the telluric voltage at any dipole, to the voltage on the initial dipole (0-250 m). Because only changes in voltage are important geologically, the higher frequency curves have been shifted vertically for ease of viewing.

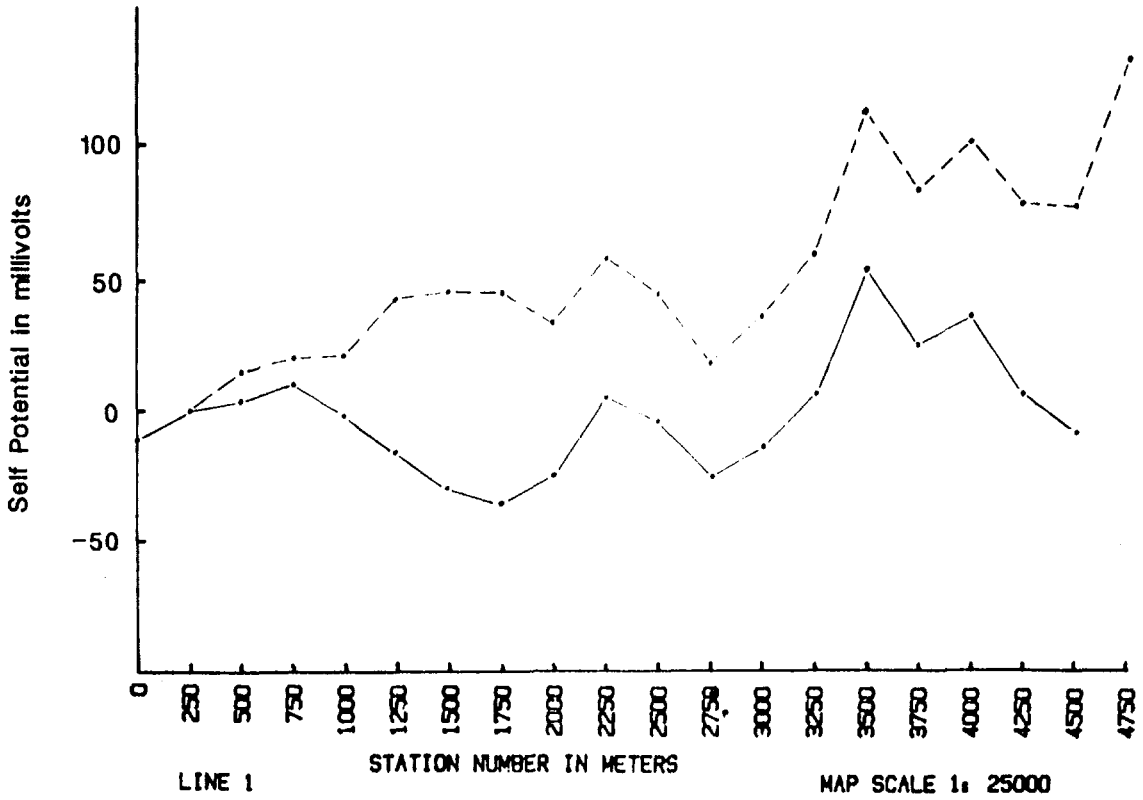

Fig. IV.20. Self potential data for Chupadero line 1. The solid curve shows data for the two back pair of electrodes, and the dashed line for the forward pair of electrodes of the telluric profile.

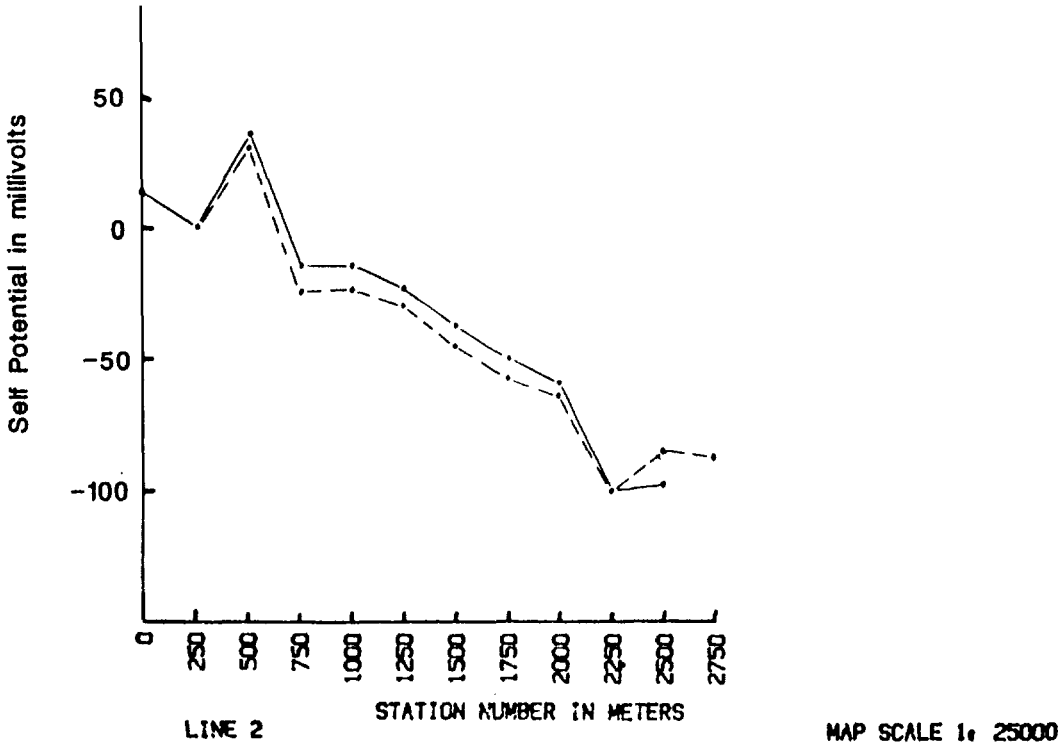

Fig. IV.21. Self potential data for Chupadero line 2. The solid curve shows data for the two back pair of electrodes, and the dashed line for the forward pair of electrodes of the telluric profile.

Fig. IV.22. Self potential data for Chupadero line 3. The solid curve shows data for two back pair of electrodes, and the dashed line for the forward pair of electrodes of the telluric profile.

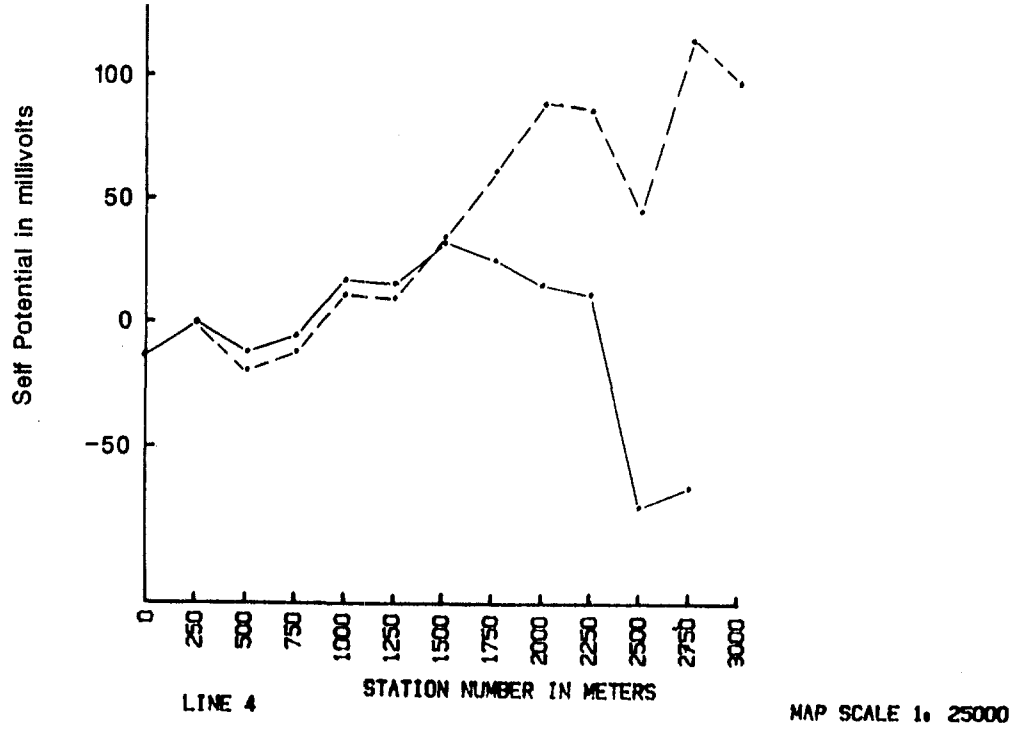

Fig. IV.23. Self potential data for Chupadero line 4. The solid curve shows data for the two back pair of electrodes, and the dashed line for the forward pair of electrodes of the telluric profile

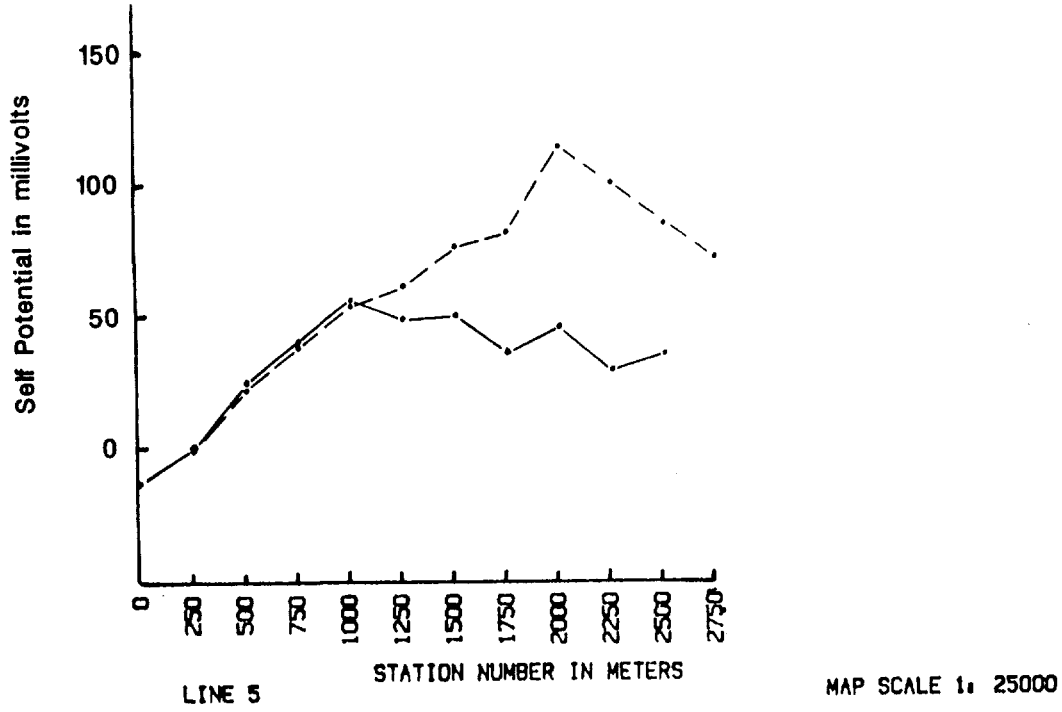

Fig. IV.24. Self potential data for Chupadero line 5. The solid curve shows data for the two back pair of electrodes, and the dashed line for the forward pair of electrodes of the telluric profile.

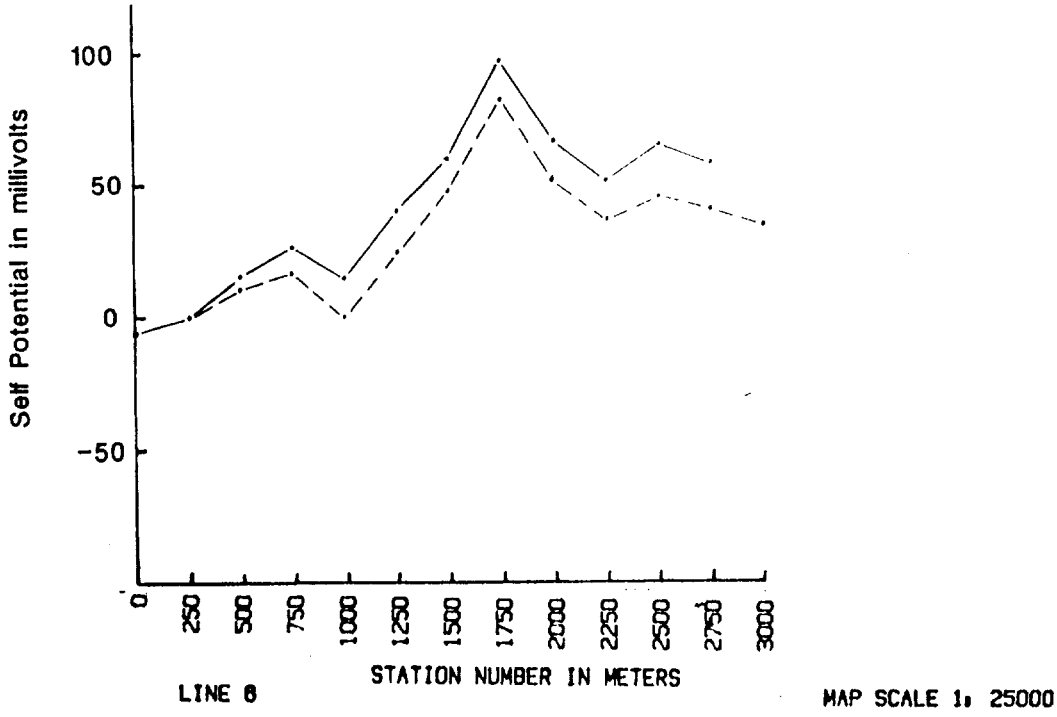

Fig. IV.25. Self potential data for Chupadero line 6. The solid curve shows data for the two back pair of electrodes, and the dashed line for the forward pair of electrodes of the telluric profile.

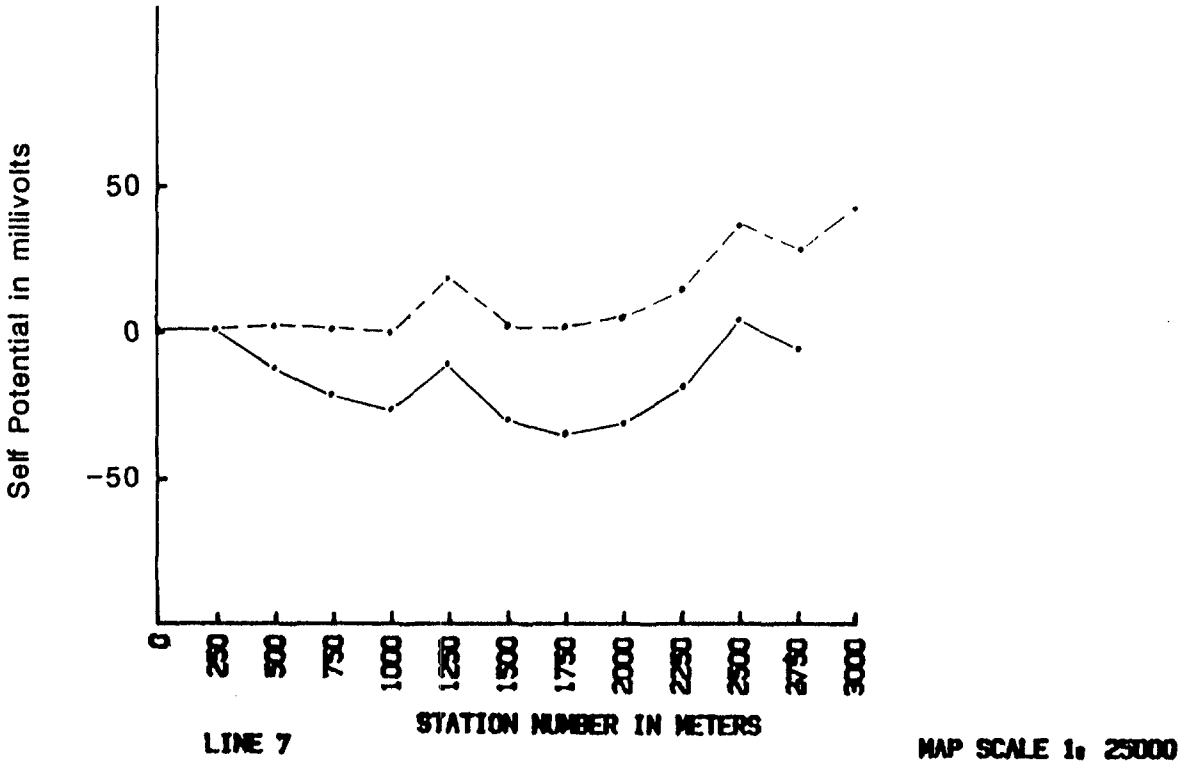

Fig. IV.26. Self potential data for Chupadero line 7. The solid curve shows data for the two back pair of electrodes, and the dashed line for the forward pair of electrodes of the telluric profile.

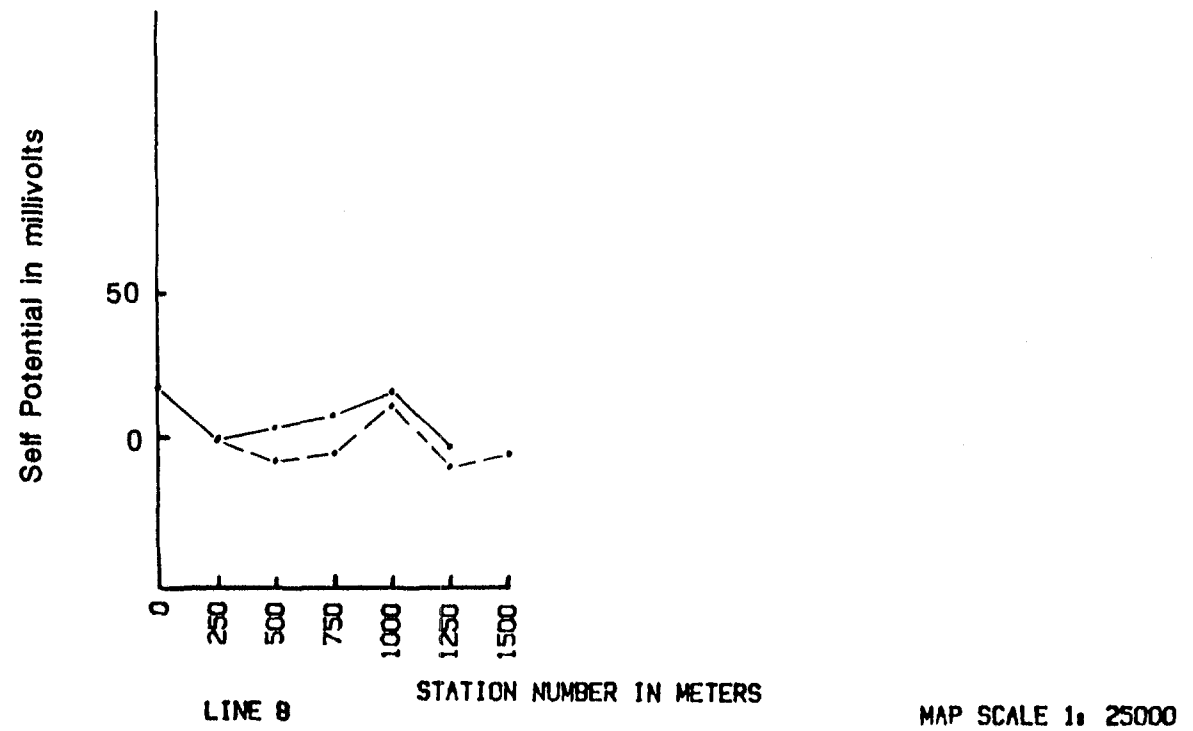

Fig. IV.27. Self potential data for Chupadero line 8. The solid curve shows data for the two back pair of electrodes, and the dashed line for the forward pair of electrodes of the telluric profile.

D. DISCUSSION OF DATA

Telluric lines 1, 2, and 3 (Figs. IV.12, IV.13, and IV.14), oriented in an EW direction, were run to try to identify any NS-trending structures which may be related to normal faulting that defines the Tecuamburro graben. No clear evidence for a NS-trending feature can be seen in the data of lines 1 through 3. Obvious interference from power lines can be seen on line 1, at dipoles 2.5-2.75 km and 4.5-4.75 km and on line 2 at dipoles 1.75-2.25 km, particularly on the 75-Hz traverse data. Line 3 is free of this problem.

Examination of the high-frequency, 14 000-Hz data shows good correlation with the mapped surficial geology (W. A. Duffield, U.S. Geological Survey, personal communication 1989). On line 1, a high-resistivity zone is seen between 2.25 and 3.0 km that corresponds with the position of the phreatic tuff ring from Ixpaco Crater. From 3.0 to 4.4 km, a younger debris avalanche flow of basaltic andesite is crossed showing much lower resistivity. The contact of this flow with an older andesitic pumice occurs at 4.4 km and appears to be marked by a small resistivity low on dipole 4.25-4.50 km. However, this low persists on the lower-frequency data indicating that this electrical feature extends to depth. This may be an expression of the ring fracture of the Chupadero crater. The western margin of the Chupadero crater on line 4 is crossed near position 0.25 km. To the west are andesites from the Miraflores sratovolcano, whereas Quaternary alluvium is present east of 0.25 km to the contact with the phreatic tuff ring from Ixpaco. No sharp electrical boundary is apparent where the line crosses the western boundary of the Chupadero crater, although the data show an increase in resistivity as might be expected over the older Miraflores volcanics. A resistivity minimum at dipole 0.50-0.75 km on the lower-frequency data could be an expression of increased fracturing along the ring fracture of the Chupadero crater at depth. The offset of the resistivity minimum from the mapped surface expression may be due to the dip of the ring fracture. In all cases where the ring fracture was crossed or approached, the inferred electrical expression is offset about 250 m inside the mapped location. This is also true for the INDE VES data northeast of Ixpaco Lake where there was sufficient detail to define the resistivity transition across the crater rim (see the VES map, Fig. IV.28).

Line 2 is on alluvium within the Chupadero crater, except on each end. The crater rim on the western end is mapped at 0.25 km, and the electrical expression is inferred to be represented by the abrupt change in resistivity at 0.5 km for the 75-Hz data and the subtle low on dipole 0.50-0.75 km at 7.5 and 27 Hz. The lowest resistivity zone, near position 1.25 km, correlates with a zone of fumaroles west of Ixpaco.

Line 3 is on Miraflores volcanics from 0 to 1.2 km, then on alluvium to 1.8 km, and the remainder on a debris avalanche flow of basaltic andesite. The 14-kHz data appear to define these three lithologic units. The line does not cross any known margin of the Chupadero crater. Data at 75 Hz and

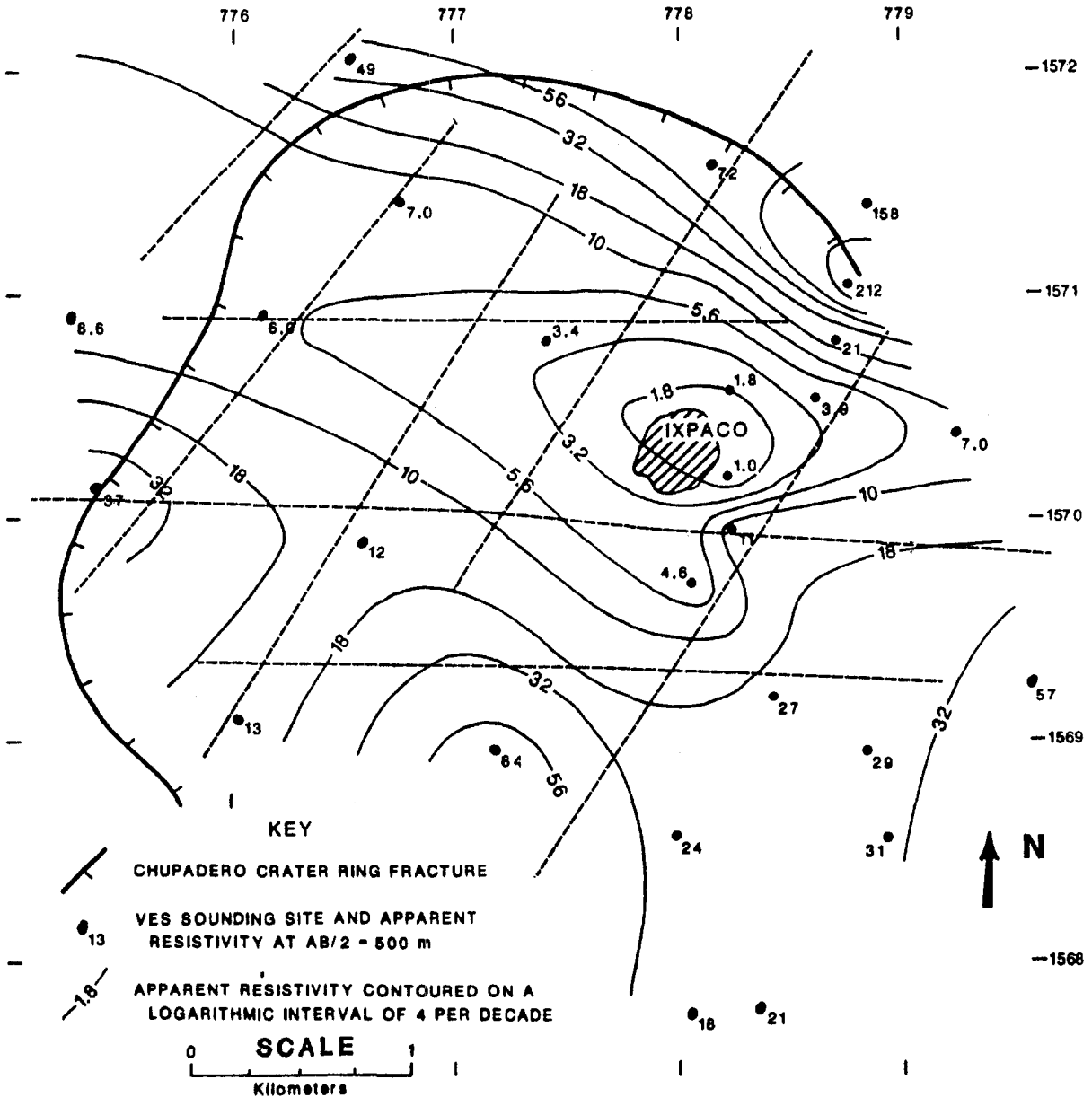

Fig. IV.28. Apparent resistivity map derived from INDE VES data in the Chupadero Crater area using an AB/2 current separation of 500 m. The location of the telluric traverses are indicated by the thin dashed lines.

lower show a distinct electrical boundary at 0.5 km with resistive units to the west. The Chupadero crater boundary is mapped 600 m west of the start of line 3, so this is not an expression of the mapped ring fracture.

The Cuilapa geologic map (plate 1, in pocket) shows the appropriate location of two NS-trending faults that cross lines 1 and 3. One of these, just west of the Chupadero crater margin, crosses line 1 on dipole 0-0.75 km and is not evident in the data. The other fault runs through Ixpaco Lake crossing line 1 at 3.0 km and line 2 at 2.0 km. This fault also, if present, has no clear expression in the electrical data.

Traverse lines 4-8 were run in a NE-SW direction to identify NW-trending structural features within the crater. This is a prominent structural trend northeast of the Chupadero crater, and covered structures with this orientation within the crater could be significant in localizing the existing hydrothermal system. Lines 4-7 (Figs. IV.15-IV.18) are within the crater. On each of these lines, a resistivity low is seen in the northern part of the crater that defines a WNW trend running through Ixpaco Lake and fumarolic vents each and west of the lake. This low is fairly broad on lines 4 and 5 centered on dipoles 2.0-2.25 and 1.75-2.0 km, respectively. On line 4, this low correlates directly with the location of known fumaroles. On lines 6 and 7, the lows are not quite as prominent but occur on dipoles 2.75-2.5 and 1.75-2.0 km, respectively. The low on line 6 also correlates directly with known fumaroles a few hundred meters east of the line. We infer that this electrical low seen on the four lines within the Chupadero crater is an expression of a major fracture of fault zone controlling the upward movement of fluids and gasses within the crater. Line 8 outside the crater shows relatively little change in resistivity at the lower frequencies. The lowest values, however, are on the southwestern end of the line where the line enters an area of altered rock (Cuilapa geologic map, in pocket). The electrical data are consistent with the presence of altered rock on the southwest end. Unfortunately, the line is not long enough to provide much evidence for extension of the WNW trend, seen within the crater, to line 8.

Line 4 is entirely within the Chupadero crater. A power line was crossed on dipoles 0.75-1.0 and 2.5-2.75 km. Noise from this source creates the peaks seen on 75- and 450-Hz data on each of the dipoles. The crater rim is mapped 250 m off the southwestern end of the line. Miraflores volcanics are present on the first 500 m and alluvium along the rest of the line.

Line 5 is quite similar to line 4 in general appearance, with the northern half of the crater defined by a broad low-resistivity zone at depth. The first dipole on the line exhibits a pronounced resistivity low that may be an expression of the crater ring fracture mapped 100 m south of the line. An abrupt rise in resistivity on the northern end is inferred to mark the crossing of the ring fracture into more competent rock. The boundary, however, is mapped at approximately 3.0 km on the line.

Line 6 shows a much broader zone of high resistivities at depth, with the lowest resistivities near the northern margin of the crater. The low on dipole 2.25-2.50 km, referred to previously, is believed to mark the trace of a prominent low-resistivity zone trending WNW across the crater. THe low on the last dipole (2.75-3.0 km) is inferred to be an expression of the ring fracture zone at depth. VES data provided by INDE show that resistivities rise abruptly 250 m north of the end of this line in support of this inference. Minor power line interference is present on dipoles 0.75-1.0 and 2.75-2.50 km, but it is evident only on the 75-Hz data.

Line 7 was intended to provide added definitions of the low-resistivity zone within the crater as well as provide a signature for the ring fracture and a major WNW-trending fault outside of the crater. Dipole 0.25-0.50 km crosses normal to the trace of a WNW-trending fault. The low-resistivity zone on this dipole is inferred to be an expression of increased fracturing associated with the fault zone. The Chupadero ring fracture is also inferred to be positioned on dipole 0.75-1.0 km. The minimum on dipole 1.75-2.0 km identifies the axis of the WNW-trending conductive zone in the northern part of the Chupadero crater.

Line 8 is entirely outside the Chupadero crater on andesitic lava flows (Chap. I). The lower-frequency data show that lowest resistivities are on the southwest end of the line at the two dipoles. The Cuilapa geological map shows these two dipoles to be in an area of hydrothermal alteration, which could be responsible for the lower resistivities. The electrical data are insufficient to determine of the low-resistivity zone on line 8 is related to an extension of the WNW-trending resistivity low seen within the Chupadero crater. However, note that the altered area encountered on line 8 is mapped in an L-shape with arms oriented northeast and northwest.

A resistivity map (Fig. IV.29) is derived from the AMT soundings on each of lines 4, 5, 6, 7, and 8, by computing resistivities along the traverses. The ring fracture of the Chupadero crater is also shown for reference. A low-resistivity zone is clearly shown within the northern part of the crater with values of resistivity <10 ohm-m. This resistivity map shows a strong NE-oriented low-resistivity trend defined along traverse 4 and a definite WNW-low-resistivity trend crossing the Ixpaco phreatic crater. The prominent northeast trend suggests that traverse 4 may have been made subparallel and close to faulting within the crater. Faulting of this orientation in the vicinity has not been mapped, although faulting of this orientation is prominent 10 km east of Ixpaco.

Examination of the cross lines 1, 2, and 3 shows no strong consistent feature crossing the lines where intersected by traverse 4, but it does show some evidence of electrical changes near their intersections with traverse 4. On line 3, a distinct transition from resistive to conductive rock occurs 250 m west of line 4. Where line 4 crosses line 1, a region of uniformly conductive rock to the west changes on going east to a region of gradually increasing resistivity. On line 2, line 4 crosses at the region of lowest

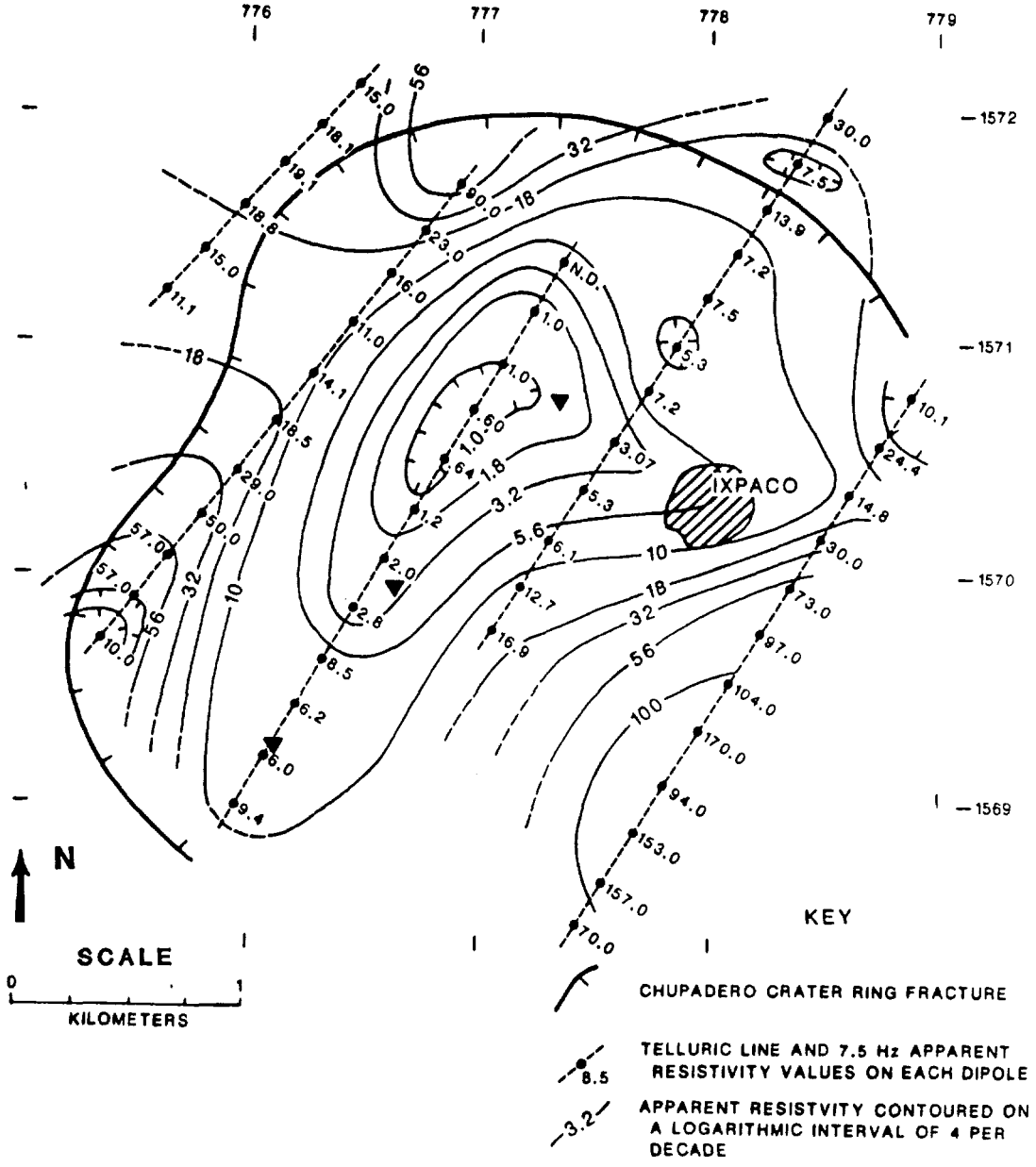

Fig. IV.29. Apparent resistivity map at 7.5 Hz derived from telluric data on lines 4, 5, 6, 7, and 8 in the Chupadero Crater area. Resistivity values were obtained by using the AMT apparent resistivity at 7.5 Hz for each of the soundings on the lines and calculating resistivities along each line as explained in the text. Black triangles show the center location of three INDE VES soundings made near traverse 4.

resistivity in an area of fumaroles west of Ixpaco. Additional data in this area would be desirable to confirm a NE-trending fault or fracture system.

Some additional evidence exists in the INDE VES data in the Chupadero area. A map of apparent resistivity in the Chupadero area (Fig. IV.28) is

derived from the INDE VES data for a one-half current electrode distance of 500 m. This map shows a WNW-trending resistivity low corresponding well with a similar low defined by the telluric data. Three VES soundings were made close to traverse 4. Two are on the southwestern part of traverse 4 very close to the line and expanded along the direction of the line. These two data points also show evidence for a NE-trending low-resistivity zone along traverse 4. The third sounding (number 30) near traverse 4 is located 0.75 km northwest of Ixpaco and was expanded in a northwest direction approximately normal to the traverse and subparallel to the inferred WNW fault through Ixpaco.

The SP data are particularly noisy on lines 3, 4, and 5, whereas the separate curves show fair agreement on the other lines. However, there is no evident correlation with known or inferred thermal or structural features. Geologic noise contributed by near-surface and topographic effects and electrode drift appear to be masking any signal, if present, related to the thermal features.

E. SUMMARY

The telluric measurements within Chupadero crater defined a WNW-trending conductive trend within the northern part of the crater, which is inferred to be related to fracturing and alteration along a WNW fault zone that is controlling the location of fumaroles within the crater. A second NE-trending zone of high conductivity is defined along traverse 4 that may relate to faulting adjacent to the line. However, no consistent evidence for such faulting is seen on three lines that cross traverse 4, suggesting that if faulting is present it has not been a major conduit for geothermal fluids in the upper part sampled by the electrical data.

The margins of the Chupadero crater as mapped are consistent with the electrical geophysical data. The deep-looking electrical data define the margin inside the mapped margin approximately 250 m, consistent with an inward dip of the ring fracture.

F. REFERENCES

Hoover, D. B., C. L., Long, and R. M., Senterfit, 1978. Some results from audio-magnetotelluric investigations in geothermal areas. Geophysics, Dec. 1978.

Hoover, D. B., A. R., de Silva, H. A., Pierce, and Roberto, Amaral, 1984. The application of audiomagnetotelluric surveys on São Miguel Island, Azores, Portugal. GRC Transactions, 8, 499-503.

Slankis, J. A., W. M., Telford, A., Becker, 1972. 8-Hz telluric and magnetotelluric prospecting. Geophysics, 37 (5), 862-878.

APPENDIX A

GEOLOGIC CROSS-SECTIONS

(for cross-section lines, see Plate 1 in pocket)

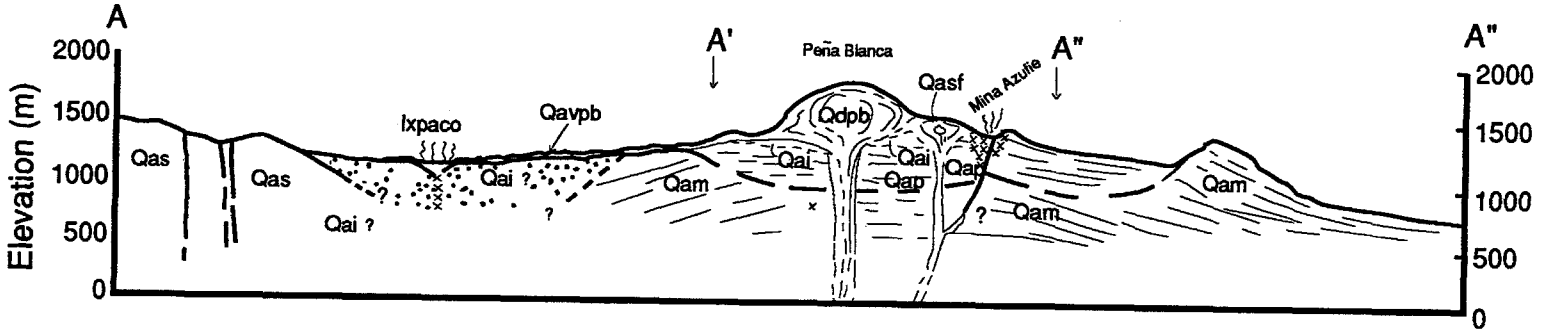
A
A'
A"
A"
Peña Blanca
Mina Azufre
Elevation (m)
2000
1500
1000
500
0
Qas
Qas
Qai ?
Ixpaco
Qavpb
Qai ?
Qam
Qai
Qdpb
Qasf
Qai
Qap
Qap
Qam
Qam
Qam

B
B'
B"
B'"
Peña Blanca
La Soledad
Tecuamburro
Elevation (m)
2000
1500
1000
500
0
Qam
Qdpb
Qap
Qat
Qai
Qri
Qae
Vents for V. Miraflores,
older Tecuamburro
and Peña Blanca

C
C'
Miraflores
San Francisco
Mina
Azufre
Tecuamburro
Qasf
Qasb
Qap
Qaf
Qai
Qam
Qavm
Tai
Rio Los Esclavos
Elevation (m)
2000
1500
1000
500
0
1000
500
0
?
Possible vents for Miraflores,
Pena Blanca, older Tecuamburro
and San Francisco

D
D'
D"
Elevation (m)
1500
1000
500
0
Azufre
Ixpaco
Phreatic Crater
and tuff ring
CRATER
Qal
Qai
Qas
?

E
1000
500
0
Elevation (m)
Tqu
Qri
?
Qal
Qri
Qae
?
Qtapg
Qtapg
Tqu
Qtapg
Qri
Qb
Tau
Jalpatagua
f.z.
E′
1000
500
0

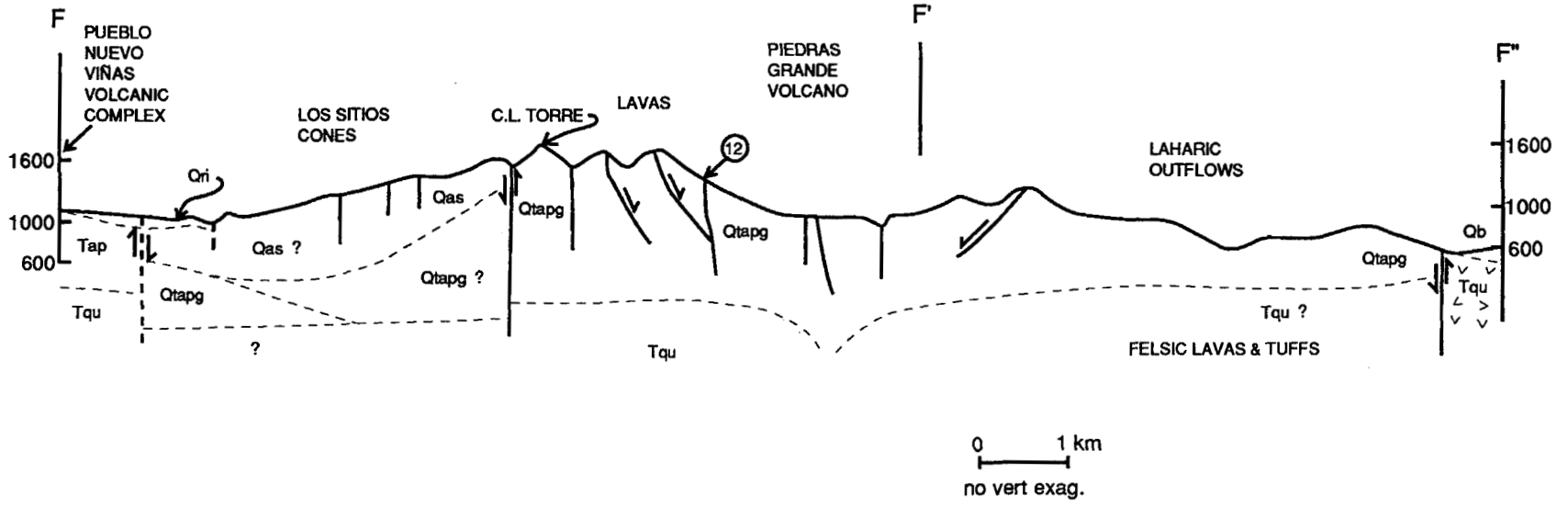
F
PUEBLO
NUEVO
VIÑAS
VOLCANIC
COMPLEX
LOS SITIOS
CONES
C.L. TORRE
LAVAS
PIEDRAS
GRANDE
VOLCANO
F'
F"
LAHARIC
OUTFLOWS
1600
1000
600
Qri
Qas
Qtapg
Tap
Qas ?
Qtapg ?
Tqu
?
Tqu ?
Qb
FELSIC LAVAS & TUFFS
0
1 km
no vert exag.

APPENDIX B

PETROGRAPHIC ANALYSES

Unit Name	Ixpaco tuff ring	Link	
Sample No.	2-25-89-3A	Rock type	Breccia

Description

Lower most massive unit of Ixpaco tuff ring; white, silicified breccia. The rock consists of 10- to 1000-μm-long, angular clasts of hydrothermally altered pumice(?), shards(?), and feldspar clasts. There are also traces of angular quartz grains in the deposit. Clasts are altered to pale brown clay and silica phases. Some clasts could be interpreted as altered fragments of porphyritic lava.

Mode			
Groundmass		Matrix	
Plagioclase		Quartz	
Cpx		K-feldspar	
Fe-Ti oxides		Biotite	
Olivine		Opx	
Hornblende		Pumice	
Glass		Shards	
Vesicles		Scoria	
Lithic clasts			

Unit Name	Ixpaco tuff ring	Link	
Sample No.	2-25-3B	Rock type	Phreatic tuff

Description

Poorly bedded silicified clastic material in beds 4 cm to 1 m thick. Alternating pink and white layers.

This rock has only the vaguest relict outlines of individual clasts; appears to have been a tuff, containing pumice with phenocrysts and rare lithic clasts. It is so silicified that little more can be said.

Mode			
Groundmass		Matrix	
Plagioclase		Quartz	
Cpx		K-feldspar	
Fe-Ti oxides		Biotite	
Olivine		Opx	
Hornblende		Pumice	
Glass		Shards	
Vesicles		Scoria	
Lithic clasts			

Unit Name	Ixpaco tuff ring	Link	
Sample No.	2-25-89-3C	Rock type	Phreatic tuff

Description

Sample over the soil sample collected for C14 dating. Colored, bedded clastic unit.

Only relict textures remain the 0.1- to 1-mm-diameter clasts. Most appear to have been porphyritic lavas, but some resemble pumices (~35-50% vesicularity), with small (<100-μm long), ovoid vesicles.

Mode			
Groundmass		Matrix	
Plagioclase		Quartz	
Cpx		K-feldspar	
Fe-Ti oxides		Biotite	
Olivine		Opx	
Hornblende		Pumice	
Glass		Shards	
Vesicles		Scoria	
Lithic clasts			

Unit Name	Jalpatagua fault breccia	Link	
Sample No.	2-22-89-1	Rock type	"Rock flour"

Description

The rock consists of mostly angular broken phenocrysts of plagioclase and K-feldspar, and lesser biotite and Fe-Ti oxide. Larger phenocrysts (>2 mm) are fractured; smaller clasts appear to be "rock flour."

In the field, this looks like a nonwelded tuff. Is this what a sheared tuff looks like? There are no remnant shards or pumices if this is the case.

Mode			
Groundmass		Matrix	
Plagioclase		Quartz	
Cpx		K-feldspar	
Fe-Ti oxides		Biotite	
Olivine		Opx	
Hornblende		Pumice	
Glass		Shards	
Vesicles		Scoria	
Lithic clasts			

Unit Name	Valley ignimbrite-east	Link	
Sample No.	7-9-88-16	Rock type	Vitric ash

Description

Nonwelded, medium- to fine rhyolitic ash (check composition later). Consists of: (1) Colorless shards; mostly derived from pumice with narrow, elongate vesicles; final products are ~50- to 500-μm-long needle-like and tubular pyroclasts. (2) 1-mm-diameter rounded pumice clasts; 30 to 70% vesicularity; mixture of elongate (15 x 200 μm) and ovoid (100-150 μm) vesicles. (3) 100- to 300-μm-long phenocrysts of biotite, plagioclase, sanidine, hornblende, and Fe-Ti oxides. Most are broken, anhedral, with some adhering glass. (4) Rounded lithic clasts, consisting of andesitic lavas; altered to varying extent.

	Mode	g.c.		
Groundmass			Matrix	
Plagioclase	5.6		Quartz	
Cpx			K-feldspar	1.6
Fe-Ti oxides	1.0		Biotite	1.6
Olivine			Opx	
Hornblende	0.6		Pumice	17.0
Glass			Shards	63.0
Vesicles			Scoria	
Lithic clasts	ands.=6.0; sltst=3.3			

Unit Name	Ayarza Pumice; fine-gr. ign.	Link	
Sample No.	7-16-88-2	Rock type	Vitric ash

Description

Fine-grained ash, with est. med. grain size of 70 μm. Mostly angular shards derived from a highly inflated pumiceous melt, with thin bubble walls. Most shards are thin, curved needles or "Y" shapes. Some pumice remnants have deformed ovoid (almost polygonal) vesicles, 100- to 150-μm-long; bubble walls are <5-μm thick. There are rare small pumice clasts with smaller, more densely packed vesicles.

Phenocrysts are angular, small clasts of plagioclase, sanidine, and biotite.

XRD analyses

Mode			
Groundmass		Matrix	
Plagioclase	0.6	Quartz	
Cpx		K-feldspar	1,6
Fe-Ti oxides		Biotite	tr
Olivine		Opx	tr
Hornblende		Pumice	5.3
Glass		Shards	92.3
Vesicles		Scoria	
Lithic clasts			

Unit Name	Ayarza caldera pumice fall	Link	
Sample No.	7-16-88-1	Rock type	Pumice

Description

The pumice contains ~1% phenocrysts, including plagioclase (up to 2.5-mm long), biotite (up to 1 mm), and hypersthene (to 400 μm). Vesicularity is ~40%.

Vesicles are radial around phenocrysts, form coalesced voids up to 1-mm long, but consist mostly of elongate, 10- to 100-μm-long ovoid shapes; the latter "groundmass" vesicles make up the visible flow structure, around coalesced vesicles and phenocrysts.

XRD analyses

Mode			
Groundmass		Matrix	
Plagioclase	7.6	Quartz	
Cpx		K-feldspar	0.9
Fe-Ti oxides		Biotite	tr
Olivine		Opx	
Hornblende		Pumice	
Glass	46.7	Shards	
Vesicles	44.5	Scoria	
Lithic clasts			

Unit Name	Valley fill ignimbrite-west	Link	
Sample No.	KW7-88-1	Rock type	Pumice

Description

Colorless glass. Vesicularity of 40%, mostly highly elongate pipe vesicles, with the exception of bundles of large coalesced vesicles.

Phenocrysts are all subhedral to anhedral fragments and include biotite (400- to 1500-μm long), plagioclase (~600 μm), and hornblende (400- to 600-μm long).

Mode			
Groundmass		Matrix	
Plagioclase	tr	Quartz	
Cpx		K-feldspar	
Fe-Ti oxides		Biotite	3.0
Olivine		Opx	
Hornblende	tr	Pumice	
Glass		Shards	
Vesicles		Scoria	
Lithic clasts			

Unit Name	Valley fill ignimbrite-west	Link	
Sample No.	KW-7-88-2	Rock type	Coarse vitric ash

Description

(1) 0.5- to 1.5-mm-long, slightly elongate, subrounded pumice pyroclasts. Mostly with highly elongate parallel vesicles and 50-60% vesicularity.

(2) 50- to 200-μm-long colorless shards, mostly derived from pumiceous magma with larger vesicles and thicker vesicle walls than the pumices described above (could be the part of the melt with coalesced vesicles).

(3) Phenocrysts consist of mostly 0.2- to 1-mm-long plagioclase (osc. zoning), aegerine-augite, biotite.

(4) Rounded basalt lithic clasts, weathered to varying extent. Rare rounded andesitic lava and siltstone clasts.

XRD analyses

Mode	g.c.		
Groundmass		Matrix	
Plagioclase	16.6	Quartz	
Cpx	tr	K-feldspar	3.0
Fe-Ti oxides	0.6	Biotite	tr
Olivine		Opx	tr
Hornblende	2.6	Pumice	37.0
Glass		Shards	32.0
Vesicles		Scoria	granu lith=0.3
Lithic clasts	andes=2.3; sltst=1.3; bas=4.0		

Unit Name	Valley fill ignimbrite-west	Link	
Sample No.	KW7-88-4	Rock type	Coarse vitric ash

Description

Highly vesicular pumice clasts, up to 1-cm long, are in a matrix of med. to coarse vitric ash.

(1) Pumices-colorless glass; rare phenocrysts and 60-70% vesicularity. Elongate vesicles and large, ovoid groups of coalesced vesicles.

(2) Shards. Mostly Y- or fork-shaped shards, derived from a highly vesicular pumice with large ovoid vesicles. Most are in the range of 100- to 300-μm long.

(3) Phenocrysts include plagioclase, K-feldspar, hypersthene, and biotite.

(4) Lithic clasts are hydrothermally altered andesitic (?) lavas.

XRD analyses

Mode			
Groundmass		Matrix	
Plagioclase	0.6	Quartz	
Cpx		K-feldspar	1.3
Fe-Ti oxides		Biotite	0.3
Olivine		Opx	tr
Hornblende		Pumice	10.3
Glass		Shards	87.3
Vesicles		Scoria	
Lithic clasts			

Unit Name	Valley fill ignimbrite-west	Link	
Sample No.	KW7-88-3	Rock type	Vitric ash

Description

Moderately well-sorted vitric ash consisting of:

(1) Colorless shards; 100- to 300-μm-long, bubble walls derived from a pumiceous melt with elongate vesicles and 20- to 80-μm-thick vesicle walls.

(2) Pumice; 200- to 900-μm-long, subequant, rounded; 50- to 70% vesicularity.

(3) Phenocrysts of hornblende, aegerine-augite, K-feldspar, and plagioclase.

Mode	g.c.		
Groundmass		Matrix	
Plagioclase	2.3	Quartz	
Cpx	tr	K-feldspar	0.6
Fe-Ti oxides	0.6	Biotite	1.6
Olivine		Opx	
Hornblende	tr	Pumice	9.6
Glass		Shards	81.6
Vesicles		Scoria	granu lith=0.3
Lithic clasts	andes.=0.3; slst=1.0; baslt=2.6		

Unit Name	Cerro Peña Blanca Dome	Link	
Sample No.	7-14-88-7	Rock type	Andesite

Description

Phenocrysts. Plagioclase; up to 2 mm; complexly zoned; ext angles 10°, 14°, 22°, 13°, 35°, 33°, 28°; andesine-labradorite.
Hornblende; 1.5- to 2-mm long; mostly replaced by Fe-Ti oxides.
Fe-Ti oxides and mostly less than 50 μm and occur in mafic clots.
Groundmass. Hyalopilitic; glass is partly devitrified.

XRD analyses

Mode			
Groundmass	52.7	Matrix	
Plagioclase	31.3	Quartz	
Cpx		K-feldspar	
Fe-Ti oxides	3.7	Biotite	
Olivine		Opx	8.2
Hornblende	4.1	Pumice	
Glass		Shards	
Vesicles		Scoria	
Lithic clasts			

Unit Name	Cerro Peña Blanca Dome	Link	
Sample No.	7-8-88-1	Rock type	Andesite

Description

Mostly plagioclase phenocrysts (up to 1 mm) in a hyalopilitic groundmass. There are a few glomerocrysts of hornblende-plagioclase-orthopyroxene. Mesostasis consists of plagioclase microlites and Fe-Ti oxides in glass.

Plagioclase phenocrysts--zoned; 23°, 20°, 18-33°. An40-An60. Some glass inclusions. Some zoned cores now altered to clay. Hypersthenes up to 2.0 mm. Oxyhornblende, 0.5 to 1.2 mm. Fe-Ti oxides 100- to 300-μm long. Some rutile in plagioclase grains.

Mode			
Groundmass	49.2	Matrix	
Plagioclase	35.6	Quartz	
Cpx		K-feldspar	
Fe-Ti oxides	3.8	Biotite	
Olivine		Opx	6.9
Hornblende	4.6	Pumice	
Glass		Shards	
Vesicles		Scoria	
Lithic clasts			

Unit Name	Cerro Peña Blanca Avalanche	Link	
Sample No.	7-13-88-7	Rock type	Lithic-crystal tuff

Description

Lithic clasts are all biotite-orthopyroxene andesite, consisting of: (1) 50-μm- to 1-mm-long plagioclase, with strong oscillatory zoning (18°, 15°, 21°, 21°; ~An40); also contain apatites; (2) hypersthene; (3) quartz; (4) zircon, with strong p. haloes; (5) augite; (6) Fe-Ti oxides; (7) oxyhornblende; and (8) biotite(?).

Shards are less than 50-μm long, but there are rare pumices. Most glass appears to be broken from lava groundmass.

Crystals range from 50- to 500-μm long.

Mode			
Groundmass		Matrix	
Plagioclase	20.63	Quartz	4.37
Cpx	2.8	K-feldspar	3.0
Fe-Ti oxides	5.6	Biotite	
Olivine		Opx	3.2
Hornblende	2.4	Pumice	0.4
Glass		Shards	12.3
Vesicles		Scoria	
Lithic clasts	andesite=35.3; tuff=7.1		

Unit Name	San Francisco Andesite	Link	
Sample No.	7-8-88-3	Rock type	Andesite

Description

Phenocrysts. Plagioclase; oligoclase-andesine(?), mostly 1-mm long. Many are fractured and appear to be resorbed in the more calcic cores. Hypersthene; 0.2-1.5 mm; the larger (2 mm) phenocrysts are strongly altered, having reacted with the groundmass. Hornblende; mostly altered to Fe-Ti oxides and are small (20 to 50 μm). Clinopyroxene; rims are altered; most are in 2-mm-diam. glomeroporphyritic clots with plag. and opx.

Groundmass. Is vesicular, glassy. Vesicles are irregular, oval, with some crystals intruding (diktytaxitic texture).

Mode	%		
Groundmass	54.5	Matrix	
Plagioclase	24.3	Quartz	
Cpx	5.0	K-feldspar	
Fe-Ti oxides	4.4	Biotite	
Olivine		Opx	8.3
Hornblende	0.8	Pumice	
Glass		Shards	
Vesicles		Scoria	
Lithic clasts	Gabbro=2.8		

Unit Name	Cuilapa-Barberena basalt	Link	
Sample No.	LM-3	Rock type	Pyroxene basalt

Description

Porphyritic basalt, consisting of 50-μm- to 2-mm-long phenocrysts of subhedral plagioclase and clinopyroxene in a diktytaxitic groundmass of feldspar, Fe-Ti oxides, and cpx. Some chloritic alteration of the groundmass.

Plagioclase phenocrysts--400-μm- to 2-mm-long, complexly zoned. The cores of larger phenocrysts have sieve textures and are often altered to chlorite and silica phases. Cpx phenocrysts--pigeonite and aegerine-augite, 400 to 600 μm; usually as G-P clots or as gabbroic inclusions. Some resorbed and altered olivines.

Quartzose sandstone inclusions; quartz with reaction rims and clay matrix altered to chlorite. Some thin qtz. veins.

Mode			
Groundmass	66.0	Matrix	
Plagioclase	24.6	Quartz	
Cpx	2.3	K-feldspar	
Fe-Ti oxides		Biotite	
Olivine	0.3	Opx	
Hornblende		Pumice	
Glass		Shards	
Vesicles		Scoria	
Lithic clasts	arkose=0.6; veins=1.3; chl=4.6		

Unit Name	Cuilapa-Barberena basalts	Link	
Sample No.	LM-4	Rock type	Olivine basalt

Description

100- to 600-μm-long phenocrysts of olivine and plagioclase in a trachytic groundmass composed of mostly feldspar laths, 40 to 60 μm, stubby cpx(?), and granular Fe-Ti oxides. In reflected light, the texture appears to be diktytaxitic.

There are glomeroporphyritic clots of olivine and plagioclase, up to 2 mm in diam.

There is some alteration of Fe-Ti oxides to hematite and rimming of olivine with iddingsite.

Mode

Groundmass	91.3	Matrix	
Plagioclase	1.3	Quartz	
Cpx		K-feldspar	
Fe-Ti oxides	1.0	Biotite	
Olivine	5.0	Opx	
Hornblende		Pumice	
Glass		Shards	
Vesicles		Scoria	

Lithic clasts

Unit Name	Las Delicias basalt	Link	
Sample No.	LM-8	Rock type	Basalt??

Description

Relict plagioclase phenocrysts, 200- to 500-μm long in groundmass. Some with oscillatory zoning. The rock has been altered to a granophyric mixture of finely grained crystalline silica and clay.

Too altered for modal analysis

Mode			
Groundmass		Matrix	
Plagioclase		Quartz	
Cpx		K-feldspar	
Fe-Ti oxides		Biotite	
Olivine		Opx	
Hornblende		Pumice	
Glass		Shards	
Vesicles		Scoria	
Lithic clasts			

Unit Name	Y. Tec. lavas-Sulfur Mine	Link	
Sample No.	7-8-88-6	Rock type	Hyd. Alt. Andesite

Description

Porphyritic andesite, similar in many respects to 7-8-88-4. However, this is only a relict texture. The rock has been replaced entirely by silica phases in this zone of acid alteration.

Mode			
Groundmass	50.6	Matrix	
Plagioclase	39.0	Quartz	
Cpx	4.6	K-feldspar	
Fe-Ti oxides	3.0	Biotite	
Olivine		Opx	2.6
Hornblende		Pumice	
Glass		Shards	
Vesicles		Scoria	
Lithic clasts			

Unit Name	Younger Tecuamburro lavas	Link	
Sample No.	7-13-88-3	Rock type	Andesite

Description

Porphyritic, with abundant phenocrysts as single crystals and glomeroporphyritic clots; these include:

(1) 100-μm to 1.5-mm-long, euhedral and subhedral plagioclase, with oscillatory zoning; (2) 0.2- to 1.5-mm-diam. hypersthene; (3) 50- to 250-μm-diam. Fe-Ti oxides; and (4) 100- to 300-μm-diam. rounded subhedral olivines; most are slightly altered to iddingsite.

The groundmass contains irregular, elongate, 200-μm- to 1.5-mm-long vesicles. The groundmass consists mostly of less than 40-μm-long plagioclase, lesser opx (less than 30 μm), and small Fe-Ti oxides (less than 10 μm). It is all crystalline.

Mode			
Groundmass	50.0	Matrix	
Plagioclase	40.6	Quartz	
Cpx		K-feldspar	
Fe-Ti oxides	1.6	Biotite	
Olivine	Tr	Opx	4.6
Hornblende		Pumice	
Glass		Shards	
Vesicles		Scoria	
Lithic clasts			

Unit Name	Younger Tecuamburro lavas	Link	
Sample No.	7-14-88-1	Rock type	Andesite

Description

Porphyritic. Mostly subhedral, zoned plagioclase (considerable sieve textures), 400-μm to 2.5-mm long. Lesser (1) 400-μm- to 3-mm-long hypersthene, mostly in glomeroporphyritic clots; (2) subhedral, 200-μm to 1-mm olivine; (3) augite (>3 mm); and (4) Fe-Ti oxides.

Groundmass. Similar to other Tec. lavas - less than 100 μm plag, opx, and Fe-Ti oxides.

Vesicles. 500-μm- to 3-mm-long, irregular vesicles.

Mode			
Groundmass	54.3	Matrix	
Plagioclase	33.0	Quartz	
Cpx	tr	K-feldspar	
Fe-Ti oxides	0.6	Biotite	
Olivine	4.0	Opx	4.3
Hornblende		Pumice	
Glass		Shards	
Vesicles		Scoria	
Lithic clasts			

Unit Name	Younger Tecuamburro lavas	Link	
Sample No.	7-9-88-3	Rock type	Andesite

Description

Porphyritic; mostly 200-μm- to 2-mm-long zoned euhedral to subhedral plagioclase; some parallel growth, with extensions out from ends of crystals. Lesser volumes of (1) 200-μm- to 1-mm-long hypersthene; (2) a few large (up to 3 mm) augites; (4) Fe-Ti oxides (100- to 250-μm diameters); and (5) 100- to 300-μm-diam., subhedral olivines.

Groundmass. Mostly sub-100-μm feldspar laths; lesser orthopyroxene and Fe-Ti oxides.

Mode

Groundmass	53.6	Matrix	
Plagioclase	37.3	Quartz	
Cpx	2.0-	K-feldspar	
Fe-Ti oxides	0.3	Biotite	
Olivine	1.6	Opx	5.0
Hornblende		Pumice	
Glass		Shards	
Vesicles		Scoria	
Lithic clasts			

Unit Name	Younger Tecuamburro lavas	Link	
Sample No.	7-9-88-2	Rock type	Andesite

Description

Porphyritic lava, with mostly subhedral to euhedral, 250-μm- to 2-mm-long plagioclase; each with osc. zoning, and parallel growths extending out from the ends of each phenocryst. Lesser hypersthene (250-μm to 2.2-mm long, subhedral; zoned, with inclusions of Fe-Ti oxides and feldspar), some olivine (with reaction rims) and Fe-Ti oxides (100- to 600-μm diameter, rounded).

Groundmass consists of ~90% sub-100-μm-long feldspar laths, 5% sub-60-μm orthopyroxene, and 5% less than 20-μm-diam. Fe-Ti oxides.

Mode			
Groundmass	56.0	Matrix	
Plagioclase	31.3	Quartz	
Cpx		K-feldspar	
Fe-Ti oxides	1.3	Biotite	
Olivine	0.3	Opx	11.0
Hornblende		Pumice	
Glass		Shards	
Vesicles		Scoria	
Lithic clasts			

Unit Name	Older Tecuamburro lavas	Link	
Sample No.	2-22-89-5	Rock type	Andesitic lava

Description

Sample from blocks at surface (in place?) between Mina Azufre and El Silencio.

~50% phenocrysts of plagioclase (100-μm to 2-mm long), orthopyroxene (20-μm to 1.5-mm long) in a finely crystalline (almost equigranular) groundmass. Most of the larger zoned plagioclase phenocrysts have altered (sieve texture) cores and most of the pyroxenes are altered to some extent, from rims of Fe-Ti oxide to completely oxidized to deep red-brown.

No apparent flow structure

Mode			
Groundmass		Matrix	
Plagioclase		Quartz	
Cpx		K-feldspar	
Fe-Ti oxides		Biotite	
Olivine		Opx	
Hornblende		Pumice	
Glass		Shards	
Vesicles		Scoria	
Lithic clasts			

Unit Name	Older Tecuamburro lavas	Link	
Sample No.	2-22-89-6	Rock type	Andesitic lava

Description

Porphyritic, with ~30% phenocrysts, including plagioclase (400-μm to 3-mm long; oscillatory zoning) and rare opx. Well developed flow foliation, with oriented feldspar microlites. Some degree of alteration, particularly of microlites and cores of zoned feldspars.

Mode			
Groundmass		Matrix	
Plagioclase		Quartz	
Cpx		K-feldspar	
Fe-Ti oxides		Biotite	
Olivine		Opx	
Hornblende		Pumice	
Glass		Shards	
Vesicles		Scoria	
Lithic clasts			

Unit Name	Tecuam. pyx pumice fall	Link	
Sample No.	2-25-89-4	Rock type	Pumice

Description

4 m+ of pyroxene pumice fallout. Massive; pumice lapilli in a coarse ash matrix. Maximum pumice=10 cm.

Porphyritic pumice, containing ~11% phenocrysts of anhedral plagioclase (100 μm to 1 mm), 100- to 200-μm-long orthopyroxenes, and Fe-Ti oxides.

Vesicularity, using Vista is 69%, 62%, and 62% (higher than in the pyroclastic flows). Vesicles are ovoid, ranging in length from 10 to 200 μm. Vesicles are radial from phenocryst surfaces.

XRD analyses

Mode			
Groundmass		Matrix	
Plagioclase	8.0	Quartz	
Cpx	0.6	K-feldspar	
Fe-Ti oxides	1.0	Biotite	
Olivine		Opx	1.6
Hornblende		Pumice	
Glass	25	Shards	
Vesicles	64.3	Scoria	
Lithic clasts			

Unit Name	Tecuamburro pyx pumice	Link	
Sample No.	2-22-89-4	Rock type	Pyrox. pumice tuff

Description

~20% phenocrysts in the pumice. The pumice has ~40% vesicles; vesicles are spherical to ovoid and range in size from 5- to 75-μm long.
Phenocrysts: Plag > Opx > Fe-Ti oxides.

Mode			
Groundmass		Matrix	
Plagioclase		Quartz	
Cpx		K-feldspar	
Fe-Ti oxides		Biotite	
Olivine		Opx	
Hornblende		Pumice	
Glass		Shards	
Vesicles		Scoria	
Lithic clasts			

Unit Name	Tecuamburro pyroclastic rx	Link	
Sample No.	7-9-88-7	Rock type	Pumice

Description

Pumice contains ~15% phenocrysts of plag > Opx > Fe-Ti oxides. ~50% vesicles; spherical to ovoid and ranging in size from 10 to 400 μm. Considerable radial vesicle growth around phenocryst surfaces.

Mode			
Groundmass		Matrix	
Plagioclase		Quartz	
Cpx		K-feldspar	
Fe-Ti oxides		Biotite	
Olivine		Opx	
Hornblende		Pumice	
Glass		Shards	
Vesicles		Scoria	
Lithic clasts			

Unit Name	Pyx pumice ignimbrite	Link	
Sample No.	2-24-89-2	Rock type	Pumice

Description

From quarry east of Chiquimulilla. Deposit contains less than 1% lithic clasts; andesitic lava.

~1% broken phenocrysts: mostly plagioclase with oscillatory zoning, and orthopyroxene and Fe-Ti oxides.

Vesicularity measured with Vista = 44%, 44.5%, 47.4%. Ave.=45.3%. Nearly all phenocrysts are surrounded by radial vesicles. Vesicle sizes range from 10 to 100 μm; mostly ovoid.

XRD analyses

Mode			
Groundmass		Matrix	
Plagioclase	14.6	Quartz	
Cpx		K-feldspar	
Fe-Ti oxides	2.3	Biotite	
Olivine		Opx	1.6
Hornblende		Pumice	
Glass	34.3	Shards	
Vesicles	45.3	Scoria	
Lithic clasts			

Unit Name	Tecuamburro pyroclastic rx	Link	
Sample No.	7-9-88-7	Rock type	Pumice

Description

Pumice contains ~21% phenocrysts of plag > Cpx > Opx > Fe-Ti oxides.

46% vesicles; spherical to ovoid and ranging in size from 10 to 400 μm. Considerable radial vesicle growth around phenocryst surfaces.

XRD analyses

Mode			
Groundmass		Matrix	
Plagioclase	16.3	Quartz	
Cpx	3.0	K-feldspar	
Fe-Ti oxides	1.0	Biotite	
Olivine		Opx	1.0
Hornblende		Pumice	
Glass	33.0	Shards	
Vesicles	45.6	Scoria	
Lithic clasts			

Unit Name	Tecuamburro pyx pumice	Link	
Sample No.	2-22-89-4	Rock type	Pyrox. pumice tuff

Description

16% phenocrysts in the pumice. The pumice has 38% vesicles; vesicles are spherical to ovoid and range in size from 5- to 75-μm long.
Phenocrysts: Plag > Opx > Cpx > Fe-Ti oxides.

XRD analyses

Mode			
Groundmass		Matrix	
Plagioclase	11.3	Quartz	
Cpx	1.3	K-feldspar	
Fe-Ti oxides	0.3	Biotite	
Olivine		Opx	2.0
Hornblende		Pumice	
Glass	47.0	Shards	
Vesicles	38.0	Scoria	
Lithic clasts			

Unit Name	Tecuamburro pyroclastic rx	Link	
Sample No.	7-11-88-2	Rock type	Crystal tuff

Description

Coarse crystal tuff, consisting of:
(1) 100-μm- to 1.2-mm-long angular, broken plagioclase crystals; most exhibit osc. zoning. (2) 0.1 - 0.5-mm-long hypersthene; anhedral. (3) 0.5-mm-long aegerine-augite; anhedral. (4) Lithic clast-andesite groundmass; hydrothermally altered. (5) Lithic clast-metasandstone-arkose. (6) 1 to 2-mm-diam., equant pumice-colorless glass; 10- to 50-um-diam., equant vesicles. Vesicularity ~50%; plagioclase phenocrysts.

Mode	g.c.		
Groundmass		Matrix	
Plagioclase	45.6	Quartz	
Cpx	14.0	K-feldspar	7.0
Fe-Ti oxides	4.0	Biotite	
Olivine		Opx	2.6
Hornblende		Pumice	12.3
Glass		Shards	
Vesicles		Scoria	
Lithic clasts	and=13.3; ss=1.0		

Unit Name	Tecuamburro pyx pumice	Link	
Sample No.	7-9-88-12	Rock type	Pumice

Description

Porphyritic pumice with colorless glass. Phenocrysts include: (1) 240-μm to 1.2-mm-long plagioclase, osc. zoning, mostly euhedral. (2) 50- to 400-μm-long hypersthene, euhedral to subhedral. (3) Rounded, 200-μm-diam. Fe-Ti oxides. (4) Some subhedral K-feldspars??

Vesicles are mostly ovoid to elongate, and 10- to 100-μm long. Most are bent around phenocrysts. Good radial growth of vesicles from phenocryst surfaces, with some deformation by later flow.

Mode			
Groundmass		Matrix	
Plagioclase	13.0	Quartz	
Cpx		K-feldspar	2.0
Fe-Ti oxides	1.3	Biotite	
Olivine		Opx	3.6
Hornblende		Pumice	
Glass		Shards	
Vesicles		Scoria	
Lithic clasts			

Unit Name	Tecuam pyroclastic rx interb w/lavas	Link	
Sample No.	7-9-88-6a	Rock type	Lithic ash

Description

Coarse lithic ash, with a finer component that appears to be mostly alteration products or infiltrated silt. The ash consists of: (1) glassy pumice, with 5- to 20-μm ovoid vesicles. Mostly glass, with rare, small plagioclase. (2) Plagioclase phenocrysts and g-p clots; zoned, 250-μm to 2-mm long. (3) 0.5- to 1-mm-long anhedral augite. (4) 0.5 to 0.6-mm-long anhedral hypersthene. (5) 0.5- to 1-mm diam., equant, rounded andesitic lava; mostly groundmass, but some porphyritic lava. (6) Rounded metasandstone clast. (7) 0.6-mm-diam. Fe-Ti oxide. Most of the pyroclasts are rounded and show varying degrees of alteration.

Mode	g.c.		
Groundmass		Matrix	
Plagioclase	16.0	Quartz	
Cpx	14.0	K-feldspar	
Fe-Ti oxides	1.6	Biotite	
Olivine		Opx	2.0
Hornblende		Pumice	12.3
Glass		Shards	
Vesicles		Scoria	
Lithic clasts	54.0		

Unit Name	Tec. ashes interb. w/lavas	Link	
Sample No.	7-9-88-6b	Rock type	Lithic ash

Description

Coarser clasts (>500 μm) include (1) well-rounded to rounded basaltic andesite (main phenocryst is hypersthene, with lesser plagioclase), with a finely crystalline, hyalocrystalline groundmass. (2) Rounded andesite, with osc. zoned plagioclase as main pheno, in a mod. crystalline groundmass. (3) Orthopyroxenes.

The coarser clasts serve as nuclei for 1- to 3-mm diam., poorly developed accretionary lapilli. The matrix consists of fine-grained, angular plagioclase, opx, Fe-Ti oxides, small lithic clasts stained with hematite, in a pale brown (smectitic?).

XRD analyses

Mode			
Groundmass		Matrix	68.6
Plagioclase	9.3	Quartz	
Cpx	0.9	K-feldspar	
Fe-Ti oxides	0.6	Biotite	
Olivine		Opx	0.3
Hornblende		Pumice	
Glass		Shards	
Vesicles		Scoria	3.6
Lithic clasts	bas andes=15.9; andes=0.3		

Unit Name	Hummocky terrain-lithic tuff?	Link	
Sample No.	2-24-89-5	Rock type	Andesitic lava

Description

Block from block-bearing tuff(?); clastic rock anyway. Only relict texture left. A porphyritic andesite lava with ~40% phenocrysts of osc. zoned plagioclase and orthopyroxene (some of the pyroxenes are partly preserved). Finely crystalline equigranular groundmass. Replaced by authigenic silica(?), clays and hematite.

Mode			
Groundmass		Matrix	
Plagioclase		Quartz	
Cpx		K-feldspar	
Fe-Ti oxides		Biotite	
Olivine		Opx	
Hornblende		Pumice	
Glass		Shards	
Vesicles		Scoria	
Lithic clasts			

Unit Name	Miraflores andesites	Link	
Sample No.	7-11-88-1	Rock type	Andesite lava

Description

Porphyritic, with phenocrysts of plagioclase (euhedral to subhedral, from 250-μm to 2.5-mm long, with oscill. zoning), hypersthene (80 μm to over 2-mm long, euhedral to subhedral), and Fe-Ti oxides (20- to 250-μm diameters).

The largest phenocrysts are in glomeroporphyritic clots.

Groundmass. Mostly 10- to 50-μm-long feldspars, but are some 10-μm stubby pyroxenes and Fe-Ti oxides.

There are rare, less than 1-mm-long, irregular vesicles.

Mode			
Groundmass	52.3	Matrix	
Plagioclase	38.3	Quartz	
Cpx		K-feldspar	
Fe-Ti oxides	1.3	Biotite	
Olivine		Opx	5.0
Hornblende		Pumice	
Glass		Shards	
Vesicles		Scoria	
Lithic clasts			

Unit Name	Miraflores andesites	Link	
Sample No.	7-13-88-9	Rock type	Andesite

Description

Porphyritic, with many of the phenocrysts present as mono-minerallic glomerocrysts.

Phenocrysts include: plagioclase (400-μm to 1.5-mm long, mostly euhedral, and with subtle osc. zoning), hypersthene (150-300 μm, subhedral, slightly rounded), Fe-Ti oxide (100- to 250-μm diameter).

Groundmass. Mostly 10- to 25-μm-long feldspars. Well-developed flow texture in the groundmass. 5- to 10-μm-diam. Fe-Ti oxides scattered throughout. Some irregular, 0.5- to 1-mm-long vesicles.

XRD analyses

Mode

Groundmass	56.3	Matrix	
Plagioclase	30.0	Quartz	
Cpx		K-feldspar	
Fe-Ti oxides	0.6	Biotite	
Olivine		Opx	7.6
Hornblende		Pumice	
Glass		Shards	
Vesicles		Scoria	
Lithic clasts			

Unit Name	Los Sitios andesites	Link	
Sample No.	LM-7	Rock type	Andesite

Description

Porphyritic andesite; mostly groundmass.

Phenocrysts of: (1) Plagioclase, 200- to 1.8-mm long, euhedral to subhedral, with strong oscillatory zoning. (2) Hypersthene, 100-μm to 1.5-mm long, euhedral to subhedral crystals. (3) 200- to 400-μm-diam. Fe-Ti oxides. (4) K-feldspar laths, mostly less than 1 mm. (5) Subhedral cpx (pigeonite?), 0.5- to 2-mm diameter. Some glomeroporphyritic clots of all of the phases listed above.

Groundmass. Felty flow texture, consisting mostly of 10- to 50-μm-long feldspars. Traces of Fe-Ti oxide and pyroxene.

Mode			
Groundmass	68.0	Matrix	
Plagioclase	22.0	Quartz	
Cpx	1.6	K-feldspar	1.6 (check)
Fe-Ti oxides	1.3	Biotite	
Olivine		Opx	4.6
Hornblende		Pumice	
Glass		Shards	
Vesicles		Scoria	
Lithic clasts			

Unit Name	Nuevas Viñas andesite	Link	
Sample No.	none yet	Rock type	

Description

Equivalent to the Cerro la Gabia andesite of Reynolds.

Mode			
Groundmass		Matrix	
Plagioclase		Quartz	
Cpx		K-feldspar	
Fe-Ti oxides		Biotite	
Olivine		Opx	
Hornblende		Pumice	
Glass		Shards	
Vesicles		Scoria	
Lithic clasts			

Unit Name	El Sordo andesite and basalt	Link	
Sample No.	7-15-88-5	Rock type	Andesite lava

Description

Porphyritic, with phenocrysts of:

(1) Plagioclase; 200-μm to 3-mm long, subhedral, oscillatory-zoned crystals. Zoning poorly developed.

(2) Pigeonite; 100- to 750-μm long, zoned crystals.

(3) 20- to 100-μm-diam. Fe-Ti oxides.

(4) Unidentified pyx-like phase, altered to clay. Also present as glomeroporphyritic clots.

Groundmass consists of 5- to 25-μm-diam., stubby clinopyroxene and plagioclase (traces of Fe-Ti oxides).

Mode			
Groundmass		Matrix	
Plagioclase		Quartz	
Cpx		K-feldspar	
Fe-Ti oxides		Biotite	
Olivine		Opx	
Hornblende		Pumice	
Glass		Shards	
Vesicles		Scoria	
Lithic clasts			

Unit Name	El Sordo andesite and basalt	Link	
Sample No.	7-15-88-3	Rock type	Olivine basalt

Description

Porphyritic with a trachytic groundmass. Good flow texture with oriented plagioclase phenocrysts and parallel orientation of groundmass crystals.

Phenocrysts: 80-μm to 1.5-mm-long subhedral to euhedral plagioclase with oscillatory zoning. 40-μm to 1-mm diam. olivines with thin altered rims. 50- to 200-μm diam. Fe-Ti oxides.

Groundmass: 70% 10- to 60-μm-long plagioclase, 25% 5- to 50-μm-long clinopyroxene(?), and 5% 10- to 50-μm-diam. Fe-Ti oxides.

Mode

Groundmass	61.3	Matrix	
Plagioclase	33.3	Quartz	
Cpx		K-feldspar	
Fe-Ti oxides	1.6	Biotite	
Olivine	2.6	Opx	1.0
Hornblende		Pumice	
Glass		Shards	
Vesicles		Scoria	

Lithic clasts

Unit Name	El Sordo andesite and basalt	Link	
Sample No.	7-15-88-9	Rock type	Andesite lava

Description

Porphyritic, mostly phenocrysts and little groundmass.

Phenocrysts of:

(1) Plagioclase; subhedral, 200-μm- to 1.5-mm-long crystals with very pronounced oscillatory zoning.

(2) Hypersthene; rounded, 200-μm- to 2-mm-long crystals. Some are altered to a dark orange-brown mineral (iddingsite).

(3) 50- to 150-μm-diam. Fe-Ti oxides.

Glomeroporphyritic clots are common.

Groundmass; stubby, 20- to 100-μm-long plagioclase, clinopyroxene, and Fe-Ti oxides.

Mode			
Groundmass		Matrix	
Plagioclase		Quartz	
Cpx		K-feldspar	
Fe-Ti oxides		Biotite	
Olivine		Opx	
Hornblende		Pumice	
Glass		Shards	
Vesicles		Scoria	
Lithic clasts			

Unit Name	Piedra Grande andesite w.t.	Link	
Sample No.	KW7-88-5	Rock type	Andesitic welded tuff

Description

A crystal welded tuff, consisting of:
(1) 400-μm- to 3-mm-long zoned plagioclase phenocrysts.
(2) Oxidized 200-μm to 3-mm-long hornblende phenocrysts.
(3) 200- to 1000-μm-long orthopyroxene.
(4) 100- to 400-μm Fe-Ti oxides.
In a brown glass matrix (densely welded) with scattered small spherulites.
(5) 200- to 400-μm-long K-feldspar.

Mode			
Groundmass		Matrix	glass - 73.3
Plagioclase	13.6	Quartz	
Cpx		K-feldspar	4.0
Fe-Ti oxides	1.6	Biotite	
Olivine		Opx	
Hornblende	7.3	Pumice	
Glass		Shards	
Vesicles		Scoria	
Lithic clasts			

Unit Name	Ixuatan lavas	Link	
Sample No.	3-1-89-1	Rock type	Andesitic lava

Description

Porphyritic andesite lava. ~30% phenocrysts of plagioclase (0.5- to 2.5-mm long, irregular forms), rare orthopyroxene (except in glomerocrysts) and large glomerocrysts of coarsely crystalline plagioclase, orthopyroxene, and Fe-Ti oxides. These are set in a felty or trachytic groundmass with well-developed flow foliation.

Mode			
Groundmass		Matrix	
Plagioclase		Quartz	
Cpx		K-feldspar	
Fe-Ti oxides		Biotite	
Olivine		Opx	
Hornblende		Pumice	
Glass		Shards	
Vesicles		Scoria	
Lithic clasts			

Unit Name	Cinder cone on Ixuatan	Link	
Sample No.	3-1-89-2	Rock type	Andesitic scoriz

Description

Ixuatan cinder cone on summit of ridge, exposed in a cinder quarry. Similar to 3-1-89-1, only in a scoria with tachylitic groundmass. ~50% coarse phenocrysts of plagioclase and orthopyroxene. Distinctive hopper-shaped plagioclase phenocrysts.

Mode			
Groundmass		Matrix	
Plagioclase		Quartz	
Cpx		K-feldspar	
Fe-Ti oxides		Biotite	
Olivine		Opx	
Hornblende		Pumice	
Glass		Shards	
Vesicles		Scoria	
Lithic clasts			

Unit Name	Ixhuatan lavas	Link	
Sample No.	3-1-89-4	Rock type	Andesitic lava

Description

Elev. 1060 m, half way between the Llano Grande and the Pan American Highway. Platy gray andesite, exposed in a road cut.

~35% plagioclase (and minor orthopyroxene with reaction rims) phenocrysts in a trachytic groundmass with well-developed flow foliation. The large tabular and hopper-shaped plagioclase phenocrysts seem to be characteristic of the Ixuatan lavas.

Mode			
Groundmass		Matrix	
Plagioclase		Quartz	
Cpx		K-feldspar	
Fe-Ti oxides		Biotite	
Olivine		Opx	
Hornblende		Pumice	
Glass		Shards	
Vesicles		Scoria	
Lithic clasts			

Unit Name	Tuff, Llano Grande, Ixuatan	Link	
Sample No.	3-1-89-3	Rock type	

Description

Poor outcrop along road; medium-gray, massive tuff; overlain by 1.5-m of soil.

Weathered lithic(?) tuff, containing relict lava clasts, a welded tuff clast, and relict pumice and shards(?). Angular, broken phenocrysts include plagioclase, hornblende, and biotite. It seems too old and deeply weathered to be part of the Amatitlan tephras.????

Mode			
Groundmass		Matrix	
Plagioclase		Quartz	
Cpx		K-feldspar	
Fe-Ti oxides		Biotite	
Olivine		Opx	
Hornblende		Pumice	
Glass		Shards	
Vesicles		Scoria	
Lithic clasts			

Unit Name	El Corozal lavas	Link	
Sample No.	LM-1	Rock type	

Description

Porphyritic-trachytic texture. Phenocrysts of mostly subhedral plagioclase (with oscillatory zoning, in 150-μm- to 1-mm-long crystals) with minor subhedral pigeonite (300- to 500-μm long and having reaction rims of another pyroxene[?]). There are also scattered 50- to 200-μm-long Fe-Ti oxides.

The trachytic groundmass exhibits flow textures and consists of about 70% 10- to 60-μm-long plagioclase, 25% 5- to 10-μm-long clinopyroxenes, and 5- to 10-μm-diam. Fe-Ti oxides.

Mode

Groundmass	63.0	Matrix	
Plagioclase	33.3	Quartz	
Cpx	3.3	K-feldspar	
Fe-Ti oxides	0.3	Biotite	
Olivine		Opx	
Hornblende		Pumice	
Glass		Shards	
Vesicles		Scoria	

Lithic clasts

APPENDIX C

TABULAR DATA FOR THERMAL AND NONTHERMAL WATERS, TECUAMBURRO VOLCANO, GUATEMALA

TABLE C-1. FIELD DATA FOR THERMAL AND NONTHERMAL WATERS, TECUAMBURRO VOLCANO, GUATEMALA

Field Number	Date	Location[a] UTM Grid Coordinates		Temp (°C)	Field (pH)	Flow Rate (l/min)	Comments
GT-88-1	03/17/88	1570.40	778.20	88.0	2.5	None	Site #2 Laguna Ixpaco (Fig. III.3)
GT-88-2	03/17/88	1571.95	786.75	90.0	6.7	5	Colmenares hot spring (GT-88-13, Fig. III.4)
GT-88-3	03/21/88	1578.45	796.46	37.0	5.7	1	Warm spring 4.5 km E of Los Esclavos
GT-88-4	07/07/88	1570.35	778.20	77.0	2.5	None	Site #10 Laguna Ixpaco (Fig. III.3)
GT-88-5	07/07/88	1570.40	778.20	85.0	2.5	None	Site #8 Laguna Ixpaco (Fig. III.3)
GT-88-6	07/07/88	1570.45	778.05	71.5	3.0	None	Site #15 Laguna Ixpaco (Fig. III.3)
GT-88-7	07/07/88	1570.20	778.20	27.8	3.0	3000	Outflow Laguna Ixpaco
GT-88-8	07/07/88	1570.10	778.10	22.1	6.5	152	Large inflow S shore Laguna Ixpaco
GT-88-9	07/08/88	1571.95	786.75	70.0	6.8	2	Colmenares hot spring
GT-88-10	07/08/88	1571.95	786.75	60.0	7.0	10	Colmenares "coldest" spring (Fig. III.4)
GT-88-11	07/08/88	1571.95	786.75	78.2	6.5	2	Colmenares hot spring (Fig. III.4)
GT-88-12	07/08/88	1571.95	786.75	94.3	6.8	5	Colmenares hot spring (Fig. III.4)
GT-88-13	07/08/88	1571.95	786.75	90.4	6.8	1	Colmenares hot spring (GT-88-2, Fig. III.4)
GT-88-14	07/08/88	1571.95	786.75	77.2	6.8	2300	Colmenares hot spring total outflow (Fig. III.4)
GT-88-15	07/08/88	1572.80	786.15	82.5	6.5	9	Circa TM-31 hottest spring
GT-88-16	07/08/88	1570.75	787.38	83.7	6.5	6	Hot spring E side Río Esclavos
GT-88-17	07/08/88	1570.80	787.70	34.6	6.0	19	Finca Agua Tibia
GT-88-18	07/08/88	1570.70	787.70	32.7	6.0	190	Large spring 150 m E of TM-34
GT-88-19	07/08/88	1573.85	787.60	40.2	6.5	4	Warm spring near paved highway
GT-88-20	07/09/88	1558.65	783.65[b]	20.0	–	–	Rainwater at Chiquimulilla
GT-88-21	07/09/88	1565.95	778.90[b]	96.0	–	–	Sulfur mine, Tecuamburro
GT-88-22	07/09/88	1565.95	778.90[b]	96.0	–	–	Sulfur mine, Tecuamburro
GT-88-23	07/09/88	1565.90	778.80[b]	20.0	5.5	12	Cold spring at Azufral
GT-88-24	07/09/88	1570.40	776.95	32.4	2.2	2	Las Playitas
GT-88-25	07/09/88	1569.75	780.10	22.3	6.0	15	Cold spring below Finca Chupadero
GT-88-26	07/11/88	1580.95	781.65	37.4	5.3	20	Warm spring, Finca Esperanza
GT-88-27	07/11/88	1580.93	781.75	21.3	6.0	57	Cold spring, Finca Esperanza
GT-88-28	07/11/88	1564.80	779.85[b]	24.1	5.8	1	Cold spring above TM-12, Finca El Silencio
GT-88-29	07/11/88	1564.65	780.10[b]	58.1	6.0	380	Large spring Finca El Silencio
GT-88-30	07/11/88	1564.60	780.50[b]	42.0	6.0	10	Warm spring S side of Tecuamburro
GT-88-31	07/12/88	1569.40	782.50	34.5	6.0	40	Warm spring at Finca Moreno
GT-88-32	07/12/88	1570.90	776.85	23.5	4.8	8	Swamp W side Laguna Ixpaco
GT-88-33	07/12/88	1570.90	776.85	23.5	4.8	Seep	Swamp W side Laguna Ixpaco

TABLE C-1 (cont)

Field Number	Date	Location[a] UTM Grid Coordinates		Temp (°C)	Field (pH)	Flow Rate (l/min)	Comments
GT-88-34	07/12/88	1572.98	775.30	42.0	4.8	4	Finca San Lorenzo
GT-88-35	07/13/88	1581.40	776.20	23.4	6.0	2	Cold spring Finca La Pastoría
GT-88-36	07/13/88	1577.79	779.85	22.2	6.3	5	Cold spring Finca Las Delicias
GT-88-37	07/13/88	1580.95	779.60	34.8	4.0	12	Warm spring Finca Bonanza
GT-88-38	07/14/88	1572.79	779.20	51.6	5.0	50	Hot spring Finca El Chorro
GT-88-39	07/14/88	1573.33	777.91	20.4	6.3	152	Cold spring
GT-88-40	07/14/88	1573.40	776.15	25.3	6.0	57	Cold spring Finca San Cayaetano
GT-88-41	07/14/88	1571.60	775.15	33.8	5.6	3	Warm spring Finca San Isabel
GT-88-42	07/15/88	1577.80	781.15	96.6	6.5	Seep	Fumarole Infiernitos Finca Las Delicias
GT-88-43	07/16/88	1561.44	783.35[b]	24.8	6.2	8	Cold spring by paved rd 2-3 km N Chiquimulilla
GT-88-44	07/16/88	1567.80	782.75	24.7	6.2	Seep	Cold spring by paved rd 10 km N Chiquimulilla
GT-88-45	07/16/88	1572.60	787.00	96.2	6.5	20	Hot spring Río Esclavos
GT-88-46	07/16/88	1572.55	786.98	88.8	6.5	90	Hot spring 80 m downstream from TM-2
GT-88-48	07/16/88	1577.60	798.29[c]	22.7	6.5	10	Cold spring 2-3 km E of Los Esclavos on CA#1
GT-88-49	07/16/88	1582.25	780.35	22.8	6.3	2	Cold spring near Finca Bonanza
GT-89-53	02/21/89	1570.40	778.20	93.5	3.0	None	N shore Ixpaco Site #8 (GT-88-5)
GT-89-54	02/21/89	1570.35	778.20	85.2	2.8	None	N shore Ixpaco Site #10 (GT-88-4)
GT-89-55	02/21/89	1570.10	778.10	20.0	6.5	228	Ixpaco inflow (GT-88-8)
GT-89-56	02/21/89	1569.75	780.10	22.2	6.5	57	Cold spring W of Finca Chupadero
GT-89-57	02/22/89	1570.75	787.38	80.2	6.7	30	Hot spring E side Río Esclavos (GT-88-16)
GT-89-58	02/22/89	1570.75	787.39	86.2	8.0	11	Hot spring Río Esclavos 50 m upstream of 57
GT-89-59	02/22/89	1570.49	787.40	85.0	7.5	4	Hot spring 30 m downstream of TM-8
GT-89-60	02/22/89	1569.77	786.75	36.0	6.0	19	Warm spring E bank of Río Esclavos along cliff
GT-89-61	02/22/89	1569.60	786.70	53.5	6.5	<2	Hot spring 30 m downstream of GT-60
GT-89-62	02/22/89	1569.50	786.65	85.0	7.5	19	Hot spring 100 m downstream of GT-61 E of Río
GT-89-63	02/23/89	1569.22	786.63	85.2	8.0	10	Across river from TM-9
GT-89-64	02/23/89	1568.29	785.49	25.0	7.5	38	Cold spring W side of Río Los Esclavos
GT-89-65	02/24/89	1566.58	784.98[b]	20.8	7.0	19	Cold spring E wall of canyon of Río Los Esclavos
GT-89-66	02/25/89	1585.59	769.25[d]	32.5	6.0	1000	Warm spring at Finca Santa Marta
GT-89-67	02/25/89	1573.40	776.15	22.4	6.0	57	Cold spring Finca San Cayetano (GT-88-40)
GT-89-68	02/25/89	1572.98	775.30	40.8	5.0	8	Finca San Lorenzo (GT-88-34)
GT-89-69	02/25/89	1570.90	776.85	25.5	4.5	None	Swamp W of Laguna Ixpaco (GT-88-32)
GT-89-70	02/25/89	1570.40	776.95	20.1	3.5	None	Las Playitas (GT-88-24)
GT-89-71	02/25/89	1572.60	787.00	96.5	7.0	15	Hot spring Río Esclavos (GT-88-45)

TABLE C-1 (cont)

Field Number	Date	Location[a] UTM Grid Coordinates		Temp (°C)	Field (pH)	Flow Rate (l/min)	Comments
GT-89-72	02/25/89	1572.55	786.98	87.4	7.5	15	Hot spring 80 m downstream from GT-88-46
GT-89-73	03/01/89	1578.45	796.46	37.5	6.0	19	Warm spring 4.5 km E of Los Esclavos
GT-89-74	03/01/89	1578.45	796.46	41.8	6.0	6	Hottest seep at TM-1 area
GT-89-75	03/01/89	1578.45	796.46	30.0	6.5	12 000	Río Esclavos, above to mineral seeps
GT-89-76	03/01/89	1577.60	798.29[c]	21.1	6.5	10	Cold spring E of Esclavos (GT-88-48)
GT-89-77	03/03/89	1564.65	780.10[b]	58.0	5.8	304	Finca El Silencio (GT-88-29)
GT-89-78	03/01/89	1564.80	779.85[b]	25.1	5.8	11	Cold spring above TM-12, Silencio (GT-88-28)
GT-89-79	03/01/89	1565.90	778.80	17.5	5.6	5	Cold spring at Azufral (GT-88-23)
GT-89-80	03/01/89	1565.90	778.80	96.0	—	—	Sulfur mine, Tecuamburro (GT-88-21)
GT-89-81	03/04/89	1572.79	779.20	52.4	4.8	38	Finca El Chorro (GT-88-38)
GT-89-82	03/04/89	1570.40	778.20	87.3	—	None	Site #8 Laguna Ixpaco
GT-89-83	03/04/89	1571.95	786.75	82.4	7.0	1	Colmenares (GT-88-9)
GT-89-84	03/04/89	1571.95	786.75	65.4	6.5	38	Colmenares (GT-88-10)
GT-89-85	03/04/89	1571.95	786.75	95.8	7.0	30	Colmenares hottest spring (GT-88-12)
GT-89-86	03/04/89	1571.95	786.75	75.0	7.0	2280	Colmenares outflow (GT-88-14)
GT-89-87	03/04/89	1572.80	786.15	92.4	6.5	15	Hot spring (GT-88-15)
GT-89-88	03/04/89	1573.85	787.60	42.0	6.8	11	Warm spring (GT-88-19)
GT-89-90	03/06/89	1580.95	781.65	37.9	5.2	15	Hot spring Finca Esperanza (GT-88-26)
GT-89-91	03/06/89	1580.93	781.75	17.2	6.2	38	Cold spring (GT-88-27)
GT-89-92	03/06/89	1580.95	779.60	35.5	3.8	76	Warm spring Finca Bonanza (GT-88-37)
GT-89-93	03/06/89	1583.65	783.73	21.9	6.0	None	Cold well, Barbaerena drinking water
GT-89-94	03/06/89	1583.61	783.94	21.7	5.9	None	Cold well in Barbaerena S side of hwy
GT-89-95	03/07/89	1561.20	784.65[b]	20.0	—	Seep	Cold seep near GT-89-97
GT-89-96	03/07/89	1561.90	784.60[b]	28.5	6.0	10	Cold spring north of GT-89-95
GT-89-97	03/07/89	1561.40	784.75[b]	39.2	6.0	3	Warm spring SSE side of Tecuamburro Volcano
GT-89-98	03/07/89	1561.20	784.70[b]	27.8	6.0	20	Cold spring 100 m upstream of GT-88-97
GT-89-99	03/07/89	1576.99	797.91	20.0	—	—	Rainwater at Los Esclavos village
GT-89-100	03/08/89	1577.79	779.85	20.7	6.8	2	Cold spring Finca Las Delicias (GT-88-36)
GT-89-101	03/08/89	1577.80	781.15	97.0	6.5		Fumarole Infiernitos Finca Las Delicias (GT-88-42)
GT-89-102	03/08/89	1581.40	776.20	23.5	6.0		Cold spring Finca La Pastoría (GT-88-35)

[a] All locations on Cuilapa Sheet unless otherwise noted.
[b] Chiquimullia Sheet.
[c] Oratorio Sheet.
[d] Guanagazapa Sheet.

TABLE C-2. MAJOR ELEMENT ANALYSES (mg/kg) FOR THERMAL AND NONTHERMAL WATERS OF TECUAMBURRO VOLCANO, GUATEMALA[a]

Sample No.	Temp (°C)	SiO_2	Ca	Mg	Sr	Na	K	Li	CO_3	HCO_3	SO_4	Cl	F	Br	B	TDS	Cation (meq/l)	Anion (meq/l)	Balance
GT-88-1	88.0	213	32.4	26.6	0.14	13.1	9.0	<0.02	0	0	355	2.3	0.07	<0.1	0.03	670.0	7.078	7.523	-0.0609
GT-88-2	90.0	88	59.3	1.15	1.13	609	23	1.89	0	127	256	787	2.06	2.4	12.6	1973.2	30.387	30.232	0.0051
GT-88-3	37.0	117	67.9	39.6	0.95	381	25	0.98	0	849	109	335	0.20	<0.1	3.14	1929.2	23.984	25.702	-0.0692
GT-88-4	77.0	288	180	87.4	0.11	70	6.2	0.09	0	0	3560	<0.4	0.14	<0.4	0.31	4834.5	73.395	74.424	-0.0139
GT-88-5	85.0	190	64.2	30.6	0.11	26	8.1	0.03	0	0	1285	0.2	0.13	<0.2	0.18	1774.6	25.087	26.958	-0.0719
GT-88-6	71.5	92	21.8	7.17	0.13	7.5	9.1	<0.02	0	0	427	2.7	0.09	<0.1	<0.02	590.1	7.827	9.042	-0.1440
GT-88-7	27.8	70	22.4	7.21	0.14	8.0	9.9	0.02	0	0	400	2.6	0.09	<0.1	<0.02	545.3	7.401	8.473	-0.1350
GT-88-8	22.1	67	20.6	6.07	0.11	9.5	3.0	0.01	0	117	13.2	1.9	<0.05	<0.1	<0.02	241.3	2.036	2.291	-0.1178
GT-88-9	70.0	95	55.2	1.30	1.03	598	24.8	1.91	0	156	236	796	2.42	2.1	17.1	1995.9	29.768	30.808	-0.0343
GT-88-10	60.0	90	35.9	2.73	0.74	334	13.8	1.04	0	239	124	377	1.77	1.1	8.9	1232.1	17.054	17.653	-0.0345
GT-88-11	78.2	87	50.1	2.34	0.94	464	18.8	1.46	0	169	190	608	2.11	1.6	13.1	1611.5	23.595	24.536	-0.0391
GT-88-12	94.3	90	66.1	1.10	1.23	610	24.0	1.99	0	147	259	811	2.58	2.3	17.5	2042.6	30.814	31.536	-0.0231
GT-88-13	90.4	89	59.8	1.08	1.19	591	22.4	1.62	0	142	249	801	2.43	2.2	17.5	1984.3	29.573	30.961	-0.0458
GT-88-14	77.2	92	55.4	1.48	1.05	543	22.0	1.60	0	164	225	735	2.41	2.0	15.8	1864.9	27.283	28.899	-0.0575
GT-88-15	82.5	94	60.1	1.04	1.13	601	22.4	1.84	0	142	258	795	2.65	2.3	12.3	1997.3	30.056	30.752	-0.0229
GT-88-16	83.7	72	47.3	0.20	0.72	444	6.6	1.11	0	68.5	293	546	3.24	1.6	8.94	1495.8	22.013	23.181	-0.0517
GT-88-17	34.6	91	21.4	6.73	0.21	16.2	5.8	0.01	0	156	1.9	2.3	<0.05	<0.1	<0.02	304.0	2.489	2.696	-0.0799
GT-88-18	32.7	91	20.9	6.78	0.26	13.7	4.6	<0.01	0	159	0.7	1.2	<0.05	<0.1	<0.02	299.5	2.324	2.683	-0.1432
GT-88-19	40.2	115	30.3	4.78	0.29	22.0	6.9	0.02	0	168	4.1	4.0	<0.05	<0.1	<0.02	368.9	3.053	3.168	-0.0370
GT-88-23	20.0	48	10.9	2.24	0.06	5.5	2.1	0.01	0	49.1	12.5	2.5	<0.05	<0.1	<0.02	145.3	1.029	1.344	-0.2653
GT-88-24	32.4	202	214	50.8	1.55	82	9.0	0.06	0	0	5200	8.7	<0.05	<0.2	0.20	6574.3	102.234	108.736	-0.0616
GT-88-25	22.3	79	53.4	15.2	0.20	14.6	2.5	<0.01	0	152	110	2.5	<0.05	<0.1	<0.02	436.5	4.649	4.975	-0.0678
GT-88-26	37.4	63	15.8	4.82	0.09	11.8	3.5	<0.01	0	44.1	69.0	0.5	0.08	<0.1	<0.02	213.4	1.801	2.190	-0.1951
GT-88-27	21.3	68	10.7	3.84	0.12	7.8	2.3	<0.01	0	88	1.6	1.4	<0.05	<0.1	<0.02	186.6	1.442	1.516	-0.0500
GT-88-28	24.1	74	28.3	7.11	0.17	10.1	2.7	<0.01	0	159	3.0	1.2	<0.05	<0.1	<0.02	291.3	2.510	2.799	-0.1088
GT-88-29	58.1	200	115	31.8	0.60	62	9.1	0.02	0	195	376	4.1	0.07	<0.1	0.09	1013.0	11.330	11.582	-0.0220
GT-88-30	42.0	150	86.8	24.0	0.43	48	8.8	0.03	0	213	249	2.5	0.08	<0.1	0.12	780.2	8.660	8.795	-0.0155
GT-88-31	34.5	120	59.4	37.2	0.35	41	9.0	0.01	0	356	117	3.6	0.17	<0.1	0.09	739.2	8.044	8.403	-0.0436
GT-88-32	23.5	102	46.7	16.1	0.28	17.6	7.0	<0.01	0	0	412	2.8	0.06	<0.1	0.03	614.5	6.374	8.730	-0.3120
GT-88-34	42.0	55	43.1	8.74	0.18	39	7.2	0.01	0	186	109	1.3	<0.05	<0.1	0.02	449.4	4.818	5.374	-0.1091
GT-88-35	23.4	90	8.3	3.07	0.18	10.6	10.8	0.01	0	76	3.1	4.3	<0.05	<0.1	<0.02	218.7	1.481	1.606	-0.0806
GT-88-36	22.2	33	70.2	4.82	0.22	2.9	1.0	<0.01	0	242	4.3	1.6	0.19	<0.1	<0.02	361.5	4.066	4.129	-0.0153
GT-88-37	34.8	75	27.6	6.13	0.12	8.9	4.3	<0.01	0	0	149	1.2	0.24	<0.1	<0.02	277.0	3.218	3.174	0.0136
GT-88-38	51.6	85	22.8	5.67	0.02	25	9.0	<0.01	0	29.5	165	1.1	0.19	<0.1	0.03	360.7	3.836	3.990	-0.0393
GT-88-39	20.4	64	41.3	16.3	0.35	9.7	3.6	<0.01	0	56.3	8.7	14.4	<0.05	<0.1	<0.02	377.4	3.930	4.137	-0.0513
GT-88-40	25.3	88	16.3	8.53	0.09	9.7	2.7	<0.01	0	149	1.5	0.6	<0.05	<0.1	<0.02	280.6	2.011	2.562	-0.2411
GT-88-41	33.8	75	50.3	19.9	0.22	32	3.4	<0.01	0	164	156	2.5	0.18	<0.1	0.08	534.7	6.066	6.342	-0.0446
GT-88-42	96.6	25	194	19.8	0.14	1.5	0.8	<0.01	0	276	328	5.5	0.10	<0.1	<0.02	859.4	11.445	11.572	-0.0110
GT-88-43	24.8	85	35.6	11.1	0.20	17.6	3.2	<0.01	0	122	75.0	1.5	<0.05	<0.1	<0.02	351.0	3.542	3.617	-0.0208
GT-88-44	24.7	53	160	48.2	1.13	9.5	5.0	<0.01	0	53.9	80.4	25.3	<0.05	<0.1	<0.02	1036.1	12.529	12.929	-0.0315
GT-88-45	96.2	95	69.0	1.18	1.30	604	25.2	1.86	0	144	280	817	2.46	2.5	17.6	2074.5	30.707	32.109	-0.0447
GT-88-46	88.8	99	56.1	1.25	1.08	504	22.4	1.55	0	159	235	709	2.32	2.2	16.4	1814.8	25.613	28.353	-0.1016
GT-88-48	22.7	57	15.6	3.73	0.12	5.8	4.0	<0.01	0	78.3	2.7	2.2	<0.05	<0.1	<0.02	174.5	1.445	1.483	-0.0256
GT-88-49	22.8	99	52.0	57.0	0.74	17.8	3.2	<0.01	0	39.2	72.4	28.5	<0.05	<0.1	<0.02	711.9	8.162	8.472	-0.0372

TABLE C-2 (cont)

Sample No.	Temp (°C)	SiO_2	Ca	Mg	Sr	Na	K	Li	CO_3	HCO_3	SO_4	Cl	F	Br	B	TDS	Cation (meq/l)	Anion (meq/l)	Balance
GT-89-53	93.5	201	38.6	23.7	0.16	17.8	9.5	0.06	0	0	913	1.3	0.32	<0.1	<0.05	1333.9	19.761	19.223	0.0276
GT-89-54	85.2	288	103	62	0.08	48	2.1	0.05	0	0	2180	<1	0.38	<0.1	0.16	2978.1	46.774	45.671	0.0239
GT-89-55	20.0	81	25.4	7.40	0.12	10.6	3.1	<0.01	0	98.8	21.1	2.5	<0.05	<0.05	<0.05	272.9	2.497	2.491	0.0024
GT-89-56	22.2	82	59.5	16.2	0.17	17.4	2.7	<0.01	0	126	128	5.7	0.10	<0.05	<0.05	460.2	5.152	5.275	-0.0236
GT-89-57	80.2	72	43.4	0.28	0.62	417	8.3	1.07	0	68.3	283	488	2.49	0.79	9.10	1397.1	20.722	21.310	-0.0280
GT-89-58	86.2	73	49.0	0.26	0.70	457	10.0	1.16	0	51.2	311	542	3.32	1.00	12.6	1515.3	22.789	23.336	-0.0237
GT-89-59	85.0	88	51.2	0.48	0.72	485	10.2	1.21	0	53.7	307	575	3.25	1.03	12.0	1591.2	24.138	24.183	-0.0019
GT-89-60	36.0	83	24.2	7.30	0.24	62.0	5.2	0.12	0	137	32.0	61.8	0.35	0.19	1.38	416.7	4.661	4.760	-0.0210
GT-89-61	53.5	88	34.8	3.8	0.40	255	7.8	0.59	0	110	145	296	1.62	1.82	6.87	953.4	13.448	13.575	-0.0094
GT-89-62	85.0	70	59.6	0.24	0.76	508	10.0	1.24	0	35.4	293	623	3.10	1.27	14.6	1622.7	25.509	25.054	0.0180
GT-89-63	85.2	74	60.0	0.38	0.76	511	10.6	1.24	0	43.9	302	639	3.28	1.34	15.2	1665.9	25.686	25.866	-0.0070
GT-89-64	25.0	95	25.8	11.1	0.16	14.2	3.0	0.02	0	166	4.6	3.0	.06	<0.05	<0.05	328.8	2.906	3.004	-0.0330
GT-89-65	20.8	98	13.7	6.54	0.10	10.6	0.8	<0.01	0	107	3.7	1.4	<0.05	<0.05	<0.05	243.8	1.722	1.903	-0.0994
GT-89-66	32.5	111	36.2	32.2	0.25	84.5	16.6	0.13	0	288	107	61.4	0.21	0.22	0.34	743.1	8.578	8.794	-0.0249
GT-89-67	22.4	90	16.0	8.93	0.11	9.7	2.9	<0.01	0	128	2.1	0.8	0.07	<0.05	<0.05	261.7	2.037	2.216	-0.0841
GT-89-68	40.8	58	46.5	10.2	0.17	38.2	7.4	<0.01	0	183	104	2.0	0.15	<0.05	<0.05	450.2	5.040	5.247	-0.0403
GT-89-69	25.5	118	76.2	29.2	0.36	27	3.2	<0.01	0	0	456	1.4	<0.05	<0.05	<0.05	726.4	11.537	9.615	0.1817
GT-89-70	20.1	180	62.2	29.3	0.38	28	4.7	<0.01	0	0	638	7.8	<0.05	<0.05	<0.05	997.8	14.429	13.672	0.0539
GT-89-71	96.5	107	67.2	1.46	1.18	671	25.4	2.02	0	131	275	815	2.69	1.85	18.7	2123.9	33.611	31.789	0.0557
GT-89-72	87.4	102	60.9	1.62	1.10	587	3.4	1.83	0	145	246	730	2.47	1.61	16.7	1922.8	29.550	28.926	0.0213
GT-89-73	37.5	140	66.7	39.5	0.78	443	32.4	1.20	0	885	117	347	0.49	1.58	3.44	2078.9	26.841	26.835	0.0002
GT-89-74	41.8	139	84	52	1.20	680	44.0	1.89	0	1220	178	530	0.49	1.15	5.41	2938.6	39.400	38.773	0.0160
GT-89-75	30.0	61	16.2	6.07	0.14	21.3	5.2	0.04	0	121	8.8	14.4	0.13	<0.05	<0.05	254.5	2.397	2.585	-0.0755
GT-89-76	21.1	78	27.4	8.9	0.19	9.6	2.6	<0.01	0	161	1.6	1.0	0.06	<0.05	<0.05	294.5	2.588	2.775	-0.0695
GT-89-77	58.0	184	104	28.8	0.50	56	8.1	0.01	0	206	324	3.9	<0.05	<0.05	<0.05	917.0	10.248	10.299	-0.0049
GT-89-78	25.1	83	22.8	6.41	0.14	9.6	1.8	<0.01	0	115	4.2	1.5	<0.05	<0.05	<0.05	255.6	2.148	2.185	-0.0172
GT-89-79	17.5	53	9.6	2.21	0.04	5.9	1.9	0.01	0	36.6	17.7	1.7	0.13	<0.05	<0.05	132.2	0.969	1.081	-0.1088
GT-89-81	52.4	88	22.4	5.96	0.05	23.9	8.8	0.06	0	20.7	162	1.1	.07	<0.05	<0.05	349.1	3.750	3.779	-0.0079
GT-89-83	82.4	92	58	1.53	1.06	578	24.0	1.86	25.2	101	235	771	1.99	1.68	17.0	1912.9	29.031	29.950	-0.0312
GT-89-84	65.4	92	47.2	4.66	0.72	339	14.6	1.07	0	165	138	423	1.37	1.14	9.58	1239.8	18.018	18.001	0.0009
GT-89-85	95.8	95	61.2	1.28	1.12	612	23.0	1.99	27.6	74.4	270	810	2.56	1.74	18.1	2004.0	30.634	31.495	-0.0277
GT-89-86	75.0	92	55	1.84	0.94	516	20.2	1.67	26.4	96.4	217	681	2.20	1.32	15.7	1731.3	26.086	26.960	-0.0329
GT-89-87	92.4	95	60.0	1.16	1.06	579	21.8	1.89	25.2	84.2	256	772	2.49	1.61	17.4	1922.2	29.088	30.178	-0.0368
GT-89-88	42.0	123	31.1	5.31	0.29	22.5	7.1	0.02	0	162	7.0	6.1	0.05	<0.05	<0.05	380.0	3.165	3.217	-0.0161
GT-89-90	37.9	67	16.2	4.98	0.06	11.9	3.5	0.01	0	29.3	72.1	0.6	0.24	<0.05	<0.05	205.9	1.851	2.024	-0.0892
GT-89-91	17.2	88	16.6	7.10	0.15	12.0	2.9	<0.01	27.6	52.5	13.2	1.0	0.12	<0.05	<0.05	221.3	2.019	2.083	-0.0309
GT-89-92	35.5	79	27.5	6.62	0.11	9.5	4.3	0.01	0	0	149	1.7	0.19	<0.05	<0.05	282.5	2.793	3.186	-0.1315
GT-89-93	21.9	70	21.4	8.12	0.16	10.8	3.2	0.01	42.0	36.6	6.6	2.5	0.18	<0.05	<0.05	213.7	2.294	2.412	-0.0504
GT-89-94	21.7	93	26.5	12.7	0.26	10.8	2.9	<0.01	0	142	4.6	15.7	<0.05	<0.05	<0.05	320.4	2.930	3.051	-0.0406
GT-89-97	39.2	141	79.3	64.5	0.66	436	37.6	0.58	0	763	121	519	0.41	1.18	11.0	2182.8	29.482	30.103	-0.0208
GT-89-98	27.8	94	24.3	10.6	0.19	14.7	2.6	0.01	0	138	29.7	1.9	<0.05	<0.05	<0.05	318.1	2.801	2.979	-0.0615
GT-89-99	—	<1	1.0	0.30	0.06	3.1	0.7	<0.02	0	97.6	1.7	2.7	<0.05	<0.05	<0.05	107.7	0.255	1.712	-1.4810
GT-89-100	20.7	36	68.9	5.00	0.21	3.1	1.5	<0.01	0	240	6.8	1.5	0.15	<0.05	<0.05	366.9	4.109	4.148	-0.0094
GT-89-101	97.0	21	480	43.4	0.24	1.4	4.0	<0.01	0	204	1157	2.6	0.27	<0.05	<0.05	1942.6	27.785	28.086	-0.0108
GT-89-102	23.5	102	9.0	3.11	0.17	9.5	11.9	0.01	0	78.1	3.5	4.8	<0.05	<0.05	<0.05	231.1	1.522	1.603	-0.0520

[a] Analyses by P. E. Trujillo and D. Counce, Los Alamos National Laboratory.

TABLE C-3. TRACE ELEMENT ANALYSES (mg/kg) FOR THERMAL AND NONTHERMAL WATERS OF TECUAMBURRO VOLCANO AREA[a]

Sample No.	Ag	Al	As	Ba	Cd	Co	Cr	Cs	Cu	Fe	Hg	Mn	Mo	NH_4	Ni	NO_3	Pb	PO_4	Rb	Sb	Se	Zn
GT-88-1	<0.001	6.6	<0.05	0.08	<0.001	<0.002	<0.002	0.015	<0.002	8.61	<0.1	0.77	0.006	2.17	<0.002	0.2	0.003	<0.1	0.058	<0.1	<0.1	0.17
GT-88-2	<0.001	<0.1	1.9	0.01	<0.001	<0.002	<0.002	0.11	<0.002	0.11	<0.1	0.05	0.003	0.08	<0.002	0.2	<0.002	<0.1	0.12	0.1	<0.1	<0.01
GT-88-3	<0.001	<0.1	0.10	0.11	<0.001	<0.002	<0.002	0.008	<0.002	<0.01	<0.1	0.09	<0.002	<0.05	0.002	<0.1	<0.002	<0.1	0.11	<0.1	<0.1	<0.01
GT-88-4	<0.001	234	0.10	0.02	<0.001	<0.002	0.041	0.009	<0.002	411	<0.1	3.05	<0.002	13.9	<0.002	<0.4	<0.002	<0.4	0.18	<0.1	<0.1	0.41
GT-88-5	<0.001	72.6	<0.05	0.05	<0.001	<0.002	0.012	<0.005	<0.002	92.0	<0.1	1.18	<0.002	3.84	<0.002	<0.2	<0.002	<0.2	0.076	<0.2	<0.1	0.23
GT-88-6	<0.001	10.0	<0.05	0.07	<0.001	<0.002	0.005	<0.005	<0.002	11.6	<0.1	0.30	<0.002	0.74	0.003	<0.1	<0.002	<0.1	0.037	<0.1	<0.1	0.05
GT-88-7	<0.001	10.7	<0.05	0.07	<0.001	<0.002	<0.002	<0.005	<0.002	12.8	<0.1	0.30	<0.002	0.60	0.004	<0.1	<0.002	<0.1	0.038	<0.1	<0.1	0.05
GT-88-8	<0.001	<0.1	<0.05	0.03	<0.001	<0.002	<0.002	<0.005	<0.002	0.14	<0.1	<0.01	<0.002	0.11	0.004	2.6	<0.002	<0.1	0.008	<0.1	<0.1	0.02
GT-88-9	<0.001	<0.1	1.36	0.03	<0.001	<0.002	<0.002	<0.005	<0.002	0.02	<0.1	0.08	<0.002	0.21	0.012	4.5	<0.002	<0.1	0.19	0.2	<0.1	0.02
GT-88-10	<0.001	<0.1	1.46	0.03	<0.001	<0.002	<0.002	0.081	<0.002	0.04	<0.1	0.05	<0.002	0.06	0.012	1.3	<0.002	<0.2	0.11	<0.1	<0.1	0.02
GT-88-11	<0.001	<0.1	1.40	0.03	<0.001	<0.002	<0.002	0.095	<0.002	<0.02	<0.1	0.07	<0.002	0.67	0.005	<0.1	<0.002	<0.1	0.14	<0.2	<0.1	0.01
GT-88-12	<0.001	<0.1	1.83	0.02	<0.001	<0.002	<0.002	0.12	<0.002	<0.02	<0.1	0.06	<0.002	0.17	<0.002	<0.1	<0.002	<0.1	0.18	<0.2	<0.1	0.31
GT-88-13	<0.001	<0.1	1.91	0.02	<0.001	<0.002	<0.002	0.12	<0.002	<0.02	<0.1	0.04	<0.002	0.21	<0.002	<0.1	<0.002	<0.1	0.17	<0.2	<0.1	0.01
GT-88-14	<0.001	<0.1	1.76	0.03	<0.001	<0.002	<0.002	0.11	<0.002	<0.02	<0.1	0.05	<0.002	0.07	<0.002	0.6	<0.002	<0.1	0.16	<0.2	<0.1	0.01
GT-88-15	<0.001	<0.1	1.82	0.04	<0.001	<0.002	<0.002	0.11	<0.002	<0.02	<0.1	0.11	0.002	0.28	0.004	<0.1	<0.002	<0.1	0.17	0.2	<0.1	0.01
GT-88-16	<0.001	<0.1	1.23	0.02	<0.001	<0.002	<0.002	0.069	<0.002	<0.02	<0.1	0.03	0.003	0.12	<0.002	<0.1	<0.002	<0.1	0.092	<0.1	<0.1	0.01
GT-88-17	<0.001	<0.1	<0.05	0.04	<0.001	<0.002	<0.002	<0.005	<0.002	<0.01	<0.1	<0.01	<0.002	0.13	<0.002	2.1	<0.002	<0.1	0.017	<0.1	<0.1	0.01
GT-88-18	<0.001	<0.1	<0.05	0.02	<0.001	<0.002	<0.002	<0.005	<0.002	<0.01	<0.1	<0.01	<0.002	0.06	<0.002	1.7	<0.002	<0.1	0.013	<0.1	<0.1	0.01
GT-88-19	<0.001	<0.1	<0.05	0.08	<0.001	<0.002	<0.002	0.007	<0.002	0.01	<0.1	<0.01	<0.002	0.06	<0.002	13.4	<0.002	<0.1	0.021	<0.1	<0.1	0.01
GT-88-23	<0.001	<0.1	<0.05	0.01	<0.001	<0.002	<0.002	<0.005	0.002	0.01	<0.1	<0.01	<0.002	0.07	<0.002	12.8	<0.002	<0.1	0.010	<0.1	<0.1	0.02
GT-88-24	<0.001	579	<0.05	0.04	<0.001	0.36	0.068	<0.005	0.006	216	<0.1	4.12	0.006	5.09	0.058	<0.2	<0.002	<0.2	0.048	<0.2	<0.1	0.98
GT-88-25	<0.001	0.2	<0.05	0.02	<0.001	<0.002	<0.002	0.006	<0.002	0.11	<0.1	<0.01	0.003	0.05	0.007	6.5	<0.002	<0.1	<0.005	<0.1	<0.1	0.02
GT-88-26	<0.001	<0.1	<0.05	0.08	<0.001	<0.002	<0.002	<0.005	<0.002	0.13	<0.1	0.06	<0.002	<0.05	0.011	<0.1	<0.002	<0.1	0.007	<0.1	<0.1	0.02
GT-88-27	<0.001	1.2	<0.05	0.08	<0.001	<0.002	<0.002	<0.005	<0.002	0.94	<0.1	0.06	<0.002	0.06	<0.002	<0.1	<0.002	<0.1	<0.005	<0.1	<0.1	0.02
GT-88-28	<0.001	<0.1	<0.05	0.01	<0.001	<0.002	<0.002	<0.005	<0.002	<0.01	<0.1	<0.01	<0.002	<0.05	<0.002	5.9	<0.002	<0.1	<0.005	<0.1	<0.1	0.02
GT-88-29	<0.001	<0.1	<0.05	0.05	<0.001	<0.002	<0.002	<0.005	<0.002	<0.01	<0.1	1.03	<0.002	<0.05	<0.002	23.4	<0.002	<0.1	0.038	<0.1	<0.1	0.01
GT-88-30	<0.001	<0.1	<0.05	0.04	<0.001	<0.002	<0.002	<0.005	<0.002	0.07	<0.1	0.67	<0.002	0.05	<0.002	<0.1	<0.002	<0.1	0.032	<0.1	<0.1	0.02
GT-88-31	<0.001	<0.1	<0.05	0.02	<0.001	<0.002	<0.002	<0.005	<0.002	<0.01	<0.1	<0.01	<0.002	<0.05	<0.002	<0.1	<0.002	<0.1	0.021	<0.2	<0.1	0.02
GT-88-32	<0.001	0.6	<0.05	0.10	<0.001	<0.002	<0.002	<0.005	<0.002	3.46	<0.1	0.95	<0.002	4.54	<0.002	<0.1	<0.002	<0.1	0.016	<0.2	<0.1	0.01
GT-88-34	<0.001	<0.1	<0.05	0.07	<0.001	<0.002	<0.002	<0.005	<0.002	0.98	<0.1	0.18	<0.002	0.06	<0.002	<0.1	<0.002	<0.1	0.016	<0.1	<0.1	0.01
GT-88-35	<0.001	0.3	<0.05	0.29	<0.001	<0.002	0.005	<0.005	<0.002	0.11	<0.1	<0.01	<0.002	0.49	0.003	10.8	<0.002	<0.1	0.036	<0.1	<0.1	0.02
GT-88-36	<0.001	<0.1	<0.05	0.10	<0.001	<0.002	0.009	<0.005	<0.002	0.01	<0.1	0.04	<0.002	0.12	<0.002	1.0	<0.002	<0.1	<0.005	<0.1	<0.1	0.02
GT-88-37	<0.001	2.5	<0.05	0.05	<0.001	0.006	<0.002	<0.005	0.004	1.38	<0.1	0.32	0.006	0.06	0.003	<0.1	<0.002	<0.1	0.007	<0.1	<0.1	0.05
GT-88-38	<0.001	<0.1	<0.05	0.03	<0.001	<0.002	<0.002	<0.005	<0.002	16.7	<0.1	0.24	0.003	0.12	<0.002	<0.1	<0.002	<0.1	0.031	<0.1	<0.1	0.05
GT-88-39	<0.001	<0.1	<0.05	0.09	<0.001	<0.002	<0.002	<0.005	<0.002	0.03	<0.1	0.01	<0.002	0.05	<0.002	163	<0.002	<0.1	0.005	<0.1	<0.1	0.02
GT-88-40	<0.001	<0.1	<0.05	<0.01	<0.001	<0.002	0.003	<0.005	<0.002	0.02	<0.1	0.03	<0.002	<0.05	<0.002	4.4	<0.002	<0.1	0.005	<0.1	<0.1	0.02
GT-88-41	<0.001	<0.1	<0.05	0.09	<0.001	<0.002	<0.002	<0.005	<0.002	7.75	<0.1	0.34	<0.002	0.11	<0.002	18.4	<0.002	<0.1	0.010	<0.1	<0.1	0.03
GT-88-42	<0.001	<0.1	<0.05	0.11	<0.001	<0.002	<0.002	<0.005	<0.002	0.04	<0.1	0.71	<0.002	0.46	0.002	0.5	<0.002	<0.1	<0.005	<0.1	<0.1	0.02
GT-88-43	<0.001	<0.1	<0.05	<0.01	<0.001	<0.002	<0.002	<0.005	<0.002	<0.01	<0.1	0.01	<0.002	<0.05	<0.002	<0.1	<0.002	<0.1	0.005	<0.2	<0.1	0.03
GT-88-44	<0.001	<0.1	<0.05	0.19	<0.001	<0.002	<0.002	<0.005	<0.002	0.10	<0.1	<0.01	<0.002	0.26	<0.002	599	<0.002	<0.1	0.011	<0.2	<0.1	0.03
GT-88-45	<0.001	<0.1	2.00	0.02	<0.001	<0.002	<0.002	0.14	<0.002	<0.02	<0.1	0.07	0.006	0.13	<0.002	<0.1	<0.002	<0.1	0.15	<0.1	<0.1	0.02
GT-88-46	<0.001	<0.1	1.55	0.01	<0.001	<0.002	<0.002	0.12	<0.002	0.02	<0.1	0.07	0.007	0.09	<0.002	2.3	<0.002	<0.1	0.14	<0.1	<0.1	0.01
GT-88-48	<0.001	<0.1	<0.05	0.01	<0.001	<0.002	<0.002	<0.005	<0.002	0.03	<0.1	<0.01	<0.002	<0.05	<0.002	5.0	<0.002	<0.1	0.006	<0.1	<0.1	0.03
GT-88-49	<0.001	<0.1	<0.05	0.33	<0.001	<0.002	<0.002	<0.005	<0.002	<0.01	<0.1	0.01	<0.002	0.06	<0.002	342	<0.002	<0.1	0.006	<0.1	<0.1	0.02
GT-89-53	<0.001	69.7	<0.1	0.06	<0.001	0.005	0.010	0.009	<0.002	49.0	<0.2	0.68	<0.002	3.35	0.023	0.26	0.002	0.62	0.08	<0.1	<0.2	0.22
GT-89-54	<0.001	103	<0.1	0.02	<0.001	0.016	0.015	0.007	0.066	170	<0.2	2.08	<0.002	6.27	0.009	<0.1	0.006	<0.1	0.10	<0.1	<0.2	0.44
GT-89-55	<0.001	0.46	0.05	0.02	<0.001	<0.002	<0.002	<0.005	0.002	0.34	<0.1	<0.01	<0.002	0.14	0.012	22.1	<0.002	<0.05	0.046	<0.05	<0.1	0.01
GT-89-56	<0.001	0.12	<0.05	<0.01	<0.001	<0.002	<0.002	<0.005	<0.002	0.07	<0.1	<0.01	<0.002	0.09	0.004	22.2	<0.002	<0.05	0.014	<0.05	<0.1	<0.01
GT-89-57	<0.001	0.3	1.2	<0.02	<0.001	<0.002	<0.002	0.10	<0.002	0.06	<0.2	0.02	0.015	0.05	<0.002	<0.1	<0.002	<0.1	0.07	<0.1	<0.2	<0.02
GT-89-58	<0.001	0.2	1.3	<0.02	<0.001	<0.002	<0.002	0.12	<0.002	<0.02	<0.2	0.02	0.015	0.10	<0.002	<0.1	<0.002	<0.1	0.08	<0.1	<0.2	0.28
GT-89-59	<0.001	0.2	1.3	0.04	<0.001	<0.002	<0.002	0.12	0.002	<0.02	<0.2	0.07	0.011	0.08	<0.002	<0.1	0.002	<0.1	0.08	<0.1	<0.2	0.02
GT-89-60	<0.001	<0.05	0.15	0.03	<0.001	<0.002	<0.002	0.031	<0.002	<0.01	<0.1	<0.01	0.006	<0.04	<0.002	1.4	<0.002	<0.05	0.025	<0.05	<0.1	0.02

TABLE C-3 (cont)

Sample No.	Ag	Al	As	Ba	Cd	Co	Cr	Cs	Cu	Fe	Hg	Mn	Mo	NH_4	Ni	NO_3	Pb	PO_4	Rb	Sb	Se	Zn
GT-89-61	<0.001	0.1	0.6	0.08	<0.001	<0.002	<0.002	0.066	<0.002	0.10	<0.2	0.09	0.008	0.06	0.003	<0.1	<0.002	<0.1	0.05	<0.1	<0.1	<0.01
GT-89-62	<0.001	<0.1	1.5	0.02	<0.001	<0.002	<0.002	0.13	<0.002	<0.02	<0.2	<0.02	0.012	0.08	0.003	<0.1	<0.002	<0.1	0.08	<0.1	<0.2	<0.02
GT-89-63	<0.001	<0.1	1.5	0.05	<0.001	<0.002	0.002	0.13	<0.002	<0.02	<0.2	0.02	0.012	0.07	<0.002	<0.1	0.005	<0.1	0.09	<0.1	<0.2	<0.02
GT-89-64	<0.001	<0.05	<0.05	0.02	<0.001	<0.002	<0.002	<0.005	<0.002	0.03	<0.1	0.01	0.006	0.05	<0.002	5.8	<0.002	0.17	0.009	<0.05	<0.1	<0.01
GT-89-65	<0.001	0.07	0.06	0.02	<0.001	<0.002	<0.002	<0.005	0.002	0.01	<0.1	0.14	<0.002	0.06	0.009	1.79	<0.002	<0.05	<0.005	<0.05	<0.1	<0.01
GT-89-66	<0.001	<0.05	0.07	0.02	<0.001	<0.002	<0.002	<0.005	<0.002	0.03	<0.1	<0.01	0.004	<0.05	0.007	4.2	<0.002	0.37	0.05	<0.05	<0.1	<0.01
GT-89-67	<0.001	<0.05	<0.05	0.01	<0.001	<0.002	<0.002	<0.005	<0.002	0.01	<0.1	0.02	<0.002	0.08	0.003	2.7	<0.002	0.13	0.008	<0.05	<0.1	<0.01
GT-89-68	<0.001	0.05	<0.05	0.07	<0.001	<0.002	<0.002	<0.005	<0.002	0.05	<0.1	0.19	<0.002	0.19	<0.002	<0.05	<0.002	<0.05	0.025	<0.05	<0.1	<0.01
GT-89-69	<0.001	2.4	<0.1	0.05	<0.001	<0.002	<0.002	<0.005	<0.002	2.90	<0.2	1.29	<0.002	5.12	<0.002	<0.05	<0.002	0.22	0.024	<0.1	<0.2	0.02
GT-89-70	<0.001	35.5	<0.1	0.02	<0.001	<0.002	0.003	<0.005	<0.002	2.20	<0.2	0.99	<0.002	2.49	0.062	<0.05	<0.002	2.30	0.024	<0.1	<0.2	0.04
GT-89-71	<0.001	0.1	2.0	0.02	<0.001	<0.002	<0.002	0.14	<0.002	0.08	<0.2	0.04	0.007	0.41	0.007	<0.1	<0.002	<0.1	0.13	<0.1	<0.2	0.32
GT-89-72	<0.001	<0.1	1.8	<0.02	<0.001	<0.002	<0.002	0.11	<0.002	<0.02	<0.2	0.04	0.011	0.15	<0.002	<0.1	0.002	<0.1	0.12	<0.1	<0.2	0.02
GT-89-73	<0.001	<0.1	<0.1	0.22	<0.001	<0.002	<0.002	0.009	<0.002	0.12	<0.2	0.25	0.002	0.11	<0.002	<0.1	<0.002	<0.1	0.12	<0.1	<0.2	0.02
GT-89-74	<0.001	0.1	0.3	0.20	<0.001	<0.002	<0.002	<0.005	<0.002	0.10	<0.2	0.29	0.002	0.09	<0.002	<0.1	<0.002	<0.1	0.22	<0.1	<0.2	0.02
GT-89-75	<0.001	<0.05	<0.05	0.05	<0.001	<0.002	<0.002	<0.005	<0.002	0.21	<0.1	0.11	<0.002	0.09	0.011	<0.05	<0.002	0.22	0.013	<0.05	<0.1	<0.01
GT-89-76	<0.001	<0.05	0.08	0.01	<0.001	<0.002	<0.002	<0.005	0.004	0.01	<0.1	<0.01	<0.002	<0.05	<0.002	3.7	0.002	0.25	0.008	<0.05	<0.1	<0.01
GT-89-77	<0.001	<0.1	<0.1	0.04	<0.001	<0.002	<0.002	<0.005	0.003	<0.02	0.2	0.92	<0.002	0.11	<0.002	<0.05	<0.002	0.55	0.038	<0.1	<0.2	0.02
GT-89-78	<0.001	0.10	<0.05	<0.01	<0.001	<0.002	<0.002	<0.005	<0.002	0.02	<0.1	<0.01	<0.002	0.06	<0.002	10.5	0.002	<0.05	0.005	<0.05	<0.1	0.02
GT-89-79	<0.001	<0.05	0.08	<0.01	<0.001	<0.002	<0.002	<0.005	0.002	<0.01	<0.1	<0.01	0.003	<0.05	<0.002	3.2	<0.002	<05	0.013	<0.05	<0.1	0.03
GT-89-81	<0.001	0.08	0.12	0.02	<0.001	<0.002	<0.002	<0.005	<0.002	15.7	<0.1	0.23	<0.002	0.09	<0.002	<0.05	<0.002	<0.05	0.043	<0.1	<0.1	0.06
GT-89-83	<0.001	<0.1	2.0	<0.02	<0.001	<0.002	<0.002	0.11	<0.002	<0.02	<0.2	0.07	0.004	0.20	<0.002	<0.1	<0.002	<0.1	0.14	<0.1	<0.2	0.02
GT-89-84	<0.001	<0.1	1.1	0.03	<0.001	<0.002	<0.002	0.06	<0.002	0.06	<0.2	0.06	0.002	0.06	<0.002	<0.1	<0.002	<0.1	0.08	<0.1	<0.2	<0.02
GT-89-85	<0.001	<0.1	2.0	<0.02	<0.001	<0.002	<0.002	0.12	0.002	0.04	<0.2	0.07	<0.002	0.11	<0.002	<0.1	<0.002	<0.1	0.14	<0.1	<0.2	<0.02
GT-89-86	<0.001	<0.1	1.7	<0.02	<0.001	<0.002	<0.002	0.06	0.002	<0.02	<0.2	0.06	0.003	0.05	<0.002	<0.1	0.002	<0.1	0.11	0.1	<0.2	0.12
GT-89-87	<0.001	<0.1	1.8	<0.02	<0.001	<0.002	<0.002	0.12	0.003	0.04	<0.2	0.07	0.003	0.10	<0.002	<0.1	<0.002	<0.1	0.14	0.1	<0.2	<0.02
GT-89-88	<0.001	0.05	0.05	0.07	<0.001	<0.002	<0.002	0.011	<0.002	<0.01	<0.1	<0.01	<0.002	<0.05	<0.002	14.8	<0.002	<0.05	0.032	<0.05	<0.1	0.02
GT-89-90	<0.001	0.08	<0.05	0.07	<0.001	<0.002	<0.002	<0.005	<0.002	0.07	<0.1	0.06	<0.002	0.07	<0.002	<0.05	<0.002	<0.05	0.015	<0.05	<0.1	0.10
GT-89-91	<0.001	<0.05	<0.05	0.07	<0.001	<0.002	<0.002	<0.005	0.002	0.05	<0.1	<0.01	<0.002	0.05	<0.002	<0.05	<0.002	<0.05	0.010	<0.05	<0.1	0.03
GT-89-92	<0.001	2.33	<0.05	0.04	<0.001	0.004	<0.002	<0.005	<0.002	1.41	<0.1	0.32	<0.002	<0.05	0.003	<0.05	<0.002	<0.05	0.014	<0.05	<0.1	0.06
GT-89-93	<0.001	<0.05	<0.05	0.03	<0.001	<0.002	<0.002	<0.005	0.002	<0.01	<0.1	<0.01	<0.002	<0.05	<0.002	12.1	<0.002	0.45	0.009	<0.05	<0.1	0.03
GT-89-94	<0.001	0.07	<0.05	0.08	<0.001	<0.002	<0.002	<0.005	<0.002	<0.01	<0.1	<0.01	<0.002	0.05	0.003	11.6	<0.002	<0.05	0.006	<0.05	<0.1	0.04
GT-89-97	<0.001	<0.1	0.8	0.13	<0.001	<0.002	<0.002	0.012	<0.002	4.12	<0.2	0.56	0.008	0.17	0.004	<0.1	<0.002	<0.1	0.10	0.2	<0.2	<0.02
GT-89-98	<0.001	<0.05	<0.05	0.01	<0.001	<0.002	<0.002	<0.005	<0.002	0.04	<0.1	<0.01	<0.002	0.05	0.003	2.1	<0.002	0.19	0.008	<0.05	<0.1	<0.01
GT-89-99	<0.001	<0.1	<0.1	<0.02	<0.001	<0.002	<0.002	<0.005	0.004	<0.02	<0.2	<0.02	<0.002	0.48	0.006	0.04	<0.002	<0.05	<0.005	<0.05	<0.2	<0.02
GT-89-100	<0.001	<0.05	<0.05	0.07	<0.001	<0.002	<0.002	<0.005	0.002	0.01	<0.1	0.01	<0.002	0.11	0.003	0.74	<0.002	0.30	<0.005	<0.05	<0.1	2.50
GT-89-101	<0.001	<0.1	<0.1	0.19	<0.001	<0.002	<0.002	<0.005	0.002	0.08	<0.2	1.23	0.003	1.69	0.015	25.5	<0.002	<0.1	0.006	<0.1	<0.2	0.04
GT-89-102	<0.001	0.39	<0.05	0.28	<0.001	<0.002	<0.002	<0.005	0.003	0.72	<0.1	<0.01	<0.002	0.12	0.023	7.1	0.002	<0.05	0.056	<0.05	<0.1	0.01

[a] Analyses by P. E. Trujillo and D. Counce, Los Alamos National Laboratory.

TABLE C-4. ISOTOPE ANALYSES FOR THERMAL AND NONTHERMAL WATERS OF THE TECUAMBURRO VOLCANO AREA

Field Number	Date	Elev (m)	Temp (°C)	δD^a (‰)	$\delta^{18}O^a$ (‰)	$\delta^{18}O_{H_2O}{}^b$ (‰)	$\delta O_{SO_4}{}^b$ (‰)	$\delta^{13}C_{HCO_3}{}^b$ (‰)	Tritium[a] (T.U.)
GT-88-1	03/17/88	1070	88.0	-[c]	–	–	–	–	–
GT-88-2	03/17/88	490	90.0	–	–	–	–	–	–
GT-88-3	03/21/88	860	37.0	–	–	–	–	–	–
GT-88-4	07/07/88	1070	77.0	-21.9	-2.55	–	–	–	1.67
GT-88-5	07/07/88	1070	85.0	-31.2	-0.76	–	–	–	–
GT-88-6	07/07/88	1070	71.5	-41.0	-4.58	–	–	–	–
GT-88-7	07/07/88	1070	27.8	-39.2	-4.29	–	4.89	–	–
GT-88-8	07/07/88	1070	22.1	-60.3	-8.90	–	–	–	4.53
GT-88-9	07/08/88	490	70.0	-51.9	-6.45	-6.35	3.01	-6.27	0.65
GT-88-10	07/08/88	490	60.0	-51.7	-7.15	-7.16	3.12	-15.22	1.90
GT-88-11	07/08/88	490	78.2	–	–	–	–	–	0.08
GT-88-12	07/08/88	490	94.3	-49.4	-6.56	-6.71	3.66	-5.37	–
GT-88-13	07/08/88	490	90.4	–	–	–	–	–	–
GT-88-14	07/08/88	490	77.2	–	–	–	–	–	–
GT-88-15	07/08/88	480	82.5	-50.1	-6.68	–	–	–	–
GT-88-16	07/08/88	480	83.7	-51.5	-6.83	-6.95	4.25	-9.25	–
GT-88-17	07/08/88	590	34.6	-59.2	-8.26	-8.46	–	-18.18	0.55
GT-88-18	07/08/88	590	32.7	-53.4	-7.82	–	–	–	–
GT-88-19	07/08/88	530	40.2	-53.6	-7.49	–	–	–	5.24
GT-88-20	07/08/88	250	20.0	-14.5	-2.67	–	–	–	3.52
GT-88-21	07/09/88	1470	96.0	-90.8	-15.05	–	–	–	–
GT-88-22	07/09/88	1470	–	–	–				–
GT-88-23	07/09/88	1460	20.0	-59.5	-8.49	–	–	–	5.55
GT-88-24	07/09/88	1110	32.4	-44.7	-5.64	–	–	–	–
GT-88-25	07/09/88	1020	22.3	-62.5	-4.74	–	–	–	7.41
GT-88-26	07/11/88	1100	37.4	-54.6	-7.92	-7.97	10.92	-12.53	0.20
GT-88-27	07/11/88	1100	21.3	-49.2	-7.19	–	–	–	–
GT-88-28	07/11/88	1120	24.1	-51.8	-7.88	–	–	–	–
GT-88-29	07/11/88	1080	58.1	-58.0	-8.58	-8.65	4.11	-5.05	4.85
GT-88-30	07/11/88	1040	42.0	-58.0	-8.60	-8.81	3.91	-6.04	–
GT-88-31	07/12/88	750	34.5	-61.7	-8.79	-9.10	2.40	6.52	0.49
GT-88-32	07/12/88	1110	23.5	–	–	–	–	–	–
GT-88-33	07/12/88	1110	–	–	–				–
GT-88-34	07/12/88	1000	42.0	-55.7	-8.26	-8.19	7.24	-4.29	0.18
GT-88-35	07/13/88	920	23.4	-46.9	-6.93	–	–	–	8.29
GT-88-36	07/13/88	1220	22.2	-51.9	-7.84	–	–	–	7.11
GT-88-37	07/13/88	1120	34.8	-53.6	-7.81	-7.87	3.20	–	3.37
GT-88-38	07/14/88	990	51.6	-56.6	-8.40	-8.55	6.41	-17.27	0.14
GT-88-39	07/14/88	1340	20.4	-52.9	-7.72	–	–	–	4.51
GT-88-40	07/14/88	1060	25.3	-53.5	-7.91	–	–	–	2.85
GT-88-41	07/14/88	1020	33.8	-54.5	-8.09	-8.29	8.14	-7.17	3.01
GT-88-42	07/15/88	1180	96.6	-57.6	-7.25	-7.53	-5.49	0.39	2.21
GT-88-43	07/16/88	390	24.8	-54.4	-7.75	–	–	–	–
GT-88-44	07/16/88	820	24.7	-48.6	-7.04	–	–	–	–
GT-88-45	07/16/88	490	96.2	-53.9	-6.72	-6.79	3.64	-5.43	0.65

TABLE C-4 (cont)

Field Number	Date	Elev (m)	Temp (°C)	δD^a (‰)	$\delta^{18}O^a$ (‰)	$\delta^{18}O_{H_2O}{}^b$ (‰)	$\delta O_{SO_4}{}^b$ (‰)	$\delta^{13}C_{HCO_3}{}^b$ (‰)	Tritium[a] (T.U.)
GT-88-46	07/16/88	490	88.8	-47.9	-6.50	–	–	–	–
GT-88-48	07/16/88	780	22.7	-44.7	-6.82	–	–	–	3.50
GT-88-49	07/16/88	980	22.8	-40.1	-5.97	–	–	–	–
GT-89-53	02/21/89	1070	93.5	NR[d]	NR	–	–	–	2.85
GT-89-54	02/21/89	1070	85.2	NR	NR	–	–	–	–
GT-89-55	02/21/89	1070	20.0	NR	NR	–	–	–	–
GT-89-56	02/21/89	1020	22.2	NR	NR	–	–	–	5.24
GT-89-57	02/22/89	480	80.2	NR	NR	-7.16	4.15	-11.97	–
GT-89-58	02/22/89	470	86.2	NR	NR	-7.08	4.20	-10.28	0.37
GT-89-59	02/22/89	475	85.0	NR	NR	-6.99	4.23	-9.70	3.42
GT-89-60	02/22/89	480	36.0	NR	NR	–	–	–	8.28
GT-89-61	02/22/89	460	53.5	NR	NR	–	–	–	1.23
GT-89-62	02/22/89	480	85.0	NR	NR	-6.95	3.74	-9.79	0.69
GT-89-63	02/23/89	460	85.2	NR	NR	-6.96	3.82	-9.64	3.78
GT-89-64	02/23/89	440	25.0	NR	NR	–	–	–	–
GT-89-65	02/24/89	580	20.8	NR	NR	–	–	–	6.20
GT-89-66	02/25/89	980	32.5	NR	NR	-8.72	–	-4.52	1.71
GT-89-67	02/25/89	1060	22.4	NR	NR	–	–	–	–
GT-89-68	02/25/89	1000	40.8	NR	NR	-8.20	–	-4.34	0.20
GT-89-69	02/25/89	1110	25.5	NR	NR	-6.58	1.37	–	–
GT-89-70	02/25/89	1110	20.1	NR	NR	-5.97	0.18	–	–
GT-89-71	02/25/89	490	96.5	NR	NR	-6.47	2.96	-6.14	–
GT-89-72	02/25/89	490	87.4	NR	NR	-6.55	2.93	-7.92	2.74
GT-89-73	03/01/89	860	37.5	NR	NR	-7.03	2.33	-2.42	–
GT-89-74	03/01/89	860	41.8	NR	NR	-7.42	1.99	-1.97	5.95
GT-89-75	03/01/89	860	30.0	NR	NR	–	–	–	–
GT-89-76	03/01/89	780	21.1	NR	NR	–	–	–	–
GT-89-77	03/03/89	1080	58.0	NR	NR	-8.43	3.42	-5.61	–
GT-89-78	03/01/89	1120	25.1	NR	NR	–	–	–	6.15
GT-89-79	03/01/89	1460	17.5	NR	NR	–	–	–	5.53
GT-89-80	03/01/89	1460	–	NR	NR				–
GT-89-81	03/04/89	990	52.4	NR	NR	-8.56	5.74	–	1.01
GT-89-83	03/04/89	490	82.4	NR	NR	-6.74	2.81	-7.79	–
GT-89-84	03/04/89	490	65.4	NR	NR	–	–	–	3.04
GT-89-85	03/04/89	490	95.8	NR	NR	-6.64	2.77	-5.56	0.51
GT-89-86	03/04/89	490	75.0	NR	NR	–	–	–	–
GT-89-87	03/04/89	480	92.4	NR	NR	-6.74	2.82	-6.84	0.70
GT-89-88	03/04/89	530	42.0	NR	NR	–	–	–	–
GT-89-90	03/06/89	1100	37.9	NR	NR	-8.14	10.45	–	0.26
GT-89-91	03/06/89	1100	17.2	NR	NR	–	–	–	–
GT-89-92	03/06/89	1120	35.5	NR	NR	–	2.81	–	–
GT-89-93	03/06/89	1190	21.9	NR	NR	–	–	–	–
GT-89-94	03/06/89	1170	21.7	NR	NR	–	–	–	6.62
GT-89-95	03/07/89	240	20.0	NR	NR	–	–	–	–

TABLE C-4 (cont)

Field Number	Date	Elev (m)	Temp (°C)	δD^a (‰)	$\delta^{18}O^a$ (‰)	$\delta^{18}O_{H_2O}{}^b$ (‰)	$\delta O_{SO_4}{}^b$ (‰)	$\delta^{13}C_{HCO_3}{}^b$ (‰)	Tritium[a] (T.U.)
GT-89-96	03/07/89	260	28.5	NR	NR				--
GT-89-97	03/07/89	260	39.2	NR	NR	-7.41	7.01	-2.23	1.00
GT-89-98	03/07/89	240	27.8	NR	NR	--	--	--	--
GT-89-99	03/07/89	750	--	NR	NR	--	--	--	3.07
GT-89-100	03/08/89	1220	20.7	NR	NR	--	--	--	6.94
GT-89-101	03/08/89	1180	97.0	NR	NR	0.01	--	0.26	0.57
GT-89-102	03/08/89	920	23.5	NR	NR	--	--	--	--

[a] Stable isotope analyses by M. Colucci, Southern Methodist University; tritium analyses by H. G. Ostlund, University of Miami.
[b] Isotope analyses by USGS, Menlo Park, California.
[c] -- = no sample collected.
[d] NR = analyses not yet received.

APPENDIX D

TABULATED SELF-POTENTIAL (SP) AND AC VOLTAGE MEASUREMENTS

The tables give the electrode positions with values for the AC voltage and self-potential measured between electrodes given on a line between each electrode position. For the most part, two values are shown for both AC voltage and self-potential, corresponding to one measurement on the rear dipole and one on the forward dipole of each setup. The self-potential along the line is the sum of the self-potentials across each dipole relative to an arbitrary reference electrode.

Ixpaco Line 1

Sta	Dipole SP (mV) Back	Dipole SP (mV) Forward	Line SP (mV) Back	Line SP (mV) Forward	AC Voltage (mV) Back	AC Voltage (mV) Forward
0			-12		1	
0.25	12		0	0	5	8
0.50	-3	+14	+3	+14	4	5
0.75	-7	+6	10	20	4	4
1.00	+12	+1	-2	21	2	3
1.25	+16	+22	-18	43	12	14
1.50	+13	+2	-31	45	26	35
1.75	+5	+6	-36	46	22	19
2.00	-11	-12	-25	34	7	7
2.25	-32	+25	7	59	24	24
2.50	+10	-14	-3	45	66	42
2.75	+22	-26	-25	19	29	31
3.00	-12	+17	-13	36	9	10
3.25	-20	+24	+7	60	7	8
3.50	-48	+50	+55	110	11	12
3.75	+29	-26	26	84	26	25
4.00	-11	+17	37	101	35	34
4.25	+30	-22	7	79	41	44
4.50	+16	0	-9	79		91
4.75		+49		+128		

Ixpaco Line 2

Sta	Dipole SP (mV) Back	Dipole SP (mV) Forward	Line SP (mV) Back	Line SP (mV) Forward	AC Voltage (mV) Back	AC Voltage (mV) Forward
0			+15		5	
0.25	+15		0	0	6	7
0.50	-36	+31	+36	31	5	4
0.75	+52	-56	-16	-25	4	4
1.00	-1	+1	-15	-24	4	4
1.25	+8	-6	-23	-30	3	4
1.50	+16	-16	-39	-46	7	5
1.75	+13	-12	-52	-58	27	32
2.00	+8	-6	-60	-64	39	42
2.25	+40	-37	-100	-101	13	13
2.50	-1	+16	-99	-85		9
2.75		-3		-88		

Ixpaco Line 3

Sta	Dipole SP (mV) Back	Dipole SP (mV) Forward	Line SP (mV) Back	Line SP (mV) Forward	AC Voltage (mV) Back	AC Voltage (mV) Forward
0			-17		26	
0.25	-17		0	0	47	34
0.50	+64	-9	-64	-9	21	20
0.25	+26	+20	-90	+11	7	7
1.00	+19	+22	-109	+33	4	4
1.25	+41	-4	-150	29	4	4
1.50	+49	-3	-199	26	12	12
1.75	+40	-1	-239	25	12	11
2.00	+28	+2	-267	27	6	8
2.75	-1	+5	-266	32	6	5
2.50	+7	+19	-273	51	4	5
2.75	+83	-27	-356	24	6	6
3.00	-17	+79	-339	103		8
3.25		+17		120		

Ixpaco Line 4

Sta	Dipole SP (mV) Back	Dipole SP (mV) Forward	Line SP (mV) Back	Line SP (mV) Forward	AC Voltage (mV) Back	AC Voltage (mV) Forward
0			-12			
	-12				5	
0.25			0	0		
	+12	-20				
0.50			-12	-20	18	22
	-5	+8			54	55
0.75			-7	-12		
	-25	+24			77	72
1.00			+18	+12		
	+3	-2			48	37
1.25			15	10		
	-18	+24			24	25
1.50			33	34		
	+7	+28			7	7
1.75			26	62		
	+10	+27			3	3
2.00			16	89		
	+5	-2			1	2
2.25			11	87		
	+89	-41			2	2
2.50			-78	46		
	-14	+69			9	9
2.75			-64	115		
		-17				12
3.00				98		

Ixpaco Line 5

Sta	Dipole SP (mV) Back	Dipole SP (mV) Forward	Line SP (mV) Back	Line SP (mV) Forward	AC Voltage (mV) Back	AC Voltage (mV) Forward
0			-13			
	-13				8	
0.25			0	0		
	-24	+22			15	14
0.50			24	22		
	-16	+17			18	13
0.75			40	39		
	-16	+16			13	14
1.00			56	55		
	+7	+6			9	9
1.25			49	61		
	-1	+16			2	6
1.50			50	77		
	+14	+4			5	3
1.75			36	81		
	-11	+33			8	7
2.00			47	114		
	+18	-14			7	8
2.25			29	100		
	-6	-15			3	4
2.50			35	85		
		-13				18
2.75				72		

Ixpaco Line 6

Sta	Dipole SP (mV) Back	Dipole SP (mV) Forward	Line SP (mV) Back	Line SP (mV) Forward	AC Voltage (mV) Back	AC Voltage (mV) Forward
0			-7			
	-7				2	
0.25			0	0		
	-15	+10			2	1
0.50			+15	+10		
	-11	+7			11	11
0.75			26	17		
	+13	-18			15	22
1.00			13	-1		
	-25	+24			11	4
1.25			38	+23		
	-20	+23			4	6
1.50			58	46		
	-38	+36			5	4
1.75			96	82		
	+31	-31			4	3
2.00			65	51		
	+15	-16			6	6
2.25			50	35		
	-13	+8			21	23
2.50			63	43		
	+5	-4			14	14
2.75			58	39		
		-6				6
3.00				33		

Ixpaco Line 7

Sta	Dipole SP (mV) Back	Dipole SP (mV) Forward	Line SP (mV) Back	Line SP (mV) Forward	AC Voltage (mV) Back	AC Voltage (mV) Forward
0			+1			
	+1				11	
0.25			0	0		
	+12	+1			3	3
0.50			-12	+1		
	+9	-1			3	4
0.75			-21	0		
	+6	-1			3	3
1.00			-27	-1		
	-16	+19			5	6
1.25			-11	18		
	+19	-17			11	11
1.50			-30	+1		
	+4	0			41	47
1.75			-34	+1		
	-3	+4			5	4
2.00			-31	+5		
	-12	+8			7	7
2.25			-19	+13		
	-22	+24			5	5
2.50			+3	+37		
	+10	-9			4	5
2.75			-7	+28		
		+14				6
3.00				+42		

Ixpaco Line 8

Sta	Dipole SP (mV) Back	Dipole SP (mV) Forward	Line SP (mV) Back	Line SP (mV) Forward	AC Voltage (mV) Back	AC Voltage (mV) Forward
0			+17			
0.25	+17		0	0	1	
0.50	-3	-8	+3	-8	1	1
0.75	-5	+3	+8	-5		
1.00	-9	+16	17	+11	1	2
1.25	+19	-21	-2	-10	1	1
1.50		+5		-5		1

APPENDIX E

TABULATED TELLURIC DATA FOR TRAVERSES 1 THROUGH 8 CHUPADERO CRATER, GUATEMALA

TELLURIC TRAVERSE DATA
IXPACO - GUATEMALA, LINE 1
250 m DIPOLES

Station Number	Frequency in Hz	Ratio	Number of Obs.	Standard Error	Dipole Position			Relative Voltage
250	7.500	.96	6	.033	0	to	250	1.00
250	27.000	.88	6	.053	0	to	250	1.00
250	75.000	.87	6	.054	0	to	250	1.00
250	450.000	.94	7	.027	0	to	250	1.00
250	14000.000	.64	6	.083	0	to	250	1.00
500	7.500	.88	5	.019	250	to	500	.96
500	27.000	.86	5	.046	250	to	500	.88
500	75.000	.87	5	.024	250	to	500	.87
500	450.000	.75	5	.020	250	to	500	.94
500	14000.000	.77	4	.031	250	to	500	.64
750	7.500	1.11	5	.013	500	to	750	.84
750	27.000	1.02	8	.094	500	to	750	.76
750	75.000	1.05	6	.022	500	to	750	.76
750	450.000	.68	6	.027	500	to	750	.70
750	14000.000	.87	6	.021	500	to	750	.49
1000	7.500	1.01	6	.045	750	to	1000	.93
1000	27.000	1.07	6	.025	750	to	1000	.77
1000	75.000	1.07	6	.024	750	to	1000	.80
1000	450.000	1.19	6	.029	750	to	1000	.48
1000	14000.000	1.26	6	.016	750	to	1000	.43
1250	7.500	1.08	7	.031	1000	to	1250	.95
1250	27.000	.94	10	.022	1000	to	1250	.83
1250	75.000	1.13	8	.033	1000	to	1250	.86
1250	450.000	1.15	8	.031	1000	to	1250	.57
1250	14000.000	1.09	6	.045	1000	to	1250	.54
1500	7.500	.98	6	.054	1250	to	1500	1.02
1500	27.500	1.06	7	.106	1250	to	1500	.78
1500	75.000	1.41	6	.060	1250	to	1500	.97
1500	450.000	1.42	5	.021	1250	to	1500	.65
1500	14000.000	1.06	5	.020	1250	to	1500	.59
1750	7.500	1.24	5	.018	1500	to	1750	1.01
1750	27.000	1.24	6	.033	1500	to	1750	.83
1750	75.000	1.23	6	.021	1500	to	1750	1.37
1750	450.000	.74	6	.017	1500	to	1750	.93
1750	14000.000	.72	6	.035	1500	to	1750	.63
2000	7.500	.98	7	.077	1750	to	2000	1.25
2000	27.000	.96	6	.026	1750	to	2000	1.03
2000	75.000	.58	7	.036	1750	to	2000	1.69
2000	450.000	.76	4	.096	1750	to	2000	.68
2000	14000.000	1.50	6	.014	1750	to	2000	.45
2250	7.500	1.43	6	.107	2000	to	2250	1.22
2250	27.000	1.42	6	.060	2000	to	2250	.99
2250	75.000	1.77	5	.080	2000	to	2250	.98
2250	450.000	1.62	7	.087	2000	to	2250	.52
2250	14000.000	1.88	5	.358	2000	to	2250	.68
2500	7.500	.75	7	.096	2250	to	2500	1.75
2500	27.000	.87	6	.081	2250	to	2500	1.41
2500	75.000	2.59	5	.025	2250	to	2500	1.73
2500	450.000	1.86	6	.027	2250	to	2500	.84
2500	14000.000	1.00	6	.037	2250	to	2500	1.28

TELLURIC TRAVERSE DATA
IXPACO - GUATEMALA, LINE 1
250 m DIPOLES
(cont)

Station Number	Frequency in Hz	Ratio	Number of Obs.	Standard Error	Dipole Position			Relative Voltage
2750	7.500	1.03	9	.040	2500	to	2750	1.31
2750	27.000	1.00	6	.029	2500	to	2750	1.22
2750	75.000	.60	4	.014	2500	to	2750	4.48
2750	450.000	.58	6	.012	2500	to	2750	1.57
2750	14000.000	.84	5	.029	2500	to	2750	1.28
3000	7.500	1.10	8	.048	2750	to	3000	1.34
3000	27.000	1.08	9	.036	2750	to	3000	1.22
3000	75.000	.70	8	.033	2750	to	3000	2.67
3000	450.000	.54	7	.085	2750	to	3000	.92
3000	14000.000	.16	5	.407	2750	to	3000	1.08
3250	7.500	1.08	6	.026	3000	to	3250	1.48
3250	27.000	1.09	7	.024	3000	to	3250	1.31
3250	75.000	1.21	6	.024	3000	to	3250	1.86
3250	450.000	1.11	6	.036	3000	to	3250	.50
3250	14000.000	1.18	7	.031	3000	to	3250	.17
3500	7.500	1.11	7	.033	3250	to	3500	1.59
3500	27.000	1.04	6	.043	3250	to	3500	1.43
3500	75.000	1.27	6	.026	3250	to	3500	2.26
3500	450.000	1.12	5	.027	3250	to	3500	.55
3500	14000.000	1.09	6	.054	3250	to	3500	.21
3750	7.500	1.36	6	.061	3500	to	3750	1.76
3750	27.000	1.37	6	.062	3500	to	3750	1.49
3750	75.000	1.82	6	.050	3500	to	3750	2.87
3750	450.000	1.10	6	.035	3500	to	3750	.62
3750	14000.000	1.04	5	.042	3500	to	3750	.22
4000	7.500	.95	8	.068	3750	to	4000	2.39
4000	27.000	.92	6	.077	3750	to	4000	2.04
4000	75.000	1.53	6	.020	3750	to	4000	5.22
4000	450.000	.95	6	.023	3750	to	4000	.68
4000	14000.000	.95	5	.013	3750	to	4000	.23
4250	7.500	.82	6	.054	4000	to	4250	2.27
4250	27.000	.92	6	.038	4000	to	4250	1.89
4250	75.000	1.00	6	.035	4000	to	4250	8.00
4250	450.000	.92	6	.045	4000	to	4050	.64
4250	14000.000	.73	5	.080	4000	to	4250	.22
4500	7.500	2.00	7	.032	4250	to	4500	1.87
4500	27.000	1.94	7	.021	4250	to	4500	1.74
4500	75.000	2.02	6	.009	4250	to	4500	8.00
4500	450.000	1.26	7	.023	4250	to	4500	.59
4500	14000.000	1.27	6	.056	4250	to	4500	.16
	7.500				4500	to	4750	3.74
	27.000				4500	to	4750	3.38
	75.000				4500	to	4750	16.12
	450.000				4500	to	4750	.74
	14000.000				4500	to	4750	.20

TELLURIC TRAVERSE DATA
IXPACO - GUATEMALA, LINE 2
250 m DIPOLES

Station Number	Frequency in Hz	Ratio	Number of Obs.	Standard Error	Dipole Position	Relative Voltage
250	7.500	.78	6	.072	0 to 250	1.00
250	27.000	.94	8	.039	0 to 250	1.00
250	75.000	.94	7	.018	0 to 250	1.00
250	450.000	.98	6	.015	0 to 250	1.00
250	14000.000	.90	7	.033	0 to 250	1.00
500	7.500	.92	6	.014	250 to 500	.78
500	27.000	.85	6	.034	250 to 500	.94
500	75.000	.56	6	.045	250 to 500	.94
500	450.000	.83	6	.034	250 to 500	.98
500	14000.000	.95	5	.041	250 to 500	.90
750	7.500	1.08	6	.079	500 to 750	.72
750	27.000	.91	6	.042	500 to 750	.80
750	75.000	.95	6	.031	500 to 750	.52
750	450.000	.89	6	.062	500 to 750	.81
750	14000.000	1.10	5	.021	500 to 750	.86
1000	7.500	.88	6	.024	750 to 1000	.77
1000	27.000	.83	6	.018	750 to 1000	.73
1000	75.000	.97	5	.028	750 to 1000	.50
1000	450.000	.87	5	.011	750 to 1000	.72
1000	14000.000	.90	6	.032	750 to 1000	.95
1250	7.500	1.06	5	.018	1000 to 1250	.68
1250	27.000	.88	6	.073	1000 to 1250	.60
1250	75.000	.84	6	.023	1000 to 1250	.49
1250	450.000	.92	6	.021	1000 to 1250	.63
1250	14000.000	.98	6	.031	1000 to 1250	.85
1500	7.500	1.09	8	.073	1250 to 1500	.72
1500	27.000	1.15	7	.053	1250 to 1500	.53
1500	75.000	1.26	6	.040	1250 to 1500	.41
1500	450.000	1.18	6	.019	1250 to 1500	.58
1500	14000.000	1.03	6	.032	1250 to 1500	.84
1750	7.500	1.11	6	.051	1500 to 1750	.78
1750	27.000	1.24	7	.028	1500 to 1750	.61
1750	75.000	2.66	6	.039	1500 to 1750	.52
1750	450.000	1.32	6	.053	1500 to 1750	.68
1750	14000.000	1.09	7	.053	1500 to 1750	.86
2000	7.500	1.12	8	.071	1750 to 2000	.87
2000	27.000	1.10	7	.051	1750 to 2000	.75
2000	75.000	1.27	6	.067	1750 to 2000	1.37
2000	450.000	1.23	6	.042	1750 to 2000	.90
2000	14000.000	.95	6	.070	1750 to 2000	.94
2250	7.500	.97	8	.045	2000 to 2250	.98
2250	27.000	.83	8	.079	2000 to 2250	.83
2250	75.000	.37	7	.055	2000 to 2250	1.75
2250	450.000	.34	6	.292	2000 to 2250	1.11
2250	14000.000	.83	6	.038	2000 to 2250	.89
2500	7.500	.87	8	.014	2250 to 2500	.95
2500	27.000	.87	6	.032	2250 to 2500	.69
2500	75.000	.57	6	.008	2250 to 2500	.64
2500	450.000	.79	7	.034	2250 to 2500	.38
2500	14000.000	1.12	6	.011	2250 to 2500	.74
	7.500				2500 to 2750	.83
	27.000				2500 to 2750	.60
	75.000				2500 to 2750	.36
	450.000				2500 to 2750	.30
	14000.000				2500 to 2750	.84

TELLURIC TRAVERSE DATA
IXPACO - GUATEMALA, LINE 3
250 m DIPOLES

Station Number	Frequency in Hz	Ratio	Number of Obs.	Standard Error	Dipole Position			Relative Voltage
250	7.500	.74	7	.092	0	to	250	1.00
250	27.000	.81	6	.106	0	to	250	1.00
250	75.000	.89	6	.059	0	to	250	1.00
250	450.000	1.35	6	.022	0	to	250	1.00
250	14000.000	.98	5	.003	0	to	250	1.00
500	7.500	.50	7	.041	250	to	500	.74
500	27.00	.81	7	.052	250	to	500	.81
500	75.000	.58	6	.027	250	to	500	.89
500	450.000	.77	5	.011	250	to	500	1.35
500	14000.000	.95	4	.012	250	to	500	.98
750	7.500	.90	7	.106	500	to	750	.37
750	27.000	.86	6	.035	500	to	750	.66
750	75.000	.93	7	.027	500	to	750	.51
750	450.000	.92	6	.022	500	to	750	1.04
750	14000.000	1.17	5	.025	500	to	750	.92
1000	7.500	1.09	6	.054	750	to	1000	.33
1000	27.000	1.12	6	.038	750	to	1000	.56
1000	75.000	1.09	7	.018	750	to	1000	.47
1000	450.000	1.02	6	.010	750	to	1000	.96
1000	14000.000	.94	5	.017	750	to	1000	1.08
1250	7.500	.91	7	.071	1000	to	1250	.36
1250	27.500	.93	5	.026	1000	to	1250	.63
1250	75.000	.97	7	.026	1000	to	1250	.51
1250	450.000	1.01	6	.027	1000	to	1250	.98
1250	14000.000	1.47	5	.007	1000	to	1250	1.02
1500	7.500	1.28	6	.037	1250	to	1500	.33
1500	27.500	1.35	6	.071	1250	to	1500	.59
1500	75.000	1.35	6	.058	1250	to	1500	.50
1500	450.000	1.24	6	.022	1250	to	1500	.98
1500	14000.000	1.23	4	.032	1250	to	1500	1.49
1750	7.500	.79	7	.113	1500	to	1750	.42
1750	27.000	.88	6	.072	1500	to	1750	.79
1750	75.000	.95	6	.052	1500	to	1750	.67
1750	450.000	1.09	6	.027	1500	to	1750	1.22
1750	14000.000	.81	5	.012	1500	to	1750	1.83
2000	7.500	1.17	7	.057	1750	to	2000	.33
2000	27.000	1.08	7	.056	1750	to	2000	.69
2000	75.000	1.04	7	.054	1750	to	2000	.64
2000	450.000	.87	6	.040	1750	to	2000	1.33
2000	14000.000	1.07	4	.021	1750	to	2000	1.48
2250	7.500	.94	8	.054	2000	to	2250	.39
2250	27.000	.94	8	.049	2000	to	2250	.75
2250	75.000	.86	6	.049	2000	to	2250	.66
2250	450.000	1.06	6	.049	2000	to	2250	1.16
2250	14000.000	1.07	6	.047	2000	to	2250	1.58
2500	7.500	.85	7	.023	2250	to	2500	.36
2500	27.000	.92	8	.052	2250	to	2500	.71
2500	75.000	.98	7	.021	2250	to	2500	.57
2500	450.000	1.14	7	.064	2250	to	2500	1.23
2500	14000.000	1.02	5	.005	2250	to	2500	1.69

TELLURIC TRAVERSE DATA
IXPACO - GUATEMALA, LINE 3
250 m DIPOLES
(cont)

Station Number	Frequency in Hz	Ratio	Number of Obs.	Standard Error	Dipole Position			Relative Voltage
2750	7.500	.83	6	.053	2500	to	2750	.31
2750	27.000	.83	7	.042	2500	to	2750	.65
2750	75.000	.96	7	.047	2500	to	2750	.56
2750	450.000	.98	6	.038	2500	to	2750	1.40
2750	14000.000	1.02	5	.021	2500	to	2750	1.73
3000	7.500	1.07	8	.061	2750	to	3000	.26
3000	27.000	1.10	8	.057	2750	to	3000	.54
3000	75.000	1.08	7	.011	2750	to	3000	.54
3000	450.000	.84	7	.037	2750	to	3000	1.37
3000	14000.000	.57	5	.004	2750	to	3000	1.77
	7.500				3000	to	3250	.27
	27.000				3000	to	3250	.59
	75.000				3000	to	3250	.58
	450.000				3000	to	3250	1.15
	14000.000				3000	to	3250	1.00

TELLURIC TRAVERSE DATA
IXPACO - GUATEMALA, LINE 4
250 m DIPOLES

Station Number	Frequency in Hz	Ratio	Number of Obs.	Standard Error	Dipole Position			Relative Voltage
250	7.500	.80	7	.100	0	to	250	1.00
250	27.000	.76	6	.128	0	to	250	1.00
250	75.000	1.09	8	.074	0	to	250	1.00
250	450.000	.60	7	.136	0	to	250	1.00
250	14000.000	.77	4	.005	0	to	250	1.00
500	7.500	1.02	7	.115	250	to	500	.80
500	27.00	1.24	7	.056	250	to	500	.76
500	75.000	1.32	7	.040	250	to	500	1.09
500	450.000	3.13	6	.323	250	to	500	.60
500	14000.000	1.20	5	.071	250	to	500	.77
750	7.500	1.17	7	.017	500	to	750	.81
750	27.000	1.16	6	.041	500	to	750	.95
750	75.000	1.30	6	.014	500	to	750	1.44
750	450.000	1.38	5	.003	500	to	750	1.87
750	14000.000	1.93	5	.012	500	to	750	.92
1000	7.500	.58	7	.025	750	to	1000	.95
1000	27.000	.65	7	.036	750	to	1000	1.10
1000	75.000	.45	6	.020	750	to	1000	1.87
1000	450.000	.48	6	.006	750	to	1000	2.58
1000	14000.000	.68	5	.003	750	to	1000	1.78
1250	7.500	.83	7	.042	1000	to	1250	.55
1250	27.500	.89	6	.046	1000	to	1250	.72
1250	75.000	1.24	6	.056	1000	to	1250	.83
1250	450.000	1.01	6	.070	1000	to	1250	1.23
1250	14000.000	.95	5	.006	1000	to	1250	1.20
1500	7.500	.76	6	.032	1250	to	1500	.46
1500	27.500	.69	6	.036	1250	to	1500	.64
1500	75.000	.42	6	.011	1250	to	1500	1.03
1500	450.000	.56	5	.033	1250	to	1500	1.25
1500	14000.000	1.01	5	.007	1250	to	1500	1.15
1750	7.500	.79	7	.066	1500	to	1750	.35
1750	27.000	.69	7	.068	1500	to	1750	.44
1750	75.000	.56	7	.046	1500	to	1750	.43
1750	450.000	.50	6	.096	1500	to	1750	.69
1750	14000.000	.87	5	.008	1500	to	1750	1.16
2000	7.500	.94	7	.061	1750	to	2000	.26
2000	27.000	.98	7	.053	1750	to	2000	.30
2000	75.000	1.01	6	.039	1750	to	2000	.24
2000	450.000	.79	6	.022	1750	to	2000	.35
2000	14000.000	.94	5	.006	1750	to	2000	1.00
2250	7.500	1.31	6	.041	2000	to	2250	.25
2250	27.000	1.24	6	.053	2000	to	2250	.30
2250	75.000	1.44	5	.017	2000	to	2250	.24
2250	450.000	1.23	6	.015	2000	to	2250	.27
2250	14000.000	1.08	5	.003	2000	to	2250	.94
2500	7.500	.98	6	.057	2250	to	2500	.33
2500	27.000	1.28	6	.083	2250	to	2500	.37
2500	75.000	3.35	5	.489	2250	to	2500	.35
2500	450.000	2.13	6	.351	2250	to	2500	.34
2500	14000.000	.81	5	.003	2250	to	2500	1.02

TELLURIC TRAVERSE DATA
IXPACO - GUATEMALA, LINE 4
250 m DIPOLES
(cont)

Station Number	Frequency in Hz	Ratio	Number of Obs.	Standard Error	Dipole Position	Relative Voltage
2750	7.500	1.00	2	.010	2500 to 2750	.32
2750	27.000	1.09	7	.055	2500 to 2750	.47
2750	75.000	1.00	2	.010	2500 to 2750	1.18
2750	450.000	.84	1	.010	2500 to 2750	.72
2750	14000.000	1.17	5	.016	2500 to 2750	.83
	7.500				2750 to 3000	.32
	27.000				2750 to 3000	.51
	75.000				2750 to 3000	1.18
	450.000				2750 to 3000	.60
	14000.000				2750 to 3000	.96

TELLURIC TRAVERSE DATA
IXPACO - GUATEMALA, LINE 5
250 m DIPOLES

Station Number	Frequency in Hz	Ratio	Number of Obs.	Standard Error	Dipole Position			Relative Voltage
250	7.500	2.39	7	.127	0	to	250	1.00
250	27.000	2.41	8	.106	0	to	250	1.00
250	75.000	2.49	7	.015	0	to	250	1.00
250	450.000	2.08	6	.049	0	to	250	1.00
250	14000.000	.99	6	.006	0	to	250	1.00
500	7.500	1.00	8	.046	250	to	500	2.39
500	27.00	.90	7	.035	250	to	500	2.41
500	75.000	.64	7	.021	250	to	500	2.49
500	450.000	.71	6	.100	250	to	500	2.08
500	14000.000	.69	6	.033	250	to	500	.99
750	7.500	.93	7	.015	500	to	750	2.39
750	27.000	.92	7	.027	500	to	750	2.17
750	75.000	1.37	6	.067	500	to	750	1.60
750	450.000	.87	7	.006	500	to	750	1.49
750	14000.000	1.02	7	.012	500	to	750	.69
1000	7.500	.76	7	.031	750	to	1000	2.23
1000	27.000	.85	7	.085	750	to	1000	2.00
1000	75.000	.44	7	.025	750	to	1000	2.19
1000	450.000	.88	7	.027	750	to	1000	1.29
1000	14000.000	.98	6	.008	750	to	1000	.70
1250	7.500	.80	7	.013	1000	to	1250	1.71
1250	27.500	.82	7	.015	1000	to	1250	1.70
1250	75.000	.80	6	.007	1000	to	1250	.97
1250	450.000	1.01	7	.017	1000	to	1250	1.13
1250	14000.000	1.43	6	.025	1000	to	1250	.68
1500	7.500	.88	6	.013	1250	to	1500	1.36
1500	27.500	.87	7	.030	1250	to	1500	1.39
1500	75.000	.62	6	.158	1250	to	1500	.78
1500	450.000	.83	6	.032	1250	to	1500	1.15
1500	14000.000	1.03	6	.018	1250	to	1500	.97
1750	7.500	.88	7	.050	1500	to	1750	1.19
1750	27.000	.70	7	.013	1500	to	1750	1.22
1750	75.000	.79	6	.042	1500	to	1750	.48
1750	450.000	.85	6	.020	1500	to	1750	.96
1750	14000.000	.93	6	.012	1500	to	1750	1.00
2000	7.500	1.21	8	.035	1750	to	2000	1.05
2000	27.000	1.26	6	.020	1750	to	2000	.86
2000	75.000	.91	7	.020	1750	to	2000	.39
2000	450.000	1.08	6	.011	1750	to	2000	.81
2000	14000.000	1.02	7	.032	1750	to	2000	.93
2250	7.500	1.20	9	.044	2000	to	2250	1.27
2250	27.000	1.18	7	.072	2000	to	2250	1.08
2250	75.000	1.01	7	.036	2000	to	2250	.35
2250	450.000	.94	9	.061	2000	to	2250	.88
2250	14000.000	1.15	8	.019	2000	to	2250	.95
2500	7.500	1.98	10	.034	2250	to	2500	1.52
2500	27.000	1.42	7	.047	2250	to	2500	.43
2500	75.000	1.37	7	.023	2250	to	2500	.68
2500	450.000	1.10	7	.026	2250	to	2500	.60
2500	14000.000	1.31	5	.009	2250	to	2500	1.00

TELLURIC TRAVERSE DATA
IXPACO - GUATEMALA, LINE 5
250 m DIPOLES

Station Number	Frequency in Hz	Ratio	Number of Obs.	Standard Error	Dipole Position			Relative Voltage
2750	7.500	1.16	7	.041	2500	to	2750	.65
2750	27.000	1.19	7	.049	2500	to	2750	.61
2750	75.000	1.06	7	.173	2500	to	2750	.94
2750	450.000	1.12	7	.026	2500	to	2750	.66
2750	14000.000	.94	6	.008	2500	to	2750	1.31
	7.500				2750	to	3000	.75
	27.000				2750	to	3000	.73
	75.000				2750	to	3000	.99
	450.000				2750	to	3000	.74
	14000.000				2750	to	3000	1.23

TELLURIC TRAVERSE DATA
IXPACO - GUATEMALA, LINE 6
250 m DIPOLES

Station Number	Frequency in Hz	Ratio	Number of Obs.	Standard Error	Dipole Position			Relative Voltage
250	7.500	1.50	7	.113	0	to	250	1.00
250	27.000	1.51	7	.060	0	to	250	1.00
250	75.000	1.40	7	.049	0	to	250	1.00
250	450.000	1.17	8	.033	0	to	250	1.00
250	14000.000	1.18	6	.054	0	to	250	1.00
500	7.500	.99	7	.105	250	to	500	1.50
500	27.00	.84	7	.039	250	to	500	1.51
500	75.000	.88	7	.046	250	to	500	1.40
500	450.000	.97	8	.019	250	to	500	1.17
500	14000.000	.90	7	.011	250	to	500	1.18
750	7.500	.78	6	.023	500	to	750	1.48
750	27.000	.85	7	.036	500	to	750	1.28
750	75.000	1.08	7	.032	500	to	750	1.23
750	450.000	.80	8	.017	500	to	750	1.14
750	14000.000	.62	6	.018	500	to	750	1.07
1000	7.500	1.34	6	.056	750	to	1000	1.16
1000	27.000	1.43	7	.025	750	to	1000	1.09
1000	75.000	1.01	7	.069	750	to	1000	1.33
1000	450.000	1.12	7	.090	750	to	1000	.91
1000	14000.000	2.12	6	.013	750	to	1000	.66
1250	7.500	.78	6	.061	1000	to	1250	1.56
1250	27.500	.78	6	.028	1000	to	1250	1.55
1250	75.000	.64	6	.032	1000	to	1250	1.35
1250	450.000	.74	6	.022	1000	to	1250	1.02
1250	14000.000	.89	6	.025	1000	to	1250	1.40
1500	7.500	.97	6	.070	1250	to	1500	1.22
1500	27.500	.90	6	.106	1250	to	1500	1.22
1500	75.000	.94	6	.045	1250	to	1500	.86
1500	450.000	1.00	6	.020	1250	to	1500	.75
1500	14000.000	.89	6	.022	1250	to	1500	1.24
1750	7.500	.86	7	.036	1500	to	1750	1.18
1750	27.000	.82	7	.031	1500	to	1750	1.09
1750	75.000	.75	6	.031	1500	to	1750	.81
1750	450.000	.87	8	.023	1500	to	1750	.75
1750	14000.000	1.02	6	.006	1500	to	1750	1.11
2000	7.500	.64	6	.119	1750	to	2000	1.02
2000	27.000	.84	7	.063	1750	to	2000	.89
2000	75.000	1.11	6	.039	1750	to	2000	.60
2000	450.000	1.07	6	.016	1750	to	2000	.66
2000	14000.000	.83	6	.023	1750	to	2000	1.14
2250	7.500	.72	6	.063	2000	to	2250	.65
2250	27.000	.89	6	.028	2000	to	2250	.75
2250	75.000	1.88	6	.094	2000	to	2250	.67
2250	450.000	.93	6	.036	2000	to	2250	.70
2250	14000.000	.85	6	.015	2000	to	2250	.94
2500	7.500	1.28	6	.023	2250	to	2500	.46
2500	27.000	1.23	6	.053	2250	to	2500	.67
2500	75.000	.95	6	.068	2250	to	2500	1.25
2500	450.000	1.35	6	.015	2250	to	2500	.66
2500	14000.000	1.31	6	.049	2250	to	2500	.80

TELLURIC TRAVERSE DATA
IXPACO - GUATEMALA, LINE 6
250 m DIPOLES
(cont)

Station Number	Frequency in Hz	Ratio	Number of Obs.	Standard Error	Dipole Position	Relative Voltage
2750	7.500	.65	7	.047	2500 to 2750	.59
2750	27.000	.67	7	.043	2500 to 2750	.82
2750	75.000	.50	6	.027	2500 to 2750	1.19
2750	450.000	1.11	6	.036	2500 to 2750	.89
2750	14000.000	.58	5	.003	2500 to 2750	1.05
	7.500				2750 to 3000	.38
	27.000				2750 to 3000	.55
	75.000				2750 to 3000	.60
	450.000				2750 to 3000	.98
	14000.000				2750 to 3000	.61

TELLURIC TRAVERSE DATA
IXPACO - GUATEMALA, LINE 7
250 m DIPOLES

Station Number	Frequency in Hz	Ratio	Number of Obs.	Standard Error	Dipole Position			Relative Voltage
250	7.500	.50	7	.043	0	to	250	1.00
250	27.000	.54	7	.045	0	to	250	1.00
250	75.000	.45	8	.034	0	to	250	1.00
250	450.000	.67	7	.018	0	to	250	1.00
250	14000.000	.69	5	.014	0	to	250	1.00
500	7.500	1.37	8	.051	250	to	500	.50
500	27.00	1.35	7	.030	250	to	500	.54
500	75.000	1.44	7	.026	250	to	500	.45
500	450.000	1.35	7	.019	250	to	500	.67
500	14000.000	1.48	6	.005	250	to	500	.69
750	7.500	.72	7	.034	500	to	750	.68
750	27.000	.66	7	.022	500	to	750	.73
750	75.000	.67	7	.037	500	to	750	.65
750	450.000	.68	7	.008	500	to	750	.90
750	14000.000	.82	5	.005	500	to	750	1.03
1000	7.500	1.02	7	.063	750	to	1000	.49
1000	27.000	.97	6	.017	750	to	1000	.48
1000	75.000	1.24	7	.026	750	to	1000	.44
1000	450.000	1.04	7	.021	750	to	1000	.62
1000	14000.000	.94	6	.018	750	to	1000	.84
1250	7.500	.84	7	.026	1000	to	1250	.50
1250	27.500	.85	8	.047	1000	to	1250	.47
1250	75.000	1.12	7	.059	1000	to	1250	.54
1250	450.000	.96	7	.029	1000	to	1250	.64
1250	14000.000	.88	5	.015	1000	to	1250	.79
1500	7.500	1.16	8	.073	1250	to	1500	.42
1500	27.500	1.64	7	.068	1250	to	1500	.40
1500	75.000	3.51	6	.025	1250	to	1500	.60
1500	450.000	1.56	6	.024	1250	to	1500	.62
1500	14000.000	1.05	5	.018	1250	to	1500	.70
1750	7.500	.66	7	.042	1500	to	1750	.49
1750	27.000	.50	7	.052	1500	to	1750	.65
1750	75.000	.28	0	.001	1500	to	1750	2.11
1750	450.000	.60	7	.017	1500	to	1750	.97
1750	14000.000	.85	5	.001	1500	to	1750	.73
2000	7.500	1.32	7	.035	1750	to	2000	.32
2000	27.000	1.10	7	.041	1750	to	2000	.33
2000	75.000	1.08	8	.026	1750	to	2000	.59
2000	450.000	1.14	7	.011	1750	to	2000	.58
2000	14000.000	1.65	5	.004	1750	to	2000	.62
2250	7.500	1.06	8	.053	2000	to	2250	.42
2250	27.000	1.19	7	.050	2000	to	2250	.36
2250	75.000	1.08	6	.024	2000	to	2250	.64
2250	450.000	.90	7	.015	2000	to	2250	.66
2250	14000.000	.97	5	.007	2000	to	2250	1.03
2500	7.500	1.46	7	.038	2250	to	2500	.45
2500	27.000	2.15	8	.046	2250	to	2500	1.28
2500	75.000	2.46	8	.033	2250	to	2500	.36
2500	450.000	2.52	8	.017	2250	to	2500	.82
2500	14000.000	2.13	7	.031	2250	to	2500	1.09
	7.500				2500	to	2750	3.00
	27.000				2500	to	2750	2.74
	75.000				2500	to	2750	.88
	450.000				2500	to	2750	2.08
	14000.000				2500	to	2750	2.32

TELLURIC TRAVERSE DATA
IXPACO - GUATEMALA, LINE 8
250 m DIPOLES

Station Number	Frequency in Hz	Ratio	Number of Obs.	Standard Error	Dipole Position			Relative Voltage
250	7.500	1.10	8	.079	0	to	250	1.00
250	27.000	.92	7	.038	0	to	250	1.00
250	75.000	1.36	8	.069	0	to	250	1.00
250	450.000	1.69	7	.120	0	to	250	1.00
250	14000.000	1.50	5	.061	0	to	250	1.00
500	7.500	1.02	7	.025	250	to	500	1.10
500	27.00	1.00	7	.036	250	to	500	.92
500	75.000	.98	7	.031	250	to	500	1.36
500	450.000	1.06	7	.011	250	to	500	1.69
500	14000.000	1.22	5	.021	250	to	500	1.50
750	7.500	1.00	7	.055	500	to	750	1.13
750	27.000	.95	7	.034	500	to	750	.92
750	75.000	.93	7	.025	500	to	750	1.33
750	450.000	.92	7	.006	500	to	750	1.79
750	14000.000	.86	5	.006	500	to	750	1.83
1000	7.500	.89	7	.025	750	to	1000	1.12
1000	27.000	.81	8	.047	750	to	1000	.88
1000	75.000	.81	7	.036	750	to	1000	1.23
1000	450.000	.80	6	.017	750	to	1000	1.65
1000	14000.000	.96	5	.007	750	to	1000	1.58
1250	7.500	.85	7	.014	1000	to	1250	1.00
1250	27.500	.86	7	.036	1000	to	1250	.71
1250	75.000	.83	7	.016	1000	to	1250	1.00
1250	450.000	.75	6	.017	1000	to	1250	1.32
1250	14000.000	.93	5	.027	1000	to	1250	1.51
	7.500				1250	to	1500	.86
	27.500				1250	to	1500	.61
	75.000				1250	to	1500	.83
	450.000				1250	to	1500	.99
	14000.000				1250	to	1500	1.40

APPENDIX F

TABULATED AMT SOUNDING DATA FOR TELLURIC TRAVERSES 1 THROUGH 8 CHUPADERO CRATER, GUATEMALA

STATION ID = 1

NUMBER OF FREQUENCIES = 10

FREQ	AP-RES	N OBS	STD ERR
7.500	13.25	4	1.19
14.000	16.39	8	3.25
27.000	26.68	9	13.16
45.000	34.19	12	3.56
75.000	35.83	11	2.43
270.000	59.87	8	8.75
450.000	52.69	8	6.85
4500.000	67.96	10	10.36
7500.000	59.68	9	13.40
14000.000	202.49	7	49.75

STATION ID = 2

NUMBER OF FREQUENCIES = 14

FREQ	AP-RES	N OBS	STD ERR
4.500	4.34	7	0.52
7.500	7.01	10	0.26
14.000	7.55	11	1.61
27.000	5.74	11	0.40
45.000	11.15	14	0.43
75.000	17.07	12	1.54
140.000	15.08	12	1.27
270.000	23.93	12	1.28
450.000	21.28	10	1.25
750.000	10.20	11	0.73
1400.000	3.80	5	1.08
2700.000	3.30	7	1.52
7500.000	5.60	6	1.04
14000.000	9.79	8	1.04

STATION ID = 3

NUMBER OF FREQUENCIES = 14

FREQ	AP-RES	N OBS	STD ERR
4.500	54.47	2	6.70
7.500	73.08	6	8.97
14.000	98.23	10	12.98
27.000	87.90	9	13.18
45.000	67.63	12	5.44
75.000	105.35	10	15.17
140.000	81.24	12	4.16
270.000	120.90	12	5.81
450.000	79.37	9	1.18
750.000	37.01	11	1.47
2700.000	42.69	11	7.50
4500.000	144.62	12	10.86
7500.000	113.87	11	4.89
14000.000	254.59	9	5.59

STATION ID = 4

NUMBER OF FREQUENCIES = 13

FREQ	AP-RES	N OBS	STD ERR
7.500	5.91	5	1.06
14.000	18.75	13	1.11
27.000	14.97	11	1.45
45.000	31.50	11	3.17
75.000	65.22	10	6.06
140.000	43.45	18	1.66
270.000	42.35	16	5.51
450.000	41.44	11	3.45
750.000	20.90	13	1.37
2700.000	72.16	10	6.70
4500.000	22.49	10	2.63
7500.000	94.54	9	11.00
14000.000	131.75	7	5.97

STATION ID = 5

NUMBER OF FREQUENCIES = 14

FREQ	AP-RES	N OBS	STD ERR
4.500	11.80	9	3.49
7.500	18.06	9	9.46
14.000	22.47	12	6.17
27.000	9.98	11	2.21
45.000	25.36	7	5.03
75.000	33.32	12	6.15
140.000	18.15	11	3.84
270.000	14.05	8	2.15
450.000	13.48	11	2.72
750.000	14.73	8	2.24
2700.000	56.28	11	5.77
4500.000	32.08	9	9.63
7500.000	29.77	14	4.26
14000.000	82.93	13	4.70

STATION ID = 7

NUMBER OF FREQUENCIES = 14

FREQ	AP-RES	N OBS	STD ERR
7.500	41.81	11	3.83
14.000	30.13	13	3.02
27.000	29.40	8	11.04
45.000	74.41	16	14.05
75.000	67.81	11	5.73
140.000	80.70	12	6.90
270.000	89.68	16	16.83
450.000	87.68	13	4.32
750.000	44.31	12	3.66
1400.000	62.29	10	2.18
2700.000	69.75	11	9.72
4500.000	76.99	13	7.81
7500.000	107.08	12	13.57
14000.000	200.44	12	7.95

STATION ID = 6

NUMBER OF FREQUENCIES = 15

FREQ	AP-RES	N OBS	STD ERR
4.500	69.00	9	63.47
7.500	119.25	11	57.46
14.000	58.78	8	14.40
27.000	23.36	11	16.57
45.000	72.67	11	16.47
75.000	63.20	14	7.79
140.000	108.11	11	15.86
270.000	113.31	12	19.48
450.000	67.99	11	10.73
750.000	33.87	12	4.16
1400.000	92.41	13	12.75
2700.000	197.09	10	32.13
4500.000	120.41	11	13.67
7500.000	121.81	10	12.82
14000.000	403.98	10	19.41

STATION ID = 8

NUMBER OF FREQUENCIES = 15

FREQ	AP-RES	N OBS	STD ERR
4.500	21.98	7	3.02
7.500	18.45	10	1.46
14.000	23.30	13	1.72
27.000	19.08	18	1.30
45.000	33.42	12	3.36
75.000	28.04	11	8.65
140.000	28.73	12	10.90
270.000	58.62	12	6.72
450.000	47.29	10	8.48
750.000	68.00	11	10.32
1400.000	58.75	12	13.44
2700.000	27.95	12	1.62
4500.000	42.60	11	4.84
7500.000	83.68	9	15.76
14000.000	69.59	11	11.52

This report has been reproduced directly from
the best available copy.

Available to DOE and DOE contractors from
the Office of Scientific and Technical Information
P.O. Box 62
Oak Ridge, TN 37831
prices available from
(615) 576-8401, FTS 626-8401

Available to the public from
the National Technical Information Service
U.S. Department of Commerce
5285 Port Royal Rd.
Springfield, VA 22161

Microfiche A01

Page Range	NTIS Price Code	Page Range	NTIS Price Code	Page Range	NTIS Price Code	Page Range	NTIS Price Code
001–025	A02	151–175	A08	301–325	A14	451–475	A20
026–050	A03	176–200	A09	326–350	A15	476–500	A21
051–075	A04	201–225	A10	351–375	A16	501–525	A22
076–100	A05	226–250	A11	376–400	A17	526–550	A23
101–125	A06	251–275	A12	401–425	A18	551–575	A24
126–150	A07	276–300	A13	426–450	A19	576–600	A25
						601-up*	A99

*Contact NTIS for a price quote.

*U.S. GOVERNMENT PRINTING OFFICE: 1990-0-773-034/20091

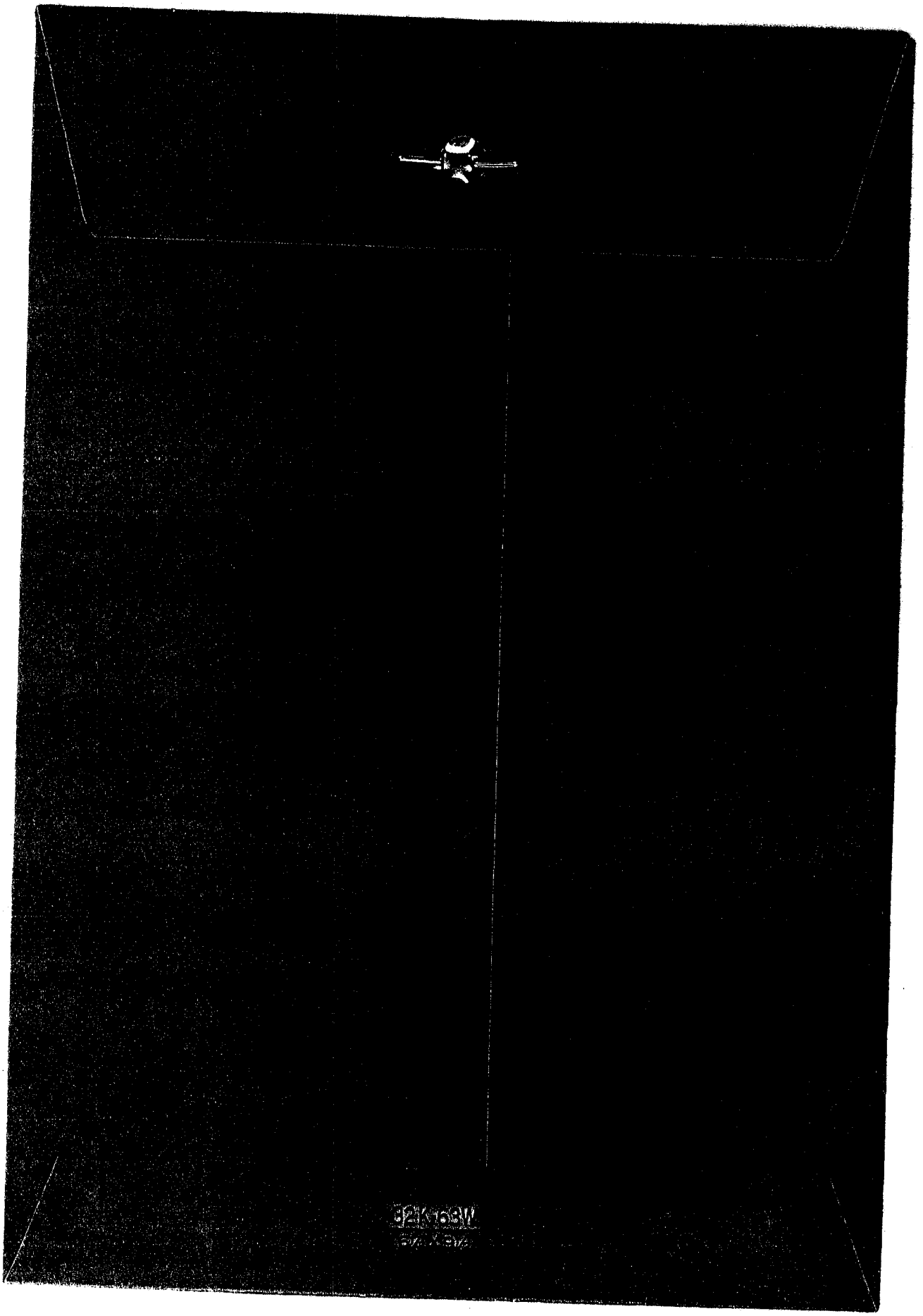
821-1638

Los Alamos National Laboratory
Los Alamos,New Mexico 87545